Isolation of Enantiomers via Diastereomer Crystallisation

Parathy Anandamanoharan

12 March 2010

A thesis submitted for the degree of Doctor of Philosophy of the University of London

Department of Chemical Engineering
University College London
Torrington Place
London
WC1E 7JE

ABSTRACT

Enantiomer separation remains an important technique for obtaining optically active materials. Even though the enantiomers have identical physical properties, the difference in their biological activities make it important to separate them, in order to use single enantiomer products in the pharmaceutical and fine chemical industries.

In this project, the separations of three pairs of diastereomer salts (**Fig1**) by crystallisation are studied, as examples of the 'classical' resolution of enantiomers via conversion to diastereomers. The lattice energies of these diastereomer compounds are calculated computationally (based on realistic potentials for the dominant electrostatic interactions and *ab initio* conformational energies). Then the experimental data are compared with the theoretical data to study the efficiency of the resolving agent.

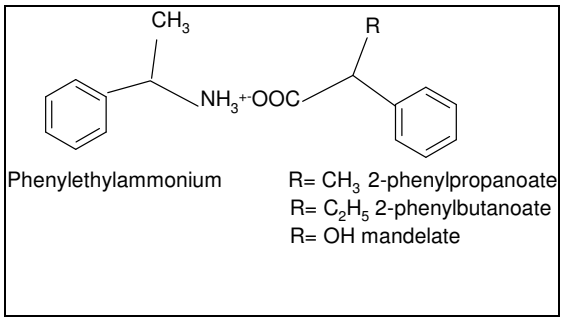

Fig1 Three pairs of diastereomer salts studied

All three fractional crystallisations occurred relatively slowly, and appeared to be thermodynamically controlled. Separabilities by crystallisation have been compared with measured phase equilibrium data for the three systems studied. All crystallisations appear to be consistent with ternary phase diagrams.

In the case of R = CH_3, where the salt-solvent ternaries exhibited eutonic behaviour, the direction of isomeric enrichment changed abruptly on passing through the eutonic composition. In another example, R = OH, the ternaries indicated near-ideal solubility behaviour of the salt mixtures, and the separation by crystallisation again corresponded.

Further, new polymorphic structures and generally better structure predictions have been obtained through out this study. In the case of R = CH_3, an improved structure of the p-salt has been determined. In the case of R = C_2H_5, new polymorphic forms of the n-salts, II and III, have been both discovered and predicted.

This work also demonstrates that chemically related organic molecules can exhibit different patterns of the relative energies of the theoretical low energy crystal structures, along with differences in the experimental polymorphic behaviour.

This joint experimental and computational investigation provides a stringent test of the reliability of lattice modelling to explain the origins of chiral resolution via diastereomer formation.

All the experimental and computational works investigated in this thesis are published (see **APPENDIX 1**).

ACKNOWLEDGEMENTS

I would like to thank my supervisors, Professor Alan Jones and Professor Peter Cains for the continuous guidance, time, advice, support and encouragement throughout my project. It has been a privilege to work with them, as they have taught me to resolve complex problems throughout my project and all I have learned from them will be invaluable tools in my future career.

I would like to say special thanks to Dr Panagiotis (Panos) Karamertzanis, Professor Sally (Sarah) Price and all the other helpful staffs from the Chemistry Department, at UCL, for guidance on using the molecular modelling tools and scientific advices throughout my studies and also for performing some of the characterisation studies.

A special thanks to Ghulam Warsi and other technical staffs for providing help with the materials necessary to carry out this project and for their patience.

Finally, I would also like to thank the EPSRC organisation for funding my research through a departmental research studentship.

TABLE OF CONTENTS

Abstract i

Acknowledgements iii

Table of contents iv

List of Tables ix

List of figures xi

1 INTRODUCTION 1

2 SURVEY OF LITERATURE AND METHODS 9

2-1 Stereochemistry and Crystallisation 9

2-1-1 Stereochemistry 9

2-1-2 Enantiomeric molecules or enantiomers 11

2-1-3 Diastereomeric molecules or diastereomers 13

2-1-4 Crystallisation 14

2-1-5 Racemic crystallisation 15

2-1-6 Diastereomeric crystallisation 15

2-1-7 Separation of racemates via classical resolution 18

2-1-8 Separation of racemates via resolution by direct and preferential crystallisations 18

2-1-9 Separation of racemates via kinetic resolution 20

2-1-10 Resolution of racemates by diastereomeric salt formation 21

2-2 Crystallography and polymorphs 22

2-2-1 Crystallography 22

2-2-1-1 Crystal structures 23

2-2-1-2 Packing and symmetry 27

2-2-1-3 Space group nomenclatures 29

2-2-1-4 Forces responsible for crystal packing – Hydrogen bonding 30

2-2-1-5 A given substance can crystallise in different ways 34

2-2-1-6 How crystals form? 34

2-2-1-7 Nucleation 35

2-2-1-8 Crystal growth 38

2-2-1-9 Survey of crystallisation methods 38
2-2-2 Polymorphism 40
2-2-2-1 Definitions 40
2-2-2-2 Effect of additives 43
2-2-2-3 Examples 44
2-2-2-4 Polymorphic compounds in the Cambridge Structural Database 45
2-2-2-5 Powder Diffraction File 46
2-2-2-6 What polymorphism can do in resolution? 46
2-2-2-7 How to choose polymorphs in pharmaceutical applications? 47
2-3 Phase Equilibria 48
2-3-1 Phase Equilibria 48
2-3-1-1 The Gibbs phase rule 48
2-3-1-2 Triangular phase diagrams 50
2-3-1-3 The lever rule 51
2-3-1-4 Solubility diagrams of diastereomer salt mixtures 52
2-3-2 Solubility Measurements 57
2-4 Analysis and characterisation methods and techniques 60
2-4-1 Chromatographic methods-HPLC 60
2-4-2 Diffraction methods 64
2-4-2-1 X-ray powder diffraction methods 65
2-4-2-2 Single-crystal X-ray diffraction methods 65
2-4-3 Calorimetric methods 66
2-5 Previous work in this field 67
2-6 Molecular modelling 70
2-6-1 Introduction 70
2-6-2 The assumptions which may allow lattice energy calculations to be used to predict diastereomeric resolution 71
2-6-3 Lattice energy 74
2-6-3-1 Modelling the lattice energy of simple ionic solids 74
2-6-3-2 Lattice energy for molecular salts 76
2-6-3-3 Molecular flexibility 77
2-6-3-4 Programs used for calculations in this thesis 77

2-7 Summary 79

3 EXPERIMENTAL AND MODELLING METHODS 80
3-1 Experimental methods 80
3-1-1 Solubility measurements 81
3-1-2 Ternary equilibrium measurements 84
3-1-3 Separability measurements 87
3-1-4 HPLC measurements 88
3-1-5 Preparation of RRA2 single-crystal diastereomer salt samples for structure determination 90
3-1-6 Further experimental work to determine different RRA2 polymorphs 91
3-1-6-1 By changing acid:base ratio 91
3-1-6-2 By replacing ethanol with other solvents 92
3-1-6-3 By changing the pH of ethanol 92
3-1-7 Slurry experiments 93
3-1-7-1 Choice of solvent 93
3-1-7-2 Slurry experiment 94
3-1-8 Characterisation of crystallisation samples 94
3-1-9 Experimental relative stabilities 95
3-2 Modelling methods 96
3-2-1 Experimental lattice energy minimisation calculation – ExptMinExpt 96
3-2-2 Ion conformational energy or Intramolecular energy - ΔEIntra 98
3-2-3 Theoretical lattice energy minimisation calculation accounting for conformational contributions to lattice energy – ExptMinCOpt 100
3-3 Summary 101

4 EXPERIMENTAL RESULTS AND DISCUSSION 102
4-1 Experimental crystal structures and their structural characteristics 102
4-1-1 Experimental crystal structures 102
4-1-2 Experimental relative stability 109
4-2 Solubility measurements 111

4-2-1 Solubility curve of (R)-1-phenylethylammonium-(R,S)-2-phenylpropanoate A1 112
4-2-2 Solubility curve of (R)-1-phenylethylammonium-(R,S)-2-phenylbutyrate A2 113
4-2-3 Solubility curve of (R)-1-phenylethylammonium-(R,S)-mandelate A3 114
4-3 Phase equilibria 115
4-3-1 Phase equilibria of system (R)-1-phenylethylammonium-(R,S)-2-phenylpropanoate A1 115
4-3-2 Phase equilibria of system (R)-1-phenylethylammonium-(R,S)-2-phenylbutyrate A2 118
4-3-3 Phase equilibria of system (R)-1-phenylethylammonium-(R,S)-mandelate A3 120
4-4 Separability Measurements 121
4-4-1 Separability measurements of (R)-1-phenylethylammonium-(R,S)-2-phenylpropanoate A1 122
4-4-2 Separability measurements of (R)-1-phenylethylammonium-(R,S)-2-phenylbutyrate A2 124
4-4-3 Separability measurements of (R)-1-phenylethylammonium-(R,S)-mandelate A3 126
4-5 Further study on polymorph determination 127
4-5-1 Extra work results to determine different (R)-1-phenylethylammonium-(R)-2-phenylbutanoate (RRA2) polymorphs 127
4-5-2 Slurry experiment results 128
4-6 Discussion on the experimental results 129
4-7 Summary 133

5 MODELLING RESULTS AND DISCUSSION 134
5-1 Experimental lattice energy minimisation calculations (ExpMinExpt) 134
5-2 The crystal energy to predict the relative thermodynamic stability 136
5-3 Discussion on the modelling results 139
5-4 Summary 143

6 CONCLUSION 144

7 FUTURE WORK 147

LIST OF PUBLICATIONS 150

REFERENCES 151

APPENDIX 1: PUBLISHED JOURNALS 161

APPENDIX 2: THE CRYSTALLOGRAPHIC INFORMATION FILES (CIF) FOR THE DETERMINED AND REDETERMINED STRUCTURES 186

APPENDIX 3: PACKING DIAGRAMS 190

APPENDIX 4: THERMAL MEASUREMENTS FOR A2 192

APPENDIX 5: THERMAL MEASUREMENTS FOR A3 194

APPENDIX 6: DATA CORRESPONDING TO ENTHALPY ΔH AND ENTROPY ΔS CALCULATIONS 196

APPENDIX 7: EQUILIBRIUM OF A1 AT 30 AND 50°C 198

APPENDIX 8: EQUILIBRIUM OF A2 AT 30 AND 50°C 204

APPENDIX 9: EQUILIBRIUM OF A3 AT 30 AND 50°C 208

APPENDIX 10: SEPARABILITY CALCULATION SHEET OF A1 AT DIFFERENT TEMPERATURES 211

APPENDIX 11: SEPARABILITY CALCULATION SHEET OF A2 AT DIFFERENT TEMPERATURES 215

APPENDIX 12: SEPARABILITY CALCULATION SHEET OF A3 30°C 218

LIST OF TABLES

Table_1 Chiral Technologies

Table_2 Commonly used resolving agents

Table_3 The symmetry elements of crystal packing

Table_4 Point symmetry elements, glide planes and/or screw axes

Tabel_5 Space group examples

Table_6 Common methods for the production of solids

Table_7 Factors that may initiate nucleation

Table_8 Different Eluants and retention times

Table_9 Summary of the systems studied

Table_10 Experimentally determined enantiomorphic crystal structures for (R)-1-phenylethylammonium, (R,S)-2-phenylpropanoate A1

Table_11 Experimentally determined enantiomorphic crystal structures for (R)-1-phenylethylammonium, (R,S)-2-phenylbutyrate A2

Table_12 Experimentally determined enantiomorphic crystal structures for (R)-1-phenylethylammonium, (R,S)-2-mandelate A3

Table_13 Summary of thermal measurements

Table_14 Thermodynamic data from solution calorimetry at room temperature and solubility measurements

Table_15 Containing the results corresponding to S_{RRA1}

Table_16 Containing the results corresponding to S_{RSA1}

Table_17 Enthalpies and entropies of dissolution of salts A1 in ethanol from solubility measurements

Table_18 Solid solution equilibrium data (mol fraction) for points on solubility curves of A1

Table_19 Comparison of the compositions of bulk crystallised products from separation measurements of A1 salts with individual crystal compositions

Table_20 Solid solution equilibrium data (mol fraction) for points on solubility curves of A2

Table_21 Solid solution equilibrium data (mol fraction) for points on solubility curves of A3

Table_22 Total crystallised solid recoveries of A1 salts at different isolation temperature

Table_23 Intermolecular potential quality of A1 system, from ExptMinExpt lattice energy minimisations

Table_24 Intermolecular potential quality of A2 system, from ExptMinExpt lattice energy minimisations

Table_25 Intermolecular potential quality of A3 system, from ExptMinExpt lattice energy minimisations

Table_26 Reproduction accuracy and predicted relative stability of A1 system, from ExptMinCopt lattice energy calculations

Table_27 Reproduction accuracy and predicted relative stability of A2 system, from ExptMinCopt lattice energy calculations

Table_28 Reproduction accuracy and predicted relative stability of A3 system, from ExptMinCopt lattice energy calculations

Table_29 Summary of modelling results of the three systems studied

Table_30 Summary of experimental and modelling results

Table_31 Summary crystal data: (R)-1-phenylethylammonium-(R,S)-2-phenylpropanoate A1

Table_32 Summary crystal data: (R)-1-phenylethylammonium-(R)-2-phenylbutyrate A2

Table_33 Summary crystal data: (R)-1-phenylethylammonium-(R)-2-phenylbutyrate A2

Table_34 Summary crystal data: (R)-1-phenylethylammonium-(R)-2-mandelate A3

Table_35 Equilibrium of A1 at T=30°C

Table_36 Equilibrium of A1 at T=50°C

Table_37 Equilibrium of A2 at T=30°C

Table_38 Equilibrium of A2 at T=50°C

Table_39 Equilibrium of A3 at T=30°C

Table_40 Equilibrium of A3 at T=50°C

Table_41 Separability measurements of A1 at T=30°C

Table_42 Separability measurements of A1 at T=20°C

Table_43 Separability measurements of A1 at T=2°C

Table_44 Separability measurements of A2 at T=30°C

Table_45 Separability measurements of A2 at T=3°C

Table_46 Separability measurements of A3 at T=30°C

LIST OF FIGURES

Fig1 Three pairs of diastereomer salts studied

Fig2 Diagram of Chirality

Fig3 Rotation of polarised light

Fig4 Asymmetric crystals of tartaric acid that are mirror images of each other

Fig5 Enantiomer pair of glyceraldehydes

Fig6 Formation of a diastereomer pair via acid-base reaction

Fig7 Phenylethylammonium diastereomer salts studied

Fig8 (R,S)-Designation

Fig9 Preferential crystallisation apparatus

Fig10 The fourteen three-dimensional Bravais lattices

Fig11 Symmetry operations of the first kind

Fig12 Symmetry operations of the second kind

Fig13 2,6-dihydroxybenzoic acid

Fig14 Hydrogen bonding in salicylamide derivatives

Fig15 Nucleation events

Fig16 Crystal packing representation of polymorphs from a same molecule

Fig17 Cholic aid – polymorphism of inclusion compounds

Fig18 Diagram of polymorphic systems

Fig19 Crystal forms of maleic acid

Fig20 The triangular coordinates used for the discussion of three-component systems

Fig21 The lever rule

Fig22 Solubility diagram of unsolvated salts

Fig23 Solubility diagram of solvated salts

Fig24 Inversion of relative solubility of diastereomeric salts with change in solvent

Fig25 Partial solid solution of salt B in the pure salt A solid phase

Fig26 Total solid solution between the two salts

Fig27 Solvation equilibria

Fig28 Sketch of crystallisation cell

Fig29 Flow chart of the HPLC system

Fig30 Flow chart of ExptMinExpt minimisations

Fig31 Acetic acid anion moiety drawn with solvent accessible surface, coloured by electrostatic potential

Fig32 Diastereomeric salt pair formed by (R)-2-phenylethylammonium (1) with (R,S)-2-phenylpropanoate (2), (R,S)-2-phenylbuyrate (3), and (R,S)-mandelate (4)

Fig33 Packing diagram of (R)-1-phenylethylammonium-(S)-2-phenylpropanoate (AFINEJ)

Fig34 Packing diagram of (R)-1-phenylethylammonium-(R)-2-phenylpropanoate polymorph I (NMACEP03)

Fig35 Packing diagram of (R)-1-phenylethylammonium-(R)-2-phenylbutyrate polymorph I (PBUPEA03)

Fig36 Packing diagram of (R)-1-phenylethylammonium-(R)-2-phenylbutyrate polymorph II (PBUPEA01)

Fig37 Packing diagram of (R)-1-phenylethylammonium-(R)-2-phenylbutyrate polymorph III (PBUPEA02)

Fig38 Packing diagram of (R)-1-phenylethylammonium-(R)-2-mandelate polymorph I (PIVGEH01)

Fig39 Solubility versus temperature for A1 individual diastereomer salts

Fig40 ln (Solubility) versus 1/Temperature of RRA1 diastereomer salt

Fig41 ln (Solubility) versus 1/Temperature of RSA1 diastereomer salt

Fig42 Solubility versus temperature for A2 individual diastereomer salts

Fig43 versus temperature for A3 individual diastereomer salts

Fig44 Isothermal ternary solution equilibria for A1 diastereomer salts at 30 and 50°C

Fig45 Representation of solid solution of A1 diastereomer salt at 30°C

Fig46 Isothermal ternary solution equilibria for A2 diastereomer salts at 30 and 50°C

Fig47 Isothermal ternary solution equilibria for A3 diastereomer salts at 30 and 50°C

Fig48 Measured separations by cooling crystallisation of A1 diastereomer salts

Fig49 Measured separations by cooling crystallisation of A2 diastereomer salts

Fig50 Measured separations by cooling crystallisation of A3 diastereomer salts

Fig51 Ephedrine

Fig52 Tartaric acid

Fig53 Packing diagram of (R)-1-phenylethylammonium-(R)-2-phenylpropanoate (RRA1) polymorph II (NMACEP01)

Fig54 Packing diagram of (R)-1-phenylethylammonium-(S)-2-phenylbutyrate (RSA2) (PEAPEA10)

Fig55 Packing diagram of (S)-1-phenylethylammonium-(R)-2-mandelate (RSA3) (PIVGEG)

Fig56 Packing diagram of (R)-1-phenylethylammonium-(R)-2-mandelate polymorph II (RRA3) (PEAMAN01)

Fig57 DSC profile for sample RSA2 showing the single endotherm accompanying fusion of the sample at ca. 408 K

Fig58 DSC (blue) and TGA (red) curves for RRA2 form I: RRA2 form I transforming to RRA2 form III at ca. 383 K

Fig59 DSC (blue) and TGA (red) curves for RRA2 form II: RRA2 form II transforming to RRA2 form III at ca. 373 K

Fig60 DSC curves for the RSA3 (the minor endothermic event at ca. 353 K is not accompanied by a noticeable change in the PXRD patterns)

Fig61 RRA3 form I diastereomeric salt pair. The mass loss is only shown for systems where decomposition is significant

Fig62 RRA3 form II diastereomeric salt pair. The mass loss is only shown for systems where decomposition is significant

Fig63 Before and after equilibrium

1 INTRODUCTION

Many molecules, required for life, exist in two conformations. These two conformations are non-superimposable mirror images of each other, i.e. they are related like our left and right hands. Hence this property is called chirality (**Fig2**), from the Greek word for hand. The two forms are called enantiomers (from the Greek word for opposite) or optical isomers, because they rotate plane-polarised light in opposite directions.

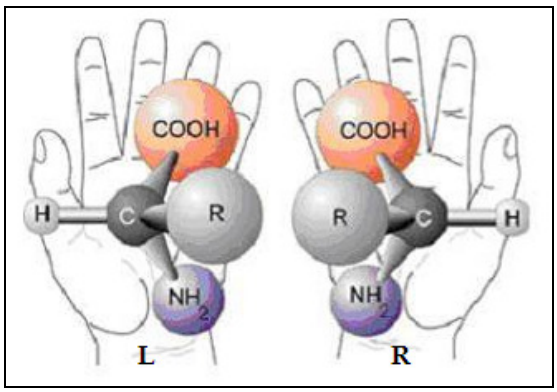

Fig2 Diagram of Chirality[1]

Whether or not a molecule or crystal is chiral is characterised by its symmetry. Chirality is a special case of symmetry. A molecule is achiral if it can be superimposed upon its mirror image. A molecule is chiral if there is no internal plane of symmetry, and the molecule and its mirror image are not superimposable. Even after rotating one of the molecules, it remains different from its enantiomer.

Louis Pasteur (1822 – 1895) was a French microbiologist and chemist who has made many discoveries in the field of chemistry, most notably the asymmetry of crystals.

In Pasteur's early works as a chemist, he resolved a problem concerning the nature of tartaric acid (1849)[2]. A solution of this compound derived from living organisms (specifically, wine lees which is a sediment settling during fermentation, especially in wines) rotated the plane of polarization of light passing through it (**Fig3**). The mystery was that tartaric acid derived by chemical synthesis (paratartrate) had no such effect, even though its reactions were identical and its elemental composition was the same.

Pasteur's experiment showed that paratartrate does not rotate polarised light while tartrate does[1].

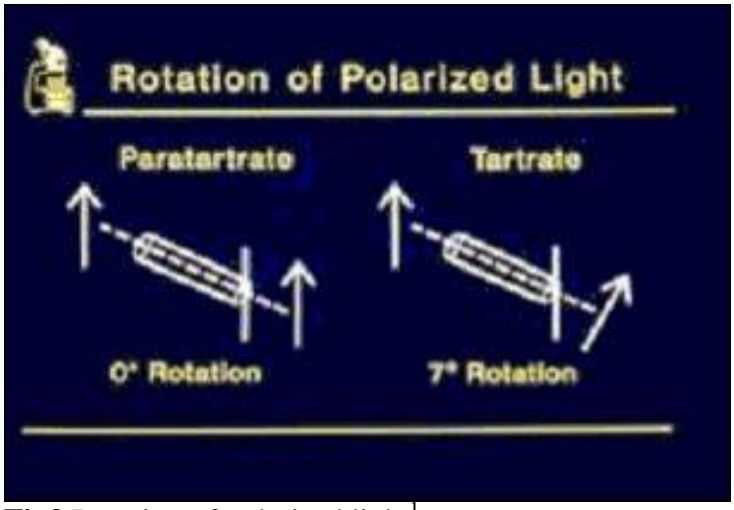

Fig3 Rotation of polarised light[1]

Upon examination of the individual crystals of tartaric acid, Pasteur noticed that the crystals came in two asymmetric forms that were mirror images of one another. Sorting the crystals by hand (**Fig4**) gave two forms of tartaric acid: solutions of one form rotated polarized light clockwise, while the other rotated light counterclockwise. An equal mix of the two had no rotating effect on light. Pasteur correctly deduced the tartaric acid molecule was asymmetric and could exist in two different forms that resemble one another as would left- and right-hand gloves, and that the synthetic form of the compound consisted of an equimolar mixture of the left and right hand rotating species[1].

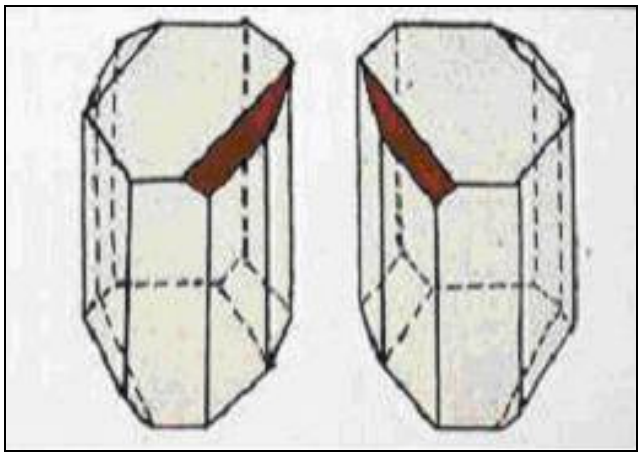

Fig4 Asymmetric crystals of tartaric acid that are mirror images of each other[3]

Enantiomers, or optical isomers, exist in pairs and represent an important and common case of stereoisomerism. Stereoisomerism in general is exhibited by molecules which are made up of the same atoms and functional groups, but which are arranged spatially, or configured, in a different way. Enantiomer pairs are non-superposable mirror images of each other, as explained and illustrated by the simple example of glyceraldehydes in **Fig5** and by tartaric acid (**Fig3**). In glyceraldehyde, four different groups are arranged tetrahedrally around the asterisked carbon atom to give the two mirror-image configurations shown[2].

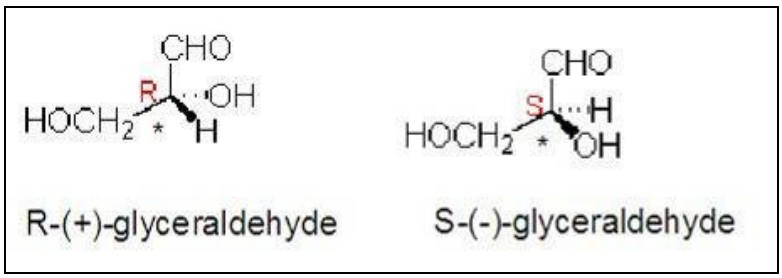

Fig5 Enantiomer pair of glyceraldehyde

Enantiomer pairs possess identical physical properties, but their biological activities and effects can be markedly different. A dramatic example of this was the thalidomide problem in the 1960s, where the drug was administered as a mixture of the two-enantiomer forms. One form mediated the desired effect as a remedy for morning sickness; the other form was severely teratogenic. More recently, the isolation and purification of single enantiomer products has become an important component of pharmaceutical and fine chemical manufacture. In 1992, for example, the US FDA promulgated a set of 'proper development guidelines' for drug activities, which requires that best efforts be made to isolate and purify enantiomeric products[4].

The world market for optically pure products has experienced a marked increase in the last decade[5] which has stimulated the development of novel methods for asymmetric synthesis and chiral separations. The revenues generated in 2003, via the application of chiral technology for pharmaceutical and agrochemical intermediates, was estimated[6] to be $8bn, with an annual growth of around 11%. To large extent this relatively new area of research was the response to drug regulatory guidelines[7] related

to the development of stereoisomeric drugs, following several cases of enantiomers exhibiting different pharmacological or toxological properties[8]. Manufacturing racemates is usually more economical than the synthesis of enantiomers[9], especially if their separation cannot be efficiently achieved with high yield and optical purity and the unwanted enantiomer utilised or recycled in some manner[5]. A wide variety of chiral separation techniques is available, which either exploit the enantioselective behaviour of biological systems or the differences in the molecular recognition of enantiomers by auxiliary chiral agents.

Manufacture of chemical products applied either for the promotion of human health or to combat pests, which otherwise adversely impact on the human food supply is now increasingly concerned with enantiomeric purity. A large proportion of such products contain at least one chiral centre[10].

The desirable reasons for producing optically pure materials include the following[10]:

1. Biological activity is often associated with only one enantiomer, or is much more marked for one enantiomer than the other;
2. Enantiomers may exhibit very different types of activity, both of which may be beneficial or one may be beneficial and the other undesirable; production of single enantiomers enables separation of the effects;
3. The unwanted isomer is at best 'isomeric ballast' gratuitously discharged to the environment;
4. The optically pure compound may be more than twice as active as the racemate because of antagonism;
5. Registration considerations; production of material as the required enantiomer is now a question of law in most countries, the unwanted enantiomer being considered as an impurity;
6. Where the switch from racemate to enantiomer is feasible, there is an opportunity effectively to double the capacity of an industrial process by a cycle of racemisation and resolution; alternatively, where the optically active component of the synthesis is not the most costly, it may allow significant savings to be made in some other achiral but very expensive process intermediate;

7. Improved cost efficacy;
8. The physical characteristics of enantiomer versus racemates may confer processing or formulation advantages.

All conceivable methods for the production of optically pure chiral materials are being actively researched. The field is served by a steady stream of monographs, reviews and specialist conferences and new journals dedicated to the topic have appeared[10].

Chirality or stereogenicity is as old as life. Nevertheless the recognition of its importance in many natural and technological processes is quite a recent achievement.

The great development in proteomics in the past twenty years has highlighted the importance of interactions between stereoisomers as a switch towards the activation or inhibition of most pathways used by nature to regulate its own behaviour[10].

Chiral-based products find application in all other bioscience fields where optimised receptor-ligand interactions may confer distinctive properties or an increased safety profile. Agro- and veterinary products, cosmeceuticals, nutraceuticals, flavours and fragrances are among the main areas where we might expect an increased future exploitation of chiral products.

Stereogenicity is an important added value also in the development of high-tech functional materials (e.g. liquid crystals, optical and electronic materials) and, more specifically, of materials for which a predefined and ordered arrangement of molecules is important. Chirality-driven product development is becoming a main strategy to be considered from the very early steps of the project, in order to maximise time-to-market potential and minimise development and production cost and waste management[10].

It is indeed a hard task to exactly quantify the potential market for chiral technologies, since many different approaches, as given in **Table_1**, towards a stereogenic molecule are possible[10].

Table_1 Chiral Technologies

Traditional methods:	• Classical resolution
	• Chromatography
	• Chiral pool synthesis
Asymmetric methods:	• Chemical synthesis
	• Asymmetric synthesis
Biological methods:	• Biocatalysis
	• Biotransformation
	• Bioresolution

Crystallisation methods are widely used for the separation, or resolution, of enantiomer pairs. Enantiomer mixtures may essentially crystallise in two different ways. In less than 8% of cases, each enantiomer crystallises separately, giving rise to a physical mixture of crystals of the two forms, known as a conglomerate. Conglomerates may usually be separated by physical methods alone. In the remaining 92% of cases, the two enantiomeric forms co-crystallise in equal amounts within the unit cell of the crystal, giving rise to a racemic crystal structure. Where such racemic crystals form, separation cannot be achieved by physical means alone, and is usually brought about by reacting the enantiomer pair with a single-enantiomer resolving agent, to form a pair of diastereomer adducts. Diastereomers are stereoisomers for which the mirror-image relationship does not exist, and which often exhibit significant differences in their physical properties that enable their separation by crystallisation[11].

The goal of this research is to identify ways in which the separability of a pair of diastereomers formed in this way can be related to the structural and thermodynamic properties of the adducts, and to the conditions under which they crystallise. By far, the commonest adduction method is via an acid-base reaction, in which the enantiomer pair containing an acid function (e.g. a carboxylic acid) is reacted with a base-resolving agent, **Fig6**, or vice-versa. At present, there are scientific guidelines by which suitable resolving agents and process conditions may be selected, and trial-and-error procedures of experimental screening are usually employed.

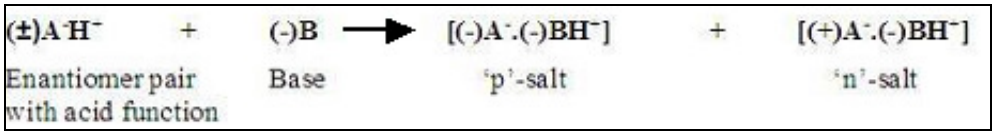

Fig6 Formation of a diastereomer pair via acid-base reaction

In this research, initial work has set out to examine the hypothesis that separability correlates with the stability difference of the two -diastereomer adducts[11], and the extent to which molecular modelling methods may be used to estimate such energy differences. A series of 1-phenylethylammonium salts in **Fig7** have been studied experimentally in some detail, and are being used as test cases to assess the performance of static lattice energy minimisations and to identify any modifications and refinements that would improve their performance.

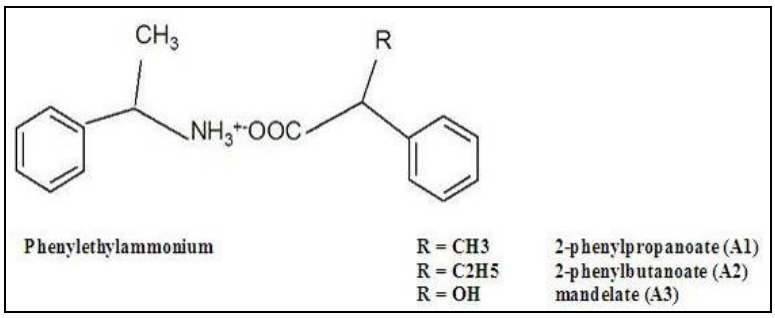

Fig7 Phenylethylammonium diastereomer salts studied

The main objectives of this project are:

1. To gain an understanding of chiral resolution based on the addition of an optically pure resolving agent to an enantiomer mixture;
2. To compare separability of diastereomer mixture by crystallisation with phase equilibrium data;
3. To predict the relative thermodynamic stability of the experimental diastereomer salt systems via lattice energy calculations and compare them with the experimental data.

This thesis consists of an introduction, a literature review, a description of the methodologies, analysis and discussion of the collected experimental data, analysis

and discussion of the predicted molecular modelling data, a conclusion and a future work.

Chapter 2 will cover theories and research findings on stereochemistry and crystallisation, crystallography and polymorphs, phase equilibria, analysis and characterisation methods and techniques, molecular modelling and previous work in this field. All these theories and research findings suggest ideas to solve the research problems as well as to help understand different methodologies and techniques, crystal behaviours and molecular modelling, to work on the chiral resolution study.

Chapter 3 will provide detailed overview of the experimental and modelling methodologies used for all the three systems studied in this thesis, as well as the analytical approaches used to examine the data.

Chapter 4 will describe the different experimental results for all the three systems studied and will also discuss whether the experimental objectives have been achieved.

Chapter 5 will describe the predicted molecular modelling results for the three systems studies in this thesis and will also discuss their implications for this study's objectives.

Chapter 6 will summarise the experimental and the predicted molecular modelling results for the three systems studied in this project and will compare the consistency between them. It will also conclude based on the objectives set at the beginning of this project and the results obtained at the end.

Chapter 7 will suggest possibilities of further research in this area of study.

2 SURVEY OF LITERATURE AND METHODS

2-1 Stereochemistry and Crystallisation

2-1-1 Stereochemistry

Stereochemistry (from the Greek stereos, meaning solid) refers to chemistry in three dimensions. Since molecules are three-dimensional, stereochemistry, in fact, pervades all of chemistry[12]. In the evolution of chemical thought, the stereochemical point of view came relatively late; much of the often-excellent chemistry of the nineteenth century ignores it. Nevertheless, there is little question that, at least in the last 25 years, the third dimension has become all important in the understanding of problems not only in organic, but in physical, inorganic and analytical chemistry as well as biochemistry, so that no chemist can afford to be without a reasonably detailed knowledge of the subject[13].

Stereochemistry was classified as either static or dynamic. Static stereochemistry, also called the stereochemistry of molecules, deals with the naming of stereoisomers, with their structure, with their energy, and with their physical and most of their spectral properties. Dynamic stereochemistry, also called stereochemistry of reactions, deals with the stereochemical requirements and the stereochemical outcome of chemical reactions[8].

The origins of stereochemistry stems from the discovery of plane-polarised light by French scientists in 1800's. In 1812[12] a French scientist, Biot, following an earlier observation of his colleague Arago, discovered that a quartz plate, cut at right angles to its crystal axis, rotates the plane of polarised light through an angle proportional to the thickness of the plate; this constitutes the phenomenon of optical rotation. Some quartz crystals turn the plane-polarised light to the right, while others turn it to the left. In 1815, Biot extended these observations to organic substances, both liquids and solutions of solids. Biot recognised the difference between the rotation produced by quartz and that produced by the organic substances he studied[12]: the former is a property of a crystal; it is observed only in the solid state and depends on the direction in which the crystal is viewed, whereas the latter is a property of individual molecules

and may therefore be observed not only in the solid, but in the liquid and gaseous states as well as in solution[12].

The discoveries of polarised light and optical rotation led to the concept of molecular chirality, which, in turn, is basic to the field of stereochemistry. Polarised light and optical rotation are therefore usually given a considerable play in elementary treatments of stereochemistry[12].

The observed angle of rotation of the plane of polarisation by an optically active liquid, solution, or (more rarely) gas or solid is usually denoted by the symbol α[13]. The angle may be either positive (+) or negative (-) depending on whether the rotation is clockwise, that is, to the right (dextro) or counter-clockwise, that is, to the left (levo) as seen by an observer towards whom the beam of polarised light travels (this is opposite from the direction of rotation viewed along the light beam.). It may be noted that no intermediate distinction can be made between rotations of $\alpha \pm 180\ n°$ (n = integer), for if the plane of polarisation is rotated in the field of the polarimeter by ± 180°, the new plane will coincide with the old one. In fact α, as measured, is always recorded as being between -90° and +90°. Thus, for example, no difference appears between rotation of +50°, +230°, +410°, or -130°[13].

Chirality (Greek handedness) is an asymmetry property important in several branches of science. An object or a system is called chiral if it differs from its mirror image, and its mirror image cannot superimpose on the original object. A chiral object and its mirror image are called enantiomorphs (Greek opposite forms) or, when referring to molecules, enantiomers. A non-chiral object is called achiral (sometimes also amphichiral) and can be superimposed on its mirror image. A chiral object may exist in two enantiomorphic forms, which are mirror images of one another. Such forms lack inverse symmetry elements, that is, a centre of inversion, a plane of inversion, or an improper axis of symmetry. The inversion centre is the most important, because there can be no inversion planes or improper rotation axes without an inversion centre. An enantiomer or enantiomorph can be defined by the fact that there is no centre of inversion[14].

2-1-2 Enantiomeric molecules or enantiomers

The expression ‘optical active substance’ may signify a pure enantiomer or a mixture containing an excess of one of the two. The composition of a mixture of two enantiomers may be characterised by its optical purity, which may in turn be determined from the ratio of the optical rotation of the mixture to that of the pure enantiomer. The optical purity (experimental value) is generally equal to the enantiomeric purity, which reflects the real composition. A pure enantiomer is often called optically pure[14].

The absolute configuration of a chiral substance is known when an enantiomeric structure can be assigned to an optically active designation of a given sign. Absolute configurations are designated by means of an alphabetic symbolism (R, S for *rectus* and *sinister*). However, the D and L descriptors (below) are still commonly used for carbohydrates and amino acids[14].

An enantiomer can also be named by the direction in which it rotates the plane of plane polarised light. If it rotates the light clockwise (as seen by a viewer towards whom the light is travelling), that enantiomer is labelled (+). Its mirror-image is labelled (−). The (+) and (−) isomers have also been termed d- and l-, respectively (for dextrorotatory and levorotatory). This labelling is easy to confuse with D- and L-.

The D/L labelling is unrelated to (+)/(−); it does not indicate which enantiomer is dextrorotatory and which is levorotatory. Rather, it says that the compound's stereochemistry is related to that of the dextrorotatory or levorotatory enantiomer of glyceraldehyde. Nine of the nineteen L-amino acids commonly found in proteins are dextrorotatory (at a wavelength of 589 nm), and D-fructose is also referred to as levulose because it is levorotatory.

The R/S system is another nomenclature system for enantiomers, which does not involve a reference molecule such as glyceraldehydes. In the R/S system of nomenclature, each chiral centre in a molecule is assigned a prefix (R or S), according to whether its configuration is right- or left-handed. No chemical reactions or interrelationship are required for this assignment. The assignment of these prefixes

depends on the application of the Sequence Rule. Since most of the chiral stereogenic centres we shall encounter are asymmetric carbons, all four different substituents must be ordered in this fashion. The basic rule for sequencing priorities is that higher atomic number proceeds lower, starting with the atoms directly attached to the asymmetric carbon, as shown in **Fig8**.

Where two or more of the atoms directly attached to the asymmetric atom are the same, the process works outward, atom by atom along the line of highest atomic number, until a point of difference is reached. Double and triple bonds are treated by assuming that each multiply-bonded atom is duplicated or triplicated respectively. Where two of the attached atoms differ isotopically, the higher atomic weight takes precedence[15].

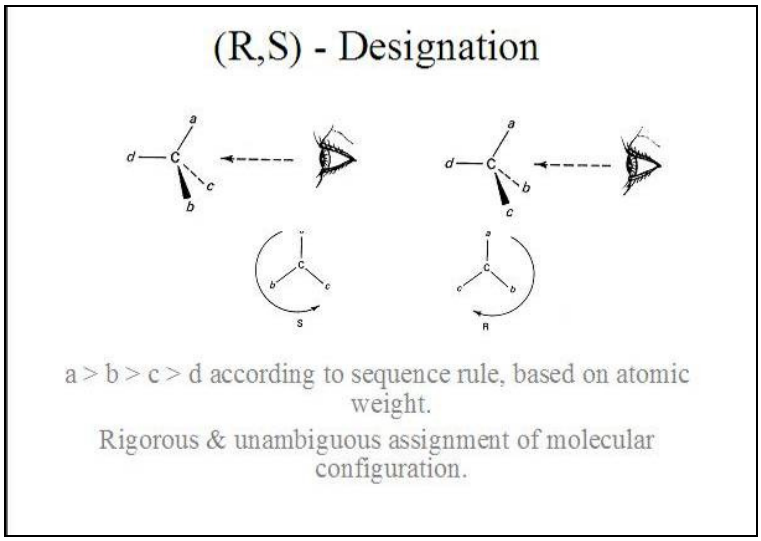

Fig8 (R,S)-Designation[15]

An equimolar mixture of two enantiomers is called a racemate. Racemates, which we generally designate by the symbol (±), are said to be optically inactive by external compensation[14].This means that the observed inactivity derives from equal propensities to rotate to the right and to the left, arising from the equal amount of each enantiomer.

The separation of the two enantiomers that constitute a racemate is called a resolution, or an optical resolution. When the separation is not complete, an unequal mixture of the two enantiomers is obtained which is often called a partially resolved racemate[14].

A crystalline racemate may be of three different types. The first is a conglomerate, which is formed as a result of spontaneous resolution of enantiomers into separate crystals. Here the two enantiomers crystallise separately and homochirally. In the second and the most common type the two enantiomers are present in equal quantities within the unit cell of the crystal lattice. The resultant homogeneous solid phase corresponds to a true crystalline addition compound called a racemic crystal. The third possibility corresponds to the formation of a solid solution between the two. Solid solution is a mixture of two solids that coexist as a single solid phase or crystalline entity. The mixing is usually accomplished by combining the two solids when they have been melted into liquids at high temperatures and then cooling to form the new solid[14]. Solid solutions can also form from solutions with mixed solutes. Solid solutions can exhibit a wide variety of structure characteristics, from isomorphous structures to 'host-guest' relations, in which the interstitial space of a (homochiral) host structure is filled or occupied by the second component.

2-1-3 Diastereomeric molecules or diastereomers

Diastereomers are stereoisomers that are not related as object and mirror image. Whereas a set of enantiomers can contain only two members, there is no such limitation for diastereomers[12].

Diastereomers differ in most, if not all, physical and chemical properties; in fact diastereomers tend to be as different from each other as many constitutional isomers. The basic reason for this difference is that enantiomers are "isometric"; that is, for each distance between two given atoms (whether bonded or not) in one isomer there is corresponding identical distance in the other. No such "isometry" exists in diastereomers or in constitutional isomers[12].

The terms enantiomer and diastereomer relate to molecules as a whole. Thus, if two molecules have the same constitution (connectivity) but different spatial arrangements of the atoms (i.e. if they are stereoisomeric), they must either be related as mirror images or not: in the former case they are enantiomers, in the latter case they are

diastereomers. The differentiation can be made without considering any particular part of the molecule[13].

Diastereomers often contain two or more chiral centres, chiral axis, or a combination thereof; however, this is not necessarily the case. On the other hand, stereogenic centres (axis or atoms), which are the foci of diastereoisomerism, might or might not be chiral. Interchange of ligands at a stereogenic centre leads to a diastereoisomerism (enantiomer or diastereomerisomer)[13].

Homochiral crystals (as in a conglomerate) necessarily crystallise in non-centrosymmetric space groups. Racemic crystals always crystallise centrosymmetrically, where the inverse symmetry elements reflect the mirror image relationship between the two component enantiomers.

2-1-4 Crystallisation

Crystallisation must surely rank as the oldest unit operation in chemical processing. Today there are few sections of the chemical industry that do not, at some stage, utilise crystallisation as a method of production, purification or recovery of solid material. Apart from being one of the best and cheapest methods available for the production of pure solids from impure solutions, crystallisation has the additional advantage of giving an end product that has many desirable and well characterised properties[16].

Most pharmaceutical manufacturing processes include a crystallisation process to achieve high purity and to produce the desired final solid form. The operating conditions of the crystallisation determine the physical properties of the products, these include the crystal purity, size, and shape distribution. For pharmaceuticals that are polymorphic or stereoisomeric, the crystallisation process also directly affects the polymorph produced and the extent of chiral separation. The solid-state phase and purity of the product affect the drug dissolution and toxicity, which are important from regulatory point of view. Therefore batch-to-batch uniformity and consistency are essential. Improved control of crystallisation processes offers possibilities for

better crystal product quality, shorter process times, and the reduction or elimination of compromised batches[17].

Recent trends in the early stage development of pharmaceutical crystallisation processes include the use of smaller size crystallisers, automation of lab-reactors, and running experiments in parallel using multiple small crystallisers. This is motivated by limited availability of pharmaceutical materials and higher throughput desired during the development stage[18].

2-1-5 Racemic crystallisation

Enantiomers have identical physiochemical properties except for the sign of optical rotation. A chemical reaction carried out in an achiral environment produces a racemate, a mixture consisting of equal amounts of two enantiomers. Therefore, the separation of an enantiomeric mixture is necessary to obtain optically pure species[19].

Optical resolution of racemates is one way to obtain pure isomers. Since Pasteur reported the first example of optical resolution in 1848[19], a significant number of compounds has been resolved, mainly by fractional crystallisation of diastereomeric salts[19]. Resolution of conglomerates by preferential crystallisation or 'entrainment' or resolution by enzymes or bacteria has also been applied to large-scale separation of some racemates (for example amino acids). Of the various methods, more chiral compounds are being resolved today by chromatography methods than crystallisation[19]. Many factors influence interactions of stereoisomeric molecules in any environment. These factors can affect chromatography of stereoisomers and must be carefully reviewed before developing a separating method[19].

2-1-6 Diastereomeric crystallisation

Diastereomeric crystallisation is based on the interaction of a racemic mixture with the single isomer of a chiral material (resolving agent) to give two diastereomeric derivatives, which are salts or complex. The salts formed are diastereomers with different physical properties, which can be separated by physical means. Generally, the most efficient method of separating the diastereomer is fractional crystallisation.

This employs differences in solubilities. This approach has the advantage of simplicity and can be accomplished with standard equipment. The Fractional crystallisation is well suited to batch production, which is the norm in the pharmaceutical industry[19].

The separation of diastereomeric salts by crystallisation is a widely used manufacturing method that provides a large fraction of single-isomer drugs produced by synthetic means. A study of a representative group of market drugs shows that more than 65% are manufactured by methods involving diastereomer salts crystallisation[19].

Amoxicillion, ampicillin, cefaclor, and cephalexin are antibiotic products that are rated, on the basis of total sales, in the top 10 products sold in single-isomer form[19]. These products contain either R-phenylglycine or R-hydroxy-phenylglycine as chiral elements. These two amino acids are produced by classical resolution processes at a scale of more than 1000 metric tons per year using (+)-10-camphorsulfonic acid and 3-bromocamphorsulphonic acid as resolving agents[19].

Optimisation of the resolving agent

The initial problem associated with diastereomeric crystallisation is to choose the right resolving agent, and the nature and composition of the solvent. This can be time consuming, tedious and labour-intensive. Some of the important points which must be taken into consideration are[20]:

- The diastereomeric salt must crystallise well, and there must be an appreciable difference in solubility between the two salts.
- The compound between the resolving agent and the substance to be resolved should be easily recoverable in a pure state from the salt following the crystallisation step.
- In general, a resolving agent should be available in an optically pure form, because the substance to be resolved cannot be obtained in a higher state of optical purity than the resolving agent by crystallisation of diastereomers.

- The chiral centre should be as close as possible to the functional group responsible for salt formation. The reason is that there is more likely to be diversity in the diastereomer physical properties.
- An agent must be chemically stable and must not racemise under the conditions of the resolution processes.
- The resolving agent should be available as both enantiomers, so that both forms of the substrate can be prepared.
- For industrial purposes, a resolving agent should be relatively inexpensive and readily recoverable in high yield after completion of the resolution.

There is no fixed set of rules that one can adhere to when it comes to choosing a resolving agent and solvent. Fortunately the number of commercial quantity resolving agent is limited, and one can devise standard protocols to screen resolving agents against solvents. Some common resolving agents are given in **Table_2**.

Table_2 Commonly used resolving agents[20]

Acids	Bases
Tartaric acid (+) (-)	1-phenylethylamine (+) (-)
Dibenzoyl tartaric acid (+) (-)	Ephedrine (+) (-)
Mandelic acid (+) (-)	2-amino-1-butanol (+) (-)
Camphoric acid (+) (-)	Quinine (+)
Malic acid (+) (-)	Quinidine (-)
1-camphor-10-sulphonic acid (+) (-)	Cinchonidine (-)
Pyroglutamic acid (+) (-)	Cinchonine (+)
α-methoxyphenylacetic acid (+) (-)	Brucine (-)
α-methoxy-α-trifluoromethylphenylacetic acid (+) (-)	Dehydroabietylamine (+)

In a process known as "Dutch Method"[21], a family of resolving agents is used instead of a single agent, for example the tartaric acid family composed of dibenzoyltartaric acid, ditoloyltartaric acid and tartaric acid. According to the author of the study, when such a mixture is added to a solution of a racemic substrate, a crystalline salt usually precipitates immediately. In most cases, the substrate contained in the precipitated salt is resolved to about 90-98% enantiomeric excess (ee)[21].

2-1-7 Separation of racemates via classical resolution

Classical resolution via diastereoisomer crystallisation is widely used industrially and in particular furnishes a large proportion of those optically active drugs, which are not derived from natural products. There are clearly many instances where resolution is both economically viable and the method of choice[13].

Attractions of classical resolution include wide applicability, provided there is suitable functionality in the molecule through which to form the diastereomer, and, usually, access to both enantiomers of the resolving agent. Classical resolution becomes particularly attractive where it can be combined with *in situ* racemisation of the unwanted enantiomer in a crystallisation-induced asymmetric transformation, a process designated 'deracemisation'. It is then possible to obtain almost complete conversion to the required enantiomer; precipitation of one enantiomer drives the equilibrium in solution in favour of that isomer[13].

2-1-8 Separation of racemates via resolution by direct and preferential crystallisations

This is an attractive method; auxiliaries and reagents, other than a solvent are not required. In simple terms, it depends on the occurrence of some substances as crystalline conglomerates (racemic mixtures of homochiral crystals) rather than racemic crystals. Although in bulk a conglomerate is optically neutral, individual crystals contain only one enantiomer, whereas in a racemic compound individual crystals contain equal amount of both enantiomers. Conglomerate formation is a prerequisite for resolution by direct crystallisation[13].

Before the method may be applied, it is obviously necessary to establish the existence of the conglomerate; this may be done in a number of ways[13]:

- By selecting small, discrete crystals and subjecting them to any sensitive method for measuring enantiomer excess (polarimetry, chiral LC or GC, NMR with shift reagent, effect on the nematic phase of a liquid crystal).

- Determination of binary or ternary phase diagrams.
- Effecting resolution by direct crystallisation.
- Powder X-ray diffraction pattern or possibly solid-state IR spectra (enantiomers give results identical with those of a racemic conglomerate, but can differ to those of racemic crystals).

There are a number of variations in the way resolution by direct crystallisation may be effected, in practice. In the first method, which is preferential crystallisation dating from 1955[14], simultaneous crystallisation of the two enantiomers is carried out in an apparatus of the type shown in **Fig9** below.

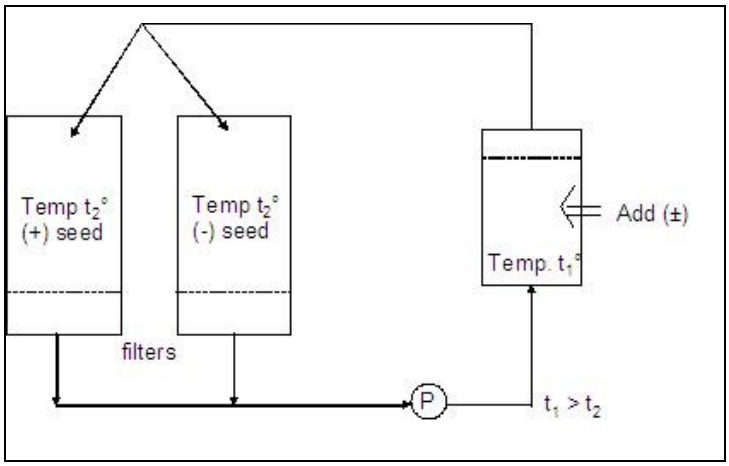

Fig9 Preferential crystallisation apparatus

Initially seeds are introduced into the two crystallisation chambers on the left, alternately with the two enantiomers corresponding to which is in enantiomeric excess at the time and crystallisation from the supersaturated solution occurs. The depleted solution is re-saturated at a higher temperature in a make-up vessel before recooling to restore the original level of supersaturation required in the crystallisers[13].

Another method consists in taking alternate crops of each of the enantiomers using a single vessel; this is the so-called method of resolution by entrainment. It has its origins in the work of Gernez[13], who in 1866 demonstrated that resolution could occur when a supersaturated solution of racemate was seeded with one of the enantiomers. To a supersaturated solution of the racemate initially artificially enriched with, say, the (+)-enantiomer is added seed crystals of the (+)-enantiomer. A crop of (+)-

enriched product is collected equal to approximately twice the amount of material used for the original enrichment. An amount of racemate equal to the weight of the (+)-crop is then dissolved in the filtrates by warming and the solution is cooled to the operating temperature to restore the original degree of supersaturation, but now with the (-)-enantiomer in excess. The solution is then seeded with the (-)-enantiomer and the whole process repeated several times. The main practical limitation on the number of cycles through which such a process can be operated is the build-up of impurities and the tolerance to these of the crystallisation. A highly purified starting racemate may be essential if an economic number of cycles is to be achieved[13].

Another attraction of direct crystallisation is that unlike classical resolution it is not necessary for substrates to possess any particular functionality for it to work. However, it is of limited, and unpredictable, applicability. The occurrence of conglomerates has been estimated at perhaps less than 10% of all crystalline racemates. However, the frequency amongst salts has been estimated to be two or three times that for covalent compounds and this provides a basis for increasing the chance of discovering a conglomerate. Note, for example, that of the naturally occurring α-amino acids virtually all are resolvable either directly or as derivatives. The technique is clearly amenable to large-scale operation but may require very fine temperature control and attention to detail in the seeding protocols. Uniform quality of feedstock, preferably of high chemical purity, will be required in order to achieve reproducible crystallisations[13].

2-1-9 Separation of racemates via kinetic resolution

This is a process in which one of the enantiomers '**A**' of a racemate '**A●B**' is more rapidly converted to a product than the other as in equations **(1)** and **(2)**, as the two enantiomers show different reaction rates:

$$\mathbf{A} \xrightarrow{k_A} \mathbf{y} \qquad \textbf{(1)}$$

$$\mathbf{B} \xrightarrow{k_B} \mathbf{z} \qquad \textbf{(2)}$$

The enantiomer conversion ratio or enantiomeric ratio, **E**, dictates the efficiency of resolution as in equation **(3)**:

$$\mathbf{E = k_A / k_B} \qquad \mathbf{(3)}$$

Where $\mathbf{k_A}$ and $\mathbf{k_B}$ represent the percentage of enantiomers '**A**' and '**B**' in the mixture.

E is related to the enantiomeric excess of the recovered reactant ($\mathbf{ee_R}$) and of the product ($\mathbf{ee_P}$) at a given degree of conversion (**c**), by the following equations **(4)** and **(5)**:

$$\mathbf{E = \ln [(1-c) (1- ee_R)] / \ln [(1-c) (1+ ee_R)]} \qquad \mathbf{(4)}$$

$$\mathbf{E = \ln [(1-c) (1+ ee_P)] / \ln [(1-c) (1- ee_P)]} \qquad \mathbf{(5)}$$

The attraction of kinetic resolution is that the **ee** of the residual substrate improves with the degree of conversion and with only modest selectivity it is still possible to recover the substrate with high **ee**[13].

Kinetic resolution may be realised by chemical or enzymic methods; in the former case the reaction may be either catalytic or stoichiometric with respect to the optically active auxiliary; from an economic standpoint catalysis is obviously preferred. Kinetic resolutions and high **E** values are more commonly found with enzymic than chemical processes[13].

2-1-10 Resolution of racemates by diastereomeric salt formation

To date, the resolution of racemic mixtures via diastereomeric salt formation has been the most commonly used industrial technique[13].

Diastereomeric crystallisation is used so widely that it provides a measure for judging alternative processes[13]. It is based on the interaction of a racemic product with an optically active material (resolving agent), to give two diastereomeric derivatives (usually salts) (see **Fig6**).

The salts formed are diastereomers with different physical properties and may be separated in a number of ways, for example by chromatography, but the most efficient method of separating such diastereomers is by crystallisation. Many significant pharmaceuticals are resolved using diastereomeric crystallisation[13].

In many pharmaceutical developments, for economic or other process reasons, an intermediate is resolved rather than the end product. Technology utilising diastereomeric crystallisation has the advantage of relative simplicity and requires only standard production equipment. From the practical point of view, the method is flexible and suited to intermittent batch production, which is often the norm in pharmaceutical manufacture. However, in spite of this simplicity, the procedure has some disadvantages on a large scale, including the need for a great deal of process equipment – reactors, holding tanks, etc. The storage of the various liquors, and second and third crops held pending future re-work, it takes up considerable space in the plant and can create a bottle neck in plant utilisation. Recovery of the resolving agent is necessary for environmental and economic reasons, but the cost of recovery, particularly for inexpensive resolving agents, can be relatively high. The feasibility of racemisation of the 'unwanted' enantiomer has a major effect on the economics[13].

2-2 Crystallography and polymorphs

2-2-1 Crystallography

Crystallography is the science of crystals. A crystalline solid is characterised by the regular repetition of its structural characteristics in three-dimensional space. The basic structural unit containing the information that defines the crystal structure and packing is called the unit cell[22].

There are two distinct classes of crystals found[22]:

- Molecular crystals in which molecules are bound together via intermolecular and intramolecular interactions.

- Ionic crystals, which consist of ions bound together by their electrostatic attraction.

Amorphous solids are solids, which lack the regular order of crystalline materials. They generally fall into two categories: one is truly amorphous solids comprised of randomly arranged molecules, rather akin to the liquid state and the second one is microcrystalline materials, in which the crystallites are of insufficient size to diffract X-rays. Historically, solids have been considered non-crystalline if they do not have an X-ray diffraction pattern; to do this, there needs to be periodic order over dimension of ~100 nm[22].

2-2-1-1 Crystal structures

Crystal structure is often discussed in terms of its unit cell. The unit cell is a minimum spatial arrangement of atoms, which is tiled in three-dimensional space to construct the complete crystal. The unit cell is defined by its lattice parameters, the length of the cell edges and the angles between them, while the positions of the atoms inside the unit cell are described by the set of atomic coordinates (x_i,y_i,z_i) measured from a lattice point[22].

The unit cell is the basic building block of a crystal, repeated infinitely in three dimensions[22]. It is characterised by:

- Three vectors (a, b, c) that form the edges of a parallelepiped.
- The angles between the vectors (α between b and c, β between a and c, γ between a and b).

For each crystal structure there is a conventional unit cell, which is the smallest unit that has the full symmetry of the crystal. However, the conventional unit cell is not always the smallest possible choice. A primitive unit cell of a particular crystal structure is the smallest possible unit cell one can construct such that, when tiled, it completely fills space. This primitive unit cell does not, however, display all the symmetries inherent in the crystal[22].

It is important to know that crystallographers talk about the unit cell and the asymmetric unit, designated Z and Z', in X-ray structure determinations, and they are not the same. Also crystal structures are usually characterised by their space group symmetries that take account of translations along the cell axes. The unit cell may therefore not contain all information about symmetry[22].

An asymmetric unit is the smallest part of a crystal structure from which the complete structure can be built using space group symmetry[22].

The crystal systems are a grouping of crystal structures according to the axial system used to describe their lattice. Each crystal system consists of a set of three axes in a particular geometrical arrangement. There are seven unique crystal systems. The simplest and most symmetric, the cubic (or isometric) system, has the symmetry of a cube, that is, the three axes are mutually perpendicular and of equal length. The other six systems, in order of decreasing symmetry, are hexagonal, tetragonal, rhombohedral (also known as trigonal), orthorhombic, monoclinic and triclinic. Some crystallographers consider the hexagonal crystal system not to be its own crystal system, but instead a part of the trigonal crystal system. The geometry of the crystal systems implies inherent point group symmetry elements[22].

When the crystal systems are combined with the various possible lattice centerings, we arrive at the Bravais lattices. They describe the geometric arrangement of the lattice points, and thereby the translational symmetry of the crystal. In three dimensions, there are fourteen unique Bravais lattices, which are distinct from one another in the translational symmetry they contain. All crystalline materials recognised, until now, fit in one of these arrangements. The fourteen three-dimensional lattices, classified by crystal system, are shown in **Fig10**. The Bravais lattices are sometimes referred to as space lattices[22].

The crystal structure consists of the same group of atoms, the basis, positioned around each and every lattice point. This group of atoms therefore repeats indefinitely in three dimensions according to the arrangement of one of the fourteen Bravais lattices.

The characteristic rotation and mirror symmetries of the group of atoms, or unit cell, is described by its crystallographic point group[22].

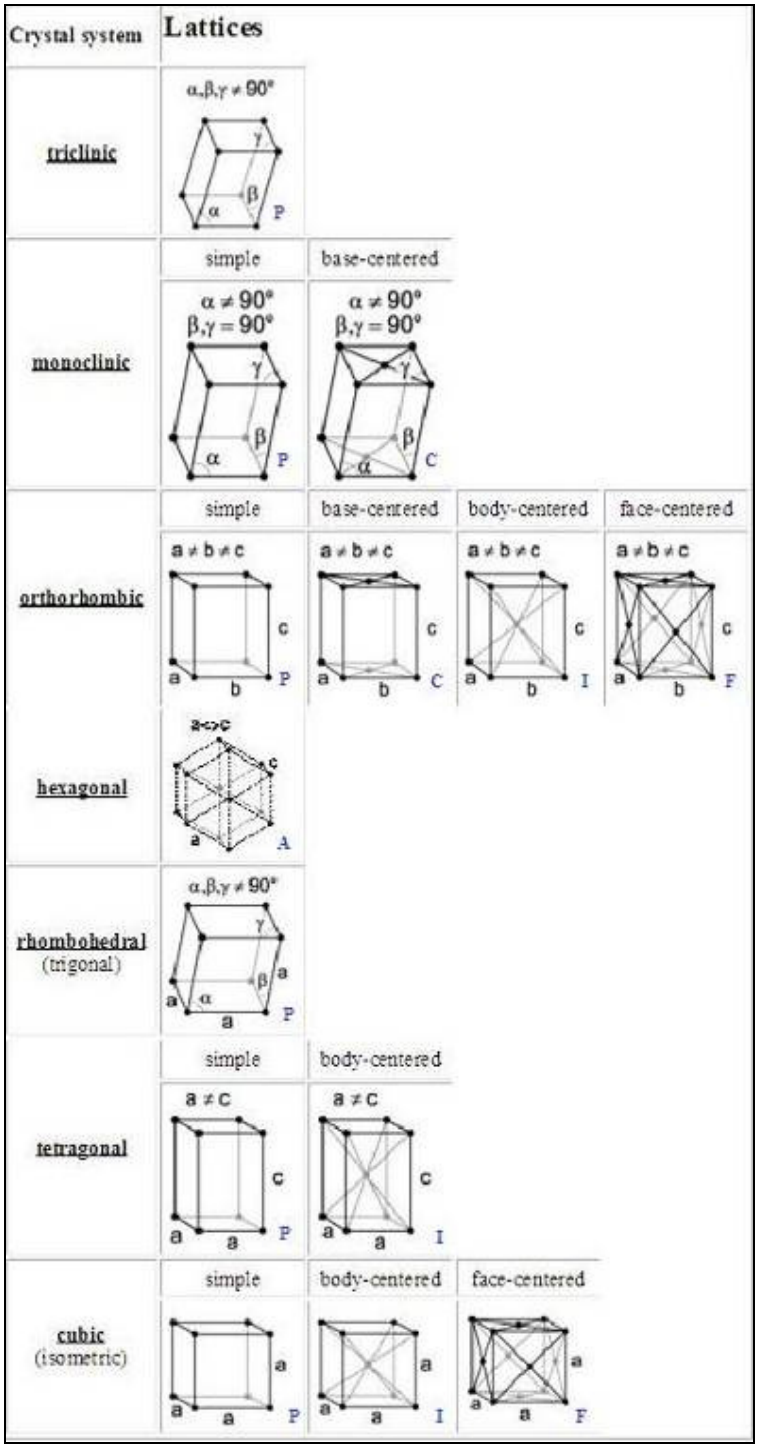

Fig10 The fourteen three-dimensional Bravais lattices[23]

There are four lattice centering types[22]. They are:

1. Primitive centering (**P**): lattice points on the cell corners only.
2. Body centred (**I**): one additional lattice point at the centre of the cell.
3. Face centred (**F**): one additional lattice point at centre of each of the faces of the cell.
4. Centred on a single face (**A**, **B** or **C** centering): one additional lattice point at the centre of one of the cell faces.

A symmetry operation is performed about a symmetry element. A symmetry element is a lattice element about which a symmetry operation is performed[24]. The axes of rotational symmetry, the mirror plane and the centre of inversion are called symmetry elements[25].

The symmetry operations are listed in **Table_3**[24].

Table_3 The symmetry elements of crystal packing[α]

Symmetry element	Description
Rotation axis Non-translational symmetry	When a rotation of 360°/n results in the same structure, then the crystal contains an n-fold rotation axis. For crystals, n is restricted to 1, 2, 3, 4 and 6
Inversion centre or centre of symmetry Non-translational symmetry	A molecule has a centre of symmetry when, for any atom in the molecule, an identical atom exists diametrically opposite this centre an equal distance from it. E.g. benzene (C_6H_6) where the inversion centre is at the centre of the ring
Rotatory-inversion axis Non-translational symmetry	An n-fold-rotatory inversion axis exists when a rotation of 360°/n followed by inversion results in the same structure
Mirror plane Non-translational symmetry	A mirror plane exists when a reflection through that plane results in the same structure
Pure translation Translational symmetry	A pure translation exists when a structure moving along a vector without rotation
Glide plane Translational symmetry	A glide plane exists when a mirror reflection followed by a parallel translation brings the structure into coincidence
Screw axis Translational symmetry	An n-fold screw axis exists when a rotation of 360°/n followed by a translation parallel to the axis of rotation brings the structure into coincidence

[α] note that a crystal containing only one enantiomer of a chiral compound cannot fall into a space group containing any one of the last three symmetry elements in **Table_3**[24].

The crystallographic point group or crystal class is the set of non-translational symmetry operations that leave the appearance of the crystal structure unchanged. These symmetry operations can include mirror planes, which reflect the structure across a central plane, rotation axes, which rotate the structure a specified number of degrees, and a centre of symmetry or inversion point, which inverts the structure through a central point. There are thirty-two different point group combinations that represent the so-called crystal classes. Each one can be classified into one of the seven crystal systems[22].

The space group of the crystal structure is composed of the translational symmetry operations in addition to the operations of the point group. These include pure translations, which move a point along a vector, screw axes, which rotate a point around an axis while translating parallel to the axis, and glide planes, which reflect a point through a plane while translating it parallel to the plane. There are 230 distinct space groups. Most of these 230 are extremely rare and in practice, we deal with a much smaller number[22].

2-2-1-2 Packing and symmetry

One definition of a crystal is that of a solid in which the component molecules are arranged or packed in a highly ordered fashion. When a specific local order, defined by the unit cell, is rigorously preserved without interruption throughout the boundaries of a given particle it is called a single crystal[24].

The term centrosymmetric, as generally used in crystallography, refers to a space group which contains an inversion center as one of its symmetry elements. In such a space group, for every point (x, y, z) in the unit cell there is an indistinguishable point at (-x, -y, -z). Crystals with an inversion centre cannot display certain properties, such as the piezoelectric effect [24] (the production of electricity by applying a mechanical stress to certain crystals).

Space groups lacking an inversion centre (non-centrosymmetric) are further divided into polar and chiral types. A chiral space group is one without any rota-inversion

symmetry elements. Rota-inversion (also called an 'inversion axis') is rotation followed by inversion. Chiral space groups must therefore only contain rotational and translational symmetry[24].

The symmetry elements are of two kinds. The symmetry operation of the first kind (**Fig11**) e.g. a pure rotation axis, when operating on a right-handed object (say) produces a right-handed object from it and all subsequent repetitions of this object are also right-handed. The symmetry operation of the second kind (**Fig12**) repeats an enantiomorphous object from an original object (transform a right-handed object into a left-handed object and vice versa). It involves a reverse of sense in the operation of repetition[25].

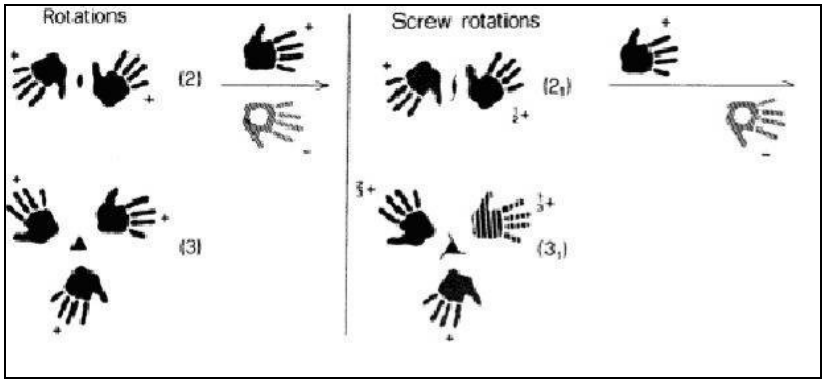

Fig11 Symmetry operations of the first kind[24]

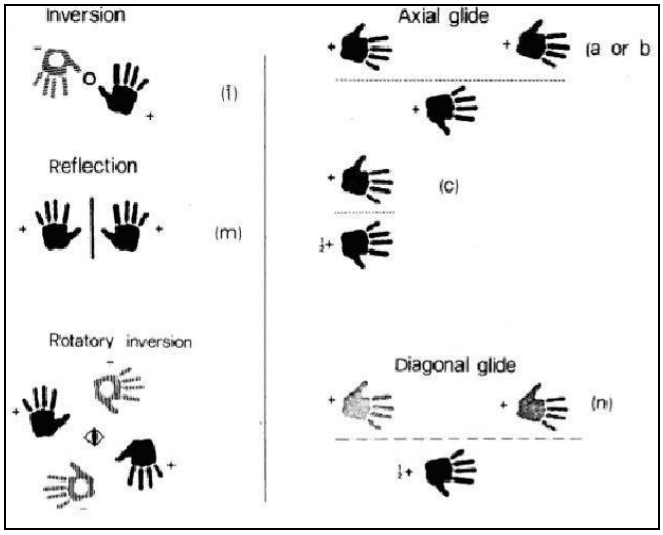

Fig12 Symmetry operations of the second kind[24]

Table_4 lists what specific elements or operations may be included with the categories of first and second kinds of symmetry operations.

Table_4 Point symmetry elements, glide planes and/or screw axes

Symmetry element	**Point group symmetry elements**	**Symmetry elements involving translations**
of the first kind (proper)	*rotation axes* 1 2 3 4 6	*screw axes* 2_1 3_1 3_2 4_1 4_2 4_3 etc
of the second kind (improper)	*rotary inversion axes* 1 2 3 4 6	*glide planes* *a b c n d*

A molecule belongs to a symmetry point group if it is unchanged under all the symmetry operations of this group[24].

Certain properties of a molecule (vibrational and electronic states, normal vibrational modes, orbitals) may behave in the same way or differently under the symmetry operations of the molecule point group. This behaviour is described by the irreducible representation[24].

2-2-1-3 Space group nomenclatures

Space group symbols are made of two parts[26]:

- The first is the capital letter designating the Bravais lattice type [**P**, **C** (**B** or **A**), **I** or **F**].
- The second part of the symbol tells the principle elements of symmetry the unit cell possesses.

It is important to note that the symbols used specify the minimum symmetry to uniquely identify the space group. All implied symmetries are not mentioned in the symbol[26].

Some examples of space groups and their descriptions are given in **Table_5**[27].

Tabel_5 Space group examples

Space groups	**Descriptions**
Orthorhombic $P2_12_12_1$	A primitive orthorhombic cell with screw axis along the 3 cell-edge directions
Orthorhombic Aba2	An orthorhombic A-face centred cell with a b-glide plane perpendicular to a, an a-glide plane perpendicular to b and a diad axis (rotation axis whose multiplicity is equal to 2) along c. The diad axis is automatically generated by other 2 symmetry elements
Monoclinic $P2_1/c$	A Primitive monoclinic cell with 2_1 axis (screw rotation) along b and a c-glide plane perpendicular to it
Monoclinic Cm	A monoclinic C-face centred cell with the mirror plane (reflection) perpendicular to the unique axis

2-2-1-4 Forces responsible for crystal packing – Hydrogen bonding

In a crystal packing, ionic crystals are held together by ionic bonds while organic crystals are held together largely by non-covalent interactions. These non-covalent interactions are either hydrogen bonding or non-covalent attractive forces. Both hydrogen bonding and non-covalent attractive interactions result in the formation of regular arrangements of molecules in the crystal. Non-covalent attractive interactions, which are sometimes called non-bonded interactions, depend on the dipole moments, polarisability, and electronic distribution of the molecules. Another important factor is the symmetry of the molecules[24].

The symmetry (or lack of symmetry) of a molecule determines how it is packed in the crystal and, in some cases, determines the overall symmetry of the crystal. Molecules with symmetries that allow them to fit together in a close-packed arrangement generally form better quality crystals and crystallise more easily than irregular molecules. This factor is not always evident from molecular models[24].

Hydrogen bonding is the most important structure directing determinant and the most useful interaction for assessing the packing modes present in crystal structures. A hydrogen bond is an attractive intermolecular interaction between a hydrogen atom

and that is covalently bonded to an electronegative atom, and an electron rich atom on another molecule (intermolecular hydrogen bond) or to an electron rich atom that is part of a different functional group on the same molecule (intramolecular hydrogen bond)[24].

Hydrogen bonds are classified as very strong, strong and weak[28]. Very strong hydrogen bonds are formed by unusually activated donors and acceptors, often in an intramolecular situation. Frequently they are formed between an acid and its conjugate base, X—H···X^-, or between a base and its conjugate acid, X^+—H···X. Very strong hydrogen bonds are of great importance in the context of chemical reactivity. The energy range for very strong hydrogen bond is 15-40 kcal/mol[28].

Strong hydrogen bonds are able to control crystal and supramolecular structure effectively. This certainly includes O—H···O=C, N—H···O=C and O—H···O—H. The transition from very strong to strong hydrogen bonds (4-15 kcal/mol) represents a transition from quasi-covalent to electrostatic character. All hydrogen bonds have some electrostatic character, but this particular characteristic is dominant in this large and most familiar category of hydrogen bonds[28].

Weak hydrogen bonds (< 4 kcal/mol) form the final category. They are hydrogen bonds, whose influence on crystal structure and packing is variable. These weak hydrogen bonds are electrostatic but this characteristic is modified by variable dispersive and charge-transfer components that depend substantially on the nature of the donor and acceptor group[28]. The strongest of these, say bonds such as O—H···Ph and C≡C—H···O, are quite electrostatic and comparable to a bond like O—H···O—H. They lie in the energy range -2 to -4 kcal/mol. The weakest of these are formed by unactivated methyl groups and are barely stronger than Van der Waals interactions (about -0.5 kcal/mol). All kinds of hydrogen bonds are different and, likewise, all kinds of weak hydrogen bonds are also different[28].

The electrostatic nature of the C—H···O/N hydrogen bond determines its role in influencing crystal packing. Electrostatic interactions between point charges (separated by a distance r) are relatively long range, falling off as $-r^{-1}$. For comparison, the short range Van der Waals interactions fall off as $-r^{-6}$. It may be thus

inferred that even incipient C—H···O bonds have an orienting effect on crystallising molecules, and before the effects are felt of the van der Waals interactions that will ultimately determine the close-packing characteristics. For this reason, crystal structures may be viewed as a complex mélange of isotropic and anisotropic interactions. The hydrogen bonds (weak and strong) determine general connectivity patterns of molecules, while the isotropic interactions determine both intramolecular conformations and intermolecular close-packing within the basic scaffolding established by the hydrogen bonds. For this reason it is particularly hard to ascertain which type of interaction is structure-determining. For the typical organic molecule that contains a small number of O and/or N atoms, the entire range of interaction hierarchy may be observed. Crystal structures are seen wherein the role of the weak hydrogen bond could be either inconsequential, or vary from supportive to intrusive. In the first (very large) category, C—H···O hydrogen bonds are found, but these are neither distinctive nor significant. They merely exist within a structure that is almost entirely determined by other interactions. When the C—H···O bonds play a supportive role, their orientational requirements are in consonance with those of the other interactions[28].

Etter[24] has reviewed the extent and types of hydrogen bonding that can exist in solids and pointed out that polar organic molecules in solution tend to form hydrogen-bonded aggregates. These aggregates are precursors to the crystals, which form when the solution is supersaturated. This concept helps to explain the many different hydrogen bonding motifs seen in different solids.

Davey et al[29] have investigated the role of solvents in the nucleation stage of crystal formation from supersaturated solutions. It is during nucleation that the structural template of the crystal is formed, which is determined by hydrogen bonding and other non-covalent interactions between the molecular entities present in the crystal. By entering into similar bonding relationships with the solute molecules, the solvent can influence form selectivity by inhibiting particular modes of intermolecular attraction relative to others.

A simple example is provided by the crystallisation of 2,6-dihydroxybenzoic acid[30,31] (**Fig13**), which occurs in two polymorphic forms:

1. A monoclinic form, based around centrosymmetric carboxylic acid dimers
2. An extended non-centrosymmetric catemer structure containing intermolecular and intramolecular carbonyl-hydroxyl and hydroxyl-hydroxyl interactions.

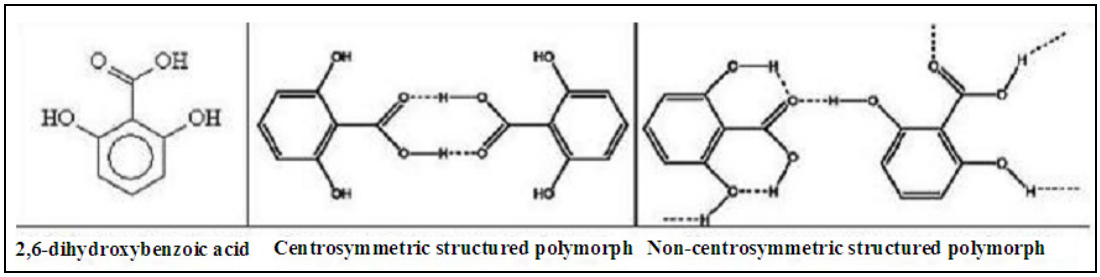

Fig13 2,6-dihydroxybenzoic acid

The first form nucleates preferentially from toluene solutions, where there is a preferential assembly of dimers. The second form was obtained from solutions in chloroform, where the phenolic catemers were strongly solvated. In both cases, solvent-solute interactions play a major role in determining the form selectivity at the nucleation stage.

Etter et al[24] also studied the hydrogen bonding in salicylamide derivatives (**Fig14**) and pointed out that two types of hydrogen bonding patterns are possible in these compounds. One pattern involves an intramolecular —N—H···OH— hydrogen bond and an intermolecular —O—H···O=C hydrogen bond while the other pattern involves an intermolecular —N—H···OH— hydrogen bond and an intramolecular —O—H···O=C hydrogen bond.

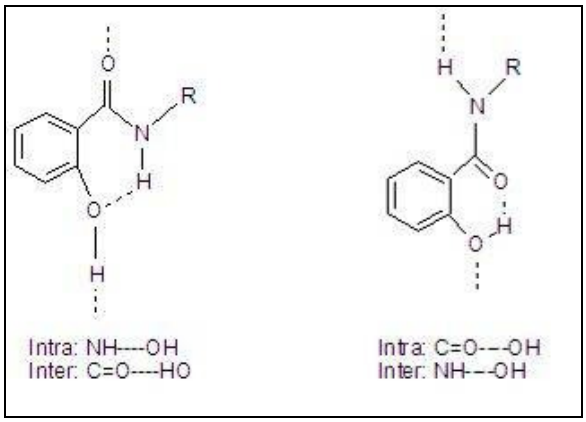

Fig14 Hydrogen bonding in salicylamide derivatives

Hydrogen bonds are the highest energy interactions in non-ionic molecular crystals, and they greatly affect the way in which certain molecules pack in the crystalline environment, only if there are no ion-pairs present. It is also important to note that the distinctions between strong hydrogen bonds and proton transfers (creating ion pairs) can be ambiguous, particularly in cocrystals (e.g. pyridine-benzoic acid interactions). Hydrogen bonding consists of a donor and acceptor, D—H···A, with stronger hydrogen bonds associated with the most electronegative atoms, mainly N, O, F and Cl[24].

2-2-1-5 A given substance can crystallise in different ways

Apart from exhibiting differences in size, crystals of a substance from different sources can vary greatly in their shape. Typical particles in different samples may resemble, for example, needles, rods, plates, prisms, etc. Such differences in shape are collectively referred to as differences in habit[24].

Naturally, when different compounds are involved, different crystal shapes would be expected as a matter of course. When batches of the same substance display crystals with different morphology, however, further work is needed to determine whether the different shapes are indicative of polymorphs, solvates or just habits. Because these distinctions can have a profound impact on, for example, drug performance, their careful definition is very important to our discourse[24].

However sometimes dramatically different shapes have been obtained upon changing crystallisation solvents[24].

2-2-1-6 How crystals form?

Table_6 contains a list of common crystallisation methods employed for pharmaceuticals[24]. Crystals could be formed from various methods as shown below.

Table_6 Common methods for the production of solids

Evaporation (including spray drying and slurry fill. Spray drying will often give an amorphous form)
Cooling a solution
Seeding a supersaturated solution with crystals of the desired form
Freeze drying (including from mixed solvents). Freeze drying will almost always give an amorphous form
Addition of antisolvents
Salting out
Changing pH
Addition of reagent to produce a salt or new compound
Deliberate phase transitions during slurry, washing or drying steps
Simultaneous addition of two solutions

2-2-1-7 Nucleation

Nucleation can occur from supersaturated solutions. However supersaturated solutions can sometimes remain metastable without forming crystals. For example, slow cooling of very clean water to well below its freezing point of 0°C can occur without the formation of ice crystals taking place. The first step in forming crystals from a supersaturated solution requires the assembly of a critical number of ordered molecules (unit cells) into viable nuclei. This process is termed primary nucleation. Assemblies below the critical number tend to dissolve while those above the critical number persist and grow into recognisable crystals. This behaviour is based on the simple fact that the surface area of a spherical body increases with a square of its radius but the volume increases with the cube of the radius. In other words, as an assembly becomes larger, the internal bonds holding it together become relatively more significant than the surface forces (solvent-solute interactions) acting to pull the particle apart[24].

For nucleation, unlike a chemical reaction, the viability of an assembly depends on its size. In creating the nucleus of a crystal a new interface is created for which a penalty must be paid in terms of free energy. The amount of free energy available to create this interface depends on the supersaturation, and to ensure overall viability of the nucleus, this penalty has to be recoverable from the free energy gain of creating the bulk material. Thus, in a supersaturated solution, there will be a steady state

distribution of assemblies and depending on the supersaturation imposed, there will be a critical size, above which the assemblies can grow and below which they are unstable. The higher the supersaturation the smaller the size, the easier nucleation becomes and the more crystals will be formed[32]. This is the classical theory of nucleation. Generally speaking, it does not work well for crystallisation.

In terms of classic formalism, this process is represented in the overall reaction as **(6)**:

$$z\mathbf{A} \leftrightarrows \mathbf{A_c} \qquad \textbf{(6)}$$

in which a number, z, of **A** molecules self-assemble to create a single critical nucleus $\mathbf{A_c}$. The equilibrium constant $\mathbf{K_z}$ associated with this process is then written as **(7)**:

$$\mathbf{K_z = [A_c] / [A]^z} \qquad \textbf{(7)}$$

and the associated free energy $\mathbf{\Delta G_c}$ is given as **(8)**:

$$\mathbf{\ln K_z = -\Delta G_c / RT} \qquad \textbf{(8)}$$

From this, it becomes apparent that the larger $\mathbf{K_z}$, and hence the higher the proportion of critically sized nuclei, the more favourable the nucleation process will be. In other words, self-assembly favours nucleation. Overall, this type of analysis gives rise to the exponential relationship between nucleation rate and supersaturation, which explains the existence of a metastable zone and indicated the difficulty of controlling crystallisation processes which are dominated by primary nucleation[32].

Despite various tidy theoretical analyses of nucleus formation that have been derived, nucleation in the laboratory or industrial setting remains very difficult to control in perhaps the majority of cases, due to the many disparate factors that are observed to affect nucleation (**Table_7**). In addition to primary nucleation, there is a phenomenon known as secondary nucleation which involves further crystallisation after initial crystals are formed (either from deliberate seeding or primary nucleation). Among the factors, which affect secondary nucleation, are: agitation (including the design and type of crystallisation vessel and agitator); temperature and concentration gradients;

friable (breakable) crystal form or habit; and crystal irregularities caused by impurities. Secondary nucleation sometimes has undesirable consequences, since it tends to produce excessive numbers of very small particles. Furthermore, once crystallisation begins, factors like concentration, supersaturation, and many of the parameters in **Table_7** may change, producing a dynamic environment that makes continued control of the process exceedingly difficult[24].

Table_7 Factors that may initiate nucleation

Pre-existing nuclei on equipment or in air
Foreign particles of a suitable nature
Deliberate seeding with desired phase
Local supersaturation by soluble metastable phase
Separation of a liquid phase during processing (e.g., temperature change or addition of antisolvent)
Local supersaturation at an immiscible solvent interface
Ultrasonic or shock waves
Scratched surfaces
Local temperature irregularities
Local concentration gradients (e.g., created by surface evaporation or reagent addition)

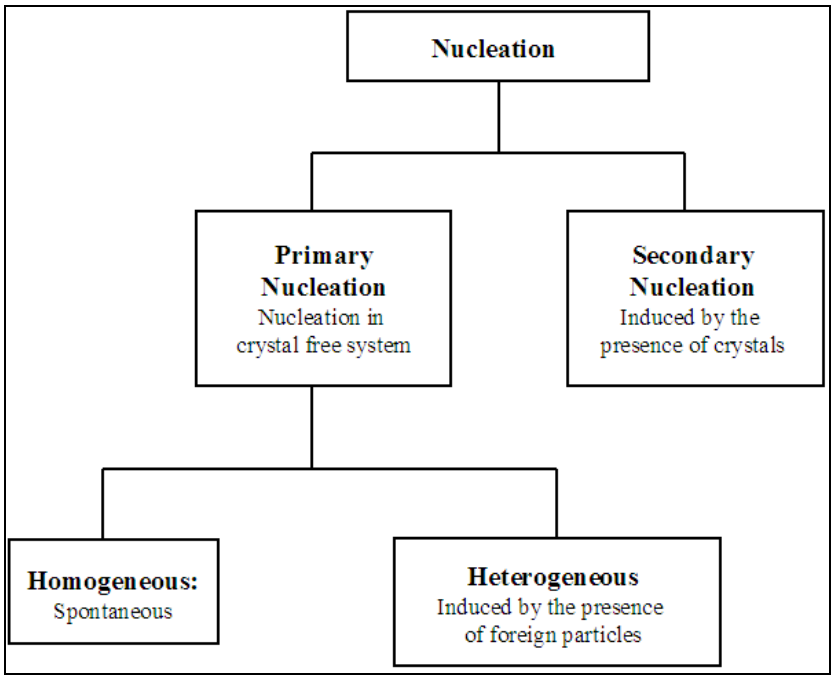

Fig15 Nucleation events[33]

There are two classes of nucleation events, known as homogeneous and heterogeneous nucleation (**Fig15**). Homogeneous nucleation involves the spontaneous

formation and subsequent growth of small particles of the new phase. In heterogeneous nucleation, the new phase is initiated on a foreign material such as a particle or a surface layer. Homogeneous nucleation occurs when there are no heterogeneous nuclei present. A heterogeneous nucleation agent provides a lower barrier to the initial formation of the new phase. Most nucleation processes, including crystal nucleation, in the real world are heterogeneous, but the process depends on the nucleating agent involved, and so the details defy a generic description. The homogeneous nucleation process involves only the one material, and also it is intrinsic to the material. The conditions for homogeneous nucleation to occur represents a limit on the stability of the phase. It can be analysed more readily than heterogeneous nucleation that involves a foreign, often unknown, material[33].

2-2-1-8 Crystal growth

Crystal growth appears during the solidification of materials. A structurally disordered (or hardly ordered) phase (liquid/gaseous) transforms into a structurally ordered crystalline phase. On a microscopic lengthscale, the growing solid phase can develop beautiful patterns during such a process.

Most crystal growth processes involve the following steps[34]:

1. Generation of growth units
2. Transport of growth units to the growth surface
3. Adsorption at the growth surface
4. Nucleation
5. Growth (advance of the liquid-solid or vapour-solid interface)
6. Removal of unwanted reaction products from the growth surface.

2-2-1-9 Survey of crystallisation methods

Solution methods

The solution methods are the most flexible and widely used methods. They are suitable for use with molecular compounds that are the subject of most crystal

structure determinations. The use of solvents means that the crystals can grow separately from each other. It is therefore important not to let a solution dry out, as crystals could become encrusted and may not remain single. When choosing solvents, it is important to look for a solvent that is similar to the compounds (in terms of polarity, functional groups, etc.). Mixing solvents allows manipulation of solubility; a mixture of solvent **A** (in which a compound is too soluble) and a second solvent **B** (in which it is not sufficiently soluble) may be more useful than either alone. If crystals grown from one solvent are poor, it is better try different solvents or mixtures of solvents. Solution methods can be extremely flexible; a number of crystallisations, differing in the proportions of solvents **A** and **B** used, can be set up to run in parallel. If a particular range of proportions appears to be more successful in producing crystals, it can be investigated more closely by decreasing the difference between successive mixtures of **A** and **B**[35].

It is important that any vessels used for crystal growth should be free of contaminants. Older containers tend to have a large number of scratches and other surface defects, providing multiple nucleation points and tending to give large numbers of small crystals. Two factors, which favour the formation of twinned crystals, are the presence of impurities and uneven thermal gradients. Conversely, if the inner surface of the container is too smooth, this may inhibit crystallisation. If this appears to be the case, gently scratching the surface with a metal spatula a few times may be effective[35].

Sublimation

Sublimation is the direct conversion of a solid material to its gaseous state. It has been harnessed to produce solvent-free crystals of electronic materials but it is applicable to any solid with a significant vapour pressure at a temperature below its decomposition or melting point. The basic experimental arrangement is simple: a closed, usually evacuated vessel in which the solid is heated and a cold surface on which crystals grow. If possible, heating of the solid is avoided, as lower sublimation temperatures often lead to better crystals[35]. The crystals are actually formed on condensation of the vapour, the reverse process of sublimation.

Fluid phase growth

It is possible to grow crystals directly from liquids or gases, often by employing *in situ* techniques. Fluid phase methods encompass both high-temperature growth from melts and low-temperature growth from compounds that melt below ambient temperature. High temperature methods (zone refining, etc.) are used widely in the purification and growth of semiconductors and other electronic materials, but are limited to compounds that melt without decomposition, thereby excluding many molecular compounds. Moreover, it is much more difficult to prevent unwanted phenomena such as twinning than with solution methods, and often impossible to separate overlapping or adjacent crystals. Liquids or gases must be contained, for example in a capillary tube. Once crystals have grown it is usually impossible to separate them physically. Unlike crystal growth from solution, there is essentially only one variable, namely the temperature of the sample. However, there are several ways to control the temperature and the method can be chosen to give coarse or fine control. A typical strategy for crystal growth involves the establishment and manipulation of a stable interface between liquid and solid phases[35].

2-2-2 Polymorphism

Polymorphism is important in the development of pharmaceutical ingredients. Many drugs receive regulatory approval for only a single crystal form or polymorph. Polymorphism in drugs can have direct medical implications. Medicine is often administered orally as a crystalline solid and dissolution rates depend on the exact crystal form of a polymorph[36].

2-2-2-1 Definitions

Polymorphism is an important phenomenon in solid state chemistry because the chemical and physical properties are dependent on polymorphs[37]. Polymorphism of a molecular crystal is the ability of a substance to exist in different crystalline arrangements.

A 2-dimensional representation of polymorphs is as in **Fig16**.

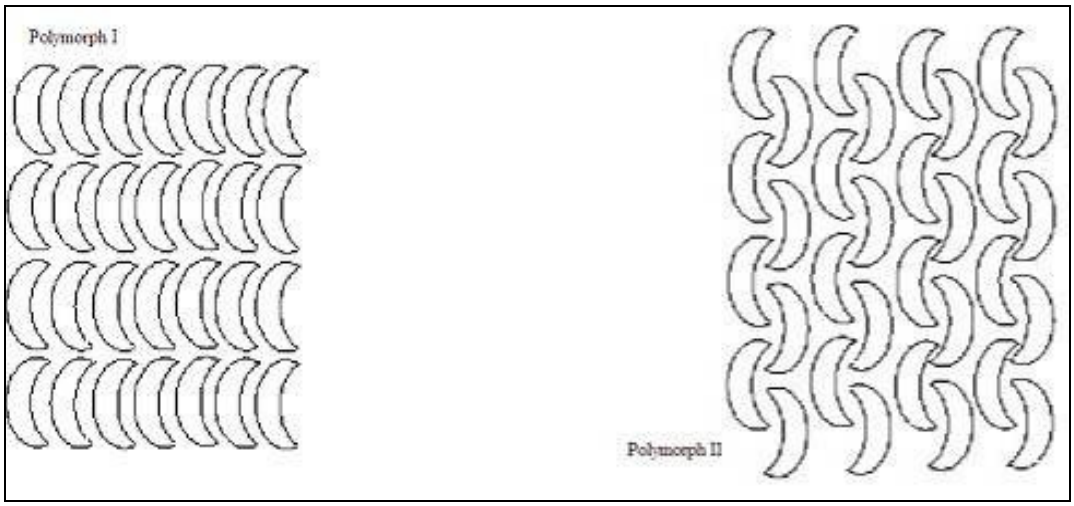

Fig16 Crystal packing representation of polymorphs from a same molecule[37]

Commonly, polymorphism is divided into two types[38,39,40]:

1. Conformational polymorphism or packing polymorphism in which the molecules adopt different conformations within different crystal packings
2. Non-conformational polymorphism in which the constituent molecules (or ions, etc) have the same molecular conformations.

Most studies of polymorphism have been applied to one-component systems. However, more recently, polymorphism of inclusion compounds has been reported for two host compounds, urea and cholic acid. Structure of cholic acid and the packing diagrams of cholic acid with inclusion compounds are given in **Fig17**[41,42].

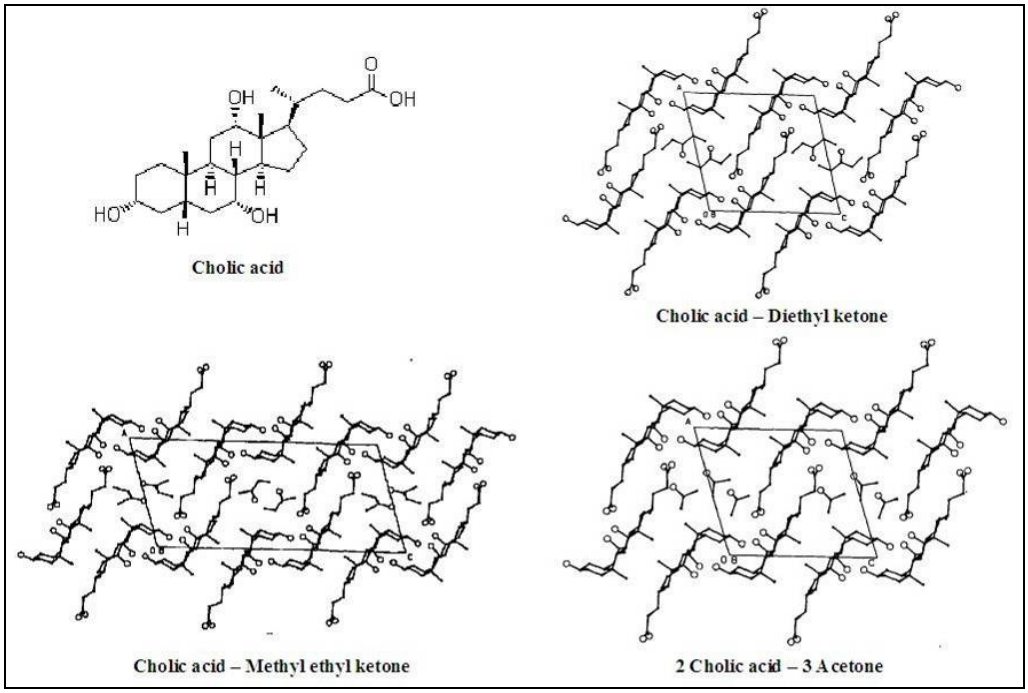

Fig17 Cholic aid – polymorphism of inclusion compounds

These two compounds yield two types of inclusion crystals that have the same host-guest combinations and host-guest ratios[43,44]. In the crystal structures, the host and guest have the same conformations but different molecular arrangements. This indicates that they are classified as polymorphism of two-component system.

Pseudopolymorphism is a term that refers to different crystalline forms with solvent molecules as an integral part of the structure. In a supramolecular sense, polymorphism is the existence of more than one type of network superstructure for the same molecular building blocks and pseudopolymorphism is the case where the solvent is one of the molecular components of the network. Thus polymorphism is regarded as a type of supramolecular isomerism and pseudopolymorphism as a type of cocrystal[45].

An analogous phenomenon for amorphous materials is polyamorphism, when a substance can take on several different amorphous modifications. Polyamorphism is the ability of a substance to exist in several different amorphous modifications. Even though amorphous materials exhibit no long-range periodic atomic structure, the different phases can vary in other properties, such as the density[46,47].

In terms of thermodynamics, there are two types of polymorphism[45] (**Fig18**):

1. For a monotropic system, one polymorph is metastable relative to the other form at all temperatures and pressures. In this case, the polymorphs are not interconvertible, except via recrystallisation. The solubility of the stable form is always lower than the metastable form
2. For an enantiotropic system, the polymorphic form is dependent upon the temperature and pressure of the system. The relative thermodynamic stability of the polymorphs changes at a transition point that is reversible. The transition point is always below melting point for any of the solid phases.

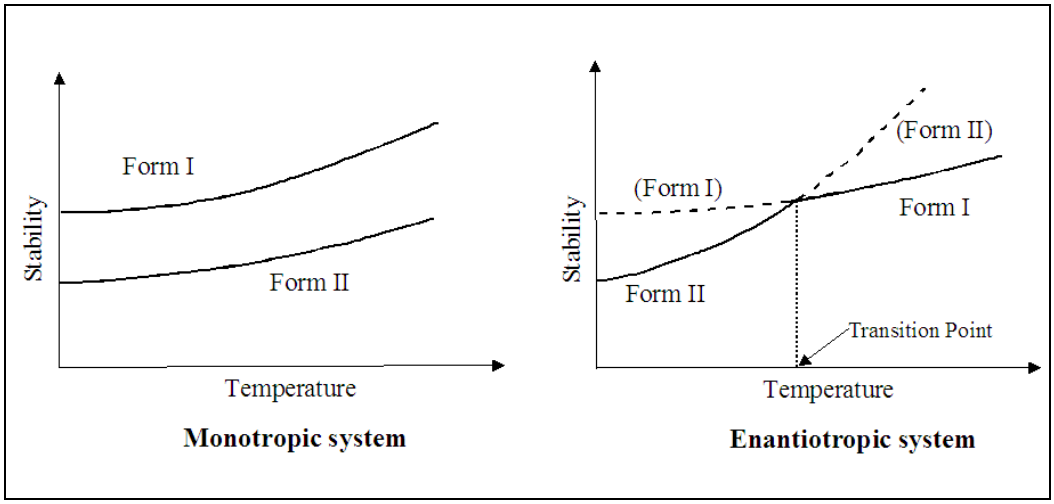

Fig18 Diagram of polymorphic systems

2-2-2-2 Effect of additives

To obtain a desired polymorphic form, additives can be used. Additives can be designed to bind specifically to the surfaces of particular polymorphs and so inhibit their achieving the critical size of nucleation, allowing a desired phase to grow without competition. Lahav and co-workers[48] have shown that additives at levels as low as 0.03% can inhibit nucleation and crystal growth of a stable polymorph, thus favouring the growth of a metastable polymorph. They also showed that it is possible to design crystal nucleation inhibitors to control polymorphism.

Davey et al[48] found that polymorph I crystals of terephthalic acid could be obtained by crystallisation only in the presence of p-toluic acid. Form II, the more stable polymorph at ambient temperatures, was recovered from a hydrothermal recrystallisation experiment.

Ikeda et al[48] determined that indomethacin can exist in three different crystal forms, denoted α, β and γ, with the α-form possessing a higher solubility than the γ-form. On recrystallisation, crystals of the α-form were the first to be deposited, but these converted gradually to the less soluble γ-form. However, in the presence of hydroxypropylmethylcellulose, conversion from the α-form to the γ-form was inhibited, leading to an increase in the solubility of indomethacin.

2-2-2-3 Examples

In 2006, a new crystal form was discovered of maleic acid 124 years after the first crystal structure determination[49]. Maleic acid (**Fig19**) is a chemical manufactured on a very large scale in the chemical industry and is a salt forming component in medicine. The new crystal type is produced when a caffeine - maleic acid co-crystal (2:1) is dissolved in chloroform and when the solvent is allowed to evaporate slowly. Whereas form I has monoclinic space group $P2_1/c$, the new form has space group Pc. Both polymorphs consist of sheets of molecules connected through hydrogen bonding of the carboxylic acid groups but in form I the sheets alternate with respect of the net dipole whereas in form II the sheets are oriented in the same direction.

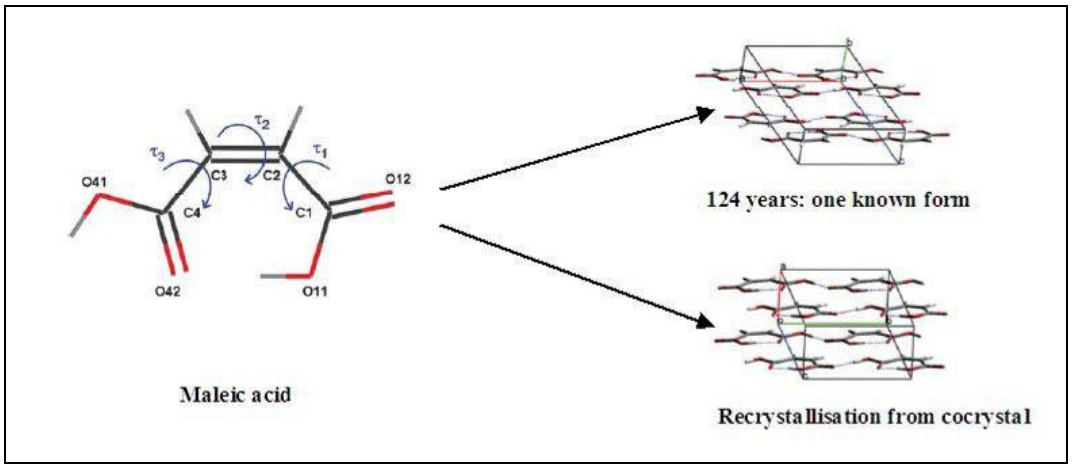

Fig19 Crystal forms of maleic acid

1,3,5-Trinitrobenzene is more than 125 years old and was used as an explosive before the arrival of the safer 2,4,6-trinitrotoluene. Only one crystal form of 1,3,5-trinitrobenzene has been known in the space group Pbca. In 2004, a second polymorph was obtained in the space group $Pca2_1$, when the compound was crystallised in the presence of an additive, trisindane. This experiment shows that additives can induce the appearance of polymorphic forms[50].

The existence of polymorphic forms provides a unique opportunity for the investigation of structure-property relationships, since by definition the only variation among polymorphs is that of structure. For a polymorphic system, differences in properties between the polymorphs must be due to differences in structure[51].

2-2-2-4 Polymorphic compounds in the Cambridge Structural Database

The Cambridge Structural Database (CSD) is the repository for the results obtained from the X-ray crystal structure analysis of organic and organometallic compounds. The October 2000 release of the database contained over 240,000 entries, and as of this date approximately 20,000 structures are added annually. It is now also serving as a depository for crystallographic data that may not be published elsewhere. In the past three decades, the database has increasingly influenced the way structural chemists carry out their work. An enormous amount of geometric and structural information is available in a very short time for searches, correlations, model compounds, packing arrangements, reaction coordinates, hydrogen-bonding patterns and a variety of other studies[52].

As the repository for all organic and organometallic crystal structures, the CSD naturally contains entries for polymorphic materials. As of the October 2000 release, approximately 5,000-6000 compounds may possibly be classified as polymorphic. Each entry in the CSD contains 1D, 2D and 3D information. The 2D information is used to generate the structural formula and chemical connectivity, which clearly will be the same for polymorphs. The 3D information contains the results of the X-ray structure determination: cell constants, space group, atomic coordinates, and atomic positions attributed needed to generate the three-dimensional molecular and crystal

structures. The 1D data contains bibliographical and chemical information (name and empirical formula)[52].

2-2-2-5 Powder Diffraction File

The second crystallographic database, which can serve as a source of examples of polymorphic structures is the Powder Diffraction File (PDF). This is the repository of over 130,000 powder diffraction patterns of solids (2000 release), roughly divided into organic, inorganic and metallic compounds, of which organics are about 25%. Bibliographic searches may be done on compound name or formula[52].

2-2-2-6 What polymorphism can do in resolution?

Polymorphism is also an important issue in resolution since either the desired component or the unwanted component (i.e. impurity) could exist in more than one crystalline form. In particular, diastereoisomer salts can be reluctant to crystallise, and if they do crystallise, the thermodynamically most favoured form does not necessarily appear straight away. In particular, the classical method of resolution screening, whereby samples of a concentrated racemate solution are taken with various resolving agents, does not give the best chance for the most stable crystal form of the diastereoisomer to deposit, or indeed for anything to crystallise at all. It is advocated that it is better to make some pure diastereoisomer first and study its crystallinity properties before proceeding to whether it will resolve from the other isomer, provided that pure material for this investigation is available. The possibilities of crystal twinning could also complicate the picture of polymorphism in crystallisation resolution studies. Either wanted or unwanted diastereoisomer crystals might twin with and therefore promote morphology of the other isomer that is not seen if that other isomer crystallises alone. If both diastereoisomers are polymorphic, then the system might deliver results, in theory, in which the form of the first that crystallises will dictate the form of the other diastereoisomer. So, polymorphism is clearly a factor that must be considered when developing any crystallisation-based resolution or purification procedure[24].

2-2-2-7 How to choose polymorphs in pharmaceutical applications?

Because polymorphs have different physical properties, it is often advantageous to choose the best polymorph for the desired pharmaceutical application. In general, the pharmaceutical applications of polymorphism depend on the answers to the following questions[24]:

1. What are the solubilities of each form?
2. Can pure, stable crystals of each form be prepared?
3. Will the form survive processing, micronising, and tableting?

Furthermore, several more basic questions about polymorphs also need to be answered[24]:

1. How many polymorphs exist?
2. What is the chemical and physical stability of each of these polymorphs?
3. Can the metastable states be stabilised?

These basic questions can be answered as follows: the number of polymorphs can be determined by microscopic examination and by subsequent analytical studies using DSC, IR, solid-state NMR, X-ray powder diffraction, and single-crystal X-ray studies. The physical stability of each form can be determined using the solution phase transformation method. This method involves placing two polymorphs in a drop of saturated solution under the microscope. Under these conditions, the crystals of less stable form will dissolve and crystals of the more stable form will grow until only the most stable form remains. Comparison of the relative stability of pairs of forms in succession gives the order of stability of the various forms. In this case, the temperature is increased or decreased to the temperature where the metastable form is most stable and then the experiment repeated[24].

2-3 Phase Equilibria

2-3-1 Phase Equilibria

Phase equilibria deals with the existence of phases, namely what phases exist when equilibrium occurs. For a research scientist, knowledge of phase equilibria provides a road map to the chemical system(s), the ingredients, the state of matter with which one is dealing. It is particularly important for work on a new material or systems studied to first examine what is known about the phase equilibrium in the system under study[53].

2-3-1-1 The Gibbs phase rule

The Gibbs phase rule (or just phase rule) establishes a relationship among phases and components and intensive variables. Phase rule is usual and crucial to understanding thermodynamics[53].

J. W. Gibbs has deduced the phase rule[54], which is a general relationship between the variance (the number of degree of freedom, that is the number of parameters like pressure, temperature and composition that can be independently varied while maintaining the same phase state of the system.), **F**, the number of components, **C**, and the number of phases at equilibrium, **P**, for a system of any composition, as expressed in **(9)**:

$$\mathbf{F = C - P + 2} \qquad \mathbf{(9)}$$

For a one-component system, such as pure water, F = 3 – P. When only one phase is present, F = 2 and both p and T can be varied independently, without changing the number of phases. In other words, a single phase is represented by an area on a (p,T) phase diagram. When two phases are in equilibrium F = 1, which implies that pressure is not freely variable if the temperature is varied, at a given temperature, a liquid has a characteristic vapour pressure. It follows that the equilibrium of two phases is represented by a line in the phase diagram. Instead of selecting the

temperature, we could select the pressure, but having done so the two phases would be in equilibrium at a single definite temperature. Therefore, freezing (or any other phase transition) occurs at a definite temperature at a given pressure[54]. It is important to point out that liquid-solid transitions (including freezing) are not usually influenced greatly by pressure, so although rigorously the freezing point will be determined by the pressure selected, the variations are very small. It is also common to eliminate pressure as a variable in dealing with liquid and solid phases, and modify the rule to F = C – P + 1 for practical purposes.

When three phases are at equilibrium, F = 0 and the system is invariant. This special condition can be established only at a definite temperature and pressure that is characteristic of the substance and outside our control. The equilibrium of three phases is therefore represented by a point, the triple point, on the phase diagram[54].

In the modern classification, phase transitions are divided into two broad categories[54]:

1. First-order phase transitions.
2. Second order phase transitions.

The first-order phase transitions are those that involve a latent heat (an amount of energy in the form of heat required for a material to undergo a change of phase). During such a transition, a system either absorbs or releases a fixed (and typically large) amount of enthalpy or internal energy. Because enthalpy or internal energy cannot be instantaneously transferred between the system and its environment, first-order transitions are associated with "mixed-phase regimes" in which some parts of the system have completed the transition and others have not. This phenomenon is familiar to anyone who has boiled a pot of water. The water does not instantly turn into gas, but forms a turbulent mixture of water and water vapour bubbles. The (Gibbs) free energy does not change significantly going through the transition, as the chemical potentials of the two phases will be the same at their point of equilibrium. There is, therefore, a difference in the entropies of the two phases, which can be calculated from calorimetric data[54].

The second class of phase transitions are the continuous phase transitions, also called second-order phase transitions. These have no associated latent heat. Examples of second-order phase transitions are the ferromagnetic transition and the superfluid transition[54].

2-3-1-2 Triangular phase diagrams

A phase diagram of a substance shows the regions of pressure and temperature at which its various phases are thermodynamically stable. The lines separating the regions are called phase boundaries, showing the conditions at which two or more phases coexist in equilibrium[54].

One of the best ways of showing how phase equilibria vary with the composition of the system is to use a triangular phase diagram. This section explains how these diagrams are constructed and interpreted[54].

The mole fractions of the three components of a ternary system (C = 3) satisfy **(10)**:

$$\mathbf{x_A + x_B + x_C = 1} \qquad \textbf{(10)}$$

where $\mathbf{x_A}$, $\mathbf{x_B}$ and $\mathbf{x_C}$ are the mol fractions of the three components **A**, **B** and **C** respectively.

A phase diagram drawn as an equilateral triangle ensures that this property is satisfied automatically, because the sum of the distances to a point inside an equilateral triangle measured parallel to the edges is equal to the length of the side of the triangle (**Fig20**), and that side may be taken to have unit length[55].

Fig20 shows how this approach works in practice. The edge **AB** corresponds to $\mathbf{x_c}$ = 0, and likewise for the other two edges. Hence, each of the three edges corresponds to one of the three binary systems (**A**,**B**), (**B**,**C**), and (**C**,**A**). An interior point corresponds to a system in which all three substances are present. The point **P**, for instance, represents $\mathbf{x_A}$ = 0.50, $\mathbf{x_B}$ = 0.10 and $\mathbf{x_C}$ = 0.40[55].

Any point on a straight line joining an apex to a point on the opposite edge (the broken line in **Fig20**) represents a composition that is progressively richer in **A** the closer the point is to **A** apex, but which has the same proportions of **B** and **C**. Therefore, if we wish to represent the changing composition of a system as **A** is added, we draw a line from the **A** apex to the point on **BC** representing the initial binary mixture. Any ternary system formed by adding **A** then lies at some point on this line[55].

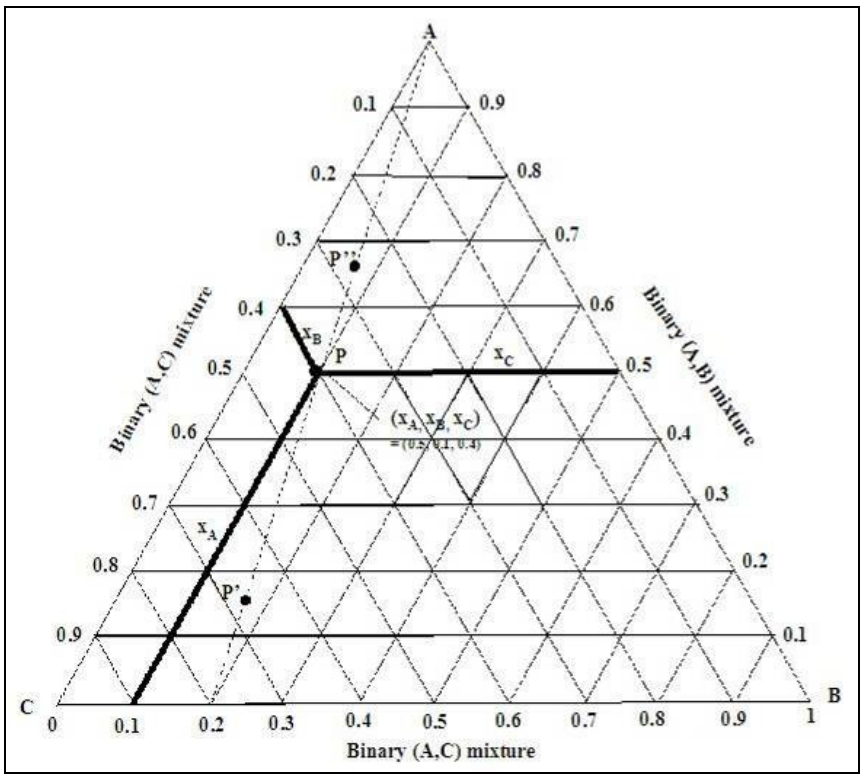

Fig20 The triangular coordinates used for the discussion of three-component systems

2-3-1-3 The lever rule

If a system consists of more than one phase, the amount of each phase present can be found by applying the lever rule to the phase diagram[54].

A point in the two-phase region of a phase diagram indicates not only qualitatively that both phases are present, but represents quantitatively the relative amounts of each. To find the relative amounts of two phases **α** (such as vapour) and **β** (for

example liquid) at equilibrium, we measure the distances $\mathbf{l_\alpha}$ and $\mathbf{l_\beta}$ along the horizontal tie-line, and then use the lever rule, as in **(11)**[54]:

$$\mathbf{n_\alpha l_\alpha = n_\beta l_\beta} \qquad \textbf{(11)}$$

where $\mathbf{n_\alpha}$ is the amount of phase **α** and $\mathbf{n_\beta}$ is the amount of phase **β**. In the case illustrated in **Fig21**, because $l_\beta \approx 2l_\alpha$, the amount of phase **α** is about twice the amount of phase **β**[54].

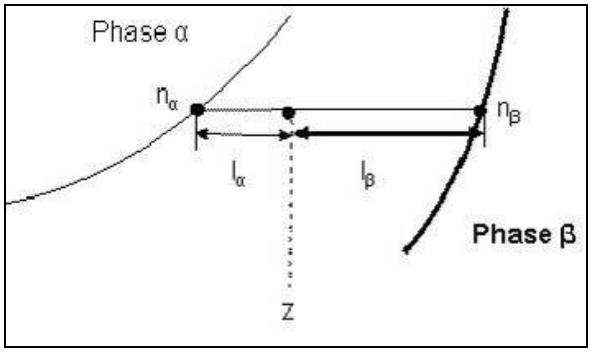

Fig21 The lever rule

2-3-1-4 Solubility diagrams of diastereomer salt mixtures

There were only few diastereomeric salt pairs that have been studied from the standpoint of solubility difference or other property with a view to applying the measured difference rationally to the improvement of a resolution. However, particularly in the case of industrial resolutions where optimisation is economically justifiable, such investigation may lead to the desired improvement[56].

Unsolvated salts

For unsolvated salts, the solubility diagram illustrates the simplest case where no formation of solid solutions occurs. The interpretation of the ternary diagram of such unsolvated salts is given in **Fig22**. **N** and **P** represent the solubilities of the pure **n** (RR-diastereomer) and **p** (RS-diastereomer) salts. From an equimolar mixture of **p** and **n** (labelled **M**) in the presence of solvent at temperature $\mathbf{T_0}$, the following situations obtain after the attainment of equilibrium[56]:

1. A concentrated solution (given by **A**) deposits a solid mixture (n,p) of composition $\mathbf{A_s}$ of mother liquors of composition **E** and whose enantiomeric composition is given by $\mathbf{E_s}$.
2. A more dilute solution (**C**) deposits crystals of pure p-salt. The maximum yield of pure p-salt is obtained when the overall composition of the mixture is given by **B**.
3. Above the isotherm **PEN**, the solution is unsaturated. Crystallisation carried out under equilibrium conditions thus always allows one to obtain the less soluble salt pure.

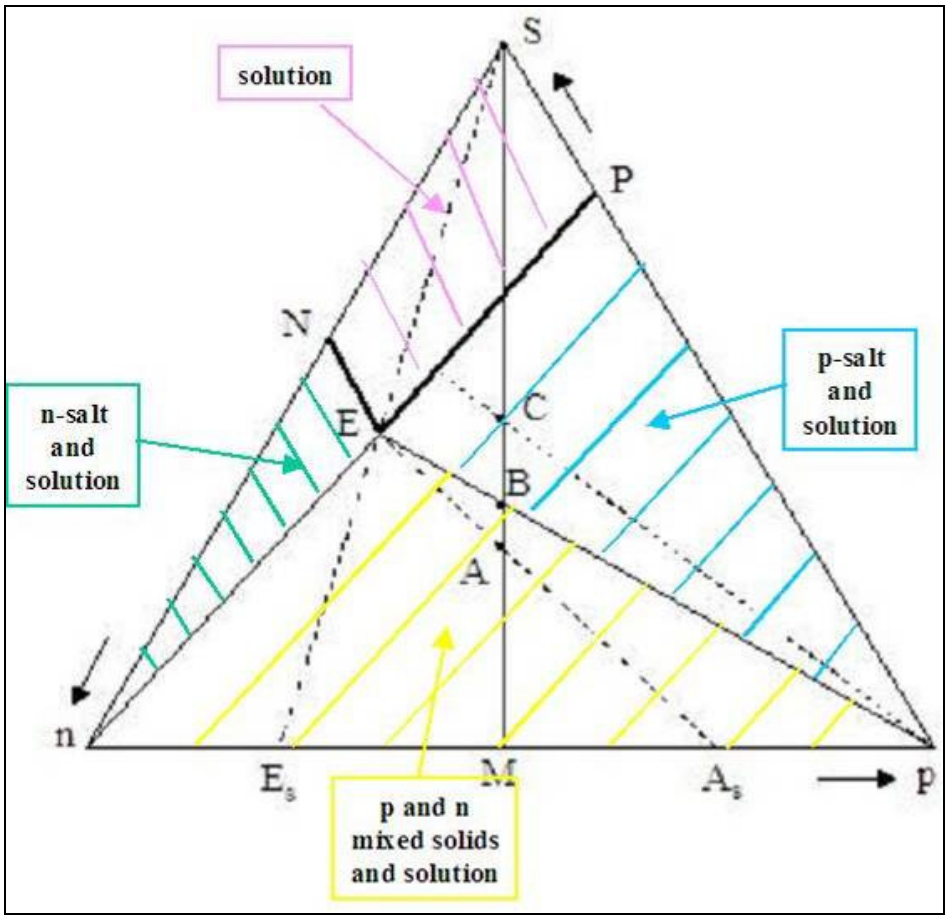

Fig22 Solubility diagram of unsolvated salts

Solvated salts

Solvation of salts (generally by water or by polar solvents) is a common phenomenon. The interpretation of such ternary diagram of solvated salt is similar to that of the

ternary diagram of an unsolvated salt. With the exception that the crystals depositing are the hydrated p' and n' salts and not the anhydrous ones (**Fig23**). This system consists of salts p and n in solvated form in the presence of solvent **S**; p' and n' represent the solvates; **P'** and **N'** are the solubilities of the pure solvates.

Taking a concentrated solution (**A**) at temperature $\mathbf{T_0}$, one obtains a mixture of solid p' and n' represented by $\mathbf{A_s}$ whose enantiomeric composition is given by **A'**. A more dilute solution (**B**) of the same diastereomer mixture deposits crystals of pure solvate p'[56].

The interaction between diastereomeric constituents in solution is neither simple nor easy to deal with. Nevertheless, it is hardly likely that the nature of the solvent would exercise a very large selective influence on the entities in solution. Rather, the solvent might well play a decisive role in the structure of crystalline products, particularly when the two salts present in a mixture are solvated to different degrees[56].

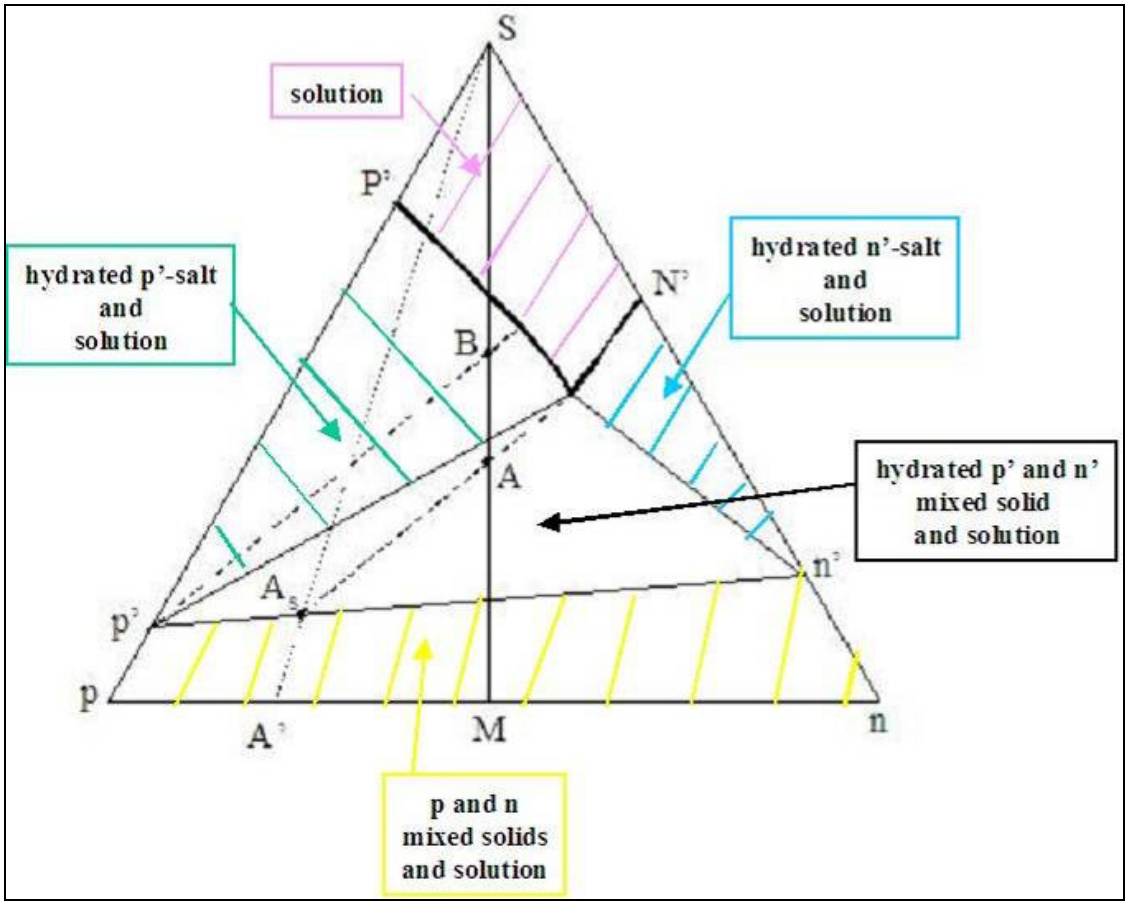

Fig23 Solubility diagram of solvated salts

Unfortunately, it is rare, that analyses of salts isolated in a resolution are published; hence the solvation of most diastereomeric salts is unknown. The researcher must content himself with the observation that occasionally the relative solubilities of p and n salts are altered as a consequence of a change in crystallisation solvent and particularly in the presence of water.

The interpretation of such phenomena in terms of solubility diagrams is simple. In the absence of experimental data, a typical case may be represented by the hypothetical isothermal diagrams **(a)** and **(b)** of **Fig24**. These describe what may take place when a pair of salts p and n crystallise in two different solvents. The degree of solvation of diastereomeric salts may change as a function of solvent. **Fig24** describes the same diagrams with the system remaining the same and **(a)** and **(b)** representing the solubilities of the system in two different solvents. In solvent 1, the two salts (p and n) are unsolvated and n is more soluble than p. In solvent 2, salt n forms solvate n' which is less soluble than p[56].

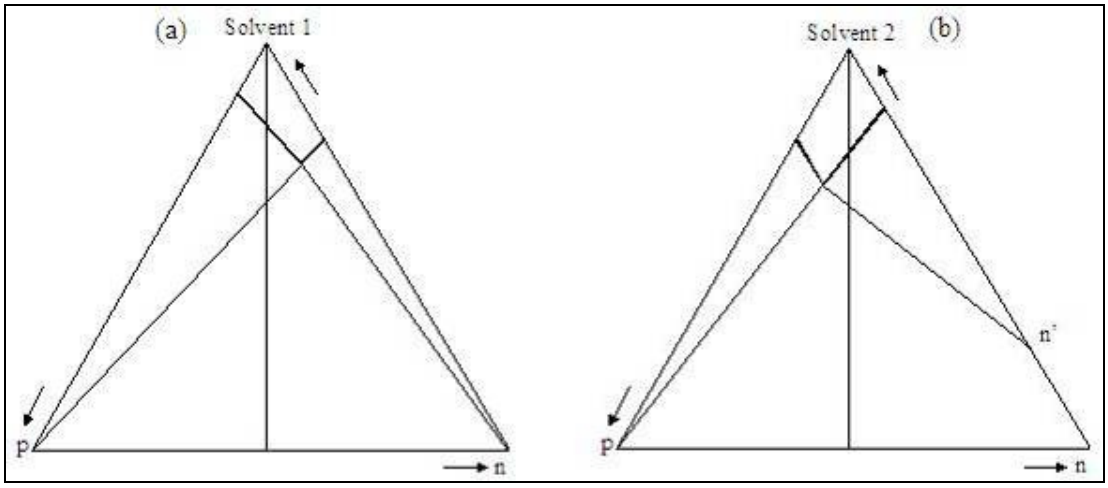

Fig24 Inversion of relative solubility of diastereomeric salts with change in solvent

Solid solutions

Phase diagrams of diastereomeric salts could contain complicated cases: partial or total miscibility in the solid state can be encountered along with intermediate solid compounds. This can lead to a diminution of the quality of the resolution. The first

case envisaged is a partial miscibility of a salt B in the salt A solid phase, as in **Fig25**[57].

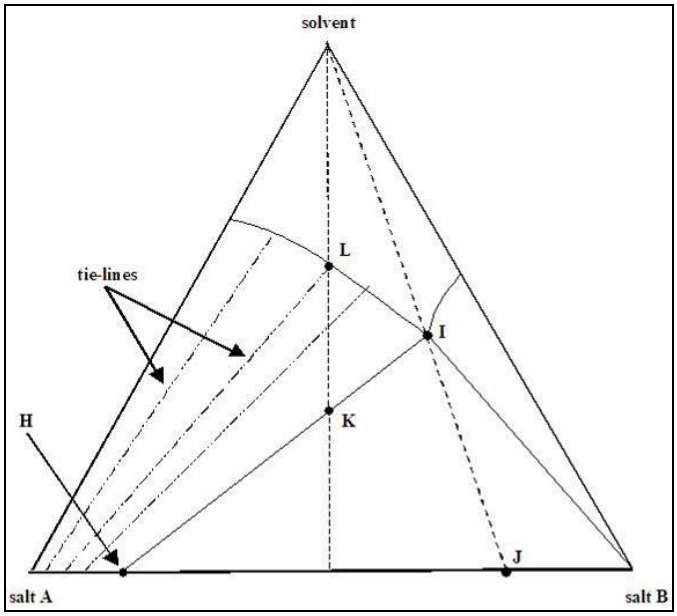

Fig25 Partial solid solution of salt B in the pure salt A solid phase

If the process is performed at point **K**, the solid collected by filtration will contain a single solid phase, which is a homogeneous mixture of the two diastereomers whose composition is given by the extremity of the tie-line **IK** (in **Fig25**, point **H** corresponds to the solid solution saturated in salt B at a given temperature)[57].

The tie-lines connect the representative composition points of the phases in equilibrium: the solid phase and its saturated solution. From composition **K** to composition **L**, the quantity of solid to filtrate tends to zero. In order to increase the purity of the solid phase, several recrystallisations are needed. Unfortunately in this case, as the excess in salt A tends to 100%, the yield tends to 0%[57].

A total solid solution can also be encountered, as in **Fig26**. This type of crystallisation behaviour often leads to a poorly efficient resolution. There is no polysaturated solution and all along the equimolar composition line, the composition of the solid phase in equilibrium never corresponds to a pure component. Several recrystallisations may increase the excess of salt A in the solid phase, but, as for the partial solid solution, if the excess in salt A tends to 100%, the yield would tend to 0%[57].

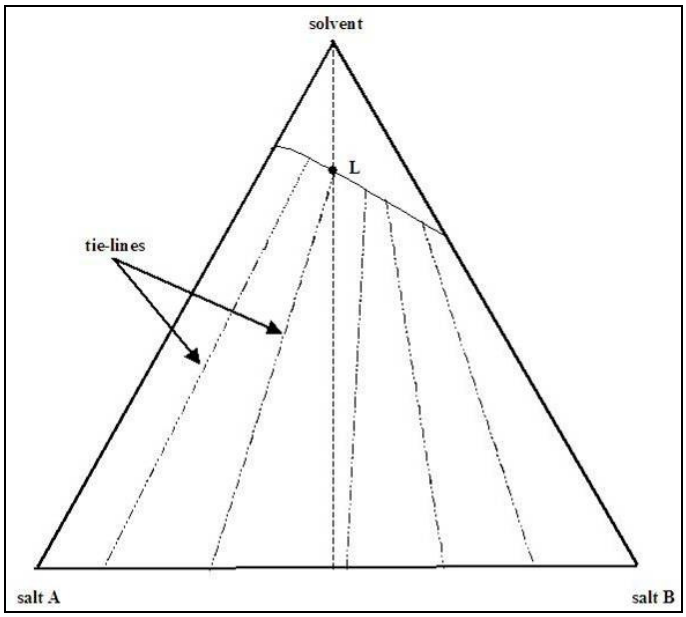

Fig26 Total solid solution between the two salts

A solid solution is a solid-state solution of one or more solutes in a solvent. Such solid solution mixture is considered as a solution rather than a compound:

- as the crystal structure of the solvent remains unchanged by the addition of the solutes. The solute may incorporate into the solvent crystal lattice substitutionally, by replacing a solvent particle in the lattice, or interstitially, by fitting into the space between solvent particles. Both of these types of solid solution affect the properties of the material by distorting the crystal lattice and disrupting the physical and electrical homogeneity of the solvent material[58]
- as the mixture remains in a single homogeneous phase[59].

2-3-2 Solubility Measurements

The solubility of a substance is the concentration at which the solution phase is in equilibrium with a given solid phase at a stated temperature and pressure. Under these conditions, the solid in equilibrium is neither dissolving nor continuing to crystallise. Note that the definition implies the presence of a specific solid phase in contact with the solution. Once determined under the state conditions, however, we can talk about

the “solubility” of a given phase as a quantity, even in the absence of that solid phase[24]. Key features are:

1. The chemical potential ultimately determines the solubility order, but in practice it is very closely approximated by the free energy of formation in the solid state. At equilibrium (saturation), the chemical potential of the solid substance is equal to that of the dissolved substance in solution[24].
2. Undersaturation pertains to solutions at a lower concentration than the saturation value (i.e. diluted solutions). Crystals will dissolve in undersaturated solutions[24].
3. Supersaturation pertains to solutions that, for one reason or another (e.g., cooling of a saturated solution without forming crystals) are at a higher concentration than the saturation value. Supersaturation is required for crystals to form and grow[24].
4. Accurate temperature control is essential during all the experimental procedures for solubility determination, not only during equilibration, but also during the sampling of saturated solution for analysis. The saturation concentration represents the solubility of the material in that solvent at that temperature. Under conditions of supersaturation, the potential of the solute in solution exceeds that of the solid phase, and there is a driving force for the solid to come out of the solution[16].
5. The allowable limits of temperature variation depend on the system under investigation and the required precision of the solubility measurement. Much greater care has to be taken when the solubility changes appreciably with a change in temperature[16].
6. Agitation is generally necessary to bring liquid and solid phases into intimate contact and facilitate equilibration. Agitation with a stirrer in an open vessel is not normally recommended, on account of the potential loss of solvent by evaporation, but sealed-agitated vessels are commonly used. Agitation in tightly stoppered vessels, that are rocked, rotated or shaken whilst immersed in a thermostat bath, is also a popular method, particularly when many samples have to be tested at the same time[16].

7. Once equilibrium has been attained, the mixture is allowed to stand for an hour or more, at a relevant constant temperature, to enable any finely dispersed solid particles to settle.

Working from undersaturation has the disadvantage that the crystals immediately precipitate, and the solution must be stirred and sampled until a steady-state composition is reached. The oversaturation method assures that the initial solution is saturated with solid. The withdrawal of a sample of clear supernatant liquid for analysis can be effected in a number of ways, depending on the characteristics of the system. For example, a temperature-conditioned pipette, with the tip protected by piece of cotton wool, glass wool or similar substance, is often quite adequate. The pipette may be warmed to the appropriate temperature by leaving it standing in a stoppered tube immersed in the thermostat bath alongside the solution / suspension to be sampled. Alternatively, a variety of sintered glass filters can be utilised. The achievement of equilibrium presents one of the major experimental difficulties in solubility determination. Prolonged agitated contact is required between excess solid solute and solution at a constant temperature, usually for several hours. In some cases, however, contact for days or even weeks may be necessary. Viscous solutions and systems at relatively low temperatures often require long contact times and so do substances of low solubility[16].

The so-called ‘synthesis’ methods of solubility determination involve a preparation of a solvent-solute mixture of known composition, initially containing excess solute. The complete dissolution of the solid phase is then observed, either when the mixture is subjected to slow controlled heating or at constant temperatures when small quantities of fresh solvent are sequentially added over a period of time. The disappearance of the solid phase can be observed visually or monitored by recording some appropriate physical or physicochemical property of the system. It is very important to be careful with this method, because it is very easy to add too much solvent and end up with an undersaturated solution or heat too quickly and overshoot the dissolution point[16].

2-4 Analysis and characterisation methods and techniques

2-4-1 Chromatographic methods-HPLC

Chromatographic methods are commonly used for the quantitative and qualitative analysis of raw materials, drug substances, drug products and compounds in biological fluids. The components monitored include chiral or achiral drugs, process impurities, residual solvents, excipients such as preservatives, degradation products, extractables and leachables from container and closure or manufacturing process, pesticide in drug product from plant origin, and metabolites[60].

Chromatography is a technique by which the components in a sample, carried by the liquid or gaseous phase, are resolved by sorption-desorption steps on the stationary phase. High Performance Liquid Chromatography (HPLC) is based on interaction and differential partition of the sample between the mobile liquid carrier and the stationary phase. The commonly used chromatographic methods can be roughly divided into the following groups:

1. Chiral
2. Ion-exchange
3. Ion-pair/affinity
4. Normal phase
5. Reversed phase
6. Size exclusion

Chiral chromatography is a method used for the separation of the enantiomers, which can be achieved on chiral stationary phases by formation of diastereomers via derivatising agents or mobile phase additives on achiral stationary phases. When used as an impurity test method, the sensitivity is enhanced if the enantiomeric impurity elutes before the required enantiomeric product[61].

Diastereomers differ in energy content and therefore have different physical and chemical properties. Enantiomers, by contrast, have identical physical properties and consequently are difficult to separate and quantitate. Chromatographic methods such as thin-layer chromatography, gas-liquid chromatography, and high performance liquid chromatography offer distinct advantages over other techniques in the separation and analysis of stereoisomers, especially enantiomers. These methods show promise for moderate-scale separations of synthetic intermediates as well as for final products. Chiral HPLC is frequently used for large-scale preparation of optical isomers[19].

Transport of solute zones in column chromatography occurs entirely in the mobile phase. Transport is an essential component of the chromatographic system since the common arrangement for the experiment employs a simple inlet and detector at opposite ends of the column with sample introduction and detection occurring in the mobile phase[62].

The position of a peak in a chromatogram is characterised by its retention time ($\mathbf{t_R}$) or retention volume ($\mathbf{V_R}$). Retention volumes are fundamentally more correct than time, but require further experimental information for their determination[62].

If the sample is introduced as a sharp rectangular pulse into a column, the individual separated sample components, when they leave the column, are broadened about their characteristic retention value, in proportion to the time each component remains in the column. This characteristic change in the appearance of bands in the chromatogram results from kinetic factors referred to in total as band broadening. Zone is sometimes used for band, and dispersion or spreading for broadening, resulting in a number of names for the same process. For consistency, we will call the process band broadening. The extent of band broadening determines the chromatographic efficiency, conventionally expressed as either the number of theoretical plates or simply the plate number (**N**), or the height equivalent to the theoretical plate (**HETP**) or simply plate height (**H**)[62].

The separation factor ($\boldsymbol{\alpha}$) is a useful measure of relative peak position in the chromatogram. This function, however, is not adequate to describe peak separations

since it does not contain any information about peak widths. The separation of two peaks in a chromatogram is defined by their resolution, $\mathbf{R_S}$, the ratio between the separation of the two peak maxima ($\mathbf{\Delta t}$) and their average width at base[63].

Equipment for liquid chromatography can be considered to contain eight basic units consisting of, solvent reservoirs, a solvent programmer, one or more pumps, a sample injector, a column oven/cooler, a detector, a computer and a printer[63].

There are two types of solvent programmer. The high-pressure programmer has a pump for each solvent and the composition of the solvent mixture is controlled by the flow rates from each pump. The output of each pump is blended in a mixer and then passed to the sample valve and column. The low-pressure programmer employs timed valves, one for each solvent, and the solvent mixture is determined by the frequency and opening period of each valve. The output from the valves is blended in a mixing chamber and then passed to a high-pressure pump[63].

In most liquid chromatographic phase systems, temperature has minimal effect on the magnitude of retention, or on selectivity, as the free energy change is often similar in both cases of component analysing. However, in chiral chromatography, slight differences in retention can be very important to achieve resolution. Consequently, temperature is an essential operating variable in chiral chromatography[63].

Of the numerous different liquid chromatographic detectors available, the UV absorption detector is the most commonly used. The UV detector measures the light absorbed by the column eluent at wavelength ranging from 200Å to 350Å, employing a photoelectric sensor. The concentration of solute is not linearly related to the sensor output, which thus must be electronically modified, in order to obtain accurate quantitative measurements. The most popular UV detector is the diode array multi-wavelength detector. Light from a broad emission source passes through the sample and is then dispersed by a holographic grating across an array of photosensitive diodes. The output from each diode is continuously sampled at regular time periods and stored on a computer disk[63].

The output from the detector is usually acquired by a computer, which integrates the signal to find the peak area, and relates the area to a calibration to give the results as a quantity or concentration and the analytical results calculated when the analysis is complete and printed out[63].

Virtually, all chiral stationary phases are bonded or coated onto silica gel particles. Silica gel is an amorphous solid consisting of silicon atoms joined by oxygen atoms, on the surface of which are free hydroxyl groups to which other molecules can be chemically bonded. The surface contains various amounts of adsorbed free water that can be removed by heating to an appropriate temperature. The important chromatographic properties of silica gel are determined by its pore size, its surface area and the diameter of the silica gel particles. In most liquid chromatographic analysis, the mean pore size is about 100Å. The most common particle diameter is 5μm. In general, the stationary phase is attached to the silica by first bonding a silane compound containing an appropriate reaction group to the silica, and then bonding the molecules of the chiral stationary phase to the attached silane group[63].

The readings used to account for a chromatographic separation are pressure and time. The maximum pressure is limited by the tolerance of the sample valve and the capability of the pump. In HPLC, the usual pressure used is between 1000 and 5000 psi. Sometimes, over-pressurisation occurs when the following situations arise:

- Viscosity of mobile phase too high.
- Particle size of packing too small.
- Salt precipitation.
- Contamination at the column inlet.
- Microbial growth in the column.
- When the injector is disconnected from the column.
- Accumulation of solid at the column head.
- In aqueous / organic solvent systems, precipitation of buffer components.
- Insufficient flow from the pump.
- Air bubble in the pump.

The analysis time can be reduced by increasing the linear velocity or by reducing the column length, the latter being the more efficient[63]. Sometimes, it is also advised to increase column length to get adequate resolution and peak separation.

2-4-2 Diffraction methods

Diffraction is commonly accepted as the most suitable method for crystal structure determination. Using diffraction methods, it is possible to measure the direction and intensity of X-ray beams diffracted by a crystal. The intensity and phase of each diffracted beam depends on the nature and position of all the atoms within the unit cells. The directions in which diffractions occur are a property of a crystal lattice, determined by the lengths and angles of the unit cell[64].

The fundamental phenomenon underlying diffraction is the scatter of radiation by matter. Neutron and electron beams are considered as radiation in this context, as well as electromagnetic radiation such as X-rays. The radiation quantum (e.g. X-ray) excites the unit of matter (e.g. electron), which, on relaxation, emits radiation at the same wavelength, but scattered in all directions. Scattered waves from various electrons of the same atom interfere, so that the total atomic scatter (called the scattering factor) is the function of the radial atomic electron density distribution and the angle of scatter, with respect to the direction of incidence. The core electrons, which are more tightly bound scatter more effectively at high angles, whereas the more loosely bound valence electrons only scatter at small angles[64].

Scattered waves, from neighbouring atoms, interfere in exactly the same way and unless the atoms are ordered as in a crystal, the total diffraction pattern is a function of the radial distribution of scattering density (atoms) only. This is the mechanism whereby diffraction patterns arise during gas-phase electron diffraction, scattering by amorphous materials, and diffraction by dissolved species. The only information contained in this type of diffraction pattern is a function describing the radial distribution of scattering centres. For a pure substance in the gas phase, this is strictly an intermolecular distribution. All possible interatomic distances are represented, but it contains no conformational information[64].

In the application of X-ray diffraction methods, a distinction is made between powder methods and single-crystal methods.

2-4-2-1 X-ray powder diffraction methods

The X-ray powder diffraction method is used for the qualitative identification of individual polymorphic phases or mixture of phases[52].

X-ray powder diffraction deals with a randomly oriented collection of small crystallites, which is midway between the total disorder of the gas phase and the perfect order of an ideal single crystal. Each crystallite produces a three dimensional diffraction pattern, but because of their random orientation, the directional properties are modified by the superposition of diffraction patterns, in all possible orientations. It follows that any powder pattern can be generated from a known single crystal molecular structure[64].

The preparation of samples for powder diffraction can lead to variations and inconsistencies among measurements on the same sample. Jenkins and Snyder (1996) have summarised the possible causes for compositional variations between the original sample and that prepared for the diffraction experiment; grinding of the sample (generally required to reduce preferred orientation) can lead to amorphism, strain in individual particles, decomposition, solid-state reaction or contamination; the radiation used in the diffraction experiment can induce changes in the material, such as solid state reaction (e.g. polymerisation), decomposition or transformation to an amorphous state; the environment (humidity, temperature) can also effect the addition or loss of solvent, onset of reaction, decomposition, etc. All of these factors should be taken into account in determining and comparing powder patterns[52].

2-4-2-2 Single-crystal X-ray diffraction methods

The single-crystal X-ray diffraction method had been employed for the determination of detailed molecular and crystal structure[52].

In single-crystal X-ray diffraction, a beam of X-rays strikes a single crystal, producing scattered beams. When they land on a charge-coupled device (CCD) or other electronic area detector, these beams make a diffraction pattern of spots; the strengths and angles of these beams are recorded, as the crystal is gradually rotated. Each spot is called a reflection of the X-ray from one set of evenly spaced planes within the crystal. For single crystal of sufficient purity and regularity, X-ray diffraction data can determine the mean chemical bond lengths and angles to within a few thousandths of an Ångström and to within a few tenths of a degree respectively[64].

To use the single-crystal X-ray diffraction method, the crystal should be sufficiently large (> 100 μm in all dimensions), pure in composition and regular in structure, with no significant internal imperfection such as cracks or twinning. A small or irregular crystal will give fewer or less reliable data, from which it may be impossible to determine the atomic arrangement. This commonly happens with crystals of unfavourable habit, such as plates or needles. The crystal is placed in an intensive beam of X-rays, usually of a single wavelength (monochromatic X-rays), producing a regular pattern of reflections. The crystal is gradually rotated and the reflection intensities, at every orientation of the crystal, are recorded. These recorded data are combined computationally with complementary chemical information to produce and refine a model of the arrangement of atom within the crystal. The final refined model of the atomic arrangement, called crystal structure, is stored in the Cambridge Crystallographic Data Centre (CCDC)[64].

2-4-3 Calorimetric methods

Whereas hot stage microscopy can be used to obtain qualitative information on polymorphic behaviour, thermal analysis provides information about the relative stability of polymorphic modifications, the energy involved in phase changes between them and the monotropic or enantiotropic nature of these transitions[52].

Calorimetric methods are based on the principle that a change in the physical state of a material is accompanied by the liberation or absorption of heat. The various techniques of thermal analysis are designed for the determination of the enthalpy accompanying the changes by measuring the difference in heat flow between the

sample under study and an inert reference. These methods are all now commonly referred to as DSC (Differential Scanning Calorimetry), since there are a number of ways of carrying out these experiments, each yielding slightly different information[52].

Thermogravimetric analysis (TGA) measures the change in mass of a sample as a function of temperature. It therefore provides information on the presence of volatile components, in the present context particularly solvents or water, which form the basis of solvates or hydrates respectively, as well as process such as decomposition and sublimation[52]. TGA is not a calorimetric method, as it does not measure enthalpy changes.

2-5 Previous work in this field

The field of prediction of separation of enantiomers via diastereomer crystallisation has not been studied very much in the past. But there are still papers, which are important for our work. A summary of those papers is given below.

In 1975, Lecqlerc and Jacques[65] published a series of three dimensional phase diagrams of the substances we are using. They found that the separation of enantiomers via crystallisation of their diastereomers can be difficult and they have given various reasons for it. Firstly, the diastereomers have to form crystalline salts instead of amorphous solid. Secondly, the differences in the solubilities between the salts have to be sufficiently large. Finally, there is possibility of formation of a double salt between the two diastereomers. Also the formation of solid solutions leads to impurities. In this case, one form may be dissolved in the phase of the other form. They have also stated that repeated crystallisation is often necessary to purify the diastereomers. The crystallisation of the propionate was possible while the butyrate and mandelate have formed mixed phases.

In 1981, Brianso[66] described the crystal structure of 1-phenylethylammonium-2-phenylbutyrate. It has been stated in this paper that “syncrystallisation” or co-crystallisation of both diastereomers is supported when the phenyl functions have a

similar configuration in the cell, especially if one molecule, for example the R-acid, can replace its enantiomer mirror in the cell lattice.

Fogassy et al[67] published a paper in 1986 about pseudosymmetry and chiral discrimination in optical resolution via diastereomeric salt formation. With the example of both forms of (R,S)-N-methylamphetamine bitartrate, the importance of second-order interactions like hydrogen bonds in the crystal lattice has been underlined in this paper.

In 1993, Leusen, Noordik and Karfunkel[68] have worked on thermodynamics and molecular mechanics calculations for racemic resolutions via crystallisations of diastereomeric salts. It has been suggested in this paper that the differences in the lattice energies play a major role in determining the resolution of the diastereomer salt pair. The work has been done on ephedrine and phosphoric acids as diastereomeric salt pairs. A resolution efficiency parameter has also been introduced in this paper, which is related to the difference in the Gibbs free energy of formation of a diastereomeric salt pair, and also the concept that these Gibbs energies can be approximated by computational methods by providing evidence for six different mixtures. As there were not enough computational methods in 1993, Leusen has suggested the general procedure that we are using in our work. In a different manner, we try his approach by calculating differences in lattice energies instead of Gibbs free energies. This should be easier to measure in the experimental part since the lattice energy is an enthalpy or internal energy related term and the Gibbs free energy includes an entropic contribution.

In 1996, Caira et al[69] resolved a mixture of 4-amino-p-chlorobutyric acid lactam that exhibited co-crystallisation. It has been found through this research that in this case no proton transfer takes place and that the hydrogen bonds are the main factor for the separation via diastereomer crystallisation. The two diastereomers exhibit different bonding characteristics, hence different properties.

Kinbara has published a paper[70] where the importance of hydrogen networks in crystals has been underlined while resolving enantiomer amines with non-chiral carboxylic acids. In the same year, he has published another paper[71] about the design

of resolving acids for 1-arylalkylamines. It has been found through this study that para-substituted mandelic acid is suitable as resolving agent. Furthermore, the influence of the size of the substituents on the phenyl ring on the resolution efficiency has been described. In this paper, it has also been reported that substituents that elongate the molecular length of the amines have decreased the resolution efficiency. The influence of substitutions at the ortho-position has also been examined through this work. Ortho-substituted mandelic acid could efficiently resolve 1-phenylpropylamine and 1-arylethylamines.

In 1998, Hansen, Frydenvang and Jensen researched the crystal structure of 3-(N,N-dimethylammonium)-1,1-diphenyl-1-butanol hydrogen tartrate[72]. Similar to the former papers, the importance of hydrogen bonds, which are responsible for the crystal structure, have been established in this paper.

In 1998, De Vries et al[21] introduced the "family" approach to the resolution of racemates. In this approach, the separabilities of amine with different acids like unsubstituted or substituted mandelic acid, substituted phenylpropionic acids and others have been measured. These measurements were carried out in different solvents. The efficiency and necessary recrystallisations for purification with a given resolving agent mixture have been given in this paper. It was shown that a mixture of different resolving agents works better than one pure resolving agent. This forms the basis of what is now known as 'Dutch' resolution[21].

In 1999, Dyer, Henderson and Mitchel[73] reported the use of differential scanning calorimetry for establishing three dimensional phase diagrams. The use of automatic differential scanning calorimetry, done by a machine, simplifies the screening process for a resolving agent.

In 2000, Kinbara et al[74] published a paper about introducing the naphthyl group into the resolving agent. By introducing naphthyl moiety into an enantiopure α-hydroxy acid, its resolution ability for p-substituted 1-aylethylamines was considerably increased, compared with those of enantiopure mandelic acid and its p-substituted derivatives. The authors came to the conclusion that a hydrogen bond between C—H

and the increased π system of the naphthyl ring is responsible for the better resolution. The effect of the molecule length is also described in this paper.

In 2003, Leusen[75] has succeeded in predicting the structure of a single diastereomer salt without using any measured crystal structure data for the prediction. He has used a system of chlorcyphos and ephedrine for his research. He has used Cerius2 with a CFF95 force field and polymorph predictor for his calculations. His results were in an error of just a few kcal/mol. If the crystal structure can be predicted, then calculations of lattice energy could be performed before expensive chemicals are used.

2-6 Molecular modelling

2-6-1 Introduction

Molecular modelling is concerned with the equations of quantum and classical mechanics. Molecular modelling programmes allow scientists to generate and present molecular data including geometries (bond lengths, bond angles, torsion angles), energies (heat of formation, activation energy, etc.), electronic properties (moments, charges, ionisation potential, electron affinity), spectroscopic properties (vibrational modes, chemical shifts) and bulk properties (volume, surface areas, diffusion, viscosities, etc.). Comparison to experimental data, where available, is also important to guide both laboratory and computational work.

In this thesis, lattice energies of the salts were calculated. First we justify why the lattice energy calculations might be used to predict what I have been studying experimentally, because the aim of this project was to provide experimental results. This is followed by the explanation of the lattice energy and the description of the programs that I used.

2-6-2 The assumptions which may allow lattice energy calculations to be used to predict diastereomeric resolution

At present, there is no systematic methodology to choose the optimal resolving agent that could convert enantiomers to a diastereomeric salt pair that can be effectively resolved by fractional crystallisation. This has to be found on a trial and error basis[11]. For example, a recent study of the resolution efficiency of 1,4-benzodioxane-2-carboxylic acid by (S)-1-arylethylamines revealed no systematic variations in the physicochemical properties of the diastereomeric salts with the functional groups present[76]. Hence, there would be considerable industrial benefit to a computational method of designing the optimal resolving agent and process conditions.

The most important determinant for an efficient resolution is the solubility ratio C_{RS}/C_{RR} of the two diastereomers. The efficient resolution is determined by the solvation equilibria of the two-diastereomeric salts, as in **Fig27**:

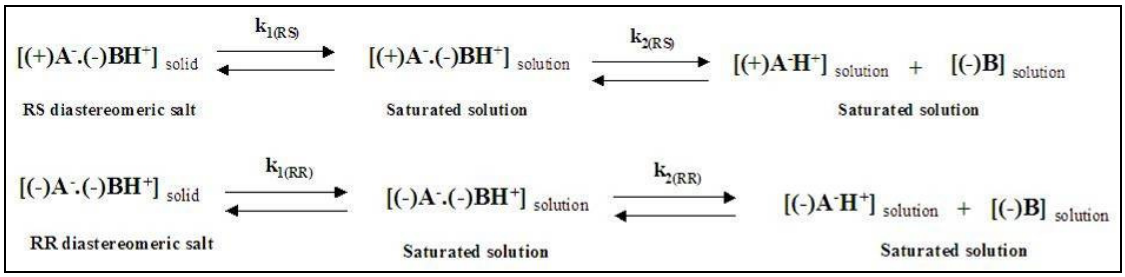

Fig27 Solvation equilibria

If we assume that the difference in pKa values between the base (-)B and the acid (±)A-H^+ is large[68], then the free energies of solvation, ΔG_{RS} and ΔG_{RR} of the diastereomer salts, are directly related to the equilibrium constants K_{RS} and K_{RR} **(12)** and **(13)**:

$$K_{RS} = k_{1(RS)} \times k_{2(RS)} \quad \text{and} \quad K_{RR} = k_{1(RR)} \times k_{2(RR)} \qquad \textbf{(12)} \text{ and } \textbf{(13)}$$

Which could also be written as a function of concentrations **(14)** and **(15)**:

$$K_{RS} = \frac{[(+)A^-H^+] \quad [(-)B]}{[(+)A^-.(-)BH^+]_{solid}} \qquad \textbf{(14)}$$

and

$$K_{RR} = \frac{[(-)A^{-}H^{+}] \quad [(-)B]}{[(-)A^{-}.(-)BH^{+}]_{solid}} \qquad (15)$$

As by convention, the concentration of a solid is taken as 1, the equations **(14)** and **(15)** could be written as **(16)** and **(17)**:

$$K_{RS} = [(+)A^{-}H^{+}]\ [(-)B] = C_{RS} \times C_{RS} = C^{2}_{RS} \qquad (16)$$

and

$$K_{RR} = [(-)A^{-}H^{+}]\ [(-)B] = C_{RR} \times C_{RR} = C^{2}_{RR} \qquad (17)$$

Where C_{RR} and C_{RS} are concentrations of RS and RR diastereomer salts respectively. The difference in Gibbs free energy, ΔG, is written as **(18)**:

$$\Delta G = \Delta H - T\Delta S = -RT\ln K \qquad (18)$$

Where ΔH is the enthalpy difference, ΔS the entropy difference, T the temperature, K the equilibrium constant and R the ideal gas constant (8.314472 $J.K^{-1}mol^{-1}$). For a pair of diastereomeric salts equation **(18)** could be written as **(19)**:

$$\Delta\Delta G = \Delta G_{RS} - \Delta G_{RR} = (\Delta H_{RS} - \Delta H_{RR}) - T(\Delta S_{RS} - \Delta S_{RR}) = RT(\ln K_{RS} - \ln K_{RR}) \qquad (19)$$

As the equilibrium constants K_{RS} and K_{RR} are proportional to the square of the concentrations C_{RS} and C_{RR} [equations **(16)** and **(17)**], the difference in Gibbs free energy could be calculated as **(20)**:

$$\Delta G_{RS} - \Delta G_{RR} = (\Delta H_{RS} - \Delta H_{RR}) - T(\Delta S_{RS} - \Delta S_{RR}) = 2RT\ln(C_{RS}/C_{RR}) \qquad (20)$$

Under these simplifying assumptions, the solubility ratio is linked to the solid-state properties and does not depend on the solution chemistry.

Approximate estimates of the diastereomers' stability difference have been made by visually examining the crystal structures of the less and more soluble diastereomer for the presence or lack of stabilising hydrogen-bond motifs[77,78], CH•••π interactions[79] and the overall packing efficiency. Although such qualitative analyses can recognise trends, when there are marked differences in the dominant intermolecular interactions, they cannot quantify the stability difference. On the other hand, the computational prediction of the free energy difference [$\mathbf{\Delta G_{RS} - \Delta G_{RR}}$ from equation **(20)**] is very demanding, as the zero-point energy, entropy, and temperature-dependent contributions to the enthalpy need to be accurately estimated, accounting for molecular flexibility and thermal expansion[80]. However, a systematic study of the resolution efficiency of diastereomeric salt pairs of ephedrine with phenyl-substituted cyclic phosphoric acids showed that the solubility ratio correlates well with the enthalpy difference between the diastereomeric salt pairs[68]; i.e., the entropies of the two diastereomers are approximately equal. If we further assume that the zero-point energy and specific heats of the two diastereomers are similar, then, to a first approximation, the solubility ratio can be estimated by comparing the diastereomers' static lattice energies. The static lattice energy $\mathbf{U_{latt}}$, which includes the intermolecular contributions $\mathbf{U_{inter}}$ and the intramolecular energy penalties $\mathbf{\Delta E_{intra}}$ for the deformation of the ions' conformation in the solid-state, is amenable to theoretical predictions and thus the type of modelling tested in this thesis. Early computational studies[68,75,81] showed that the models for the intermolecular forces and the ion conformational energies were not sufficiently accurate for reliable relative lattice energy estimates, and in some cases, the experimental crystal structures did not correspond to a minimum on the lattice energy surface as modelled with the available force fields.

The ultimate aim of computational studies is the prediction of the stability difference of the diastereomeric salt pair without relying on experimental information, which also requires the *ab initio* prediction of the diastereomers' crystal structures. The prediction of the crystal structure of chiral salts is a challenging problem[75] for two reasons. First, the number of possible packing arrangements that need to be considered is significantly larger compared with typical crystal structure prediction studies for rigid, non-ionic systems. This is because the smallest asymmetric unit in a salt crystal structure comprises two crystallographically independent ions. In addition,

chiral ions generally contain single bonds around which rotation, in response to the crystal packing forces, is energetically feasible, and hence, the ions' conformations should also be varied within the search. Second, accuracy in the calculated energies is vital for the quantitative prediction of the solubility ratio, as the latter depends exponentially on their relative thermodynamic stability [see equation **(20)** above]. Nonetheless there are methods available which can be used to predict crystal structures, based on the global minimisation of the lattice enthalpy of the crystal[82]. These can be used for molecules with significant flexibility,[83], such as salts and in deed, there have been successful searches done for predicting the crystal structures.

2-6-3 Lattice energy

The crystal lattice energy ($\mathbf{U_{latt}}$) is an important thermodynamic quantity for calculating the structure, properties and behaviour of solids. The lattice energy is approximately as the amount of energy, which had to be supplied to transfer the species from the crystal lattice to the gaseous phase, where no interactions occur. For molecular crystals, where the component species in the solid and gaseous phases consist of the same molecules, the lattice energy is effectively the sublimation energy[84]. In this case, this quantity can be measured directly. For ionic substances, the situation is different as the species existing and interacting in the solid phase are actually the ions. In this case, the lattice energy is the energy required to transfer ions from the lattice to the gaseous phase[85].

A solid phase exists as a result of attractive and repulsive interactions between the molecules forming the lattice. The lattice energy is calculated by summing up all these interactions within the crystal lattice. The main contributions are the repulsive interactions from the overlap of the charge clouds, the attractive long range dispersion interactions and the electrostatic Coulombic interactions between the molecules.

2-6-3-1 Modelling the lattice energy of simple ionic solids

For simple ionic solids where each ion is a sphere, the interaction between two ions depends only on their separation $\mathbf{r_{ij}}$, the lattice energy is then calculated by summing this interactions overall ion pairs in the lattice. The repulsion and dispersion terms are

combined in either the Lennard-Jones (or 6-12 interaction) or the Buckingham (or exp-6 potential). In addition the ions interact through the Coulomb term[86].

The most well-known dispersion-repulsion model is the Lennard-Jones potential $\mathbf{V_{LJ}}$ **(21)**[86]:

$$\mathbf{V_{LJ}(r_{ij}) = \frac{C_{ij}^{(12)}}{r_{ij}^{12}} - \frac{C_{ij}^{(6)}}{r_{ij}^{6}}} \qquad \mathbf{(21)}$$

where the inverse 12th power terms models the repulsion, which quickly decays with increasing interatomic separation and the inverse 6th power term models the longer-range dispersion. $\mathbf{C_{ij}^{(12)}}$ and $\mathbf{C_{ij}^{(6)}}$ are parameters which depend on the types of the atoms **i** and **j**.

Buckingham[86] modified the Lennard-Jones potential to combine an exponential-based model **(22),** $\mathbf{V_{bh}}$**,** for the repulsive term with the same term for the dispersion to produce an 'exp-6' model:

$$\mathbf{V_{bh}(r_{ij}) = A_{ij} \exp(-B_{ij} r_{ij}) - \frac{C_{ij}}{r_{ij}^{6}}} \qquad \mathbf{(22)}$$

where $\mathbf{A_{ij}}$, $\mathbf{B_{ij}}$ and $\mathbf{C_{ij}}$ are parameters that can be fitted to experimental data.

The Coulomb potential, $\mathbf{V_C}$, between two charged particle, is given by equation **(23)**[86]:

$$\mathbf{V_C = \frac{1}{4\pi\varepsilon_0} \frac{q_i q_j}{r_{ij}}} \qquad \mathbf{(23)}$$

Where $\mathbf{r_{ij}}$ is the interatomic separation, **q** is the electric charge on the ion, and $\boldsymbol{\varepsilon_0}$ is the electrical permittivity of space. In ionic substances, the repulsion and dispersion energies do not usually exceed 10 percent of the value of the electrostatic term, and as they have opposite signs, their sums become negligible. Therefore, for simple ionic solids, the lattice energy is dominated by the electrostatic energy.

2-6-3-2 Lattice energy for molecular salts

For molecules, the repulsion and dispersion energies are usually described by a Backingham model between every intermolecular pair of atoms. The parameters in equation **(22)** are fitted to organic crystal structures with values that depend on the types of atoms.

Electrostatic (Coulombic) forces will also dominate the lattice energy for diastereomeric salts and are particularly important in describing the orientation dependence of the hydrogen-bonding interactions in the crystal structure. The electrostatic forces around a molecule (or molecular ion) can be accurately calculated from a distributed multipole representation of an *ab initio* wave function of the molecule. This represents the molecular charge distribution by sets of point multipoles (charge, dipole, quadrupole etc.) usually at every nucleus in the molecule. These distributed multipoles provide an accurate representation even close to the Van der Waals surface of the molecules, because the expansion around each atomic site remains valid, unlike a central multipole expansion. The higher atomic multipole moments represent the electrostatic effects of lone pair, π electron, and other non-spherical features in the charge distribution. This is crucial to the success of the model in modelling the structures of Van de Waals complexes of polar molecules, particularly when hydrogen bonding or π-π interactions are involved. Because molecular crystals also involve molecules in Van der Waals contact, the use of distributed multipoles electrostatic models is expected to be important for a generally successful approach to predicting crystal structures[87].

The most commonly adopted method used to represent the electrostatic part of the intermolecular potential for a molecule is to represent the charge distribution of the isolated molecule, as calculated from the *ab initio* wave function using an affordable basis set and a high level calculation. In this thesis, the electrostatic interactions were modelled with a Distributed Multipole Analysis (DMA)[88] of the MP2 correlated[89] ion charge densities calculated a 6-31G(d,p) basis set.

The intermolecular lattice energy, $\mathbf{U_{inter}}$, is calculated by summing the repulsion, dispersion and electrostatic terms between every intermolecular pair of atoms within

the crystal. However, for the distributed multipole electrostatic model, the electrostatic energy contribution depends on the relative orientation of the atomic multipole moments[87].

2-6-3-3 Molecular flexibility

The molecular ions studied in this thesis can change their conformation by rotation above the Carbon-Carbon and Carbon-Oxygen single bonds. These changes in conformation will change the distributed multipole moments and the internal energy of the ion. For these ions, the molecular conformation could distort with small energy penalty, the *ab initio* conformational energy, $\mathbf{\Delta E_{intra}}$, which could be more than compensated for by the improved lattice energy $\mathbf{U_{latt}}$[90,91] as in equation **(24)**:

$$\mathbf{U_{latt} = U_{inter} + \Delta E_{intra}} \qquad \mathbf{(24)}$$

A procedure for allowing the flexible torsion angle to respond to the intermolecular packing forces has been developed. DMAflex Calculations minimise the value of the lattice energy $\mathbf{U_{latt}}$ by simultaneously using the program DMAREL to calculate $\mathbf{U_{inter}}$ for a crystal structure with the ions held rigid, and using GAUSSIAN to calculate $\mathbf{\Delta E_{intra}}$ and the distributed multipoles for each of the ion conformations[92].

2-6-3-4 Programs used for calculations in this thesis

GAUSSIAN

GAUSSIAN[93] is an *ab initio* quantum chemistry package. It is an electronic structure program. Starting from the basic laws of quantum mechanics, the program predicts the energies, molecular structures and vibrational frequencies of molecular systems. Computation, using this program, can be carried out on systems of nuclei and electrons which can be used to study reactions and to find the geometries and properties of molecules in their ground or in their excited states. This program is capable of predicting many properties of molecules including the following:

- Molecular structures and other low energy conformations
- Differences in energies between conformations ΔE_{intra}
- Energies and structures of transition states between conformations
- Atomic charges and electrostatic potential around the molecule
- Total and distributed multipole moments, atomic charges
- Vibrational frequencies, etc.

In this project, GAUSSIAN is used to compute the charge density, molecular geometries and intramolecular energies.

GDMA

GDMA[94] is a program used to carry out Distributed Multipole Analysis (DMA) of wavefunctions calculated by the Gaussian system of programs, using the formatted checkpoint files that they produce. The result is a set of multipole moments at sites defined by the user (usually at the positions of the atomic nuclei) which, given an accurate wavefunction, provide an accurate description of the electrostatic field of the molecule.

NEIGHBOURS

NEIGHBOURS[95] is a utility program for setting up input files for DMAREL, which models crystals of the rigid organic molecules, using anisotropic atom-atom intermolecular potentials. The program converts crystallographic data files (csd fdat) and SHELX to a Cartesian coordinate system. The molecular fragments are treated as rigid identities. It sets up the molecule-fixed local axis system on each molecule. The first run of NEIGHBOURS is usually performed to obtain the coordinates of the molecule in the local axis system prior to *ab initio* calculations. This sets the origin at the centre of mass and the local molecular axis parallel to specified intramolecular bonds. The coordinates can be used in GAUSSIAN to calculate the atomic multipoles (DMA) for the electrostatic model, or as a starting point for an *ab initio* optimisation of the geometry.

DMAREL

DMAREL[96] is a program in which the lattice energy is calculated and then minimised for a particular crystal structure, with the assumption that the molecules within the unit cell are rigid. DMAREL can handle realistic and anisotropic intermolecular potentials such as the distributed multipole moments. One of the key features is the ability of DMAREL to use atomic multipoles[88,97] generated by GDMA. This program minimises lattice energy while maintaining space group symmetry[98]. The electrostatic sums for charges and dipoles are evaluated using the Ewald approach[99,100], higher multipole interactions use a molecule based cut-off for a direct summation, with the short range potentials summed using an atom based cut-off.

2-7 Summary

In order to define the isolation of enantiomers via diastereomer crystallisation, one should understand:

- Stereochemistry (special arrangement of atoms within molecules)
- Crystallography (arrangement of atoms in solid)
- Polymorphism (ability of solid material to exist in more than one form or crystal structure)
- Phase equilibria (what phases are present at a given temperature and pressure)
- Molecular modelling (lattice energy calculation)
- Analytical tools (characterisation of experimental outcome).

With all the information provided in this chapter, one should be able to understand and carry out the chiral resolution study.

The experimental and molecular modelling methodologies, which are used to gather and analyse the data in this thesis, are discussed in the next chapter.

3 EXPERIMENTAL AND MODELLING METHODS

In the following sections the three sets of diastereomer salts studied will be called A1, A2 and A3 (see **Fig7**), where:

- **A1**: (R)-1-phenylethylammonium-(R,S)-2-phenylpropanoate
- **A2**: (R)-1-phenylethylammonium-(R,S)-2-phenylbutyrate
- **A3**: (R)-1-phenylethylammonium-(R,S)-mandelate.

In the previous chapter (Survey of Literature and Methods), important terms and information needed to understand enantiomer isolation via diastereomer crystallisation have been discussed.

In this chapter, experimental and molecular methodologies, used in this research, are discussed.

3-1 Experimental methods

(R)-1-phenylethylamine (99+%) and the six enantiomer acids were obtained from Lancaster Synthesis and Alfa Aesar; the acids were sourced as both single enantiomers (97-99%) and as racemates (98+%). These were used without further purification. All experiments were carried out using the R-form of the base, in combination with acids and acid mixtures to give the desired stereoisomer combinations. The ethanol solvent was of HPLC grade. Individual diastereomer salts were prepared by mixing stoichiometric quantities of base and acid in ethanol solution and evaporating to dryness at room temperature in an open vessel.

A simple picture of the jacketed vessel used for the equilibrium and crystallisation experiments below and the equipment attached to it for all the experimental work is shown in **Fig28**.

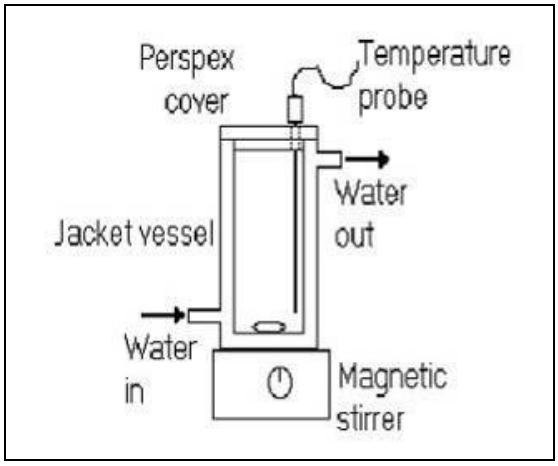

Fig28 Sketch of crystallisation cell

3-1-1 Solubility measurements

The solubilities of individual diastereomer salts were measured by contacting 10 mL aliquots of solvent with excess solid salt at a particular temperature in a water bath for periods of one week, with gentle stirring. Solution samples were extracted using a pre-heated, filtered syringe, diluted and analysed by HPLC using a 100 mm C18 column.

Solubility measurements were carried out from the highest temperature to the lowest one employed for each pure R and S form of the acids as the corresponding pure RR and RS diastereomer salts (n and p salts respectively). Equimolar amount of pure S or R acids and R-enantiomer pure base were added into a jacketed-vessel containing ethanol and connected to the water bath. The point of the solubility measurement is to take saturated liquid samples out of the vessel for HPLC analysis, to determine the concentration of the sample, at different temperatures. Therefore it is necessary to have both solid and liquid in contact at the equilibrium point of sampling. When there was only liquid in the vessel, more acid and base were added to the vessel in equimolar proportions (acid after base all the time during solubility measurements in order to get the right compound formation).

The intention was to get a creamy product in the vessel. When a creamy solid was becoming thicker like a solid in the vessel, more ethanol was added (1mL at a time) until the formation of creamy product. When there was appearance of crystals at the

sides of the vessel, the solid was rubbed off and added into the solution of the vessel, to make sure that the entire solid is in contact with the solvent, for the formation of saturated solution. After obtaining what was believed to be a saturated solution in contact with excess solid, the whole mixture was left for a further 48 hours to equilibrate.

To take the saturated sample for analysis, a syringe with a filter was used. In order to avoid the solid crystallising while taking the sample out, the syringe was kept inside the water bath for 30 to 45 minutes to condition it to the same temperature as the saturated liquid. While the saturated sample was taken out, the stirrer used to agitate the vessel was stopped and the liquid was taken into the syringe without the filter fitted. Then the saturated sample was taken very quickly out of the vessel. The filter was then immediately fixed to the syringe to trap any solids present as the sample is transferred to the dilution flask. The exact temperature inside the vessel was also noted at this point.

The solubility measurements have been started at 55°C. After taking the first saturated liquid sample out, the temperature of the vessel was decreased by 10°C and left at that temperature for 48 hours, in order to let the equilibrium be re-established. The syringe used for the extraction of the saturated solution was washed with ethanol and used again for further extraction at different temperatures. The samples were taken out at 55, 45, 35, 25, 15 and 5°C and analysed.

Preparation of samples for HPLC measurements

Preparation of standard solution: The standard solution was made of a known quantity of acid and base of the pure diastereomer salt (of RR or RS A1, A2 or A3) left in the jacketed vessel, after solubility measurements. A measured volume of ethanol was added to the solid for dilution.

The concentration of the standard solution was calculated as in **(25)**:

$$C_{standard} \times V_{ethanol} = \frac{m_{A1}}{MW_{A1}} \qquad \textbf{(25)}$$

Where $\mathbf{C_{standard}}$ is the concentration, $\mathbf{V_{ethanol}}$ the volume, $\mathbf{m_{A1}}$ the weight of the salt (A1, A2 or A3), and **MW** the molecular weight of the salt (A1, A2 or A3). This equation **(25)** could also be written as in **(26)**:

$$\mathbf{C}_{\mathbf{standard}} = \frac{\mathbf{m}_{\mathbf{A1}}}{\mathbf{MW}_{\mathbf{A1}} \times \mathbf{V}_{\mathbf{ethanol}}} \qquad \mathbf{(26)}$$

The concentration calculations, in equations **(25)** and **(26)**, were done with molal concentrations (moles of solute /L of solvent). We are not working with molar concentration (moles of solute /L of solution). The difference between molar and molal concentrations will correspond with how different the solution density is to unity. In the experiments conducted in our case, the difference will be very small, i.e. negligible.

Dilution of samples in ethanol: 200µL of each sample taken out at different temperatures was diluted in 6000µL of ethanol (6mL of ethanol was added to the sample). Then the diluted samples were HPLC analysed.

Calculation of concentration of the diluted samples: The concentration of the standard solution has been calculated, by weighing out a quantity of the sample and making up the solution to a given volume. After doing a HPLC analysis of the standard solution, a peak area corresponding to the calculated concentration was obtained. For the other diluted samples, the concentrations were unknown, but the area was given by the HPLC measurements. By using all these data, the concentrations of the diluted samples were calculated as in equation **(27)**:

$$\mathbf{C}_{\mathbf{diluted\ sample}} = \frac{\mathbf{C}_{\mathbf{standard}} \times \mathbf{Area}_{\mathbf{sample}}}{\mathbf{Area}_{\mathbf{standard}}} \qquad \mathbf{(27)}$$

Where **C** is the concentration of diluted or standard samples and **Area** is the surface area under the chromatographic peak corresponding to sample or standard solution.

After doing all the calculations, the solubility curves were plotted as **Concentration (solubility) = f (Temperature)**.

3-1-2 Ternary equilibrium measurements

For the ternary equilibrium measurements, salt mixtures were prepared by mixing base with acid mixtures of various enantiomer compositions prepared by combining single enantiomers and racemates, and evaporating as above. Excess quantities of the solids thus obtained were then contacted with 8 mL aliquots of solvent (ethanol), and held for 7-10 days in sealed vessels in a water bath with gentle stirring. The contents of the vessels were then filtered rapidly at temperature, and the quantities of the solid and filtrate recovered were determined. Filtrates were evaporated to dryness and the recovered solids weighed.

Throughout the equilibrium measurements, ternary data of A1, A2 and A3 were measured at 30 and 50°C.

From the single-salt solubility curves, the solubilities of A1, A2 or A3 diastereomer salts are determined at different temperatures. In this particular project, the temperatures considered were 30 and 50°C. The ternary equilibrium experiments were designed by basing the salt:solvent ratio on the higher of the two single salt solubilities, and then taking diastereomer ratio of 100/0, 75/25 etc.

The amount of acid and base were calculated as per equations **(28)** to **(31)** for the equilibrium experiment.

The amount of acid needed was calculated as:

$$\frac{\mathbf{M}_{\mathbf{acid}}}{\mathbf{MW}_{\mathbf{acid}}} = \mathbf{Solubility} \times \mathbf{V}_{\mathbf{ethanol}} \qquad \textbf{(28)}$$

And therefore $\mathbf{m}_{\mathbf{acid}} = \mathbf{Solubility} \times \mathbf{V}_{\mathbf{ethanol}} \times \mathbf{MW}_{\mathbf{acid}}$ **(29)**

The amount of base needed was calculated as:

$$\frac{\mathbf{V\ base \times d\ base}}{\mathbf{MW\ base}} = \mathbf{Solubility \times V\ ethanol} \qquad \mathbf{(30)}$$

And therefore

$$\mathbf{V}_{\mathbf{base}} = \frac{\mathbf{Solubility \times V}_{\mathbf{ethanol}} \mathbf{\times MW}_{\mathbf{base}}}{\mathbf{d}_{\mathbf{base}}} \qquad \mathbf{(31)}$$

Where **V** is the volume of ethanol or base, **MW** molecular weight of acid or base, **M** weight of the acid and **d** density of the base.

Equimolar amounts of acid, with different proportions of R and S acid as 100/0, 75/25, 50/50, etc, and base were weighed. In pre-weighed vials, the weighed amount of acid proportions were added and measured volume of ethanol was added. Then a stoichiometric quantity of base was poured into the vial. Then the vials were sealed and shaken. As this acid-base reaction is exothermic and released heat, the vials were left under room temperature until some solid appeared in the vials. Then all the vials were put inside the jacketed vessel, heated by a water bath, which is set at 30 or 50°C. The vials were immersed in water, which was heated by the water supply inside the jacketed vessel, and magnetic stirrer stirred the whole system. An electric thermometer inside the vessel monitored the temperature. The jacketed vessel was then closed and left to stand for a week to let the equilibrium take place.

After equilibrium the solid and liquid phases were separated and collected. The liquid phase was collected in a pre-weighed vial and diluted in ethanol. The solid phase was filtered off with a Buchner funnel, washed with hexane and dried and weighed and kept in a pre-weighed Petrie dish. The collection of the solid and liquid phases was done very quickly in order not to let any temperature change induce any compositional changes in the liquid and solid phases. The solid and liquid phases were weighed and then HPLC analysed.

Using the HPLC measurements, the proportions of RS and RR forms of A1, A2 and A3 in the solid and liquid phases were determined and the overall mol fractions were also calculated to draw the phase diagram.

The mol fraction of RA1 in the liquid phase was calculated as indicated in **(32)**:

$$\textbf{Mol fraction}_{\textbf{RA1 liquid phase}} = \frac{\mathbf{n}_{\mathbf{RA1}}}{\mathbf{n}_{\mathbf{RA1}} + \mathbf{n}_{\mathbf{ethanol}} + \mathbf{n}_{\mathbf{SA1}}} \qquad \textbf{(32)}$$

Where **n** is the number of moles of RR or RS diastereomer or the number of moles of ethanol.

As the density $\mathbf{d_{ethanol}}$ of ethanol, at room temperature, is 0.79 g/mL and its molecular weight $\mathbf{MW_{ethanol}}$ is 46 g/mol, the expression **(32)** could be written as the expression **(33)**:

$$\textbf{Mol fraction}_{\textbf{RA1 liquid phase}} = \frac{\dfrac{\mathbf{m}_{\mathbf{RA1\ liquid}}}{\mathbf{MW}_{\mathbf{RA1\ liquid}}}}{\left[\dfrac{\mathbf{m}_{\mathbf{RA1\ liquid}}}{\mathbf{MW}_{\mathbf{RA1\ liquid}}} + \dfrac{\mathbf{V}_{\mathbf{ethanol}} \times \mathbf{0.79}}{\mathbf{46}} + \dfrac{\mathbf{m}_{\mathbf{SA1\ liquid}}}{\mathbf{MW}_{\mathbf{SA1\ liquid}}}\right]} \qquad \textbf{(33)}$$

Where **m** is the weighed weight A1, A2 or A3 diastereomers (RR or RS), **V** the volume of ethanol and **MW** the molecular weight of RR or RS diastereomer (A1, A2 or A3).

The mol fraction of RA1 in the solid phase was calculated as **(34)**, using the percentage of RR and RS diastereomer salts of A1, A2 or A3 systems:

$$\textbf{Mol fraction}_{\textbf{RA1 solid phase}} = \frac{\%\,\mathbf{R}_{\mathbf{A1}}}{\%\mathbf{R}_{\mathbf{A1}} + \%\mathbf{S}_{\mathbf{A1}}} \qquad \textbf{(34)}$$

After calculating and gathering all these information, the phase diagram was drawn for A1, A2 and A3 at 30 and 50°C.

3-1-3 Separability measurements

Separability measurements of the salts A1, A2 and A3 were carried out to understand the role of crystallisation kinetics and phase equilibria on the separability of the diastereomers. Generally crystallisation will be affected by both kinetics and equilibria, and the results of this work show the equilibria to be all-important. Through the separability measurements, diastereomer salt mixtures, with different compositions, have been crystallised to characterise the enrichment of the crystals and the most suitable temperature regime for crystallisation.

For the measurements of separation by fractional crystallisation, solutions (10 mL) were made up using (R)-1-phenylethylamine and acid enantiomer mixtures in various ratios of concentrations corresponding to the solubility limits given by the 50°C solubility curves in the phase diagrams.

From the ternary phase diagram, mol fractions, corresponding to different compositions of RR and RS forms of the diastereomer salt (final product), were determined and used to calculate the quantities of acid and base corresponding to prepare these final products as follows, in expressions from **(35)** to **(37)**:

The number of moles of final product is calculated as:

$$\mathbf{n_{final\ product} = n_{RR\ diastereomer\ salt} + n_{RS\ diastereomer\ salt} = n_{acid} = n_{base} = \frac{m_{acid}}{MW_{acid}} = \frac{V_{base} \times d_{base}}{MW_{base}}} \quad \textbf{(35)}$$

The mol fraction of the RR or RS diastereomer salt is calculated based on the experssion **(36)**:

$$\mathbf{mol\ fraction_{RR\ diastereomer\ salt} = \frac{n_{RR\ diastereomer\ salt}}{n_{RR\ diastereomer\ salt} + n_{ethanol} + n_{RS\ diastereomer\ salt}}} \quad \textbf{(36)}$$

The expression **(36)** could be written in detail as **(37)** to calculate the molfraction of the diastereomer salt:

$$\text{mol fraction}_{\text{RR diastereomer salt}} = \frac{n_{\text{RR diastereomer salt}}}{\left[n_{\text{RR diastereomer salt}} + \frac{V_{\text{ethanol}} \times d_{\text{ethanol}}}{MW_{\text{ethanol}}} + n_{\text{RS diastereomer salt}} \right]} \quad (37)$$

Where **n** is the number of moles of acid, base or ethanol, **d** the density of ethanol, **V** the volume of base or ethanol and **MW** the molecular weight of acid, base or ethanol.

In pre-weighed vials, the calculated amount of acid was introduced and the solvent was added to it. Then the measured volume of the base was added. The corresponding acid-base reaction was exothermic and because of this heat release, the crystals were found dissolved in the solution. Therefore the vials were left at room temperature until crystals were visible. The temperature of the solution was increased to 55°C prior to the start of each crystallisation, to ensure complete dissolution at the beginning. The solution aliquots were placed in jacketed vessels fitted with a thermostat, and were cooled at a constant 0.5 $Kmin^{-1}$ until the reported isolation temperature was attained. The vessels were held at the isolation temperature until no further solid appeared, by visual inspection, to separate from solution. Where the solution remained clear on attaining the final temperature, the vessel was maintained at this temperature for periods of 24 hours to 30 days. Isolation was carried out by rapid filtration. The solid and liquid phases were weighed and then diluted in ethanol before HPLC analysis. From the HPLC results, the real percentage of RR and RS form of the diastereomer salts (final product) in the solid and liquid phases were calculated, using the peak areas.

3-1-4 HPLC measurements

The flow chart corresponding to the HPLC system is given below in **Fig29**.

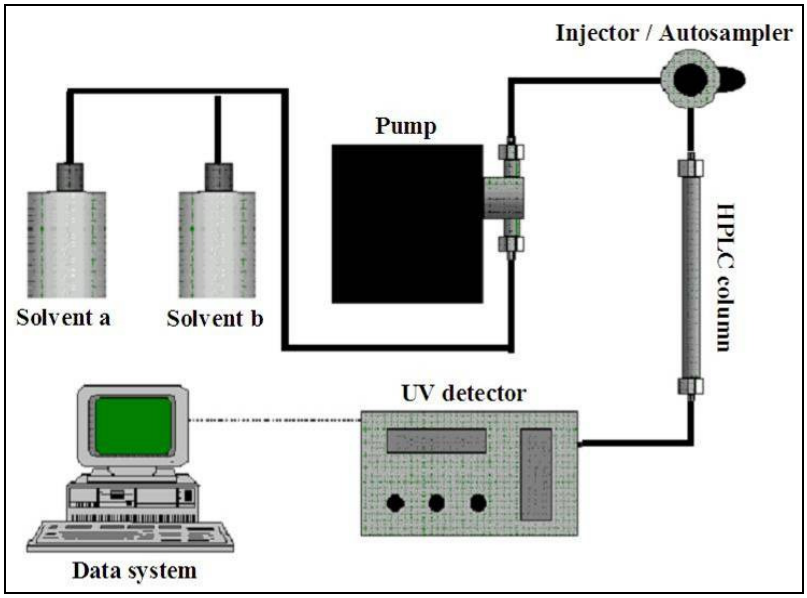

Fig29 Flow chart of the HPLC system

The acid enantiomer ratios were determined by chiral HPLC, using a 250 mm length Regis Whelk-01 reverse-phase column. For 2-phenylpropionic acids and 2-phenylbutyric acids, an eluant of 45:45:10 hexane/dichloromethane/2-isopropanol (IPA) with an acetic acid/ammonium acetate ($HOAc/NH_4Oac$) buffer (0.02%) was initially employed at a flow rate of 1.5 $mLmin^{-1}$ (the retention time information is given in **Table_8**). However, difficulties with the precipitation of the buffer solids led to the eluent being modified to 98:02 hexane / IPA with 0.1% acetic acid at the same flow rate. This much simpler eluant composition gave adequate resolutions and was much easier to work with.

For mandelic acids, a more polar eluant of 95:05 water / ethanol with 0.1% trifluoroacetic acid (TFA) was employed. In all cases, the salts were completely dissociated in ethanol solution, with the (R)-1-phenylethylamine base moiety eluting at a retention time RT > 12 min.

Table_8 Different Eluants and retention times

Samples	Eluants	Retention times (min)
(R)-2-phenylpropionic acid (S)-2-phenylpropionic acid	45:45:10 hexane/dichloromethane/IPA with a HOAc/NH_4OAc buffer (0.02%)	8.3 9.5
(R)-2-phenylbutyric acid (S)-2-phenylbutyric acid	45:45:10 hexane/dichloromethane/IPA with a HOAc/NH_4OAc buffer (0.02%)	6.3 5.6
(R)-2-phenylpropionic acid (S)-2-phenylpropionic acid	98:02 hexane / IPA with 0.1% acetic acid	6.1 7.5
(R)-2-phenylbutyric acid (S)-2-phenylbutyric acid	98:02 hexane / IPA with 0.1% acetic acid	6.2 5.5
(R)-mandelic acid (S)-mandelic acid	95:05 water / ethanol with 0.1%TFA	6.2 8.1

Equations, which were used to calculate the percentage of RR and RS forms of the diastereomer salt, are as equations **(38)** to **(40)**.

$$\textbf{Total area}_{\textbf{R and S salts}} = \textbf{Area}_{\textbf{S-acid}} + \textbf{Area}_{\textbf{R-acid}} \quad \textbf{(38)}$$

$$\%\ \textbf{R salt} = \frac{\textbf{Area}_{\textbf{R-acid}}}{\textbf{Total area}_{\textbf{R and S salt}}} \quad \textbf{(39)}$$

$$\%\ \textbf{S salt} = \frac{\textbf{Area}_{\textbf{S-acid}}}{\textbf{Total area}_{\textbf{R and S salt}}} \quad \textbf{(40)}$$

Where **Area** corresponds to the surface area of each R and S acid peak obtained from HPLC measurements.

3-1-5 Preparation of RRA2 single-crystal diastereomer salt samples for structure determination

Using the solubility curve of the RRA2 system, the equimolar amount of acid and base and the quantity of solvent to make up the saturated solution were calculated at 25°C. The acid:base ratios were adjusted as appropriate to accommodate other stoichiometries. When the pH was changed to alkaline, then sodium hydroxide (NaOH) was added to the solvent to make the pH change to 9 to 11.

Using the same acid:base ratio and changing the solvents, some crystals were formed and the structure of those crystals were determined using X-ray diffraction.

Acid and base were mixed together in ethanol and taken to 25°C, using a water-bath heat supply. When crystals were formed at 25°C, then the temperature of the samples was kept constant and after 48 hours the crystals were separated from the solution. When there was no spontaneous crystal formation, then the sample was taken down to lower temperature, at constant rate, until crystal formation. Then the crystals were separated from the solution and analysed.

Here are other crystallisation solvents used:

- 1-butanol
- 2-butanol
- 2-methoxyethanol
- 2-propanol
- dichloromethane
- nitromethane
- t-butylmethylether
- tetrahydrofurane (THF)

3-1-6 Further experimental work to determine different RRA2 polymorphs

In order to find out the existence of various polymorphs of RRA2, a few different samples were prepared as explained in the following sections.

3-1-6-1 By changing acid:base ratio

Using the solubility curve of RRA2 at 25ºC, the weight of acid, the volume of base and the volume of the ethanol were calculated. The basic equations used to determine the quantities needed for the experiments, with the ratio of 1:1 are as equations **(28)** and **(30)**.

In a small vial, weighed quantity of acid was placed. Then the calculated volume of ethanol (solvent) was added to it. After mixing them, the calculated volume of base was added and mixed with the rest. The crystals appeared in the vial in few seconds after adding the base. The vial was placed then into jacketed vessel at 25ºC and left at that temperature for few days in order to make sure that the equilibrium took place. Then the solid samples were filtered and analysed using X-ray diffraction. The same method was used with different ratios of acid:base (i.e. 3:1, 1:2, 1:3, 2:1).

3-1-6-2 By replacing ethanol with other solvents

Several polar solvents other than ethanol have been used, by assuming that ethanol and these other solvents have same solubility order. And therefore the solubility curve of RRA2 in ethanol at 25ºC was used to calculate the quantity of the acid / base samples and the solvent needed to do the experimental work. The rest of the work is done as explained in the previous section ***3-1-6-1***.

3-1-6-3 By changing the pH of ethanol

Sodium hydroxide (NaOH) was added to ethanol to change the pH of the solvent to make it more alkaline, to examine whether or not the change of pH gives rise to the formation of a different polymorph of RRA2. Sodium hydroxide was not very soluble in ethanol and therefore it was ground first before being added into the ethanol solution and the ethanol was also heated at 50ºC to dilute the sodium hydroxide quickly. Then the pH of the solution was checked using pH indicator paper. More sodium hydroxide was added until the desired pH was obtained.

The rest of the experiment was conducted as explained in the section ***3-1-6-1***.

It is important to note here that the concept of pH does not really apply to non-aqueous solvents, because it is based on $[H^+]\ [OH^-] - 10^{-14}$. Here the addition of base is just used to condition the solution in a measurable and reproducible way.

3-1-7 Slurry experiments

Slurry experiments were carried out in solvents in which the test substance has low to medium solubility. The function of the test is to allow polymorph transitions down the scale of free energy of formation, with the solvent providing the kinetic pathway. If the substance is insoluble, then this pathway does not exist.

Slurry experiments have been done on the polymorphs of each RR diastereomer salt of the systems A2 and A3, to find out which of the 2 polymorphs found is the more stable one. When we put the same amount of each polymorph of the same compound into a vessel and add solvent into it and leave for three weeks in the solvent, with stirring, at room temperature, then the less stable polymorph of the compound will be converted into the most stable polymorph.

3-1-7-1 Choice of solvent

To choose a solvent in which diastereomer salts corresponding to the acids A2 and A3 are slightly soluble, the following testing has been done on two different solvents, toluene and chloroform ($CHCl_3$):

A few crystals of diastereomer salts of A2 or A3 were spread on a microscopic slide and a few drops of chloroform was poured on top of the solid and observed under a microscope to see what is exactly happening. The solid did not dissolve in the chloroform, and when we moved the liquid around on the whole microscopic slide surface, there was no trace of solid on the pathway of the liquid, indicating that the solid was very insoluble in it. Therefore chloroform has not been used, because some solubility of crystals in the solvent was necessary for this experiment.

Then a same experiment was tried again using toluene as solvent. When the liquid was moved on the glass, small traces of solid were found on the pathway of the liquid, showing that the solid was slightly soluble in toluene. Therefore toluene has been used as solvent throughout the slurry experiments.

3-1-7-2 Slurry experiment

Weighed solid samples were added into pre-weighed vials with lid and solvent was added to it until formation of a paint-like thick suspension, which could be stirred using a magnetic stirrer. Then the vial was placed on a stirrer plate and the vial was stirred continuously for three weeks. When there was no liquid found inside the vial, a further measured volume of solvent was added to it. After three weeks, the solvent was evaporated and the crystals were analysed using X-ray powder diffraction.

Four different types of experiments were set up:

1. On RSA3 diastereomer salt crystals.
2. On a mixture of diastereomer salts of RRA2 polymorph I and RRA2 polymorph II, using 1:2 acid:base ratio, for form I and form II obtained at 25°C in ethanol.
3. On diastereomer salts of RRA3 polymorph I and RRA3 polymorph II, using 100/0 at 50°C of polymorph I obtained in the phase equilibrium experiment and 60/40 at 50°C of polymorph II obtained in the equilibrium experiment.
4. On diastereomer salt of RSA2, using 0/100 sample from measurements done at 30°C.

3-1-8 Characterisation of crystallisation samples

X-ray powder diffraction, single crystal X-ray diffraction studies and thermal measurements (TGA and DSC) were performed by Professor Sally Price's group (Chemistry Department, UCL).

The samples obtained from the crystallisations were characterised by powder and single crystal X-ray diffraction. Powder X-ray diffraction was used when the crystallisation does not give adequate quality crystals for single crystal X-ray diffraction. Single crystal X-ray diffraction was used for unit cell checking when there are adequate single crystals available and for a full data collection when necessary (usually at 150K) so that the crystal structure can be fully solved and refined.

3-1-9 Experimental relative stabilities

The solution calorimetric measurements were done by Mr Lars Menken, a former PhD student (Chemical engineering Department, UCL). Solution calorimetry was used to determine the differences in the enthalpies of formation of the pairs of diastereomers salts studied[101]. For each salt, the enthalpy change, associated with the transition from the crystallised solid to a dilute aqueous solution (nominally at approaching infinite dilution), was measured.

The enthalpies and entropies of dissolution of salts (R)-1-phenylethylammonium – (R,S) 2-phenylpropanoate (A1) in ethanol were also calculated, from solubility data, as a means of assessing the differences in the state functions of formation of the solids. The solubility data obtained for the other two salt pairs was not suitable for fitting an appropriate model function.

The enthalpy and entropy of dissolution terms of the salts, from the solubility data, were obtained by fitting the function $\mathbf{lnS_{olubility} = -A/T + B}$, using the Gibbs free energy equation **(18)** (see section **2-5-5**).

After rearranging the equation **(18)** and replacing **lnK** by $\mathbf{ln_{solubility}}$, the equation **(41)** was obtained:

$$\mathbf{lnS_{olubility} = \frac{-\Delta H}{RT} + \frac{\Delta S}{R} = \frac{-A}{T} + B} \qquad \mathbf{(41)}$$

With $\mathbf{A = \Delta H/R}$ and $\mathbf{B = \Delta S/R}$, where R represents the gas constant of value 8.3144 $J.mol^{-1}K^{-1}$. It is important to note that here the solubility is dimensionless, as would be the case if expressed in terms of mole fractions.

3-2 Modelling methods

3-2-1 Experimental lattice energy minimisation calculation - ExptMinExpt

The initial studies of the lattice energy calculations involved testing the computational model for the intermolecular potential, which comprises an empirical exp-6 repulsion-dispersion potential[102] as described in the introduction and atomic multipoles computed with a distributed multipole analysis[88] from the MP2/6-31G(d,p) molecular charge density[93]. The solid state crystal structure (determined using X-ray data with the X-H bond lengths adjusted to standard neutron values[103]), obtained from the Cambridge Structural Database[104] or determined in this work, is lattice energy minimised using DMAREL[87] and is denoted ExptMinExpt. This rigid-body minimisation does not alter the molecular conformations. Hence, these preliminary minimisations aim to judge the quality of the intermolecular potential based on how well the crystal structure is reproduced. The experimentally determined molecular structure is the fundamental input in the ExptMinExpt minimisations.

ExptMinExpt minimisations were done, as shown in **Fig30** and as explained below:

- 1st NEIGHBOURS was run, using data from Cambridge Structural Database (CSD) file or data obtained through this work, to get crystal structure set up in Cartesian axes and the molecular structures in the local axis system from the output file fort.21. This NEIGHBOURS software extracts symmetry information from CSD file or data obtained through this work, to prepare the input files for calculation. Fort.21 is the output punched file from NEIGHBOURS, which contains all the information about the crystal structure in a Cartesian axis system.
- Then the molecular structure of each molecular ion was used in GAUSSIAN to give an *ab initio* charge density. The electronic structure energy calculations are complex and were second order Møller-Plesset calculations with a 6-31G(d,p) basis set. The GAUSSIAN calculation results are saved into a checkpoint file (*.chk).

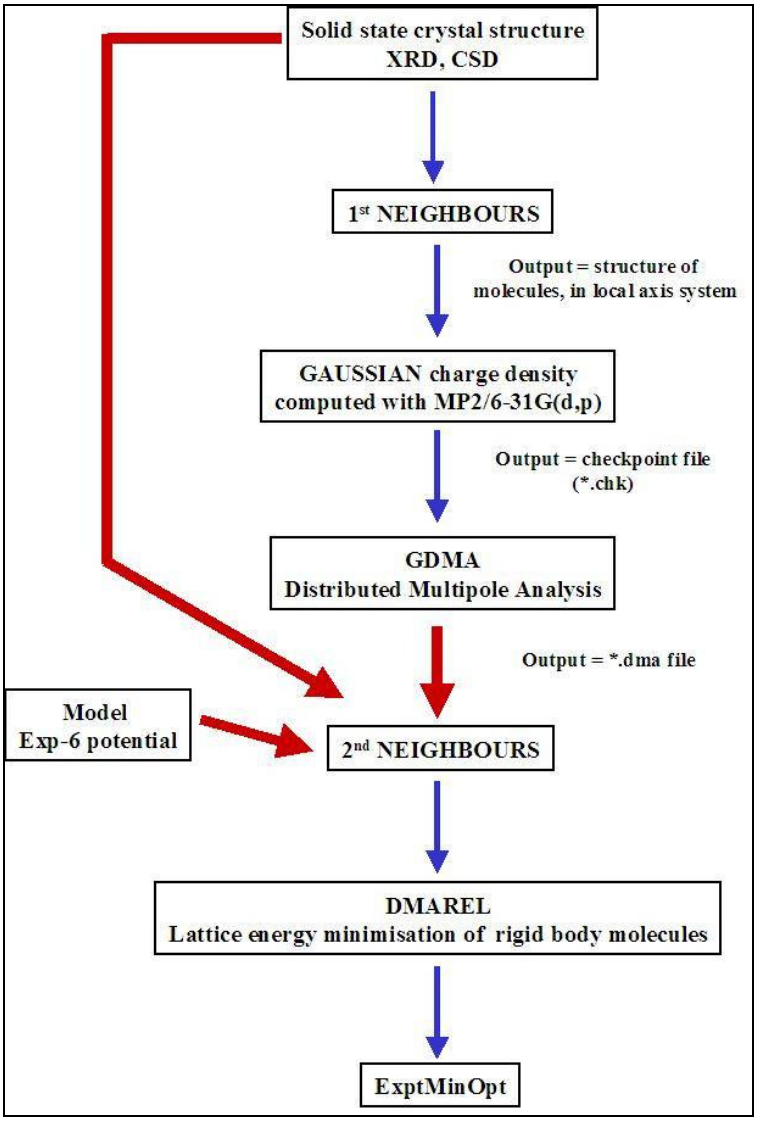

Fig30 Flow chart of ExptMinExpt minimisations

- Then the *ab initio* charge density was used to calculate a Distributed Multipole Analysis DMA punch file from GAUSSIAN with GDMA. The GDMA software uses the *.chk file as the input file for the analysis of Distributed Multipole Analysis (DMA), which describes electrostatic interactions. The GDMA code produces a set of atomic multipoles to represent the charge density of the molecule. These atomic multipoles can be used to calculate the electrostatic potential around the molecule. For the instance shown below (**Fig31**), acetic acid anion, where red surface relates to electron rich regions of the surface.

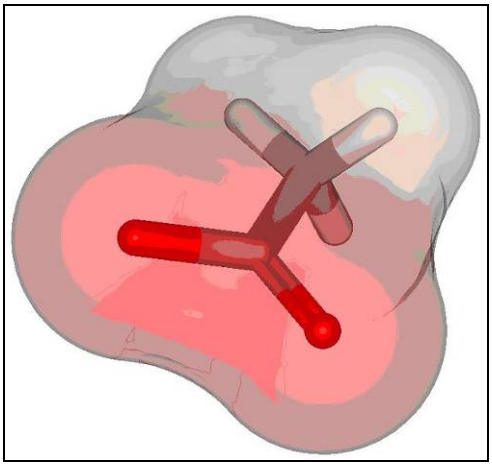

Fig31 Acetic acid anion moiety drawn with solvent accessible surface, coloured by electrostatic potential

The above image shows acetic acid anion within a charged envelope. As a repeated molecular ion is used to construct an ordered repeated three-dimensional structure, only the unique molecular ion's molecular conformation and DMA crystal need to be input explicitly in the calculation of bulk properties.

- 2nd NEIGHBOURS was run again with previously obtained DMA punch file, in addition to model exp-6 potential, the file containing the parameters and the initial crystal structure, to obtain a complete input for DMAREL.
- DMAREL was run to obtain the minimised lattice energy and 'ExptMinExpt' structure. DMAREL performs a lattice energy minimisation, where molecules are kept rigid, and the relative positions of the molecules and the cell parameters of the crystal structure are allowed to vary to find the most stable structure (lattice energy minimum).

3-2-2 Ion conformational energy or Intramolecular energy - ΔE_{Intra}

The most stable conformation of each ion in the gas phase was found by *ab initio* optimisation of the MP2/6-31G(d,p) electronic energy using Gaussian, to give the minimum of conformational energy $\mathbf{E_{min}}$. It was clear that these molecular conformations differed significantly from those in the crystal, but only in the torsions angles shown in **Fig32**. This showed that these angles were significantly affected by the crystal packing forces.

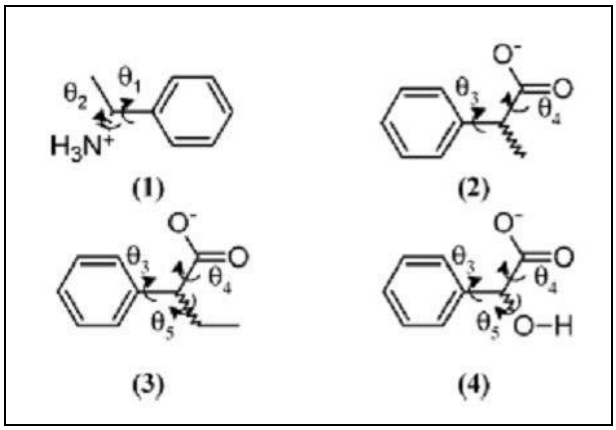

Fig32 Diastereomeric salt pair formed by (R)-2-phenylethylammonium (1) with (R,S)-2-phenylpropanoate (2), (R,S)-2-phenylbuyrate (3), and (R,S)-mandelate (4)[a]

[a] Torsion angles significantly affected by the packing forces and conatrained to their experimental values for evaluating ΔE_{intra} are indicated.

To evaluate the contribution to the lattice energy from the change in conformation, the ion conformations had the flexible torsion angles θ identified in **Fig32** constrained to their experimental values. The rest of the ion geometry was determined by MP2/6-31G(d,p) *ab initio* constrained optimisation using the electronic structure program GAUSSIAN[93]. This ensures that there is no contribution to $\mathbf{\Delta E_{intra}}$ from experimentally insignificant changes in bond lengths between the different experimental crystal structures. The ion conformational energies $\mathbf{\Delta E_{intra}}$, are expressed as the energy difference between the θ-constrained and global $\mathbf{E_{crystal}}$, and the unconstrained *ab initio* minima $\mathbf{E_{min}}$:

Intramolecular energy calculations were done as follows:

- For each of the ions in the system studied, an unconstrained GAUSSIAN optimisation was run at MP2/6-31G(d,p) level to find $\mathbf{E^{ion}_{min}}$.
- For each molecular ion in each crystal structure, a constrained GAUSSIAN optimisation at the same MP2/6-31G(d,p) level was performed with the θ_i of **Fig32** held at the experimental values to give the constrained optimisation ion geometries and $\mathbf{E^{ion}_{crystal}}$ energies.
- For each crystal structure $\mathbf{\Delta E_{intra}}$ was evaluated as **(42)**:

$$\Delta E_{intra} = \sum \Delta E_{intra} = (E^{anion}{}_{crystal} - E^{anion}{}_{min}) + (E^{cation}{}_{crystal} - E^{cation}{}_{min}) \qquad (42)$$

3-2-3 Theoretical lattice energy minimisation calculation accounting for conformational contributions to lattice energy - ExptMinCOpt

To obtain the intermolecular lattice energy that corresponds to other molecular conformations, the same procedure as described in for ExpMinExpt (**3-2-1**) was used, but with the *ab initio* constrained structure COpt.

ExptMinCOpt minimisations were done as explained below:

- A GAUSSIAN geometry optimisation was run first for each ion, with the angles in **Fig32** constrained to experimental values to obtain the constrained optimised molecular geometry. (The COpt calculation used to evaluate ΔE_{intra})
- These geometries were used to make a new crystal structure file, by overlaying each constrained optimised ion (COpt) geometry on the experimental ion by minimising the RMS difference in the positions of non-hydrogen atoms.
- 1st NEIGHBOURS was run to get the constrained optimised molecular structures in their local axes system.
- Then GAUSSIAN was run again on each ion to obtain the MP2/6-31G(d,p) *ab initio* charge distribution.
- This was then analysed to calculate a new DMA output (punch) file for each constrained optimised ion.
- Then 2nd NEIGHBOURS was run again with the DMA punch file, the crystal structure with the corresponding COpt ion calculations and the exp-6 potential parameters file.
- Then DMAREL was run to obtain the lattice energy minima ExptMinCOpt, with the ions held rigid in the constrained conformation. This gives the lattice energy $\mathbf{U_{inter}}$ from ExptMinCOpt lattice energy minimisations.
- The lattice energy **U** was evaluated as in equation **(43)**, as the sum of intermolecular contributions (ExptMinCOpt) $\mathbf{U_{inter}}$ and the ion conformational (intramolecular) energies $\mathbf{\Delta E_{Intra}}$:

$$U = U_{inter} + \Sigma \Delta E_{Intra} \quad (43)$$

- To assess how well a crystal structure has been reproduced after lattice energy minimisation, root-mean-square (RMS) percentage errors in the unit cell lengths and RMS error deviation in the overlay of all non-hydrogenic atoms in a 15-ion coordination sphere were analysed[105].

A comparison between ExptMinExpt and ExptMinCOpt can highlight the influence of molecular conformation on the crystal structure and hence elucidate the effect of the packing forces on the molecular geometries. If the ExptMinCOpt reproduction is much poorer than the ExptMinExpt, it means that assuming that only the constrained angles differ in vacuo and solid state is a gross oversimplification. We checked this in determining the angles in **Fig32,** which were constrained.

3-3 Summary

To investigate the chiral resolution via diastereomer salt formation, the following step-by-step methods were performed:

- Solubility measurements (to determine the relative stability of the enantiomers)
- Ternary equilibrium measurements (to maximise the information and understanding of the studied systems)
- Separability measurements (to determine the isomeric enrichment of the studied systems)
- Characterisation measurements (to determine the enantiomer ratio and characterise the samples)
- Modelling calculations (to predict the enantiomer stability of the studied systems).

The results of these experimental and modelling studies are presented in the following chapters.

4 EXPERIMENTAL RESULTS AND DISCUSSION

In the following sections the three sets of diastereomer salts studied will be called A1, A2 and A3 (see **Fig7**), where:

- **A1**: (R)-1-phenylethylammonium-(R,S)-2-phenylpropanoate
- **A2**: (R)-1-phenylethylammonium-(R,S)-2-phenylbutyrate
- **A3**: (R)-1-phenylethylammonium-(R,S)-mandelate.

In the previous chapter (Experimental and Modelling Methods), step-by-step methods used to determine experimental results (solubility measurements, ternary equilibrium measurements, separability measurements and characterisation measurements) and modelling results have been explained.

In this chapter, the experimental results obtained using the experimental methodologies are presented and discussed.

4-1 Experimental crystal structures and their structural characteristics

4-1-1 Experimental crystal structures

Table_9 contains a summary of molecular diagrams and structural information of all the three systems studied. The structures determined or re-determined in this work are highlighted in bold.

Successful single-crystal structure determinations have been carried out on diastereomer salts RSA1, RRA1, RRA2 and RRA3 at 150K. Details of the crystallographic data of all the experimentally determined enantiomorphic crystal structures are given in **Tables_10**, **Table_11** and **Table_12**. All the structures determined or re-determined through this work are shown in bold and for literature structures, the determination with the lowest temperature and R-factor are given. The R-factor (also called residual factor, reliability factor, R-value or R-work) is a measure of the agreement between the crystallographic model and the experimental X-ray diffraction data. It is the measure of how well the refined structure predicts the

observed data. The lower the R-factor, the better the crystal structure, with more ordered crystals.

Table_9 Summary of the systems studied

Systems	Molecular diagrams	Structures
(R)-1-phenylethylammonium – (R&S) 2-phenylpropanoate (**A1**)	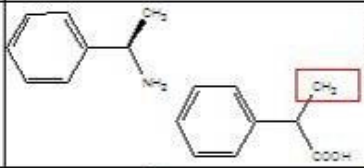	**RS-salt (p-salt)** **RR-salt I (n-salt I)** RR-salt II (n-salt II)
(R)-1-phenylethylammonium – (R&S) 2-phenylbutyrate (**A2**)	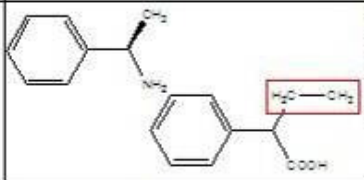	RS-salt (p-salt) **RR-salt I (n-salt I)** **RR-salt II (n-salt II)** **RR-salt III (n-salt III)**
(R)-1-phenylethylammonium – (R&S) mandelate (**A3**)	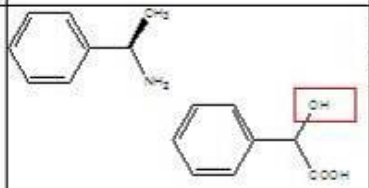	RS-salt (p-salt) **RR-salt I (n-salt I)** RR-salt II (n-salt II)

The crystallographic information, corresponding to the structures determined and re-determined through out this work (AFINEJ, NMACEP03, PBUPEA03, PBUPEA01, PBUPEA02 and PIVGEH01), are presented in **APPENDIX 2**.

The packing diagrams of the A1 structures determined through this work are given in **Fig33** and **Fig34**.

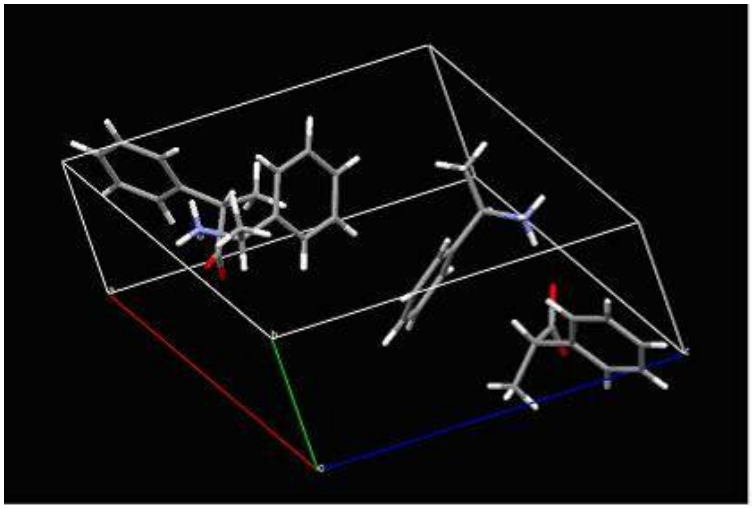

Fig33 Packing diagram of (R)-1-phenylethylammonium-(S)-2-phenylpropanoate (AFINEJ, drawn using Mercury[106])

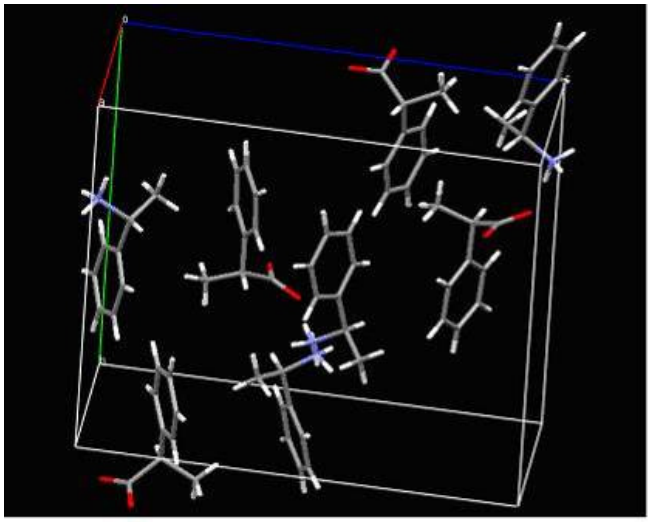

Fig34 Packing diagram of (R)-1-phenylethylammonium-(R)-2-phenylpropanoate polymorph I (NMACEP03, drawn using Mercury)

Table_10 Experimentally determined enantiomorphic crystal structures for (R)-1-phenylethylammonium, (R,S)-2-phenylpropanoate A1

Structure / CSD reference	**Symmetry** [a]	**Reduced cell**						**Density**	**Experimental details**
		a(Å)	b(Å)	c(Å)	α(°)	β(°)	γ(°)		
RS [b] (AFINEJ[107])	$P2_1$	6.539	11.008	12.160	116.0	90.00	90.00	1.146	SXRD, 150K, R-factor 4.07%
RR I [c]	$P2_12_12_1$	5.761	15.376	16.824	90.00	90.00	90.00	1.209	SXRD, 150K,

(NMACEP03[107])											R-factor 3.58%
RR II (NMACEP01[108])	$P2_12_12_1$	5.941	15.469	17.501	90.00	90.00	90.00			1.121	SXRD, RT, R-factor 3.15%

[a] Space group and number of crystallographically independent ion pairs is greater than one.

[b] Re-determined at lower temperature by SXRD, leading to smaller R-factor compared to CSD structures (PMACEP, PMACEP01)

[c] Re-determined at lower temperature by SXRD, leading to smaller R-factor compared to CSD structures (NMACEP02)

For the system (R)-1-phenylethylammonium-(R,S)-2-phenylpropanoate (**Table_10**), A1, the RR-salt has two polymorphs. The RR-salt polymorph I (with CSD ref code NMACEP03)[108] and the RR-salt polymorph II (with CSD ref code NMACEP01)[108] have already been determined in the literature[101]. The RS-salt is not polymorphic so far as only one structure is determined. The RS-salt structure is already given in the literature[109]. But RR-salt polymorph I, **Fig34** (with CSD ref code NMACEP03)[107] and RS-salt, **Fig33** (with CSD ref code AFINEJ)[107] have been re-determined in this work, with lower R-factor.

The packing diagrams of the A2 structures determined through this work are given in **Fig35**, **Fig36** and **Fig37**.

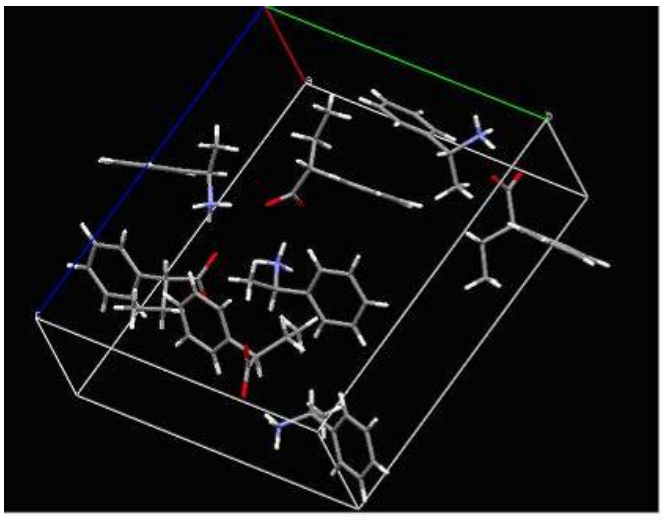

Fig35 Packing diagram of (R)-1-phenylethylammonium-(R)-2-phenylbutyrate polymorph I (PBUPEA03, drawn using Mercury)

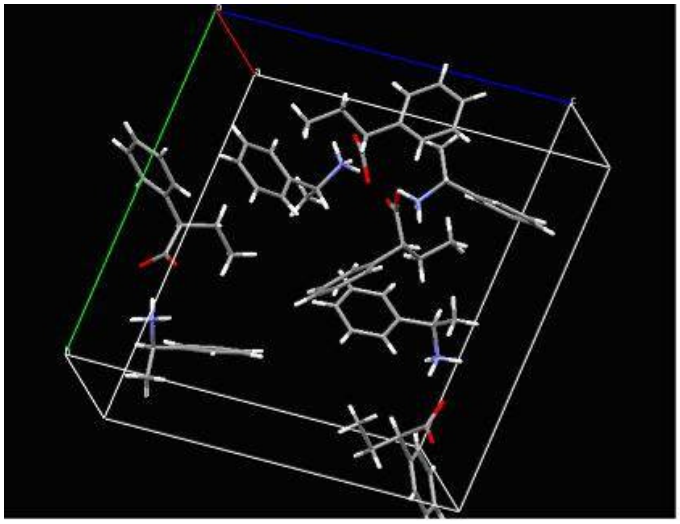

Fig36 Packing diagram of (R)-1-phenylethylammonium-(R)-2-phenylbutyrate polymorph II (PBUPEA01, drawn using Mercury)

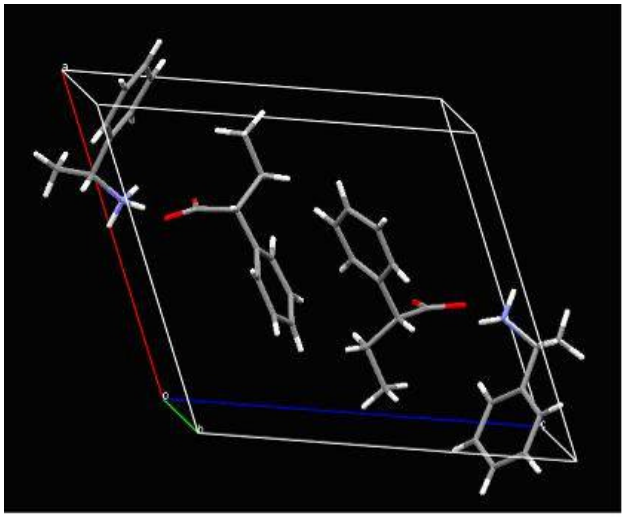

Fig37 Packing diagram of (R)-1-phenylethylammonium-(R)-2-phenylbutyrate polymorph III (PBUPEA02, drawn using Mercury)

Table_11 Experimentally determined enantiomorphic crystal structures for (R)-1-phenylethylammonium, (R,S)-2-phenylbutyrate A2

Structure / CSD reference	**Symmetry**[a]	**Reduced cell**						**Density**	**Experimental details**
		a(Å)	b(Å)	c(Å)	α(°)	β(°)	γ(°)		
RS (PEAPEA10[110])	$P4_1$	6.408	16.642	16.642	90.00	90.00	90.00	1.068	SXRD, RT, R-factor 5.06% Hydrogen atoms

									coordinates not determined
RR I[b] (PBUPEA03[107])	$P2_12_12_1$	5.757	15.433	17.571	90.00	90.00	90.00	1.214	SXRD, 150K, R_{wp} 3.98%
RR II (PBUPEA01[111])	$P2_12_12_1$	6.062	16.781	16.891	90.00	90.00	90.00	1.103	PXRD, 295K, R_{wp} 2.20%
RR III (PBUPEA02[112])	$P2_1$	5.978	11.883	13.076	113.51	90.00	90.00	1.113	PXRD, 150K, R_{wp} 3.10%

[a] Space group and number of crystallographically independent ion pairs is greater than one.

[b] Re-determined at lower temperature by SXRD, leading to smaller R-factor compared to CSD structures (PBUPEA)

For the system (R)-1-phenylethylammonium-(R,S)-2-phenylbutyrate (**Table_11**), A2, the RR-salt is polymorphic and there are three confirmed polymorphic structures. The RS-salt is not polymorphic (at present). The RS-salt structure already exists in the literature (with CSD ref code PEAPEA10)[113]. The RR-salt polymorph I is taken from the literature (with CSD ref code PBUPEA)[114], but a better structure has been re-determined through experimental results, **Fig35** (with CSD ref code PBUPEA03)[107], with lower R-factor. The RR-salt polymorphs II and III, **Fig36** and **Fig37** respectively (with CSD ref codes PBUPEA01[111] and PBUPEA02[112]), were discovered and structurally determined through this project as well.

All attempts to crystallise RSA2 produced thin needles. However, capillary PXRD measurements yielded a sufficiently good quality pattern that was indexed to the same space group and cell constants reported in an earlier determination (PEAPEA)[110].

The packing diagrams of the A3 structure determined through this work if given in **Fig38**.

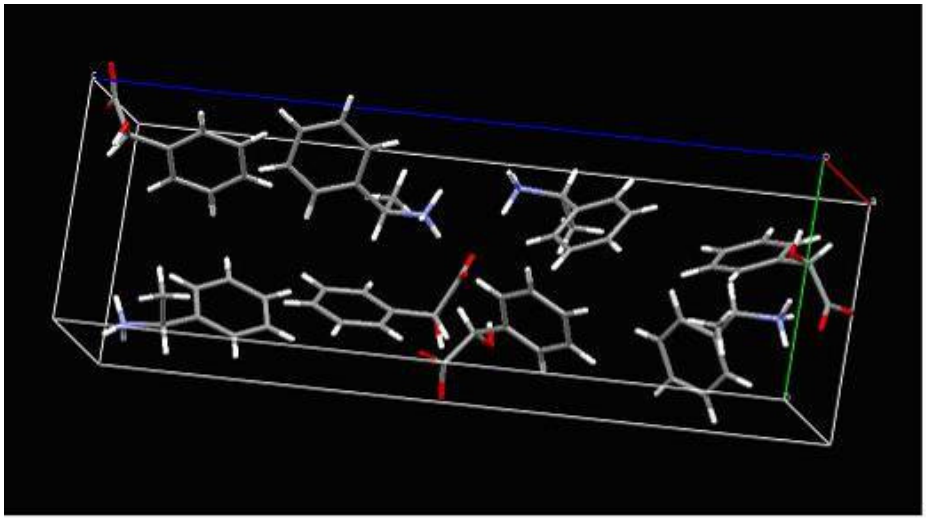

Fig38 Packing diagram of (R)-1-phenylethylammonium-(R)-2-mandelate polymorph I (PIVGEH01, drawn using Mercury)

Table_12 Experimentally determined enantiomorphic crystal structures for (R)-1-phenylethylammonium, (R,S)-2-mandelate A3

Structure / CSD reference	**Symmetry** [a]	**Reduced cell**						**Density**	**Experimental details**
		a(Å)	b(Å)	c(Å)	α(°)	β(°)	γ(°)		
RS (PIVGEG[115])	$P1$, Z' = 4	6.398	14.807	16.109	75.33	82.97	81.03	1.250	PXRD, 122K, R-factor 4.49%[e]
RR I[b] (PIVGEH01[107])	$P2_12_12_1$	6.849	8.325	25.441	90.00	90.00	90.00	1.252	SXRD, 150K, R-factor 5.88%
RR II (PEAMAN01[116])	$P2_1$	6.801	8.322	12.885	91.74	90.00	90.00	1.245	SXRD, 122K, R-factor 4.4%

[a] Space group and number of crystallographically independent ion pairs is greater than one.

[b] Re-determined at lower temperature by SXRD, leading to smaller R-factor compared to CSD structures (PEAMAN).

For the system (R)-1-phenylethylammonium-(R,S)-mandelate (**Table_12**), A3, the RS-salt (with CSD ref code PIVGEG)[117] is not polymorphic (at present), but the RR-salt exists as two polymorphs. RR-salt polymorph I, **Fig38**, has been re-determined through this work (with CDS ref code PIVGEH01)[107]. The RR-salt polymorph II already exists in the literature (with CSD ref codes PEAMAN01[116] and PEAMAN[118] for which the H atoms have been added using the SHELX program, in order to do

lattice energy minimisation calculations), but a better structure is determined through this work.

Attempts to grow single crystal RSA3 failed. Powder samples were confirmed to be the reported *P*1 crystal structure with Z' = 4 (PIVGEG). The modelling of this form required special attention as discussed in the molecular modelling methods.

The packing diagrams of the other studied structures (the ones not determined through this work) are presented in the **APPENDIX 3**.

4-1-2 Experimental relative stability

The results of the experimental measurements of the relative stability of the three diastereomeric salt pair crystal structures are summarised in **Table_13** and **Table_14**.

Table_13 Summary of thermal measurements

System[b]	Onset (K)	Peak (K)	ΔH[a] (KJ/mol)	Remarks
RS-A1	-	437.0	42.31	Melting
RR-A1 Polymorph I	-	377.9	4.74	Transformation to RR II
RR-A1 Polymorph II	-	422.0	39.66	Melting
RS-A2	405.8	408.1	44.50	Melting
RR-A2 Polymorph I	378.5	382.7	6.10	Transformation to RR III
RR-A2 Polymorph II	386.2	373.0	0.98	Transformation to RR III
RR-A2 Polymorph III	424.7 - 434.7	433.7 - 438.8	40.21 – 43.17	Melting, decomposition with > 10% mass loss[c]
RS[d]-A3	383.0	389.7	22.44	Melting
RR-A3 Polymorph I	452.9	463.9	36.82	Melting, decomposition with 9.2% mass loss[c]
RR-A3 Polymorph II	445.4	453.6	33.63	Melting, decomposition with 9.6% mass loss[c]

[a] all enthalpies reported correspond to endothermic events.

[b] for A1 system, thermal analysis data were taken from reference[119] detailed thermal measurements (DSC and variable temperature XPRD) for A2 and A3 systems can be found in **APPENDIX 4** and **APPENDIX 5** respectively.

[c] significant mass loss indicates that the heat of fusion cannot be used in quantitative comparisons with theoretical predictions due to sample decomposition. The melting temperature and heat of fusion for

RR-A2 polymorph III shows significant variation depending on the quantity of the sample used and rate of heating leading to variable degrees of mass loss and decomposition.

[d] a minor endothermic event (ΔH = -0.81 kJ/mol) is also observed with onset at 353.5K (peak 358.2K). Variable temperature PXRD showed that this event is not accompanied by appreciable changes in the structure of the system.

Table_14 Thermodynamic data from solution calorimetry[120] at room temperature and solubility measurements[121]

System	Solution calorimetry (water, room temperature)		Solubility measurements (ethanol)[a]		
	ΔH_{diss} (kJ/mol)	$\Delta[\Delta H_{diss}]^b$ (kJ/mol)	ΔH_{diss} (kJ/mol)	$\Delta[\Delta H_{diss}]^b$ (kJ/mol)	ΔS_{diss} (J/mol/K)
RS-A1	7.08	-3.88	27.54	-4.99	66.62
RR-A1 I	10.96		32.53		89.14
RS-A3	0.45	-14.98			
RR-A3 I	15.43				

[a] the enthalpy and entropy of dissolution were approximately determined in the temperature range 283-322 K by assuming unit activity coefficients and full dissociation of the salts in ethanol solution, as observed by HPLC

[b] defined as: $\Delta[\Delta H_{diss}] = \Delta H_{diss}$[RS-salt] - ΔH_{diss}[RR-salt]

Heat of fusion and solution calorimetry measurements are used to determine enthalpy differences, whilst solubility ratio measurements are typically used to establish differences in the Gibbs free energy. In this investigation, we have to assume that the free energy and enthalpy order is the same and independent of temperature, i.e. the zero-point and thermal contributions are equal for all crystal structures. This is necessary to derive an approximate stability order of the diastereomers and their polymorphs that allow a direct, qualitative comparison with static lattice energy calculations.

For the A1 system, RS diastereomer is known to exist in one form[108,114], whilst the RR diastereomer has two enantiotropically related polymorphs with RR I[108,109] being more stable than RR II[109] at low temperatures (first row of **Table_13**). The heat of the endothermic transition[119] RR I → RR II is -4.74 kJ/mol. The solution calorimetry measurements show that the RR I diastereomer has 3.88 kJ/mol (**Table_14**) lower enthalpy of formation than RS at room temperature, which agrees well with the

approximate value of 4.99 kJ/mol obtained by fitting the Van't Hoff equation to solubility measurements[121] in the temperature range 283 – 323K. However, the RS diastereomer has lower solubility[121] above 283K that indicates that its Gibbs free energy is lower at high temperatures. This is in good agreement with the RS having lower entropy of dissolution than RR I (its crystal structure has 22.5 J/mol/K higher entropy) and also being less dense at room temperature. These results clearly indicate that the interaction between enthalpic and entropic contributions to the Gibbs free energy changes the stability order of the diastereomers at different temperatures.

The A2 system has one RS and three RR diastereomeric salt structures. The endothermic transitions (second row of **Table_13**) RR I → RR III (onset 378.5K, ΔH = -6.10 kJ/mol) and RR II → RR III (onset 386.2K, ΔH = -0.98 kJ/mol) suggest[122,123] that RR III is enantiotropically related to both RR I and RR II. RR I is probably the thermodynamically most stable at low temperatures given that the transition RR I → RR III is significantly more endothermic than RR II → RR III.

The A3 system exhibits two RR polymorphs. If we ignore the decomposition during their heating, we can conclude that they are monotropically related (RR I < RR II), as the lower melting polymorph has lower enthalpy of fusion (third row of **Table_13**).

The RR polymorphs are significantly more stable than the only known RS structure, as they have significantly higher melting points and heats of fusion. This is consistent with the significantly higher enthalpy of dissolution of RR I compared with RS (and hence lower enthalpy of formation $H_{RR\ I} - H_{RS}$ = -14.98 kJ/mol at room temperature as in **Table_14**).

4-2 Solubility measurements

The solubilities of the six individual diastereomer salts studied (RRA1, RSA1, RRA2, RSA2, RRA3 and RSA3), in ethanol, were measured between 5 and 60°C, by combining (R)-1-phenylethylamine with the corresponding acid enantiomer.

4-2-1 Solubility curve of (R)-1-phenylethylammonium-(R,S)-2-phenylpropanoate A1

The A1 salts exhibit the conservative pattern of increasing solubility with temperature as shown in **Fig39**, with no phase transition detected across the temperature range investigated. The solubilities of A1 diastereomeric salt increase with the temperature. It is also observable that RS-form is less soluble than the RR-form. This indicates that the RS-form would precipitate more easily than the RR-form.

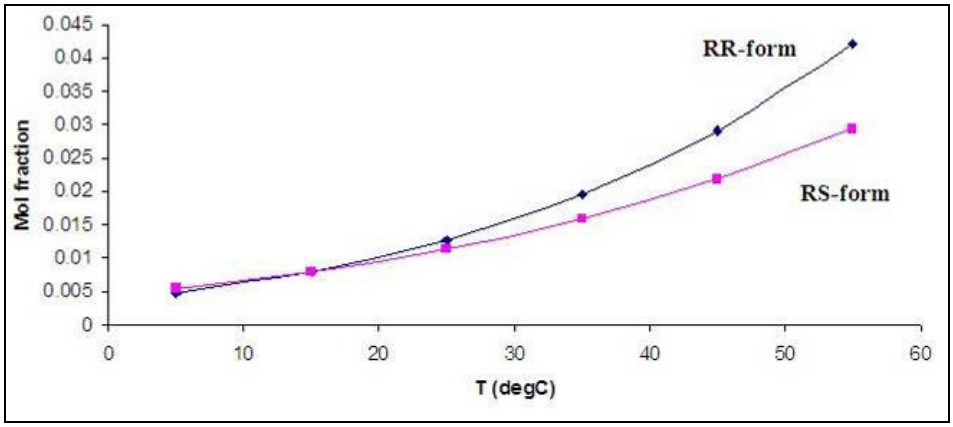

Fig39 Solubility versus temperature for A1 individual diastereomer salts

A plot of the natural logarithm of the equilibrium constant (in our case the solubility **s**) measured for certain equilibrium versus the reciprocal temperature gives a straight line, the slope of which is the negative of the enthalpy change **ΔH** divided by the gas constant and the intercept of which is equal to the entropy change **ΔS** divided by the gas constant. The graphs, corresponding to $\mathbf{ln_{Solubility}}$ versus **1/Temperature** corresponding to the calculation of **ΔH** and **ΔS** of the RRA1 and RSA1 diastereomer salts, are given in the **Fig40** and **Fig41 (APPENDIX 6)** and the results corresponding to the graphs are given in **Tables_15** and **Table_16 (APPENDIX 6)**.

Regression of these data gave the enthalpies and entropies of dissolution, which are shown in **Table_17**, with a very good fit of the data to the model equation (R^2 = 0.998). The difference between the calculated enthalpies of dissolution [$\mathbf{\Delta H_{diss}(RS) - \Delta H_{diss}(RR)}$] of -4.99 kJmol^{-1} agrees well with the corresponding value obtained for the dissolution of the diastereomers in water by solution calorimetry[65], -3.88 kJmol^{-1}.

The Van't Hoff equation in chemical thermodynamics relates the change in temperature to the change in the equilibrium constant given the enthalpy change. It assumes enthalpy change is constant over the temperature range (applicable to non-ideal solution, where $\Delta\mathbf{H}$ and $\Delta\mathbf{S}$ are averaged over the temperature range).

Table_17 Enthalpies and entropies of dissolution of salts A1 in ethanol from solubility measurements

Diastereomer	ΔH_{diss} (kJ mol^{-1})	ΔS_{diss} (J mol^{-1} K^{-1})
RS-form	27.54	66.62
RR-form	32.53	89.14

Fig39 shows that (R)-1-phenylethylamine-(S)-2-phenylpropanoate is less soluble than (R)-1-phenylethylamine-(R)-2-phenylpropanoate at temperatures above 20°C, which corresponds to a lower free energy of formation of the crystalline RS solid. The RS-form is entropically stabilised, with the entropy contribution to the free energy determining the relative stability and solubility of the diastereomer pair in this temperature region. The difference in the entropies of dissolution in **Table_17** is larger than the difference in the corresponding enthalpies. The suggested use of the differences in the enthalpies of formation of the solid as indicators of relative solubility and the propensity to separate[68,124] will therefore give the wrong ordering in this case.

4-2-2 Solubility curve of (R)-1-phenylethylammonium-(R,S)-2-phenylbutyrate A2

For the A2 system, the solubility curves of the salts are given below in **Fig42**. The RR-form is considerably less soluble than the RS-form across the temperature range investigated. This indicates that the RR-form would precipitate more easily than the RS-form.

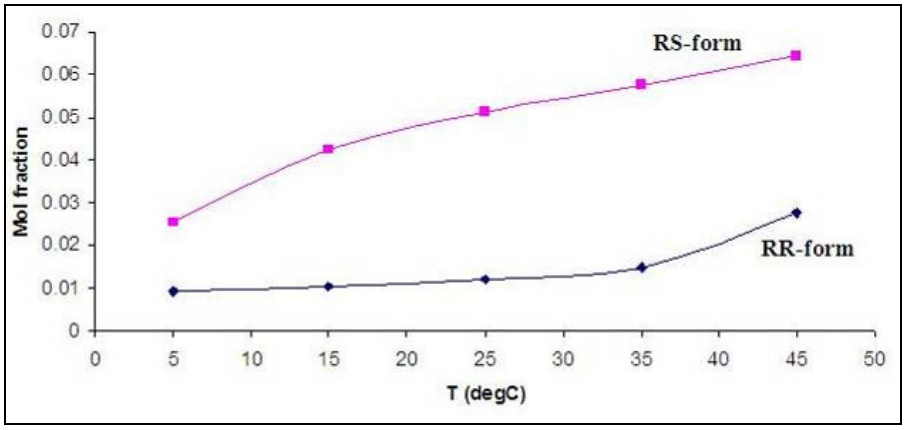

Fig42 Solubility versus temperature for A2 individual diastereomer salts

For the A2 system, the enthalpy and entropy of RRA2 and RSA2 diastereomer salts have not been calculated, by plotting the graphs **ln (solubility of R_{A2}) = f (-1/T)** and **ln (solubility of S_{A2}) = f (-1/T)**, because the solubility curves are not well represented by the modified Van't Hoff equation, and therefore the parameters cannot be fitted accurately.

4-2-3 Solubility curve of (R)-1-phenylethylammonium-(R,S)-mandelate A3

For the A3 system, the solubility curves of the salts are given below in **Fig43**. The RR-form is considerably less soluble than the RS-form across the temperature range investigated. This indicates that the RR-form would precipitate more easily than the RS-form.

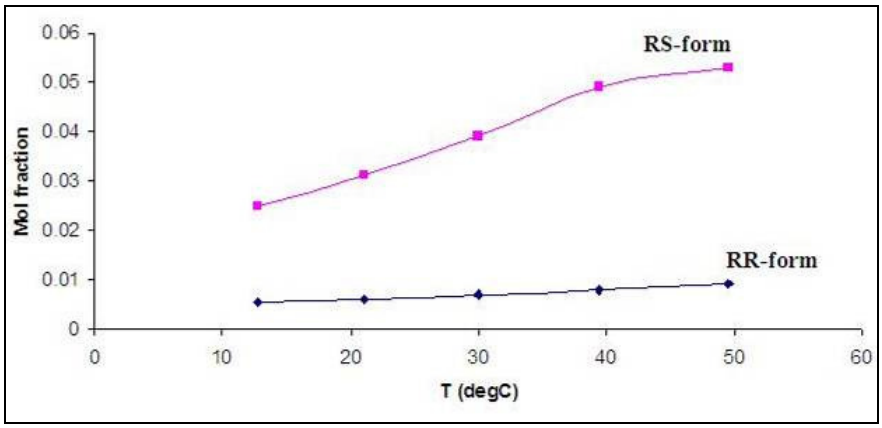

Fig43 Solubility versus temperature for A3 individual diastereomer salts

The enthalpy and entropy of RR and RSA3 salts have not been calculated, by plotting the graphs **ln (solubility) = f (-1/T)**, as for A2 curve fitting is not feasible.

4-3 Phase equilibria

Ternary phase relationships for the three diastereomeric systems (RS)-salt-(RR)-salt-ethanol have been measured at 30 and 50°C.

4-3-1 Phase equilibria of system (R)-1-phenylethylammonium-(R,S)-2-phenylpropanoate A1

Fig44 shows the equilibrium behaviour of A1 system and the solid-solution equilibrium data for points on ternary diagram is given in **Table_18**.

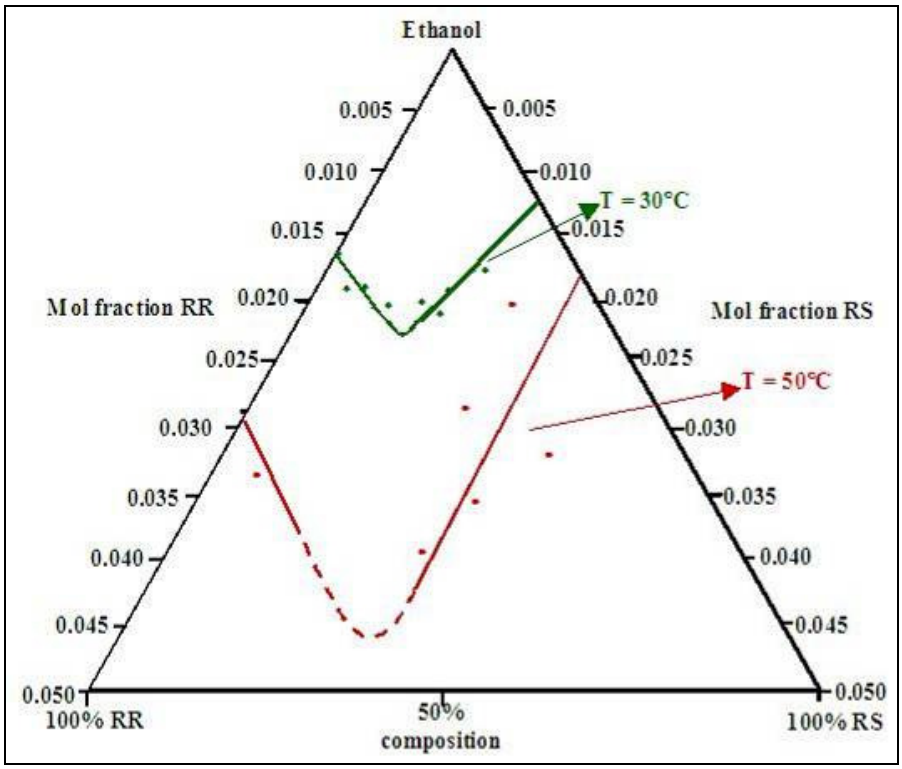

Fig44 Isothermal ternary solution equilibria for A1 diastereomer salts at 30 and 50°C

Table_18 Solid solution equilibrium data (mol fraction) for points on solubility curves of A1

Temperature °C	Starting RR:RS composition	Point on solubility curve (solution composition)		Tie-line intercept RR-RS axis (solid composition)	
		Overall molfraction	Solution composition	RR molfraction	Solid composition
30	90:10	0.0189	85.5:14.5	0.973	97.3:2.7
	40:60	0.0179	48.5:51.5	0.148	14.8:85.2
	25:75	0.0162	36.7:63.3	0.044	4.4:95.6
	20:80	0.0153	34.3:65.7	0.041	4.1:95.9
50	90:10	0.0366	88.1:11.9	0.985	98.5:1.5
	50:50	0.0354	53.5:46.6	0.386	38.6:61.4
	40:60	0.0341	44.8:55.2	0.204	20.4:79.6
	25:75	0.0253	43.5:56.5	0.181	18.1:81.9
	20:80	0.0307	28.6:71.4	0.134	13.4:86.6
	10:90	0.0189	27.0:73.0	0.114	11.4:88.6

The solid solution equilibrium data are calculated using the equilibrium results presented in **APPENDIX 7**. It also contains the work sheets corresponding to the equilibrium results of A1 at 30 and 50°C.

The phase diagram of A1 presented in **Fig44** only contains the isothermal ternary solution equilibria for A1 diastereomer salts at 30 and 50°C, as the ternary solid composition (tie-line intercept) does not fit into the scale used in **Fig44** (i.e. mol fraction from 0 to 0.050). If the ternary solid composition has also been included into this phase diagram, then it would have been very difficult to observe the solution equilibria into such a big scale (i.e. mol fraction from 0 to 1, rather than 0 to 0.050). And therefore the tie-lines have not been included in **Fig44**.

To get an idea of how the phase diagram, containing both solution equilibria data and the tie-line intercepts, would look, a ternary isotherm was redrawn (**Fig45**), ignoring the scale, exhibiting the solid solution of RSA1 salt in the pure RRA1 solid phase and RRA1 salt in the pure RSA1 solid phase.

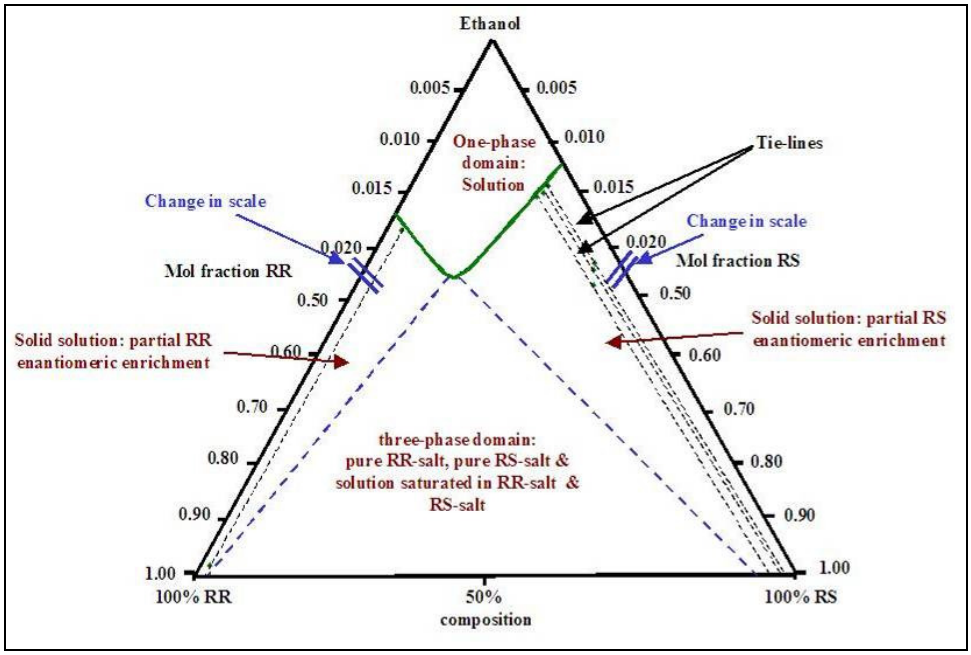

Fig45 Representation of solid solution of A1 diastereomer salt at 30°C

In **Fig44**, the red curve corresponds to ternary phase equilibria performed at 50°C and the one in green corresponds to 30°C. The equilibrium results, for the system A1 show a eutonic corresponding to RR:RS ratio around 70:30 at 30°C. At 50°C, very few data points were obtained in the near vicinity of this composition, but the data on either side of it are consistent with such a feature at the higher temperature. It is also observable that the RR diastereomer salt is more soluble than the RS diastereomer salt (i.e. RS form would precipitate more easily than the RR form of the diastereomer salt). This is consistent with the solubility data (**Fig39**). The tie-line data indicate solid solutions in the equilibrated solids. To investigate further whether solid solutions form in this case, individual single crystals were sampled from crystallised products obtained through separability measurements, and their compositions were compared with the bulked data from the corresponding separation measurement in following **Table_19**. The compositions of the individual crystals correspond quite closely to the bulk compositions, which indicated that the crystallised product comprises of a solid solution, with the composition of each individual crystal roughly equal.

Table_19 Comparison of the compositions of bulk crystallised products from separation measurements of A1 salts with individual crystal compositions

Initial RR:RS ratio	Isolation Temperature °C	RR:RS ratio of the bulk crystallised product	RR:RS ratio of selected individual crystals
75/25	20	89.9:10.1	86.3:13.7
			91.5:8.5
			90.6:9.4
			89.1:10.9
			90.1:9.9
			90.2:9.8
25/75	20	4.5:95.5	1.9:98.1
			3.2:96.8
			4.4:95.6

4-3-2 Phase equilibria of system (R)-1-phenylethylammonium-(R,S)-2-phenylbutyrate A2

Fig46 shows the ternary diagram of the A2 system and the solid solution equilibrium data for points on ternary diagram is given in **Table_20**.

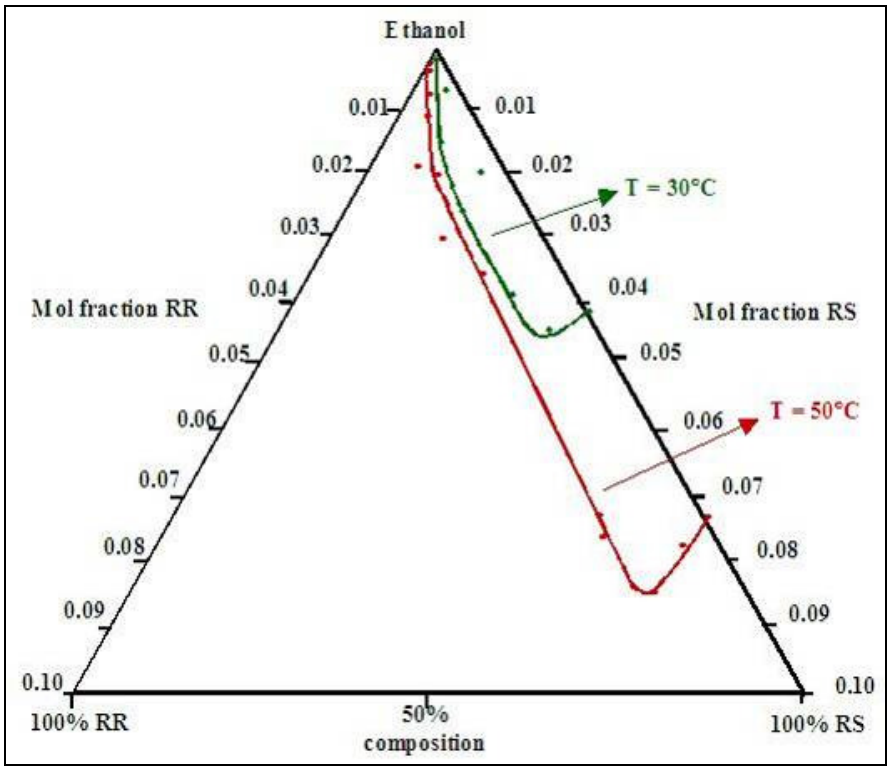

Fig46 Isothermal ternary solution equilibria for A2 diastereomer salts at 30 and 50°C

Table_20 Solid solution equilibrium data (mol fraction) for points on solubility curves of A2

Temperature °C	Starting RR:RS composition	Point on solubility curve (solution composition)		Tie-line intercept RR-RS axis (solid composition)	
		Overall molfraction	Solution composition	RR molfraction	Solid composition
30	90:10	0.0068	74.8:25.2	0.767	76.7:23.3
	25:75	0.0187	21.9:78.1	0.00	0:100
	20:80	0.0452	19.9:80.1	0.00	0:100
50	90:10	0.0048	84.4:15.2	0.968	96.8:3.2
	75:25	0.0210	26.8:73.2	0.914	91.4:8.6
	50:50	0.0313	49.5:50.5	0.882	88.2:11.8
	30:70	0.0370	26.4:73.6	0.433	43.3:56.7
	20:80	0.0728	14.5:85.5	0.681	68.1:31.9
	15:85	0.0865	13.1:86.9	0.403	40.3:59.7
	10:90	0.0811	6.4:93.63	0.333	33.3:66.7

Here again, the phase diagram of A2 presented in **Fig46** only contains the isothermal ternary solution equilibria for A2 diastereomer salts at 30 and 50°C, as the ternary solid composition (tie-line intercept) does not fit into the scale used in **Fig46**. In this A2 phase diagram, the red curve corresponds to ternary phase equilibria performed at 50°C and the one in green corresponds to 30°C. This ternary diagram exhibits a eutonic point at low RR:RS ratios (around 15:85) at 50°C. The eutonic is still detectable at 30°C, but is very much less marked than at 50°C. The phase diagram also shows that RR diastereomer salt is less soluble than the RS-salt (i.e. RR diastereomer salt would precipitate more easily than the RS salt), which is consistent with the solubility data of the A2 system (**Fig42**). The tie-line data (**Table_20**) indicate solid solutions in the equilibrated solids.

APPENDIX 8 contains the work sheets corresponding to the equilibrium results of A2 at 30 and 50°C.

4-3-3 Phase equilibria of system (R)-1-phenylethylammonium-(R,S)-mandelate A3

Fig47 shows the ternary diagram of the A3 system and the solid solution equilibrium data for points on ternary diagram is given in **Table_21**.

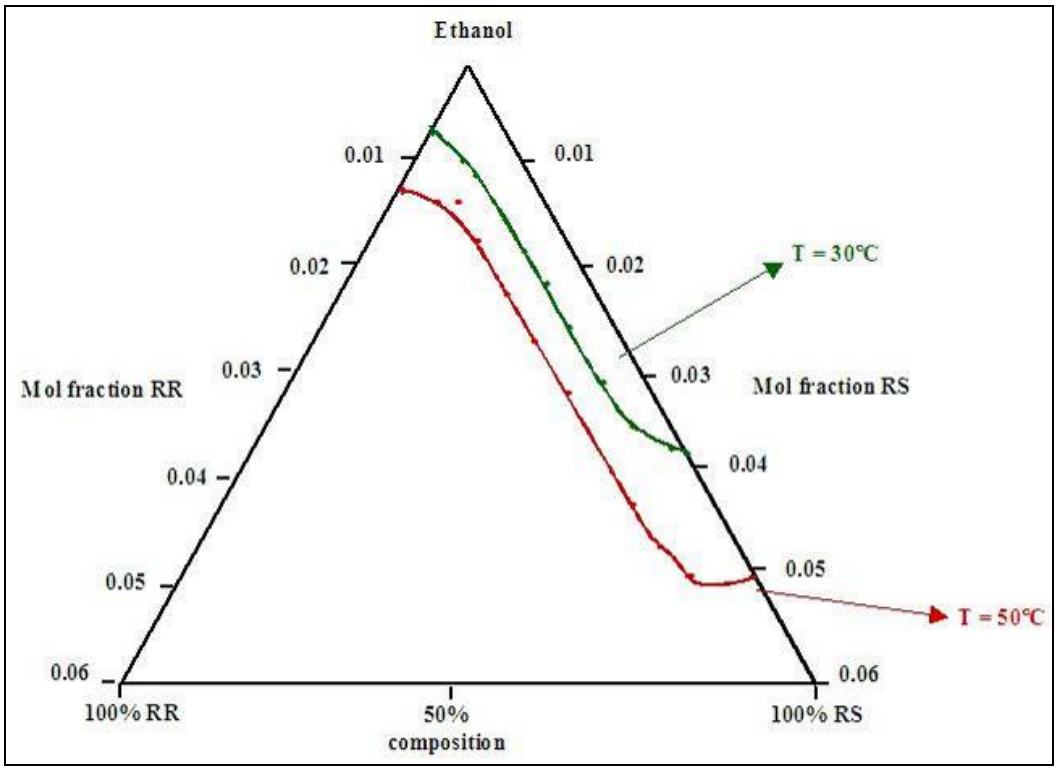

Fig47 Isothermal ternary solution equilibria for A3 diastereomer salts at 30 and 50°C

Table_21 Solid solution equilibrium data (mol fraction) for points on solubility curves of A3

Temperature °C	Starting RR:RS composition	Point on solubility curve (solution composition)		Tie-line intercept RR-RS axis (solid composition)	
		Overall molfraction	Solution composition	RR molfraction	Solid composition
30	80:20	0.0092	44.3:55.7	0.890	89.0:11.0
	75:25	0.0113	41.7:58.3	0.866	86.6:13.4
	50:50	0.0184	25.3:74.7	0.714	71.4:28.6
	40:60	0.0235	18.8:81.2	0.657	65.7:34.3
	20:80	0.0318	11.3:88.7	0.558	55.8:44.2
	10:90	0.0362	9.2:90.8	0.270	27.0:73.0
50	90:10	0.0109	78.4:21.6	0.933	93.3:6.7

	80:20	0.0133	51.8:48.2	0.902	90.2:9.8
	60:40	0.0236	35.5:64.5	0.805	80.5:19.5
	50:50	0.0284	29.7:70.3	0.736	73.6:26.4
	40:60	0.0331	24.9:75.1	0.661	66.1:33.9
	20:80	0.0464	17.4:82.6	0.566	56.6:43.4

Here again, the phase diagram of A3 presented in **Fig47** only contains the isothermal ternary solution equilibria for A3 diastereomer salts at 30 and 50°C, as the ternary solid composition (tie-line intercept) does not fit into the scale used in **Fig47**. In this A3 phase diagram, the red curve corresponds to ternary phase equilibria performed at 50°C and the one in green corresponds to 30°C.

For the mandelate salts, the curve indicates a near-ideal pattern of solubility behaviour of the salt mixtures (the effect of the less soluble species on the solvent activity is very small, giving rise to near ideal behaviour of the mixed system). However, the solubility curves do show some curvature to the ethanol-(RS)-salt axis, indicating that there may be slightly increased total solubility where small quantities of the (RR)-salt are present. The phase diagram also shows that RR diastereomer salt is less soluble than the RS salt, which is consistent with the solubility data (**Fig43**). The tie-line data in the **Table_21** accompanying **Fig47**, obtained by analysing the solids recovered at equilibrium with the solution concentrations, are all composed of mixtures of the (RR)- and (RS)-salts, and indicate that the equilibrium solid phases are probably solid solutions. Some of the individual crystals have been HPLC analysed and they have been found containing RR and RS salts.

APPENDIX 9 contains the work sheets corresponding to the equilibrium results of A3 at 30 and 50°C.

4-4 Separability Measurements

Results for the separation of the three diastereomer pairs in single cooling crystallisations are given below for each of the systems A1, A2 and A3 studied, in the form of graph. The abscissae of these graphs show the RR:RS ratio at the start of the experiments. The ordinates show the isomeric ‘enrichments’ of the crystal products

for each experiment. The enrichment expresses the extent to which the compositions of the crystallised solids approach a pure single enantiomer (100%) from the initial RR:RS ratio (0%), with the sign convention that enrichments in RR are designated positive and those in RS negative. For cases where the RR-salt is enriched in the crystallised product, the enrichment is calculated as in equation **(44)**:

$$\text{Enrichment } \% = \frac{\text{RR\% in product crystals} - \text{RR\% at start of experiment}}{\text{100\% RR} - \text{RS\% at start of experiment}} \times 100 \qquad \textbf{(44)}$$

And where the RS-salt is enriched the enrichment is calculated as in equation **(45)**:

$$\text{Enrichment } \% = \frac{-[\text{RS\% at start of experiment} - \text{RS\% in product crystals}]}{\text{100\% RS} - \text{RS\% at start of experiment}} \times 100 \qquad \textbf{(45)}$$

The following sections contain the separability diagrams for the three systems studied.

4-4-1 Separability measurements of (R)-1-phenylethylammonium-(R,S)-2-phenylpropanoate A1

APPENDIX 10 contains the separability calculation sheet of A1 system.

Fig48 contains the separability results of A1 diastereomer salts by cooling crystallisation. The enriched diastereomer salts, compared to the initial compositions, have been isolated at 4, 6, 20 and 30°C.

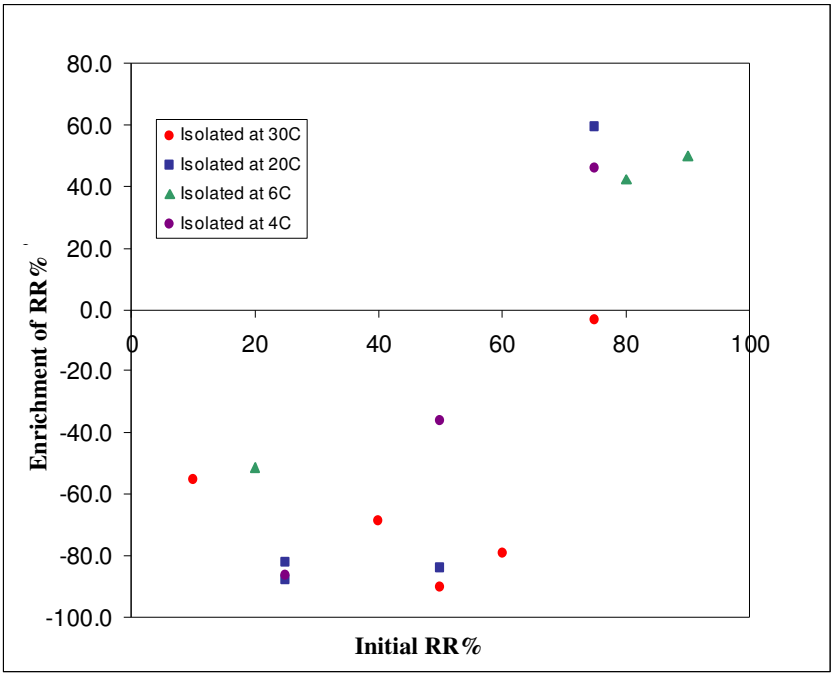

Fig48 Measured separations by cooling crystallisation of A1 diastereomer salts

For this A1 system, as shown in **Fig48**, a sharp reversal in the direction of enrichment, around RR:RS ratio of 70:30, is observed. With starting RR:RS compositions below 70%, the RS-diastereomer is enriched in the crystallised product, while the RR-isomer is enriched where the starting composition exceeds 70% of the RR-form. The (total) crystallised solid recoveries obtained at the various isolation temperatures used are given in **Table_22**.

Table_22 Total crystallised solid recoveries of A1 salts at different isolation temperature

Isolation temperature (°C)	Mean solid recovery (%)	Standard deviation (abs. %)
30	15.6	2.3
20	26.0	6.2
6	60.8	4.5
4	46.9	5.2

Initial temperature 50°C, cooling rate 0.5 $Kmin^{-1}$.

The change in direction of enrichment is entirely consistent with the eutonic behaviour exhibited in the ternary phase diagram. The existence of the eutonic as a composition of maximum total solubility implies that, in any fractional crystallisation

controlled by solubility considerations, the less soluble single salts on either side of the eutonic will preferentially separate from the solution. The reversal in the separability diagram occurs at an initial RR:RS ratio of 70:30, where the ternary diagram of A1 shows eutonic at both 30 and 50°C.

The enrichment in the separability measurements do not show significant, systematic variations with isolation temperature, although **Table_22** indicates that the recoveries generally exhibited an increase with decreasing temperature, as would be expected with the corresponding decrease in salt solubilities shown in the solubility curves of A1. The similarities in the solubilities of the two diastereomer salts below 20°C suggests that the numerical value of the enrichments on either side of the 70:30 divide should also be similar, as is the case. Generally, the enrichments appear slightly more extreme at the higher isolation temperatures, with smaller solid yields, although we cannot demonstrate that the effect is experimentally significant. Conventionally, enrichment tends to decrease with increasing solid separation, because the solution becomes progressively depleted in the preferentially separating component. However, the variation in enrichment with solid yield and isolation temperature, under equilibrium control, will depend most significantly on the difference between the eutonic and single salt solubilities at the prevailing (isolation) temperature.

4-4-2 Separability measurements of (R)-1-phenylethylammonium-(R,S)-2-phenylbutyrate A2

APPENDIX 11 contains the separability calculation sheet of A2 system.

The corresponding separability data for the A2 diastereomer salts are shown in **Fig49**. The enriched diastereomer salts have been isolated at 4, 6, 16, 20, 25 and 37°C.

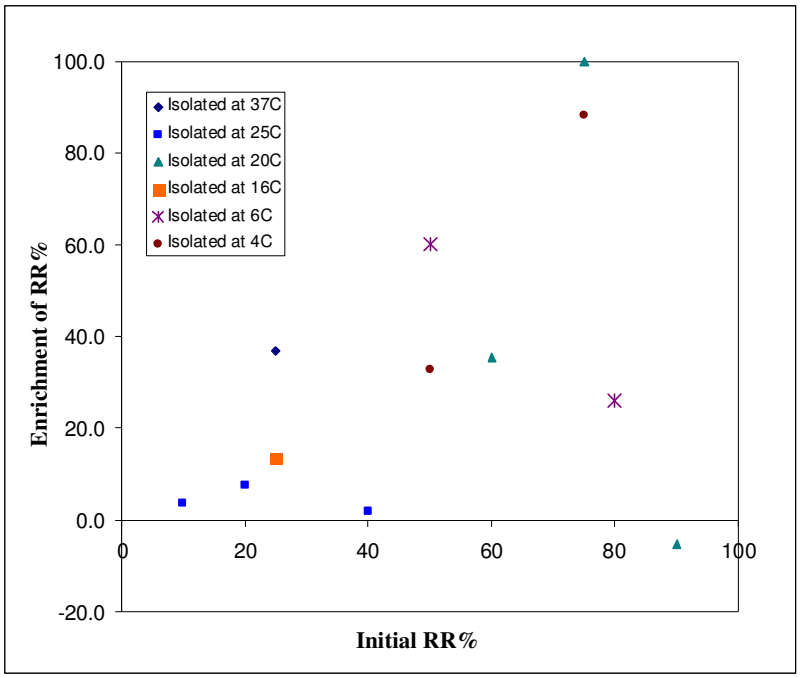

Fig49 Measured separations by cooling crystallisation of A2 diastereomer salts

Except for a single point at initial RR:RS of ratio 90:10, showing slight (5%) enrichment of the RS-isomer (which may include measurement error because of the small amounts of salts employed in this case), all crystallisations showed enrichment of the RR-form in the solid. While the scatter of data is quite extensive, there appears to be a general increase in the RR-enrichment with increasing initial RR:RS ratio.

The phase diagram at 50°C shows a eutonic close to the Solvent-RS axis, which is much less marked at 30°C. We therefore anticipated that we might see a reversal in the direction of enrichment at low RR:RS ratios. On testing this, referring to the points of the graph, we found consistent, low increases in the RR:RS ratio. We therefore believe that the phase diagram at the isolation point is the most important in determining the enrichments. This is logical because, in a thermodynamically controlled crystallisation, which is what this is, the solubilities at the end of the crystallisation process should determine the outcome rather than those at the beginning. A practical consequence of this is that where the eutonics in the phase diagram vary with temperature, it may be possible to modify the outcome by varying the end temperature of the crystallisation.

4-4-3 Separability measurements of (R)-1-phenylethylammonium-(R,S)-mandelate A3

APPENDIX 12 contains the separability calculation sheet of A3 system.

The separability results for A3 salts are shown in **Fig50**. The enriched diastereomer salts have been isolated at 15, 20, 25 and 30°C.

This is the simplest case, where the phase diagram shows near-ideal pattern of solution behaviour for the salt mixtures, and the RR-form is markedly less soluble than the RS-form. All crystallisations show enrichment in the RR-form, as would be expected from the simple axiom that the less soluble salt will separate and crystallise more readily. The relative enrichment also increases with the starting RR:RS ratio, indicating the tendency of the less soluble RR-form to separate from solution. This is a favourable condition for effective resolution, since purification may be increased by repeated crystallisations. Although crystallisation was not rapid by commonly accepted standards, it occurred more readily than in the A1 and A2 diastereomer salts, in particular at high initial RR:RS ratios. Crystallised solid recoveries were in the range 32-45% of the total salt used in each case.

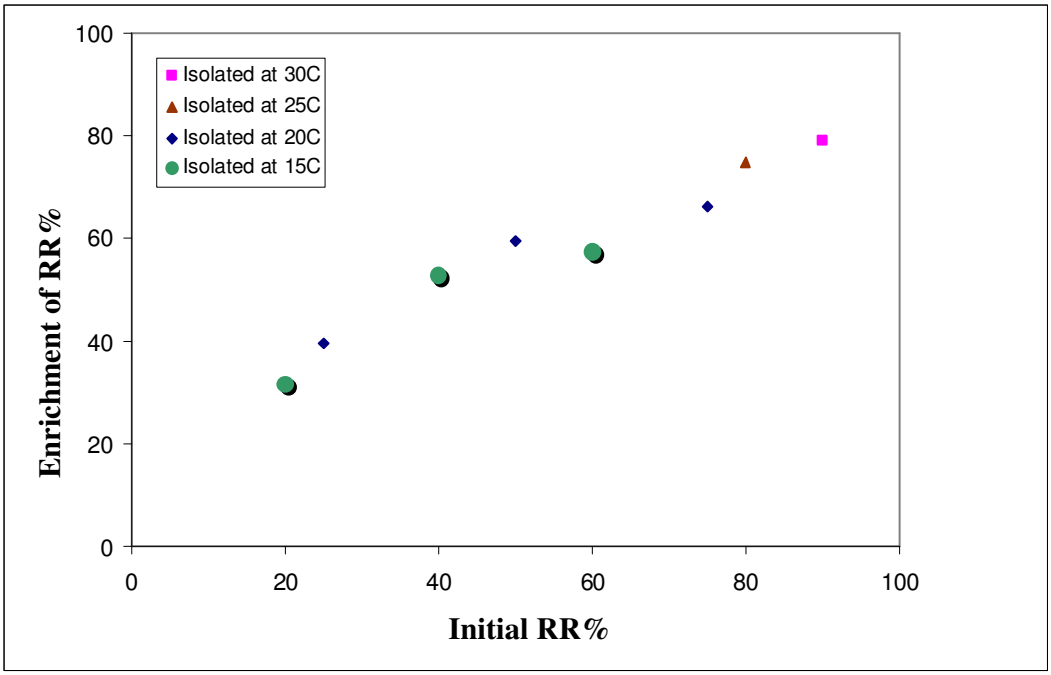

Fig50 Measured separations by cooling crystallisation of A3 diastereomer salts

4-5 Further study on polymorph determination

4-5-1 Extra work results to determine different (R)-1-phenylethylammonium-(R)-2-phenylbutanoate (RRA2) polymorphs

The following results were obtained after carrying out the structural determination of RRA2 samples, using X-ray diffraction, varying the pH, acid:base ratio and/or solvent.

Samples giving the structure of polymorph I after varying the ratio of (R)-1-phenylethylamine and (R)-2-phenylbutanoic acid, using ethanol as solvent, are:

- 3:1 acid:base
- 1:2 acid:base
- 1:1 acid:base
- 1:3 acid:base
- 2:1 acid:base.

Samples giving the structure of polymorph II, using 1:1 acid:base ratio and different solvents are:

- 1-butanol
- 2-butanol
- 2-methoxyethanol
- 2-propanol
- dichloromethane
- ethanol
- nitromethane
- tButylmethylether
- THF (Tertrahedrofuran).

The addition of sodium hydroxide to vary the basicity of ethanol did not give any new polymorphic structure of RRA2 sample.

4-5-2 Slurry experiment results

Slurry experiments were conducted in solvents, where the test substances had low to medium solubility, to induce polymorphic transformation and to find out which of the two polymorphs of the diastereomer salts of A2 and A3 are more stable.

The analysis of the solid samples via powder X-ray diffraction showed no change before and after the stirring. No change in polymorphic forms was observed and hence the choice of solvent and conditions was not optimal. In all the four different experiments set, there was no transformation of the polymorphs, in ethanol. A common approach to screen the crystallisation of a given compound is trial-and-error, where the crystallisation conditions are varied randomly to find an optimum set of conditions to crystallise a polymorph consistently. However, this approach can be very time-consuming, because many factors (e.g. solvent, supersaturation, impurity, cooling rates, stirring rates, etc) can influence the polymorph outcomes. Slurry experiments do not always work. Sometimes, transformation to stable form is very slow.

4-6 Discussion on the experimental results

The presence of polymorphism has only been determined at the end of all the experimental studies performed in this work (i.e. solubility measurements, phase equilibrium and separability measurements), while characterising the diastereomer salts (i.e. X-ray diffraction, TGA and DSC measurements). And therefore the following interpretation of the solubility measurements, phase equilibrium and the separability measurements were done with the assumption that most stable polymorphs were formed under the experimental conditions examined in this work.

In this project, the separation of the three-diastereomer salt pairs A1, A2 and A3 has been measured, by fractional crystallisation, and these separations have been correlated with the phase equilibrium behaviour of the salt pairs in solution. For one of the salt pairs A1, the ternary diagram shows a eutonic (**Fig44**), and the direction of isomeric enrichment changes markedly as the composition of salts in the crystallising solution passes through this eutonic point (**Fig48**). This is consistent with a thermodynamically controlled fractional crystallisation, where a less soluble component will be driven to separate from solution in preference to a more soluble component, in this case the eutonic.

In the case of A2 and A3 diastereomer salts, both showed the RR-form separating preferentially from solution (**Fig49** and **Fig50** respectively), in accordance with solubility measurements that showed the RR-form of both salts to be considerably less soluble than their RS-counterparts across the range of temperature employed. Although the phase diagram for A2 salts exhibited a eutonic at 50°C at RR:RS ratio around 15:85, this is not particularly well marked at 30°C (**Fig46**), and the solubility enhancement brought about by the eutonic appears insufficient to drive enrichment of the RS-isomer in the crystallised product at lower initial RR:RS ratios. All separations reported in this work are thus consistent with the ternary phase behaviour at the lower temperature, 30°C, close to the isolation temperatures. No differences in this pattern of behaviour were observed where lower isolation temperatures down to 3-5°C were employed, and the phase equilibrium data for A1 and A2 diastereomer salts at 10°C

reported by Leclercq and Jacques[65] show no qualitative differences in the ternary behaviour to that recorded here at 30°C.

While the above results establish the important role of the phase equilibrium behaviour in solution in determining the outcome of fractional crystallisation as a separation method, there are many other behaviour aspects, relating to both equilibrium and non-equilibrium conditions that can influence the efficacy of separation, and these need to be investigated further. All of the crystallisations reported here occurred relatively slowly, taking place over periods of hours rather than minutes, with nucleation occurring under fairly extreme conditions of super cooling and supersaturation. In general, such conditions are undesirable in industrial practice as there is a possibility of obtaining uncontrolled crystal growth leading to poor crystal form, and crystallisations that occur more rapidly and can be carried out at moderate supersaturations are preferred as more crystal nuclei are formed in a short time scale, giving rise to more uniform crystal growth. In such rapid crystallisations, nucleation and growth kinetics may play a critical role in determining the outcome of the separation, by controlling the relative rates at which product crystals may be formed. More rapid crystallisations of this type will be the subject of future research.

Other factors that can obstruct separation include the formation of solid solutions, double and other multiple salts, and difficulties in obtaining crystallised salts from solution. These have been briefly discussed by Leclercq and Jacques[65], even though without offering any separability data or drawing any definitive conclusions. The phase equilibrium results of A1, A2 and A3 show the existence of solid solutions (**Table_18**, **Table_20** and **Table_21**). Just looking at these experimental results, it is not possible to say whether or not a true solid solution (i.e. solid solution of one or more solute into a solvent[59,125]) exists. This needs to be investigated further, using for example DSC technique. A true solid solution would have a similar solid structure to the 'solvent' or 'host' that may be modified or distorted by the presence of the 'solute'. It would be a single phase and would therefore have a single melting point. If it is not a true solid solution and is a mixture that is microstructurally polyphasic (usually as a mixture of ‘RR in RS’ and ‘RS in RR phases), there would be two melting points. In this project work, what these experimental solid solutions show is a solid in equilibrium with the solution that showed a mixed composition (i.e. partial

enantiomeric enrichment). However the composition appeared to be consistent, macroscopically, throughout the solid, as shown in **Table_19**.

Parameters relating to the individual diastereomer components, such as differences in the enthalpies of formation of the crystalline solids, have been proposed as indicators of separability as has previously been suggested[68,124]. Predictive methods based on this approach assume initially that the solution behaviour of the diastereomer pair will be approximately ideal. Here, A3 diastereomer salts most closely meet this condition. However, the solubilities of the two-diastereomer salts in this case differ widely across the entire temperature range of the experiment, and it would be possible, at least in principle, to predict the outcome from a simple consideration of the single-salt solubility data. Generally, this pattern of near-ideal solution behaviour will be more commonly realised in cases where the two solubilities differ by a considerable margin.

However, A1 diastereomer salts give a very clear example where such correlations and predictions will not lead to the correct answer. Firstly, consideration of the difference in the enthalpies of formation as a predictor of separation behaviour will give the wrong ordering of the solubilities of the two compounds, which is dominated by the effect of the entropic contribution. Secondly, such methods take no account of the formation of eutonics, which, our results show, completely determine the direction in which enrichment via crystallisation will occur. The effects of eutonics and eutectics on diastereomer has been discussed recently, [57,126] with the general impression given that eutonic formation favours separability. These discussions also postulate eutonic behaviour as an alternative to less favourable behaviour patterns, such as solid solutions[107], implying that the two types of behaviour are mutually exclusive. However, both appear to be exhibited by A1 diastereomer salts. Furthermore, the high numerical enrichments in the separability measurements of A1 diastereomer salts combined with the lack of evidence that enrichment level falls off drastically with increased solid recovery, suggest that a separation process based on multiple recrystallisations is likely to yield a highly enriched product in spite of the solid solution behaviour.

The A2 diastereomer salt system exhibits phase characteristics common with both A1 and A3 diastereomer salts. In common with A3 diastereomer salt, the RR-form is much less soluble than the RS-form across the temperature range, and the ternary solubilities at 30°C more closely resemble the ideal pattern of behaviour than the eutonic. However, at 50°C the ternary shows a eutonic at an RR:RS ratio around 15:85 (**Fig46**). We find a small enrichment in the RR-isomer on starting from initial RR:RS ratios in excess of this value. We have also found it very difficult to prepare a good quality crystal of the RR-form of this salt, as with the corresponding diastereomer salt RRA3[107]. The separation behaviour of A2 diastereomer salts thus resembles that of A3, probably for the same underlying reasons.

It has been suggested[127] that the separability of a diastereomer pair can be predicted from an analysis of its binary melting behaviour, on the grounds that a eutectic melt composition will be congruent with a solution eutonic, and the detection of the former by differential scanning calorimetry will give information on the likely performance of a fractional crystallisation. In theory, this can only be true if a number of conditions apply: both diastereomer components must be stable up to their melting points, and the interactions of the solutes with the solvent must be similar. Also, in cases where this principle is applicable, the eutonic composition must remain invariant with temperature, and must also remain the same for all solvents from which crystallisation is to be attempted. For A2 diastereomer salts, the eutonic at higher temperature implies that a melt eutectic would be detected, if it was possible to carry out a measurement at the melting points. Our experience with these salts suggests that they are not particularly stable as solids at elevated temperatures, so it would probably be difficult to carry out such a measurement. However, at 30°C and below, the eutonic effectively disappears, and an investigation of such high temperature behaviour would not correctly predict the separations obtained by fractional crystallisation under these conditions.

There are literature reports that multiple salts may form in the A3 mandelate system. Two of these involve racemic compositions of the base with single[128] or mixed[129] enantiomer acid moieties, and the possibility of their formation has been eliminated from our experiments by the use of a single base enantiomer, as has the complex conglomerate behaviour that has recently been reported in the quaternary A1

system[119]. The other two multiple A3 diastereomer salts consist of adducts of each of the two diastereomers with two free acid moities[129,130]. Single-crystal and powder X-ray diffraction analysis shows no evidence of these forms in our crystallised products[107]. HPLC analysis has shown that all the salts employed in this study were effectively dissociated into their ions in ethanolic solutions.

4-7 Summary

Through out the experimental studies on the three systems investigated, the following results have been observed.

For (R)-1-phenylethylammonium-(R,S)-2-phenylpropanoate A1:

- RR-salt is more soluble than RS-salt
- Phase diagram exhibits a strong eutonic behaviour at 70:30 RR:RS ratio
- Enrichment of RS and RR salts are comparable
- Direction of enrichment changes when the starting composition passes through the eutonic point.

For (R)-1-phenylethylammonium-(R,S)-2-phenylbutyrate A2:

- RS-salt is significantly more soluble than RR-salt
- Phase diagram exhibits eutonic behaviour at 50°C, at 15:85 RR:RS ratio, which is not evident at lower temperature
- Enrichment of RR-salt is observed via separability measurements.

For (R)-1-phenylethylammonium-(R,S)-2-mandelate A3:

- RS-salt is significantly more soluble than RR-salt
- Phase diagram does not exhibit eutonic behaviour. A near-ideal equilibrium behaviour is observed
- Enrichment of RR-salt is observed via separability measurements.

The molecular modelling results for these three systems are discussed in the following chapter.

5 MODELLING RESULTS AND DISCUSSION

In the following sections the three sets of diastereomer salts studied will be called A1, A2 and A3 (see **Fig7**), where:

- **A1**: (R)-1-phenylethylammonium-(R,S)-2-phenylpropanoate
- **A2**: (R)-1-phenylethylammonium-(R,S)-2-phenylbutyrate
- **A3**: (R)-1-phenylethylammonium-(R,S)-mandelate.

In the previous chapter (Experimental Results and Discussion), the following results have been obtained experimentally:

- Enrichment of RSA1 and RRA1 salts are comparable and there is a change in direction of enrichment observed passing through the eutonic point
- RSA2 salt is significantly more soluble than RRA2 salt
- RSA3 salt is more soluble than RRA3 salt.

In this chapter, modelling results obtained for the three systems studied in this project are presented and discussed.

5-1 Experimental lattice energy minimisation calculations (ExpMinExpt)

In this section, we will examine the intermolecular forces of the three systems studied.

The aim of the experimental lattice energy minimisation calculation (ExptMinExpt) is to judge the quality of the intermolecular potential based on how well the crystal structure is reproduced. The lattice energy is the sum of the intermolecular interactions (i.e. the intermolecular potentials) between all the molecules in the crystals. For an organic crystal structure modelling, a reasonably realistic model is obtained if the lattice energy minimisation produces the known crystal structures to within a few percent in the lattice parameters. If the deviations are of more than 5%, then it gives serious cause for concern about the adequacy of the model.

The following **Table_23**, **Table_24** and **Table_25** contain the results of intermolecular potential quality (experimental lattice energy minimisation results) of the six model compounds studied in this work. The results for the structures determined or re-determined throughout this work are highlighted in bold. The starting points for the rigid-point lattice energy minimisations were the structures shown in **Tables_10**, **Table_11** and **Table_12** (Section **4-1**).

Table_23 Intermolecular potential quality of A1 system, from ExptMinExpt lattice energy minimisations

Structure	**U_{inter} (kJ/mol)**	**Reduced cell parameters %**			**Reproduction Quality RMS Cell length (%)**
		a	**b**	**c**	
RS p-salt	-675.94	+3.07	-1.15	-1.30	2.04
RR I n-salt	-684.42	+0.14	+0.14	-1.71	0.99
RR II n-salt	-678.81	+0.05	+1.00	-3.30	1.99

For the A1 system (**Table_23**), the percentage of reduced cell parameters is very small, which indicates that the lattice energy minimisation reproduces the known crystal structure and gives a reasonably realistic model. In all cases, the percentage of root-mean-square (RMS) cell length is also very small, indicating a good reproduction of the crystal structure.

Table_24 Intermolecular potential quality of A2 system, from ExptMinExpt lattice energy minimisations

Structure	**U_{inter} (kJ/mol)**	**Reduced cell parameters %**			**Reproduction Quality RMS Cell length (%)**
		a	**b**	**c**	
RS p-salt	-639.40	-1.55	-1.55	4.21	2.74
RR I n-salt	-687.39	-1.97	1.58	2.34	1.99
RR II n-salt	-674.00	1.69	-1.20	-1.80	1.58
RR III n-salt	-660.19	1.14	2.18	-3.00	2.24

For the A2 system (**Table_24**), the percentage of reduced cell parameters and the percentage of RMS cell lengths are very small, indicating a good reproduction of the known crystal structure.

Table_25 Intermolecular potential quality of A3 system, from ExptMinExpt lattice energy minimisations

Structure	**U_{inter} (kJ/mol)**	**Reduced cell parameters %**			**Reproduction Quality RMS Cell length (%)**
		a	**b**	**c**	
RR I n-salt	-717.33	0.81	-1.13	0.86	0.94
RR II n-salt	-709.41	0.09	-0.34	1.96	1.15

ExptMinExpt minimisation was not performed for p-salt of (R)-1-phenylethylammonium- (S)-mandelate system (RSA3), because of the large number of missing hydrogen atoms and large number of ions in the asymmetric unit.

For the other two RRA3 polymorphs studied (**Tabel_25**), the percentage of reduced cell parameters and the percentage of RMS cell lengths are very small, indicating a good reproduction of the known crystal structure.

For all the six model compounds of the three systems studied (A1, A2 and A3), the experimental crystal structure is very close to the lattice energy minimum obtained with the intermolecular potential, keeping the experimental molecular crystal conformation rigid, as the percentage of reduced cell parameters and that of RMS cell lengths are relatively small.

5-2 The crystal energy to predict the relative thermodynamic stability

In this section, we will examine crystal energy in order to predict the relative stability of the diastereomers.

The lattice energy was calculated as the sum of the intermolecular ($\mathbf{U_{inter}}$) and intramolecular ($\mathbf{\Delta E_{Intra}}$) contributions as given by the equation **(24)** in section ***2-5-3-3***,

obtained using the molecular structures in which only the main torsion angles defined in **Fig32** were held at this experimental values (ExptMinCOpt).

The following **Table_26**, **Table_27** and **Table_28** contain the results of rigid point lattice energy minimisation calculations of the six model compounds studied in this work.

Table_26 Reproduction accuracy and predicted relative stability of A1 system, from ExptMinCopt lattice energy calculations

Structure	**U_{inter} (kJ/mol)**	**ΔE_{Intra} (kJ mol^{-1}) Cation**	**Anion**	**Crystal energy U (kJ mol^{-1})**	**Quality of Reproduction[a]**		
					RMS error cell lengths (%)	**Density (% error)**	**RMS_{15} (Å)**
RS p-salt	-652.83	0.80	3.55	-648.48	1.70	1.126 (-1.75%)	0.173
RR I n-salt	-650.80	0.30	3.71	-646.79	2.94	1.158 (-1.78%)	0.211
RR II n-salt	-647.20	2.29	5.86	**-639.05**	3.50	1.103 (-1.61%)	0.287

[a] Quality of reproduction assessed via the root-mean-square error in the lattice lengths and root-mean-square discrepancy of a 15-ion pair cluster[105].

For the A1 system (**Table_26**), RS-diastereomer salt (p-salt) and RR-diastereomer salt (n-salt) polymorph I have almost equal lattice energies. This indicates that it would be difficult to separate these two diastereomer salts via fractional crystallisation. RR-diastereomer salt polymorph I is more stable than RR-diastereomer salt polymorph II. The overall geometric reproduction of the crystal structures are satisfactory, with values under 3.5% root-mean-square error in the lattice lengths and values under 0.3 Å root-mean-square discrepancy of a 15-ion pair cluster.

Table_27 Reproduction accuracy and predicted relative stability of A2 system, from ExptMinCopt lattice energy calculations

Structure	U_{inter} (kJ/mol)	ΔE_{Intra} (kJ mol^{-1}) Cation	Anion	Crystal energy U (kJ mol^{-1})	Quality of Reproduction[a] RMS error cell lengths (%)	Density (% error)	RMS_{15} (Å)
RS p-salt[c]	-616.33	0.08	10.09	-606.16	2.97	1.027 (-3.81%)	0.253
RR I n-salt	-655.77	0.24	6.56	-648.97	3.48	1.158 (-4.61%)	0.307
RR II n-salt	-650.22	0.80	6.34	**-643.08**	2.82	1.107 (+0.30%)	0.225
RR III n-salt	-635.00	1.97	4.94	**-628.09**	4.89	1.109 (-0.30%)	0.344

[a] Reference[131].

For the A2 system (**Table_27**), we can say, looking at the crystal energies of RR-diastereomer salts polymorphs I, II and III, that RR-diastereomer salt polymorph I (-648.97 KJ/mol) is most stable polymorph, followed by RR-diastereomer salt polymorph II and RR-diastereomer salt polymorph III. In addition to this information, we can also observe that there is a RS-diastereomer salt and the RR-diastereomer salts have big difference in their lattice energy, indicating that it would be easier to separate these two diastereomers. The overall geometric reproduction of the crystal structures are reasonable, with values under 5% root-mean-square error in the lattice lengths and values under 0.35 Å 15-ion coordination sphere.

Table_28 Reproduction accuracy and predicted relative stability of A3 system, from ExptMinCopt lattice energy calculations

Structure	U_{inter} (kJ/mol)	ΔE_{Intra} (kJ mol^{-1}) Cation	Anion	Crystal energy U (kJ mol^{-1})	Quality of Reproduction[a] RMS error cell lengths (%)	Density (% error)	RMS_{15} (Å)
RS I[b] p-salt	-657.65	3.35 3.52 0.75 0.01	74.86 65.87 71.38 12.65	-599.55	1.28	1.215 (-2.76%)	0.186
RR I n-salt	-687.38	8.37	85.14	**-593.87**	1.72	1.224 (-2.22%)	0.182
RR II n-salt	-676.58	6.38	85.55	**-584.65**	1.46	1.206 (-3.15%)	0.159

[a] Reference[131].

[b] Hydrogen atoms added with SHELX[132,133].

For the A3 system (**Table_28**), the RS-diastereomer salt lattice energy is very sensitive to the positioning of the two hydroxyl hydrogen atoms that have not been experimentally determined and added using SHELX program. The crystal energy for this RS-diastereomer salt corresponds to a reasonable structure where the missing hydroxyl hydrogen atom of one of the anions was assumed to form an intramolecular hydrogen bond, as there are no available acceptors in neighbouring ions. The low RS energy is mainly because the intermolecular energy of the mandelate ion that was assumed to exhibit intramolecular hydrogen bonding is approximately 50 kJ.mol-1 lower than the energy of the mandelate ions involved in only intermolecular hydrogen bonds in the RS and both RR polymorphs. It is encouraging that the overall geometric reproduction of the crystal structure is satisfactory with 1.28% and 0.186 Å root mean square error in the lattice lengths and 15-ion coordination sphere respectively, which suggests that the assumed positions of the missing hydrogen atoms are reasonably correct. However, the accurate prediction of the experimental stability order is much more demanding of the balance of the inter- and intra-molecular energy model. We predict that RR-salt polymorph II (-584.65 KJ/mol) is less stable than RR-salt polymorph I (-593.87 KJ/mol).

The geometric reproduction of the crystal structures was used to confirm that the accuracy of the intermolecular potential was sufficient and that the flexible degrees of freedom had been correctly identified. For all the six systems studied, the root-mean-square error deviation in the overlay of all non-hydrogenic atoms in a 15-ion coordination sphere[105] was smaller than 0.35Å, indicating sufficient accuracy of intermolecular potential and correct identification of flexible degrees of freedom.

5-3 Discussion on the modelling results

Crystal energies of the three systems studied and the conclusion obtained from these results about the resolving agents efficiency is summarised in **Table_29**:

Table_29 Summary of modelling results of the three systems studied

Systems studied	Salts	Crystal Energy (kJ mol^{-1})	Results	Implied resolving efficiency of (R)-1-phenylethylammonium
A1	p-salt n-salt I n-salt II	-648.48 -646.79 -639.05	p-salt and n-salt are equally stable	Not a good resolving agent from calculations
A2	p-salt n-salt I n-salt II n-salt III	-606.16 -648.97 -643.08 -628.09	n-salt significantly more stable than p-salt	Good resolving agent
A3	p-salt n-salt I n-salt II	-599.55 -593.87 -584.65	Less accurate predictions. p-salt marginally more stable than n-salt.	Poor resolving agent

For the system (R)-1-phenylethylammonium-(R,S)-2-phenylpropanoate A1, purely considering modelling results, as p-salt and n-salt have similar stability order, it is very difficult to isolate the enantiomers. But the experimental results (**Fig48**) showed that there is a significant change in the enrichment of the diastereomer salt when the solution passes through the eutonic point and it showed that both RR-diastereomer salt (n-salt) and RS-diastereomer salts (p-salt) are equally stable passing through the eutonic point. And therefore 1-phenylethylamine is a good resolving agent for (R,S)-2-phenylpropanoic acid. From the molecular modelling results, there is no possibility to figure out the existence of eutonic behaviour and therefore, in the case of presence of eutonic point, the experimental results have to be taken into account to decide whether the chosen resolving agent is effective or not.

For the system (R)-1-phenylethylammonium-(R,S)-2-phenylbutyrate A2, because of the large stability difference between the p-salt and the n-salt crystals, it is easy to isolate the two enantiomers via crystallisation. This has also been shown throughout the experimental results. On the phase diagram for the A2 system (**Fig46**), we can see that the RS-salt (p-salt) is significantly more soluble than the RR-salt (n-salt), and therefore RR-salt will precipitate more easily. Hence, our thermodynamic stability

predictions are consistent with the solubility measurements confirming that 1-phenylethylamine is a good resolving agent for (R,S)-2-phenylbutanoic acid.

For the system (R)-1-phenylethylammonium-(R,S)-mandelate A3, the RS-salt (p-salt) is predicted to be more stable (lower crystal energy). However it is more soluble (**Fig47**), i.e. experimentally less stable. Hence the calculations are not consistent. This could be due to the potential errors in the model, such as the positioning of hydroxyl hydrogen atoms that have not been experimentally determined and that have been added using standard bond lengths with SHELX. A more reliable determination of atom positions could give improved hydrogen bonding energies from calculations, and could possibly reverse the stability order.

The crystal structures and qualitative relative stability of the chemically related diastereomer pairs have been reproduced well by lattice energy calculations using a distributed multipole model for the dominant electrostatic interactions and *ab initio* estimates of the ion conformational energies. The only exception is the overestimation of the thermodynamic stability of the (R)-1-phenylethylammonium-(S)-mandelate crystal structure compared with the (R)-1-phenylethylammonium-(R)-mandelate polymorphs, due to the difficulties in establishing accurate hydrogen positions by the computational models. The intermolecular potential should be extended to account for the effect of polarisation of the ion's charge density in the crystalline environment, in order to correctly rank structures with very different hydrogen bonding motifs. Ignoring this disagreement, the computational model appears able to even predict the delicate stability ordering of the polymorphs of the same diastereomer. Thus, the effect of the uncertainties in the intermolecular potential and ion conformational energies generally appear to be small compared with the stability difference of efficiently resolving diastereomeric salt pairs.

The appearance of a new thermodynamically more stable RS form would reduce the resolution efficiency, as the lattice energy difference of the most stable RR and RS diastereomers may be limited to a few kJ/mol. This illustrates the importance of developing a methodology that will reliably predict the relative stability of diastereomers, as the discovery of an unexpected, thermodynamically more stable polymorph[134,135] may considerably change the separability behaviour in an industrial

process. In contrast, for the simplest diastereomeric salt pair (R)-1-phenylethylammonium-(R,S)-2-phenylpropanoate (A1), the thermodynamically stable forms of both diastereomers correspond to the global minima in the corresponding searches with the same model[92,131]. Hence, although the discovery of additional polymorphs cannot be ruled out, they are likely to be metastable. Although the growth of metastable polymorphs will probably have a smaller impact on the resolution efficiency than thermodynamically stable ones, there is value in their computational prediction, as the conditions of the resolution process may affect the polymorphic outcome and, hence, indirectly determine the solubility ratio and separability of the two diastereomers. This is confirmed by the polymorphic outcome of the separation experiments for (R,S)-mandelic acid and (R)-1-phenylethlyamine being dependent on the starting ratio of the two enantiomers. Theoretical calculations predict that the lattice energy of the low melting polymorph (R)-1-phenylethylammonium-(R)-mandelate II is approximately 10kJ/mol lower than (R)-1-phenylethylammonium-(R)-mandelate I. Their predicted stability difference appears sufficiently large for the polymorphic outcome to have an important effect on the observed separability behaviour to guarantee a more detailed experimental investigation.

The prediction of the resolution efficiency from lattice calculations is based on the assumption that a successful resolution is mainly dependent on the solubility ratio of the diastereomeric salt pair. This is a reasonable basis for the theoretical screening of resolving agents to eliminate unsuitable candidates. However, there are many additional factors that can affect the resolution ability of a resolving agent, even when the stability difference of the resulting diastereomeric salt pair is large. Whilst the stability ratio is independent of the solvent, the molecular structure of the latter determines the possibilities for its association with the precipitating salt and hence the formation of a solvate that may alter the separability behaviour. Moreover, the unexpected crystallisation outcomes, such as double salts or solid solutions, are also possible. Finally the crystallisation outcome may not always be thermodynamically controlled, especially for the fast separation processes which are typically of industrial interest. Despite the challenges in predicting all factors that influence the separation behaviour, the development of computational methods that will reliably compute the Gibbs free energy difference of diastereomeric salt pairs can provide a valuable guide

to experimental investigations, by short listing resolving agents whose performance is likely to be satisfactory.

5-4 Summary

The following results have been observed through the lattice energy calculations, to predict the relative thermodynamic stability of the three systems studied.

For (R)-1-phenylethylammonium-(R,S)-2-phenylpropanoate A1:

- RS-salt and RR-salt I have almost equal stability order
- RR-salt I is more stable than RR-salt II
- Experimentally, (R)-1-phenylethlyammonium is classified as good resolving agent for this system, but the modelling calculations predict that this resolving agent is not suitable for this system.

For (R)-1-phenylethylammonium-(R,S)-2-phenylbutyrate A2:

- RR-salt is much more stable than RS-salt, which is in good accord to the experimental results
- (R)-1-phenylethlyammonium is classified as good resolving agent for this system.

For (R)-1-phenylethylammonium-(R,S)-2-mandelate A3:

- RS-salt is predicted to be more stable
- Experimental results show that RS-salt is more soluble and therefore less stable
- This contradiction between experimental and modelling result is due to the addition of missing hydrogen atoms using SHELX program
- Experimentally, (R)-1-phenylethlyammonium is classified as good resolving agent for this system, but modelling calculations predicts it as a poor resolving agent.

The experimental and modelling results are summarised together, compared and concluded based on the objectives set for this project in the following chapter.

6 CONCLUSION

The objectives of this project were:

- To investigate chiral resolution based on the addition of a resolving agent to an enantiomer mixture.
- To experimentally correlate separability with phase behaviour.
- To carry out the lattice energy calculations on the investigated three systems with a view to prediction structural factors or physical properties that significantly influence resolution.

A summary of the experimental and modelling investigations, of the three pairs of diastereomer salts studied in this project, is presented in **Table_30**.

Table_30 Summary of experimental and modelling results

Systems studied	Experimental results	Modelling results
A1: (R)-1-phenylethylammonium-(R,S)-2-phenylpropanoate 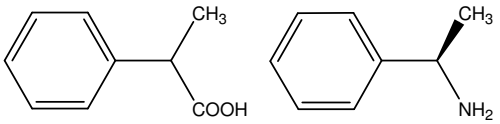	• Phase behaviour: strong eutonic behaviour at 70:30 RR:RS ratio • Separability: change in direction of enrichment (either RR-salt or RS-salt is preferentially crystallised) passing through eutonic point	RR-salt and RS-salt are equally stable
A2: (R)-1-phenylethylammonium-(R,S)-2-phenylbutyrate 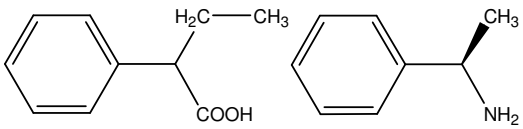	• Phase behaviour: RR-salt less soluble than RS-salt • Separability: RR-salt separating preferentially from solution	RR-salt significantly more stable
A3: (R)-1-phenylethylammonium-(R,S)-mandelate 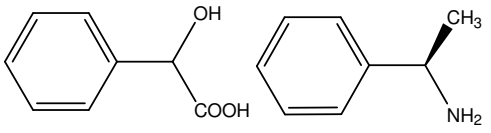	• Phase behaviour: RR-salt less soluble than RS-salt • Separability: RR-salt separating preferentially from solution	RS-salt more stable (less accurate predictions due to H addition using SHELX)

In the case of A1 system, eutonic point plays a major role in the diastereomeric enrichment. Both phase equilibrium and separability results are consistent with each other showing that

R-1-phenylethylamine is a good resolving agent for this system. Modelling results also show that there is a stability of both RR and RS salts. But with the modelling method, there is no possibility to predict the existence of eutonic behaviour. And therefore, for a system such as A1, with existence of eutonic point, it is very important to investigate both experimental and modelling methods.

In the case of A2 system, phase equilibrium shows that RR-salt would precipitate preferentially. Separability results are consistent with phase equilibrium results. And also, experimental results are in good agreement with modelling results, showing that R-1-phenylethylamine is a good resolving agent for this system. Modelling here shows that the RR-salt is significantly more stable, consistent with the observed solubilities. In such system, molecular modelling could be a rapid way to predict the chiral resolution behaviour rather than relying on trial and error screening.

In the case of A3 system, separability results show an enrichment of RR-salt at all ratios, which is consistent with the phase equilibrium data, showing that R-1-phenylethylamine is a good resolving agent for this system. But there is a contradiction between the experimental and modelling results, which is due to difficulties in positioning the hydrogen atoms and optimisation of intra- and intermolecular energies. In such system, molecular modelling would not help much to predict the right outcome.

Overall, the experimental diastereomer separation study has shown that the fractional crystallisations of the model diastereomer salts in this project follow behaviour patterns predicted from the measured equilibrium data (i.e. separability results are consistent with solubility and phase equilibrium results). All of these crystallisations take place relatively slowly, conditions which generally favour the observed thermodynamic control of the outcomes. More rapid crystallisations are likely to be more strongly influenced by kinetic factors, causing the separations to deviate from the predictions of thermodynamics. This should be examined further in future studies. The modelling study demonstrated that the stability difference of the diastereomeric salt pairs of three 1-phenylethlyammonium-2-phenylacetate derivatives is related to their resolution efficiency and varies considerably, despite the similarities in their molecular structure and hydrogen bonding motifs. Although these results are interesting and encouraging, there are drawbacks (i.e. no possibility to identify eutonic behaviour, missing hydrogen providing less accurate predictions, etc) relying

only on modelling methods. Further methodological developments will be required to rely more on lattice energy calculations. The experimental measurements gathered in this study provide a test bed for the necessary developments in computational modelling.

Therefore, based on the work carried out, it is clear that we cannot purely depend on the modelling technique to select the resolving agent due to its above-mentioned limitations and inaccuracies. However, the experimental results show that it is possible to perform chiral resolution based on the addition of resolving agent to an enantiomer mixture. This chiral resolution method could be of great interest to the pharmaceutical industry where it is important to have purified enantiomers in their products.

7 FUTURE WORK

From the results obtained so far and to get better understanding of the current systems studied (i.e. A1, A2 and A3), some extra work could be done, such as:

- The presence of polymorphs and the effects of polymorphism on diastereomer crystallisation have to be investigated further: do all polymorphs have similar enantiomeric excess?

Further investigations, on the isolation of enantiomers via diastereomer crystallisation could also be carried out, using other systems as follows:

- Experimental investigation using more complex resolving agent, such as ephedrine (**Fig51**), which has two chiral centres, so two sets of enantiomers.

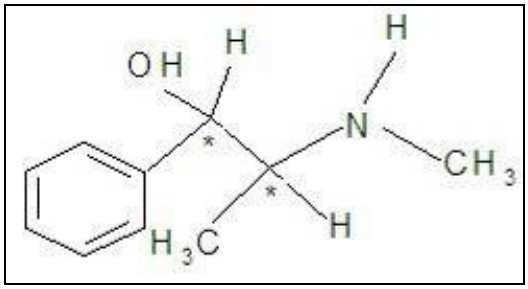

Fig51 Ephedrine

- Investigation of the resolution of bases by resolving agents based on tartaric acid (**Fig52**) and its diaroyl derivatives, which are very commonly reported in practice.

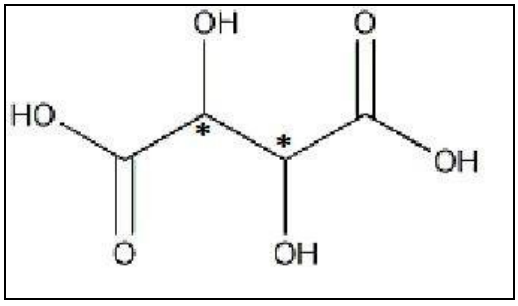

Fig52 Tartaric acid

- Experimental investigation of the 'Dutch' method[21] by which improved resolution is obtained by using mixtures of chemically similar resolving agents. In this method there is a development of "families of resolving agents", in which the members of the family bear strong structural similarities and are stereochemically homogeneous. The most significant findings of this method are:

    1) On addition of two or more resolving agents of a family to a racemate, rapid crystallisation of a diastereomeric salt containing different family members take place in good to excellent yield.
    2) The high rate of success makes the method of commercial value.
    3) The method is applicable to resolutions through formation of molecular complexes.
    4) Mixtures of racemates can be resolved to enantiomerically pure mixtures either with a single resolving agent or with several resolving agents.

- Experimental investigation of faster crystallisations where kinetic factors are likely to exert a greater influence, to see the extent to which the thermodynamic principles that we have established hold up in these cases. One of the interesting techniques to be used, in this case, is ultrasonically promoted crystallisation or sonocrystallisation[136]. Sonocrystallisation greatly improves the ability of the crystallisation scientist to reproducibly deliver high quality crystalline materials of the desired polymorphism, morphology and particle size. When ultrasound is applied judiciously, during the cooling phase of a crystallisation, it is possible to influence the process of nucleation, seeding and growth as well as to reduce particle size and to prevent agglomeration during and/or after the growth phase. Ultrasound induces nucleation in the microenvironments caused by the collapse of cavities generated by the interaction of sound waves with defects in the process fluid. In our case, to increase the crystallisation speed and study the kinetic effects, ultrasound would be very useful because:

1) A short burst of ultrasound at an intensity or energy density, above the cavitational threshold, will induce nucleation of crystallisation at significantly lower supersaturation levels than those required where no ultrasound is applied[137].
2) Ultrasound will also reduce the induction time between the establishment of supersaturation and the onset of nucleation and crystallisation. With ultrasound, there are not only marked reductions in the induction times, but also much improved reproducibility[138].

LIST OF PUBLICATIONS

Anandamanoharan, P.R.; Cains, P.W.; Jones, A.G. Tetrahedron: Asymetry 2006, 17, 1867-1874.

Karamertzanis, P. G.; Anandamanoharan, P.; Cains, P. W.; Hulme, A. T.; Vickes, M.; Tocher, D. A, J. Phys. Chem. B. 2007, 111, 5326-5336.

P. Fernandes, A. J. Florence, K. Shankland, P. G. Karamertzanis, A. T. Hulme and R. P. Anandamanoharan, Acta Cryst. 2007, E63, o202-o204.

P. Fernandes, A. J. Florence, K. Shankland, P. G. Karamertzanis, A. T. Hulme and R. P. Anandamanoharan, Acta Cryst. 2007, E63, o247-o249.

References

(1) Geison, G. L. *The Private Science of Louis Pasteur*; Princeton University Press: Princeton, NJ, 1995.

(2) Cotton, F. A.; Wilkinson, G. *Advanced Inorganic Chemistry: a Comprehensive Text*; John Wiley & Sons Inc: New York, 1980; pp 47.

(3) Eliel, E. L.; Wilen, S. H. *The Stereochemistry of Organic Compounds*; Wiley Interscience: 1994.

(4) Sheldon, R. A.; Hulshof, L. A.; Bruggink, A.; Leusen, F. J. J.; Vanderhaest, A. D.; Wijnberg, H. Crystallization Techniques for the Industrial Synthesis of Pure Enantiomers. *Chim. Oggi* **1991,** *9,* 23-29.

(5) Rekoske, J. E. Chiral Separations. *AIChE J.* **2001,** *47,* 2-5.

(6) Kaptein, B.; Vries, T. R.; Nieuwenhuyzen, J. W.; Kellogg, R. M.; Grimbergen, R. F. P.; Broxterman, Q. B. New Developments in Crystallization-Induced Resolution; In Handbook of Chiral Chemicals. Ager, D., Ed.; CRC Press: 2005.

(7) FDA's policy statement for the development of new stereoisomeric drugs. http://www.fda.gov/cder/guidance/stereo.htm . 1992. U.S.Food and Drug Administration.
Ref Type: Electronic Citation

(8) Hoffmann, F. *The Same and Not the Same*; Columbia University Press: New York, 1995.

(9) Gu, C.-H.; Grant, D. J. W. Physical Properties and Crystal Structures of Chiral Drugs; In Handbook of Experimental Pharmacology: Stereochemical Aspects of Drug Action and Disposition. Springer: Berlin, 2003.

(10) Collins, N. A.; Sheldrake, G. N.; Crosby, J. *Chirality in Industry (The Commercial Manufacture and Applications of Optically Active Compounds)*; Wiley & Sons: 1992.

(11) Jacques, J.; Collet, A.; Wilen, S. H. *Enantiomers, Racemates and Resolutions*; Krieger Publishing Company: Malabar, Florida, 1994.

(12) Eliel, E. L.; Wilen, S. H.; Doyle, M. P. *Basic Organic Stereochemistry*; John Wiley & Sons Inc: 2001.

(13) Eliel, E. L.; Wilen, S. H. *Stereochemistry of Organic Compounds*; Wiley-Interscience Publication: 1993.

(14) Jacques, J.; Collet, A.; Wilen, S. H. *Enantiomers, Racemates and Resolutions*; Wiley-Interscience: New York, 1981.

(15) Streitwieser, A.; Heathcock, C. H. *Introduction to Organic Chemistry*; McMillan: 1976.

(16) Mullin, J. W. *Crystallization*; Reed Educational and Professional Publishing Ltd: 2001.

(17) Shelkunov, B. Y.; York, P. Crystallisation Processes in Pharmaceutical Technology and Drug Delivery Design. *J. Cryst. Growth* **2000,** *211,* 122-136.

(18) Desikan, S.; Anderson, S. R.; Meenan, P. A.; Toma, P. H. Crystallisation Challenges in Drug Development: Scale-Up From Laboratory to Pilot Plant and Beyond. *Curr. Opin. Drug Discovery Develop* **2000,** *3,* 723-733.

(19) Ahuja, S. *Chiral Separations Applications and Technology*; American Chemical Society: 1997.

(20) Vaidya, N. A. Diastereomeric crystallisation - the "classical" chiral technology. Innovations in Pharmaceutical Technology . 2000.
Ref Type: In Press

(21) Vries, T.; Wynberg, H.; Echten, E. *Angewandte Chemie International Edition* **1998,** *37,* 2349-2354.

(22) Phillips, F. C. *An Introduction to Crystallography*; Oliver and Boyd: 1971.

(23) *International Tables for Crystallography, Vol. A*; Kluwer: Dordrecht, 2002.

(24) Byrn, S. R.; Pfeiffer, R. R.; Stowell, J. G. *Solid-State Chemistry of Drugs*; SSCI Inc.: West Lafayette, Indiana, 1999.

(25) Kelly, A.; Groves, G. W.; Kidd, P. *Crystallography and Crystal Defects*; John Wiley and Sons: 2000.

(26) Lifshin, E. *X-Ray Characterisation of Materials*; Wiley-VCH: 1999.

(27) Woolfson, M. M. *An Introduction to X-Ray Crystallography*; Cambridge University Press: 1997.

(28) Desiraju, G. R.; Steiner, Th. *The Weak Hydrogen Bond.*; Oxford University Press: Oxford, 1999.

(29) Davey, R. J.; Allen, K.; Blagden, N.; Cross, W. I.; Lieberman, H. F.; Quayle, M. J.; Righini, S.; Seton, L.; Tiddy, G. J. T. *CrystEngComm* **2002,** *4,* 1-8.

(30) Davey, R. J.; Blagden, N.; Righini, S.; Alison, H.; Quayle, M. J.; Fuller, S. Crystal Polymorphism As a Probe for Molecular Self-Assembly During Nucleation From Solutions: The Case of 2,6- Dihydroxybenzoic Acid. *Cryst. Growth Des.* **2001,** *1,* 59-65.

(31) Davey, R. J.; Blagden, N.; Righini, S.; Alison, H.; Ferrari, E. S. Nucleation Control in Solution Mediated Polymorphic Phase Transformations: The Case of 2,6-Dihydroxybenzoic Acid. *J. Phys. Chem. B* **2002,** *106,* 1954-1959.

(32) Davey, R. J.; Allen, K.; Blagden, N.; Cross, W. I.; Lieberman, H. F.; Quayle, M. J.; Righini, S.; Seton, L.; Tiddy, G. J. T. Crystal Engineering - Nucleation, the Key Step. *CrystEngComm* **2002,** *4,* 257-264.

(33) Jackson, K. A. *Kinetic Processes: Crystal Growth, Diffusion, and Phase Transformations in Materials*; Wiley-VCH: 2006.

(34) Vere, A. W. *Crystal Growth: Principles and Progress*; Springer: 1987.

(35) Clegg, W.; Blake, A. J.; Gould, R. O.; Main, P. *Crystal Structure Analysis, Principles and Practice*; Oxford Science Publications: Oxford, 2001.

(36) . 2007.
Ref Type: Internet Communication

(37) Gavezzotti, A.; Filippini, G. Polymorphic Forms of Organic-Crystals at Room Conditions - Thermodynamic and Structural Implications. *J. Am. Chem. Soc.* **1995,** *117,* 12299-12305.

(38) Bernstein, J. Organic Solid State Chemistry. Desiraju, G. R., Ed.; Elsevier: Amsterdam, 1987; Chapter 32.

(39) Bernstein, J.; Hagler, A. T. Conformational Polymorphism. The Influence of Crystal Structure on Molecular Conformation. *J. Am. Chem. Soc.* **1978,** *100,* 673-681.

(40) Yu, L.; Stephenson, G. A.; Mitchell, C. A.; Bunnell, C. A.; Snorek, S. V.; Bowyer, J. J.; Borchardt, T. B.; Stowell, J. G.; Byrn, S. R. Thermochemistry and Conformational Polymorphism of a Hexamorphic Crystal System. *J. Am. Chem. Soc.* **2000,** *122,* 585-591.

(41) Pauling, L. *The Nature of the Chemical Bond*; Cornell University Press: Ithaca, New York, 1939.

(42) Gilli, P.; Bertolasi, V.; Ferretti, V.; Gilli, G. Covalent Nature of the Strong Homonuclear Hydrogen-Bond - Study of the O-H---O System by Crystal-Structure Correlation Methods. *J. Am. Chem. Soc.* **1994,** *116,* 909-915.

(43) Nakano, K.; Sada, K.; Miyata, M. *Chem. Commun.* **1996,** 989.

(44) Nakano, K.; Sada, K.; Miyata, M. *Prog. Colloid Polym. Sci.* **1997,** *106,* 249.

(45) Rodriguez-Spong, B.; Price, C. P.; Jayasankar, A.; Matzger, A. J.; Rodriguez-Hornedo, N. General Principles of Pharmaceutical Solid Polymorphism: a Supramolecular Perspective. *Adv. Drug Deliver. Rev.* **2004,** *56,* 241-274.

(46) Taylor, R. E. 13C CP/MAS: Application to Glycine. *Concepts in Magnetic Resonance Part A* **2004**.

(47) He, G.; Bhamidi, V.; Wilson, S. R.; Tan, R. B. H.; Kenis, P. J. A.; Zukoski, C. F. Direct Growth of Ã-Glycine From Neutral Aqueous Solutions by

Slow, Evaporation-Driven Crystallisation. *Cryst. Growth Des.* **2006,** *6,* 1746-1749.

(48) Brittain, H. G. *Polymorphism in Pharmaceutical Solids*; 2005.

(49) Day, G. M.; Trask, A. V.; Motherwell, W. D. S.; Jones, W. Investigating the Latent Polymorphism of Maleic Acid. *Chem. Commun.* **2006,** 54-56.

(50) Thallapally, P. K.; Jetti, R. K. R.; Katz, A. K.; Carrell, H. L.; Singh, K.; Lahiri, K.; Kotha, S.; Boese, R.; Desiraju, G. R. Polymorphism of 1,3,5-Trinitrobenzene Induced by a Trisindane Additive. *Angew. Chem. ,Int. Ed.* **2004,** *43,* 1149-1155.

(51) Bernstein, J. Crystal-Growth, Polymorphism and Structure-Property Relationships in Organic-Crystals. *J. Phys. D Appl. Phys.* **1993,** *26,* B66-B76.

(52) Bernstein, J. *Polymorphism in Molecular Crystals*; Clarendon Press: Oxford, 2002.

(53) Irene, E. A. *Electronic Materials Science*; Wiley-Interscience: 2005.

(54) Atkins, P. W. *Physical Chemistry*; Oxford University Press: 1998.

(55) Atkins, P. W. *Physical Chemistry*; Oxford University Press: 1994.

(56) Jacques, J.; Collet, A.; Wilen, S. H. *Enantiomers, Racemates and Resolutions*; Krieger Publishing Company Malabar: Florida, 1994.

(57) Marchand, P.; Lefebvre, L.; Querniard, F.; Cardinael, P.; Perez, G.; Counioux, J. J.; Coquerel, G. Diastereomeric Resolution Rationalized by Phase Diagrams Under the Actual Conditions of the Experimental Process. *Tetrahedron-Asymmetry* **2004,** *15,* 2455-2465.

(58) William D.Jr. *Materials Science and Engineering: An Introduction by Callister*; John Wiley & Sons: 2006.

(59) Cottrell, A. H. *An Introduction to Metallurgy*; Institute of Materials: 1967.

(60) Reviewer guidance, Validation of chromatographic methods, center for drug evalution and methods (CDER). 1994.
Ref Type: Report

(61) Reviewer guidance, Validation of chromatographic methods, center for drug evalution and methods (CDER). 1994.
Ref Type: Report

(62) Poole, C. F. *The Essence of Chromatography*; Elsevier Science B. V: 2003.

(63) Beesley, T. E.; Scott, R. P. W. *Chiral Chromatography*; John Wiley and Sons Ltd: 1998.

(64) Gans, W.; Amann, A.; Boeyens, J. C. A. *Fundamental Principles of Molecular Modelling*; Plenum Press: New York & London, 1996.

(65) Leclercq, M.; Jacques, J. Investigation of Mixtures of Enantiomers .10. Separation of Diastereoisomeric Salts Complicated by Isomorphism. *B. Soc. Chim. Fr. II-Ch* **1975,** 2052-2056.

(66) Brianso, M.-C. *Acta Crystallogr. , Sect. B* **1981,** *37,* 740-741.

(67) Fogassy, E.; Acs, M.; Faigl, F.; Simon, K.; Rohonczy, J.; Ecsery, Z. *Chem. Soc. Perkin Trans. II* **1986,** 1881-1886.

(68) Leusen, F. J. J.; Noordik, J. H.; Karfunkel, H. R. Racemate Resolution Via Crystallization of Diastereomeric Salts - Thermodynamic Considerations and Molecular Mechanics Calculations. *Tetrahedron* **1993,** *49,* 5377-5396.

(69) Caira, M. R.; Nassimbeni, L. R.; Scott, J. L.; Wildervanck, A. F. *Journal of Chemical Crystallography* **1996,** *26,* 117-122.

(70) Kinbara, K.; Hashimoto, Y.; Sukegawa, M.; Nohira, H.; Saigo, K. Crystal Structures of the Salts of Chiral Primary Amines With Achiral Carboxylic Acids: Recognition of the Commonly-Occurring Supramolecular Assemblies of Hydrogen-Bond Networks and Their Role in the Formation of Conglomerates. *J. Am. Chem. Soc.* **1996,** *118,* 3441-3449.

(71) Kinbara, K.; Sakai, K.; Hashimoto, Y.; Nohira, H.; Saigo, K. *Tetrahedron-Asymmetry* **1996,** *7,* 1539-1542.

(72) Hansen, L. M.; Frydenvang, K.; Jensen, B. *Journal of Chemical Crystallography* **1998,** *28,* 125-132.

(73) Dyer, U. C.; Henderson, D. A.; Mitchell, M. B. *Organic Process Res. Dev.* **1999,** *3,* 161-165.

(74) Kinbara, K.; Harada, Y.; Saigo, K. A High-Perfomance, Tailor-Made Resolving Agent: Remarkable Enhancement of Resolution Ability by Introducing a Naphthyl Group into the Fundamental Skeleton. *J. Chem. Soc. Perkin T. 2* **2000,** 1339-1347.

(75) Leusen, F. J. J. Crystal Structure Prediction of Diastereomeric Salts: A Step Toward Rationalization of Racemate Resolution. *Cryst. Growth Des.* **2003,** *3,* 189-192.

(76) Bolchi, C.; Pallavicini, M.; Fumagalli, L.; Marchini, N.; Moroni, B.; Rusconi, C.; Valoti, E. *Tetrahedron-Asymmetry* **2005,** *16,* 1639-1643.

(77) Kinbara, K.; Sakai, K.; Hashimoto, Y.; Nohira, H.; Saigo, K. Chiral Discrimination Upon Crystallisation of the Diastereomeric Salts of 1-Arylethylamines With Mandelic Acid or P-Methoxymandelic Acid: Interpretation of the Resolution Efficiencies on the Basis of the Crystal Structures. *J. Chem. Soc. Perkin T. 2* **1996,** 2615-2622.

(78) Kinbara, K.; Kobayashi, Y.; Saigo, K. *J. Chem. Soc. , Perkin Trans.* **1998,** *2,* 1767-1775.

(79) Kobayashi, Y.; Kurasawa, T.; Kinbara, K.; Saigo, K. *J. Org. Chem.* **2004,** *69,* 7436-7441.

(80) van Eijck, B. P. Ab Initio Crystal Structure Predictions for Flexible Hydrogen- Bonded Molecules. Part III. Effect of Lattice Vibrations. *J. Comput. Chem.* **2001,** *22,* 816-826.

(81) Li, Z. J.; Ojala, W. H.; Grant, D. J. W. Molecular Modeling Study of Chiral Drug Crystals: Lattice Energy Calculations. *J. Pharm. Sci.* **2001,** *90,* 1523-1539.

(82) Karamertzanis, P. G.; Pantelides, C. C. Ab Initio Crystal Structure Prediction - I. Rigid Molecules. *J. Comput. Chem.* **2005,** *26,* 304-324.

(83) Karamertzanis, P. G.; Pantelides, C. C. Ab Initio Crystal Structure Prediction. II. Flexible Molecules. *Mol. Phys.* **2007,** *105,* 273-291.

(84) Kitaigorodski, A. I. *Molecular Crystals and Molecules*; Academic Press: New York, 1973.

(85) Blazejowski, J.; Lubkowski, J. Lattice Energy of Organic Ionic Crystals and Its Importance in Analysis of Features, Behaviour and Reactivity of Solid-State Systems. *J. Therm. Anal.* **1992,** *38,* 2195-2210.

(86) GROMACS User Manual. 2002. University of Groningen.
Ref Type: Computer Program

(87) Willock, D. J.; Price, S. L.; Leslie, M.; Catlow, C. R. A. The Relaxation of Molecular Crystal Structures Using a Distributed Multipole Electrostatic Model. *J. Comput. Chem.* **1995,** *16,* 628-647.

(88) Stone, A. J.; Alderton, M. Distributed Multipole Analysis - Methods and Applications. *Mol. Phys.* **1985,** *56,* 1047-1064.

(89) Leininger, M. L.; Allen, W. D.; Schaefer, H. F.; Sherrill, C. D. Is Moller-Plesset Perturbation Theory a Convergent Ab Initio Method? *J. Chem. Phys.* **2000,** *112,* 9213-9222.

(90) Vega, C.; McBride, C.; MacDowell, L. G. *Phys. Chem. Chem. Phys.* **2002,** *4,* 853-862.

(91) Wales, D. J.; Fowler, P. W. *Intermolecular Forces and Clusters*; Springer: 2005.

(92) Karamertzanis, P. G.; Price, S. L. Energy Minimization of Crystal Structures Containing Flexible Molecules. *J. Chem. Theory Comput.* **2006,** *2,* 1184-1199.

(93) Frisch, M. J.; Trucks, G. W.; Schlegel, H. B.; Scuseria, G. E.; Robb, M. A.; Cheeseman, J. R.; Zakrzewski, V. G.; Montgomery, Jr. J. A.; Stratmann, R. E.; Burant, J. C.; Dapprich, S.; Millam, J. M.; Daniels, A. D.; Kudin, K. N.; Strain, M. C.; Farkas, O.; Tomasi, J.; Barone, V.; Cossi, M.; Cammi, R.; Mennucci, B.; Pomelli, C.; Adamo, C.; Clifford, S.; Ochterski, J.; Petersson, G. A.; Ayala, P. Y.; Cui, Q.; Morokuma, K.; Malick, D. K.; Rabuck, A. D.; Raghavachari, K.; Foresman, J. B.; Cioslowski, J.; Ortiz, J. V.; Baboul, A. G.; Stefanov, B. B.; Liu, G.; Liashenko, A.; Piskorz, P.; Komaromi, I.; Gomperts, R.; Martin, R. L.; Fox, D. J.; Keith, T.; Al-Laham, M. A.; Peng, C. Y.; Nanayakkara, A.; Challacombe, M.; Gill, P. M. W.; Johnson, B.; Chen, W.; Wong, M. W.; Andres, J. L.; Gonzalez, C.; Head-Gordon, M.; Replogle, E. S.; Pople, J. A. Gaussian98, Revision A.9. 1998. Pittsburgh PA, Gaussian, Inc.
Ref Type: Computer Program

(94) Stone, A. J. GDMA: A Program for Performing Distributed Multipole Analysis of Wave Functions Calculated Using the Gaussian Program System. [1.0]. 1999. Cambridge, United Kingdom, University of Cambridge.
Ref Type: Computer Program

(95) Coombes, D. S.; Leslie, M. Online Manual for Neighbours 3.01. www.ucl.ac.uk/~ucca17p/neighmanual/index.html . 2001.
Ref Type: Internet Communication

(96) Kitaigorodskii, A. I. *Molecular Crystal and Molecules*; Academic Press: New York, 1973.

(97) Stone, A. J. Distributed Multipole Analysis, or How to Describe a Molecular Charge Distribution. *Chem. Phys. Lett.* **1981,** *83,* 233-239.

(98) Mitchell, J. B. O.; Price, S. L.; Leslie, M.; Buttar, D.; Roberts, R. J. Anisotropic Repulsion Potentials for Cyanuric Chloride (C3N3Cl3) and Their Application to Modeling the Crystal Structures of Azaaromatic Chlorides. *J. Phys. Chem. A* **2001,** *105,* 9961-9971.

(99) Ewald, P. *Ann. Phys.* **1921,** *64,* 253.

(100) Toukmaji, A. Y.; Board, J. A. Ewald Summation Techniques in Perspective: A Survey. *Comput. Phys. Commun.* **1996,** *95,* 73-92.

(101) Yff, B.; Menken, L.; Royall, P. G.; Cains, P. W. *In preparation* **2005**.

(102) Coombes, D. S.; Price, S. L.; Willock, D. J.; Leslie, M. Role of Electrostatic Interactions in Determining the Crystal Structures of Polar Organic Molecules. A Distributed Multipole Study. *J. Phys. Chem.* **1996,** *100,* 7352-7360.

(103) Allen, F. H.; Kennard, O.; Watson, D. G.; Brammer, L.; Orpen, A. G.; Taylor, R. Tables of Bond Lengths Determined By X-Ray and Neutron-Diffraction .1. Bond Lengths in Organic-Compounds. *J. Chem. Soc. Perk. T. 2* **1987,** S1-S19.

(104) Allen, F. H. The Cambridge Structural Database: a Quarter of a Million Crystal Structures and Rising. *Acta Crystallogr. , Sect. B* **2002,** *58,* 380-388.

(105) Chisholm, J. A.; Motherwell, S. COMPACK: a Program for Identifying Crystal Structure Similarity Using Distances. *J. Appl. Crystallogr.* **2005,** *38,* 228-231.

(106) CCDC. Mercury. 2004. http://www.ccdc.cam.ac.uk/products/csd_system/mercury/. Ref Type: Computer Program

(107) Karamertzanis, P. G.; Anandamanoharan, P. R.; Fernandes, P.; Cains, P. W.; Vickers, M.; Tocher, D. A.; Florence, A. J.; Price, S. L. Toward the Computational Design of Diastereomeric Resolving Agents: An Experimental and Computational Study of 1-Phenylethylammonium-2-Phenylacetate Derivatives. *J. Phys. Chem. B* **2007,** *111,* 5326-5336.

(108) Dufour, F.; Perez, G.; Coquerel, G. A Priori Assessment of the Maximum Possible Entrainment Effect Attainable During Preferential Crystallization. The Case of the Simultaneous Resolution of (+-)-Ephedrine and (+-)-Mandelic Acid. *Bull. Chem. Soc. Jpn.* **2004,** *77,* 79-86.

(109) Brianso, M. C. Structures Atomiques Et Moléculaires Des Sels Diastéréoisomères Des α-Phényl-α-Méthylacétates D'α-Phényl-Éthylammonium *p* Et *n*. *Acta Crystallogr. , Sect. B.* **1976,** *32,* 3040-3045.

(110) Brianso, M.-C. *Acta Crystallogr. , Sect. B* **1981,** *37,* 740-741.

(111) Fernandes, P.; Florence, A.; Shankland, K.; Karamertzanis, P. G.; Hulme, A.; Anandamanoharan, P. *Acta Crystallogr. ,Sect. E:Struct. Rep. Online* **2007,** *63,* 0247.

(112) Fernandes, P.; Florence, A. J.; Shankland, K.; Karamertzanis, P. G.; Hulme, A. T.; Anandamanoharan, R. P. Powder Study of (R)-1-Phenylethylammonium (R)-2-Phenylbutyrate Form 3. *Acta Crystallogr. , Sect. E* **2007,** *63,* O202-O204.

(113) Brianso, M. C. *European Crystallography Meeting* **1980,** *6,* 327.

(114) Brianso, M. C. α-Phényl-α-Éthyl-Acétate D'α-Phényl-Éthylammonium *n*. *Acta Crystallogr. , Sect. B.* **1978,** *34,* 679-680.

(115) Larsen, S.; Kozma, D.; Acs, M. Crystal-Structure at 110K of (R)-1-Phenylethylammonium Hydrogen Maleate-Water (1/0.25), and A Study of the Conformation of 1-Phenylethylammonium Ions. *Acta Chem. Scand.* **1994,** *48,* 32-36.

(116) Larsen, S.; Lopez de Diego, H. *Acta Crystallogr. , Sect. B* **1993,** *49,* 303.

(117) Lopez de Diego, H. *Acta Chem. Scand.* **1994,** *48,* 306.

(118) Brianso, M.-C.; Leclercq, M.; Jacques, J. Mandélate De Phényl-1 Éthylamine. *Acta Crystallogr. , Sect. B.* **1979,** *35,* 2751-2753.

(119) Dufour, F.; Gervais, C.; Petit, M. N.; Perez, G.; Coquerel, G. Investigations on the Reciprocal Ternary System (+/-)-2-Phenylpropionic Acid-(+/-)-Alpha-Methylbenzylamine. Impact of an Unstable Racemic Compound on the Simultaneous Resolution of Chiral Acids and Bases by Preferential Crystallisation. *J. Chem. Soc. Perkin T. 2* **2001,** *2,* 2022-2036.

(120) Yff, B.; Menken, L.; Royall, P. G.; Cains, P. W. 2006.
Ref Type: Unpublished Work

(121) Anandamanoharan, P. R.; Cains, P. W.; Jones, A. G. Separability of Diastereomer Salt Pairs of 1-Phenylethylamine With Enantiomeric 2-Substituted Phenylacetic Acids by Fractional Crystallization, and Its Relation to Physical and Phase Properties. *Tetrahedron-Asymmetry* **2006,** *17,* 1867-1874.

(122) Burger, A.; Ramberger, R. Polymorphism of Pharmaceuticals and Other Molecular-Crystals .1. Theory of Thermodynamic Rules. *Mikrochim. Acta* **1979,** *2,* 259-271.

(123) Burger, A.; Ramberger, R. Polymorphism of Pharmaceuticals and Other Molecular-Crystals .2. Applicability of Thermodynamic Rules. *Mikrochim. Acta* **1979,** *2,* 273-316.

(124) Collet, A. In *Comprehensive Supramolecular Chemistry*; Atwood, J. L., Davies, J. E. D., MacNicol, D. D., Reinhoudt, D. N., Eds.; Pergammon: Oxford, 1996; Chapter 10.

(125) Marchand, P.; Lefebvre, L.; Querniard, F.; Cardinael, P.; Perez, G.; Counioux, J. J.; Coquerel, G. Diastereomeric Resolution Rationalized by Phase Diagrams Under the Actual Conditions of the Experimental Process. *Tetrahedron-Asymmetry* **2004,** *15,* 2455-2465.

(126) Dyer, U. C.; Henderson, D. A.; Mitchell, M. B. *Organic Process Res. Dev.* **1999,** *3,* 161-165.

(127) Dyer, U. C.; Henderson, D. A.; Mitchell, M. B. *Organic Process Res. Dev.* **1999,** *3,* 161-165.

(128) Lopez de Diego, H. (*R*,*S*)-1-Phenylethylammonium (*S*)-Mandelate. *Acta Crystallogr. , Sect. C* **1994,** *50,* 1995-1998.

(129) Lopez de Diego, H. (*S*)-1-Phenylethylammonium (*S*)-Mandelate-Mandelic Acid (1/2), $C_{8H12N}{}^{+}.C_{8H7O3}{}^{-}.2C_{8H8O3}$. *Acta Crystallogr. , Sect. C* **1995,** *51,* 253-256.

(130) Larsen, S.; Dediego, H. L. Isolation of Different Enantiomers Caused by Variation in the Stoichiometric Ratio of Racemate and Resolving Agent - the Crystal-Structure of (R)-1-Phenylethylammonium (S)-Mandelate.Dimandelic Acid. *J. Chem. Soc. Perkin T. 2* **1993,** 469-473.

(131) Karamertzanis, P. G.; Price, S. L. Challenges of Crystal Structure Prediction of Diastereomeric Salt Pairs. *J. Phys. Chem. B* **2005,** *109,* 17134-17150.

(132) Sheldrick, G. M. SHELXS97. 1997. Göttingen, Germany, University of Göttingen.
Ref Type: Computer Program

(133) Sheldrick, G. M. SHELXL97. 1997. Göttingen, Germany, University of Göttingen.
Ref Type: Computer Program

(134) Chemburkar, S. R.; Bauer, J.; Deming, K.; Spiwek, H.; Patel, K.; Morris, J.; Henry, R.; Spanton, S.; Dziki, W.; Porter, W.; Quick, J.; Bauer, P.; Donaubauer, J.; Narayanan, B. A.; Soldani, M.; Riley, D.; McFarland, K. Dealing With the Impact of Ritonavir Polymorphs on the Late Stages of Bulk Drug Process Development. *Organic Process Res. Dev.* **2000,** *4,* 413-417.

(135) Dunitz, J. D.; Bernstein, J. Disappearing Polymorphs. *Accounts Chem. Res.* **1995,** *28,* 193-200.

(136) McCausland, L. J.; Cains, P. W.; Martin, P. D. *Chem. Engg. Progr* **2001,** *97,* 56.

(137) McCausland, L. J.; Cains, P. W.; Martin, P. D. *Chem. Engg. Progr* **2001,** *97,* 56.

(138) McCausland, L. J.; Cains, P. W.; Martin, P. D. *Chem. Engg. Progr* **2001,** *97,* 56.

APPENDIX 2: THE CRYSTALLOGRAPHIC INFORMATION FOR THE DETERMINED AND REDETERMINED STRUCTURES

Table_31 Summary crystal data: (R)-1-phenylethylammonium-(R,S)-2-phenylpropanoate A1

Crystal structure	**RSA1** **AFINEJ**	**RRA1 form I** **NMACEP03**
Empirical formula	$C_8H_{12}N_1^+ \bullet C_9H_9O_2^-$	$C_8H_{12}N_1^+ \bullet C_9H_9O_2^-$
Chemical formula weight **Fw (g.mol^{-1})**	271.36	271.36
Temperature **T (K)**	150	150
Crystal system	Monoclinic	Orthorhombic
Space group	$P2_1$	$P2_12_12_1$
Unit cell dimensions **a (Å)** **b (Å)** **c (Å)** **α (Å)** **β (Å)** **γ (Å)**	 11.0078(13) 6.5388(8) 12.1605(15) 90 116.014(2) 90	 5.7612(7) 15.3756(18) 16.8243(19) 90 90 90
Cell volume **V (Å^3)**	786.608	1490.329
Z	2	4
Crystal density **D_m (g.cm^{-3})**	1.146	1.209
F(000)	292	584
Crystal size [mm^3]	0.49 x 0.08 x 0.07	0.81 x 0.16 x 0.05
θ range [^{o}]	2 → 28.5	1.8 → 28.5
Reflections collected	6860	13003
Independent reflections	3577 [R_{int} = 0.0232]	2103 [R_{int} = 0.0312]
Data / restraints / parameters	3577 / 1 / 265	2103 / 0 / 265
S	1.021	1.078
R [I<2σ(I)]	R1 = 0.0407 wR2 = 0.0949	R1 = 0.0308 wR2 = 0.0880
R indices (all data)	R1 = 0.0466 wR2 = 0.0982	R1 = 0.0381 wR2 = 0.0893

Table_32 Summary crystal data: (R)-1-phenylethylammonium-(R)-2-phenylbutyrate A2

Crystal structure	**RRA2 form I** **PBUPEA03**
Empirical formula	$C_8H_{12}N^+ \bullet C_{10}H_{11}O_2^-$
Chemical formula weight **Fw (g.mol^{-1})**	285.38
Temperature **T (K)**	150
Crystal system	Orthorhombic
Space group	$P2_12_12_1$
Unit cell dimensions **a (Å)** **b (Å)** **c (Å)** **α (Å)** **β (Å)** **γ (Å)**	 5.7573(5) 15.4334(13) 17.5712(15) 90 90 90
Cell volume **V (Å^3)**	1561.284
Z	4
Crystal density **D_m (g.cm^{-3})**	1.214
F(000)	616
Crystal size [mm^3]	0.48 x 0.12 x 0.10
θ range [^{o}]	1 → 29
Reflections collected	13905
Independent reflections	3746 [R_{int} = 0.0377]
Data / restraints / parameters	3746 / 0 / 283
S	1.046
R [I<2σ(I)]	R1 = 0.0398 wR2 = 0.0935
R indices (all data)	R1 = 0.0433 wR2 = 0.0956

Table_33 Summary crystal data: (R)-1-phenylethylammonium-(R)-2-phenylbutyrate A2[a]

Crystal structure	**RRA2 form II** **PBUPEA01**	**RRA3 form III** **PBUPEA02**
Empirical formula	$C_8H_{12}N^+ \bullet C_{10}H_{11}O_2^-$	$C_8H_{12}N^+ \bullet C_{10}H_{11}O_2^-$
Chemical formula weight **Fw (g.mol^{-1})**	285.38	285.38
Temperature **T (K)**	295	295
Crystal system	Orthorhombic	Monoclinc
Space group	$P2_12_12_1$	$P2_1$
Unit cell dimensions		
a (Å)	6.0620(1)	11.88215(15)
b (Å)	16.7794(3)	5.97647(8)
c (Å)	16.8881(4)	13.07499(15)
α (Å)	90	90
β (Å)	90	113.510(1)
γ (Å)	90	90
Cell volume **V (Å^3)**	1717.802	851.424
Z	4	2
Crystal density **D_m (g.cm^{-3})**	1.104	1.113

[a] The two structures presented in **Table_33** were obtained from powder diffraction data and therefore full CIF file is not available

Table_34 Summary crystal data: (R)-1-phenylethylammonium-(R)-2-mandelate A3

Crystal structure	**RRA3 form III** **PIVGEH01**
Empirical formula	$C_8H_{12}N_1^+ \bullet C_8H_7O_3^-$
Chemical formula weight **Fw (g.mol^{-1})**	273.33
Temperature **T (K)**	150
Crystal system	Orthorhombic
Space group	$P2_12_12_1$
Unit cell dimensions **a (Å)** **b (Å)** **c (Å)** **α (Å)** **β (Å)** **γ (Å)**	 6.8488(6) 8.3253(7) 25.441(2) 90 90 90
Cell volume **V (Å^3)**	1450.603
Z	4
Crystal density **D_m (g.cm^{-3})**	1.252
F(000)	584
Crystal size [mm^3]	0.45 x 0.10 x 0.05
θ range [^{o}]	1.5 → 28.5
Reflections collected	12784
Independent reflections	3450 [R_{int} = 0.0603]
Data / restraints / parameters	3450 / 0 / 257
S	1.088
R [I<2σ(I)]	R1 = 0.0588 wR2 = 0.0980
R indices (all data)	R1 = 0.0757 wR2 = 0.1034

APPENDIX 3: PACKING DIAGRAMS

This appendix contains the packing diagrams of the structures used in this work, but not structurally determined through this work.

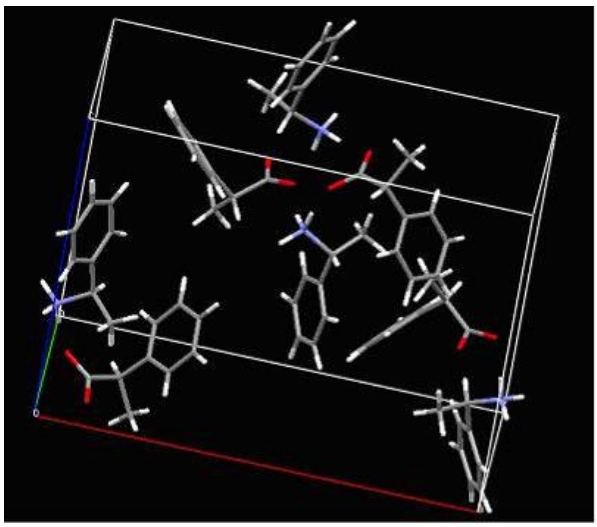

Fig53 Packing diagram of (R)-1-phenylethylammonium-(R)-2-phenylpropanoate (RRA1) polymorph II (NMACEP01, drawn using Mercury) with a space group of $P2_12_12_1$

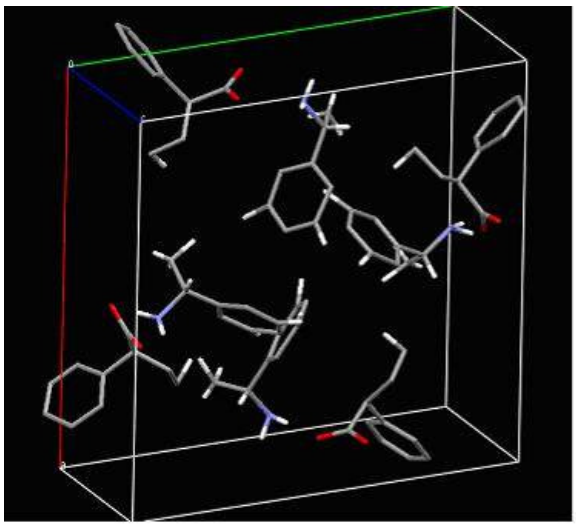

Fig54 Packing diagram of (R)-1-phenylethylammonium-(S)-2-phenylbutyrate (RSA2) (PEAPEA10, drawn using Mercury) with a space group of $P4_1$

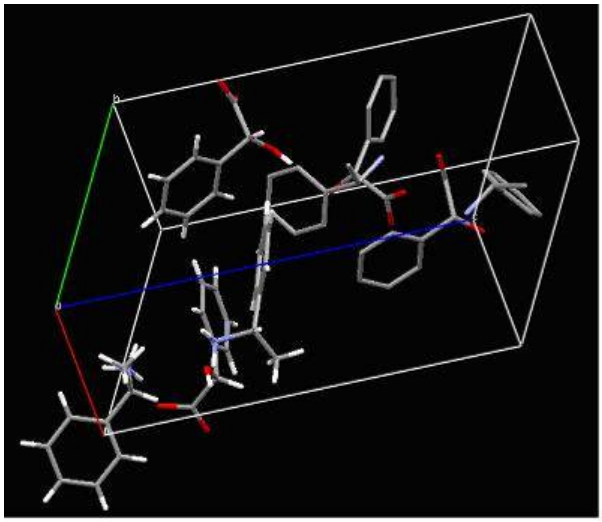

Fig55 Packing diagram of (S)-1-phenylethylammonium-(R)-2-mandelate (RSA3) (PIVGEG, drawn using Mercury) with a space group of *P*1, Z' = 4

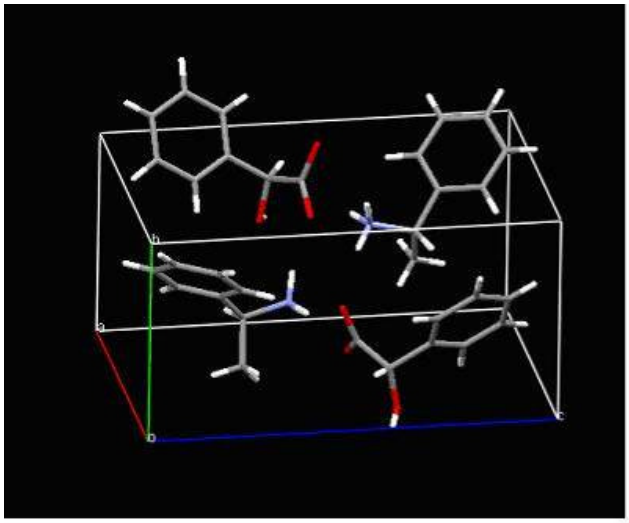

Fig56 Packing diagram of (R)-1-phenylethylammonium-(R)-2-mandelate polymorph II (RRA3) (PEAMAN01, drawn using Mercury) with a space group of $P2_1$

APPENDIX 4: THERMAL MEASUREMENTS FOR A2

The TGA and DSC results corresponding to (R)-1-phenylethylammonium-(R,S)-2-phenylbutyrate are presented in **Fig57**, **Fig58** and **Fig59**.

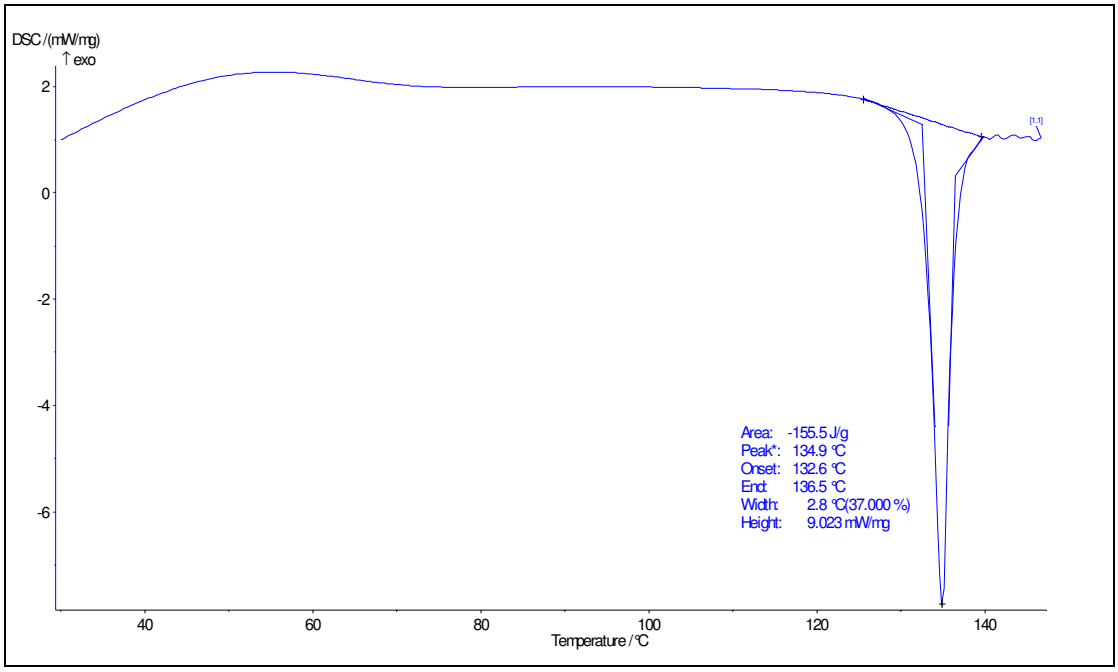

Fig57 DSC profile for sample RSA2 showing the single endotherm accompanying fusion of the sample at ca. 408 K

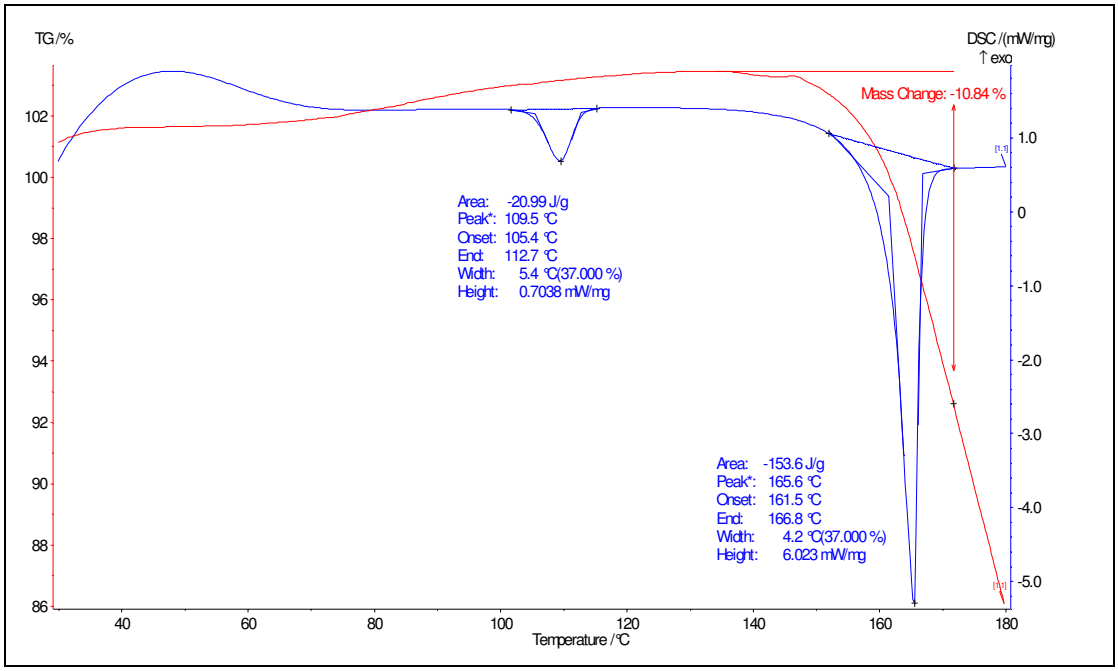

Fig58 DSC (blue) and TGA (red) curves for RRA2 form I: RRA2 form I transforming to RRA2 form III at ca. 383 K

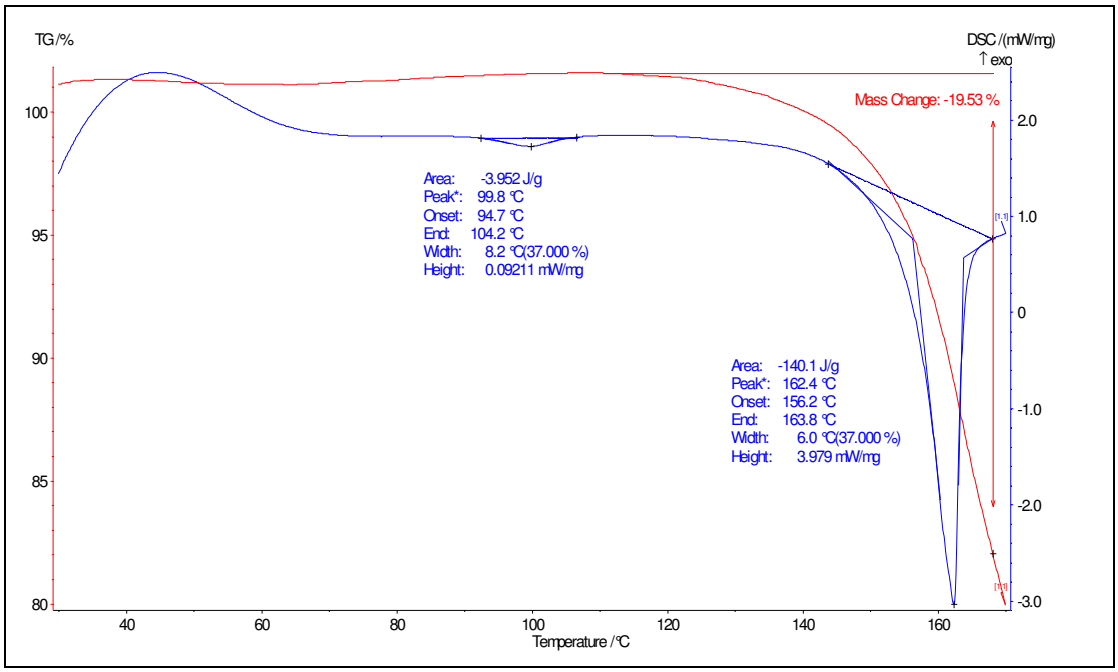

Fig59 DSC (blue) and TGA (red) curves for RRA2 form II: RRA2 form II transforming to RRA2 form III at ca. 373 K

APPENDIX 5: THERMAL MEASUREMENTS FOR A3

The TGA and DSC results corresponding to (R)-1-phenylethylammonium-(R,S)-mandelate are presented in **Fig60**, **Fig61** and **Fig62**.

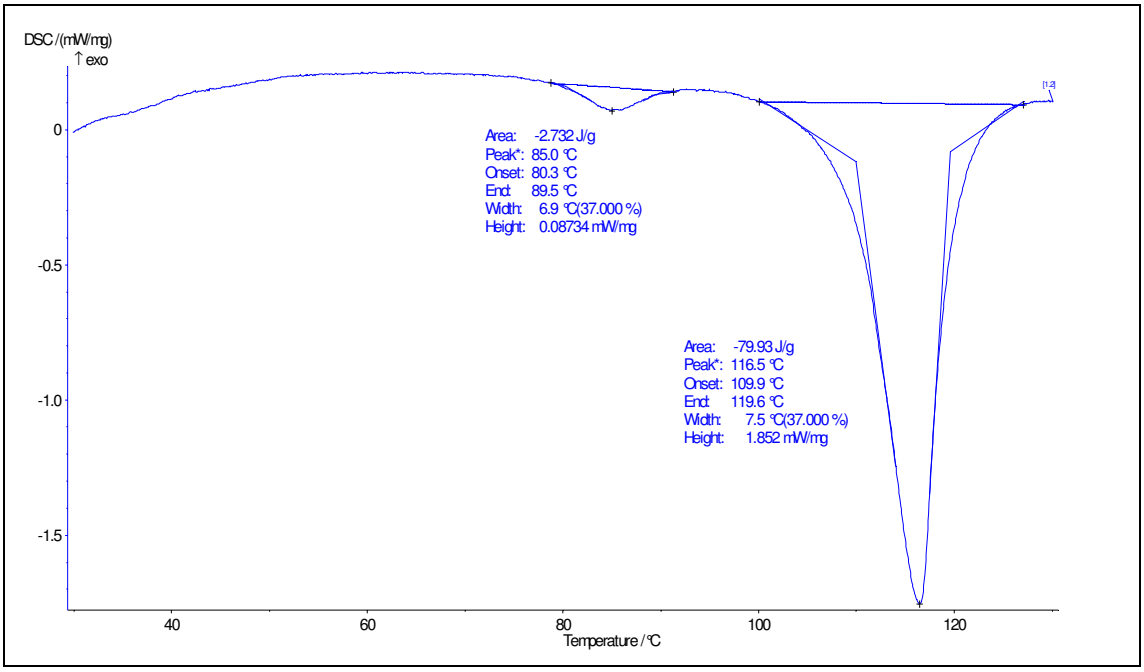

Fig60 DSC curves for the RSA3 (the minor endothermic event at ca. 353 K is not accompanied by a noticeable change in the PXRD patterns)

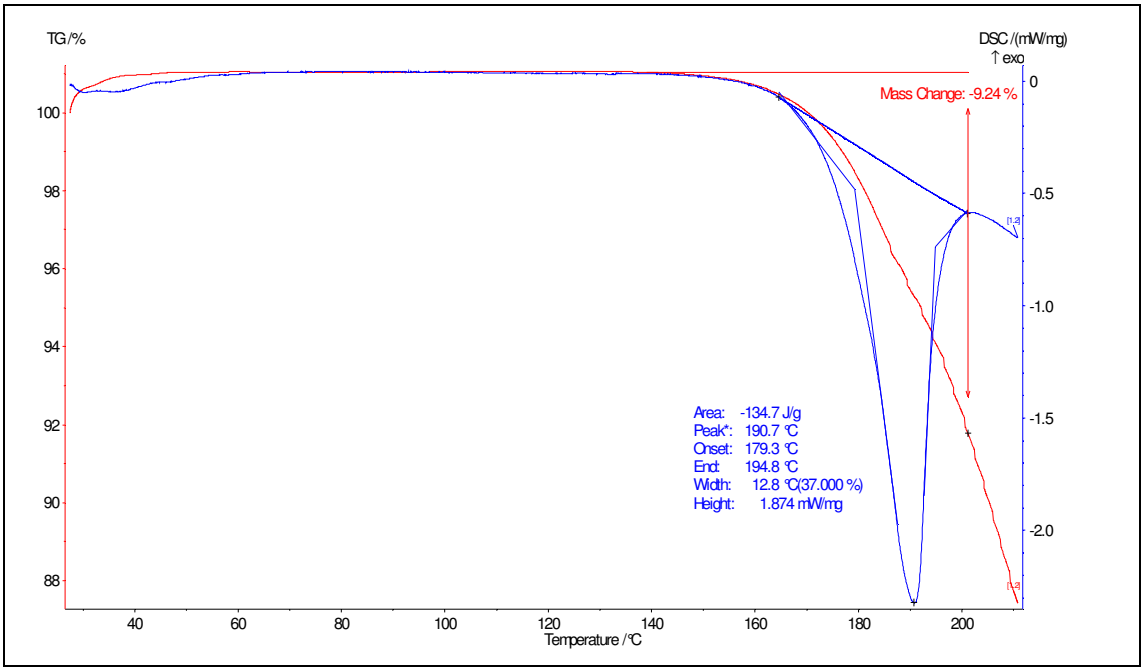

Fig61 RRA3 form I diastereomeric salt pair. The mass loss is only shown for systems where decomposition is significant

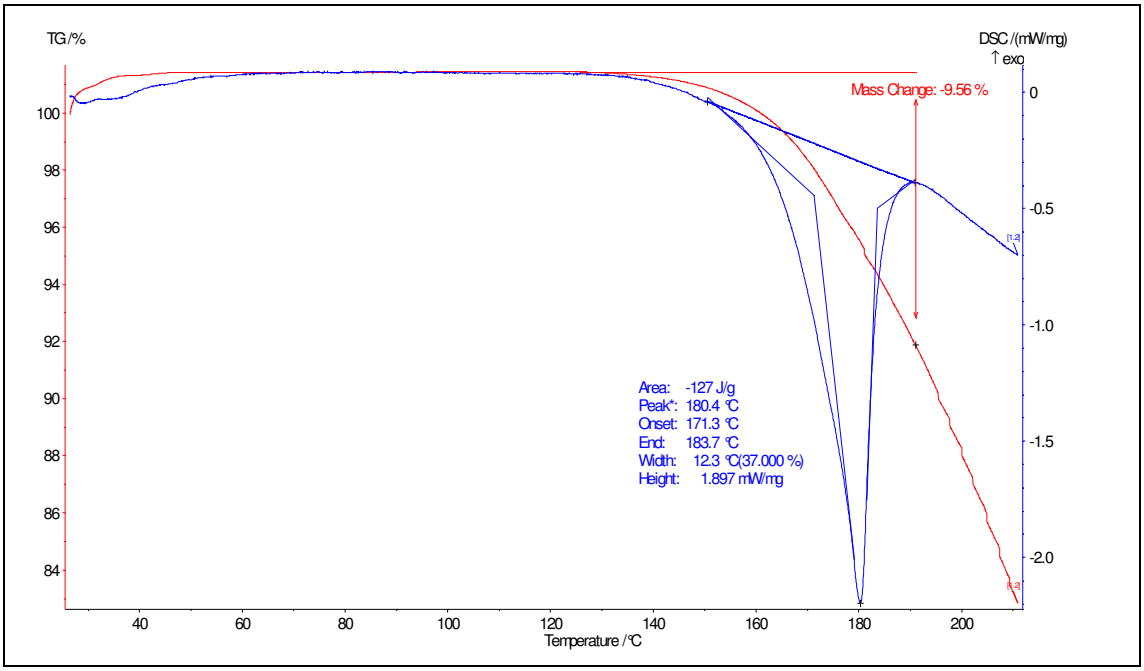

Fig62 RRA3 form II diastereomeric salt pair. The mass loss is only shown for systems where decomposition is significant

APPENDIX 6: DATA CORRESPONDING TO ENTHALPY ΔH AND ENTROPY ΔS CALCULATIONS

- Solubility S of the diastereomer salts was measured using HPLC measurements at different temperatures.
- Solubility dimensionless = Solubility / density, to keep the result dimensionless, in order to enter it into neperian logarithm Ln.
- T (K) = 273 + T (°C).
- 1/T = 1/T(K).

Table_15 Containing the results corresponding to S_{RRA1}

Solubility S_{RRA1} (mol/L)	**Temperature T (°C)**	**Solubility S_{RRA1} dimensionless**	**Ln S_{RRA1}**	**Temperature T (K)**	**1/T**
0.093059	05	0.038069	**-3.26835**	278	**0.003597**
0.137979	15	0.056445	**-2.87448**	288	**0.003472**
0.220230	25	0.090093	**-2.40691**	298	**0.003356**
0.341005	35	0.139500	**-1.96969**	308	**0.003247**
0.513698	45	0.210146	**--1.55995**	318	**0.003145**
0.754762	55	0.308762	**-1.17518**	328	**0.003049**

Density RRA1 = 2.444477 mol.L^{-1}.

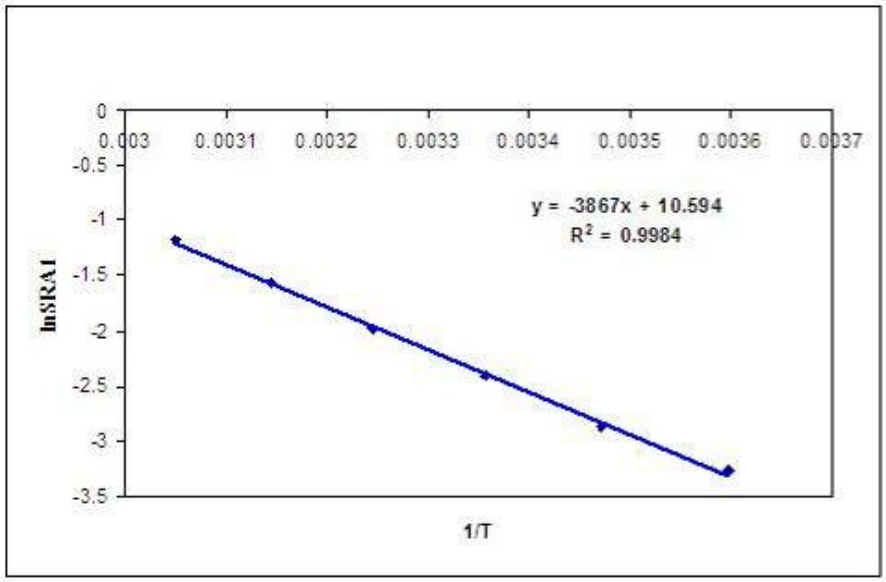

Fig40 ln (Solubility) versus 1/Temperature of RRA1 diastereomer salt

From the graph, the equation of the straight line has been deduced:

y = -3867x + 10.594, which corresponds to Ln (S_{RA1}) = -A/T + B = -ΔH/RT + ΔS/R, with R corresponding to the gas constant with a value of R ≈ 8.4122 $J.mol^{-1}.K^{-1}$.

Therefore **ΔH** = 3867 * 8.4122 = 325299.9 $J.mol^{-1}$ = **32.53 $KJ.mol^{-1}$**,

And **ΔS** = 10.594 * 8.4122 = **89.14 $J.mol^{-1}.K^{-1}$.**

Table_16 Containing the results corresponding to S_{RSA1}

Solubility S_{RSA1} (mol/L)	**Temperature T (°C)**	**Solubility S_{RSA1} dimensionless**	**Ln SSA1**	**Temperature T (K)**	**1/T**
0.083589	05	0.020189	**-3.90260**	278	**0.003597**
0.137518	15	0.033215	**-3.40476**	288	**0.003472**
0.197964	25	0.047815	**-3.04043**	298	**0.003356**
0.278318	35	0.067223	**-2.69975**	308	**0.003247**
0.382998	45	0.092506	**-2.38048**	318	**0.003145**
0.516890	55	0.124845	**-2.08068**	328	**0.003049**

Density SRA1 = 4.14025 $mol.L^{-1}$.

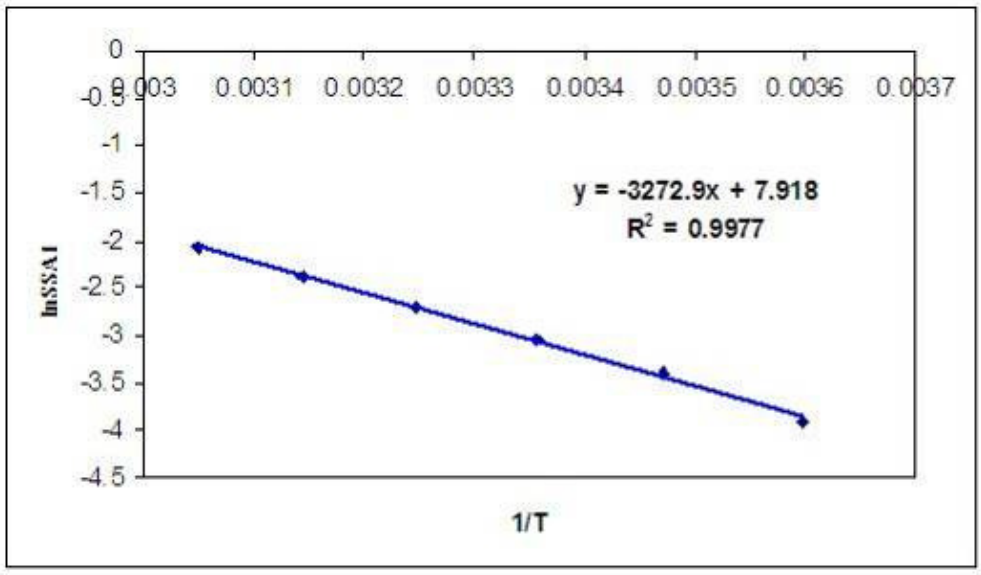

Fig41 ln (Solubility) versus 1/Temperature of RSA1 diastereomer salt

y= -3272.9x + 7.918 and therefore **ΔH = 27.54 $KJ.mol^{-1}$** and **ΔS = 66.62 $J.mol^{-1}.K^{-1}$**.

APPENDIX 7: EQUILIBRIUM OF A1 AT 30 AND 50°C

Fig63 contains a diagram of the state of salts (acid and base) and solution, before and after equilibrium.

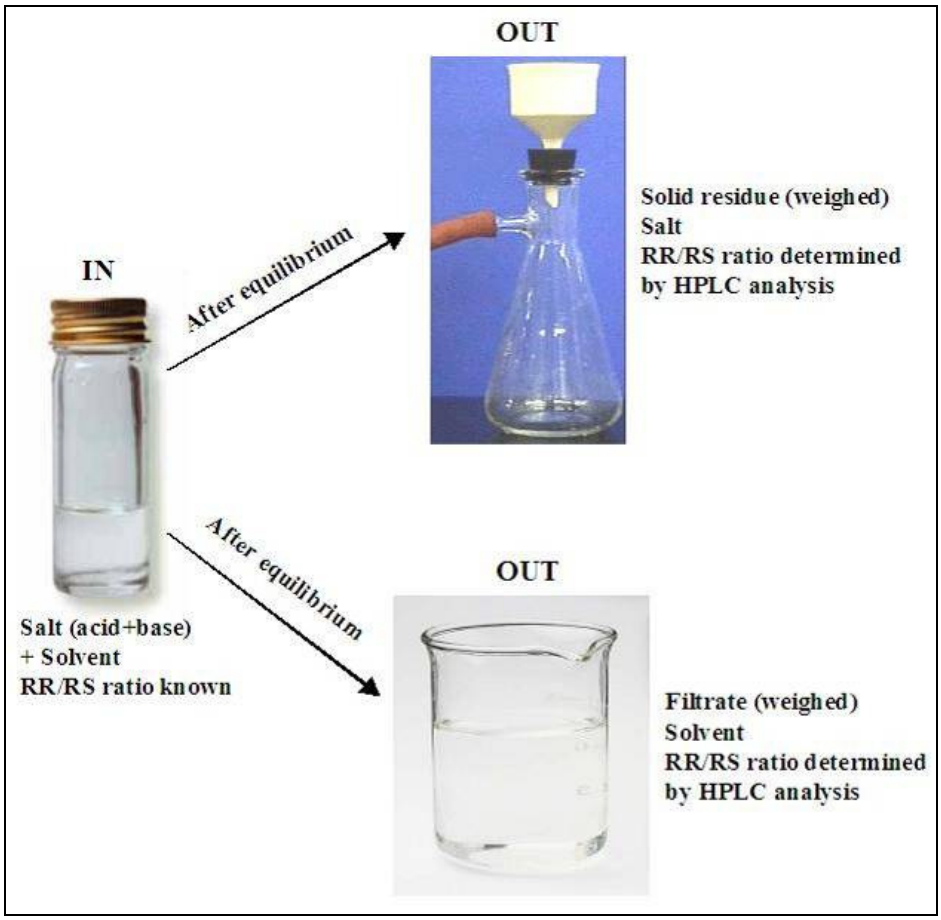

Fig63 Before and after equilibrium

The equations, which were used to calculate the values in **Table_31** and **Table_32**, are as follows.

The total amount of acid dissolved at the beginning of the experiment is calculated as in equation **(46)**:

$$\textbf{Total salt dissolved} = \textbf{Weight}_{\textbf{acid}} \times \textbf{MW}_{\textbf{A1 (or A2 or A3)}} / \textbf{MW}_{\textbf{acid}} \qquad \textbf{(46)}$$

Where $\textbf{MW}_{\textbf{A1 (or A2 or A3)}}$ corresponds to the molecular weight of the diastereomer salt A1, A2 or A3 and $\textbf{MW}_{\textbf{acid}}$ corresponds to the molecular weight of the acid used (for

the calculations presented below, the molecular weight of the acid corresponds to 2-phenylpropanoic acid).

The weight of RR-diastereomer salt, present in solution, at the beginning of the experiment is calculated by the equation **(47)**:

$$\textbf{Weight}_{\textbf{initial RR salt}} = \textbf{Total salt dissolved x Starting RR ratio / 100} \quad \textbf{(47)}$$

The weight of RS-diastereomer salt, present in solution, at the beginning of the experiment is calculated either using equation **(48)** or equation **(49)**:

$$\textbf{Weight}_{\textbf{initial RS salt}} = \textbf{Total salt dissolved x Starting RS ratio / 100} \quad \textbf{(48)}$$

$$\textbf{Weight}_{\textbf{initial RS salt}} = \textbf{Total salt dissolved - Weight}_{\textbf{initial RR salt}} \quad \textbf{(49)}$$

The weight of the RR diastereomer salt, in the solid residue, after equilibrium, is calculated as in **(50)**:

$$\textbf{Weight}_{\textbf{RR salt (crystal)}} = \textbf{Weight}_{\textbf{crystallised solid}} \textbf{ x Solid RR ratio / 100} \quad \textbf{(50)}$$

The weight of the RS diastereomer salt, in the solid residue, after equilibrium, is calculated either by equation **(51)** or **(52)**:

$$\textbf{Weight RS}_{\textbf{salt (crystal)}} = \textbf{Weight}_{\textbf{crystallised solid}} \textbf{ x Solid RS ratio / 100} \quad \textbf{(51)}$$

$$\textbf{Weight RS}_{\textbf{salt (crystal)}} = \textbf{Weight}_{\textbf{crystallised solid}} \textbf{ - Weight}_{\textbf{RR salt (crystal)}} \quad \textbf{(52)}$$

The theoretical weight of the solid in filtrate is calculated assuming that there was 100% recovery of the solid. The theoretical weight is calculated as **(53)**:

$$\textbf{Weight}_{\textbf{solid in filtrate}} = \textbf{Total salt}_{\textbf{dissolved (measured) at the beginning}} - \textbf{Weight}_{\textbf{crystals (measured) after equilibrium}} \quad \textbf{(53)}$$

The amount of RR salt present in the filtrate is calculated as **(54)**, assuming that there was 100% recovery of solid:

$$\textbf{Weight}_{\textbf{RR salt in the filtrate}} = \textbf{Weight}_{\textbf{solid in filtrate}} \times \textbf{Filtrate RR ratio / 100} \quad \textbf{(54)}$$

The amount of RS salt present in the filtrate is calculated as **(55)** or **(56)**, assuming that there was 100% recovery of solid:

$$\textbf{Weight}_{\textbf{RS salt in the filtrate}} = \textbf{Weight}_{\textbf{solid in filtrate}} \times \textbf{Filtrate RS ratio / 100} \quad \textbf{(55)}$$

$$\textbf{Weight}_{\textbf{RS salt in the filtrate}} = \textbf{Weight}_{\textbf{solid in filtrate}} - \textbf{Weight}_{\textbf{RR salt in the filtrate}} \quad \textbf{(56)}$$

The weight of the filtrate is calculated as **(57)**, assuming that there was no solvent loss during the equilibrium experiment:

$$\textbf{Weight}_{\textbf{filtrate}} = \textbf{Weight}_{\textbf{solvent added at the beginning}} + \textbf{Weight}_{\textbf{solid in filtrate}} \quad \textbf{(57)}$$

The theoretical weight of RR salt dissolved in the solution is calculated by the difference as **(58)**:

$$\textbf{Weight}_{\textbf{RR salt in solution}} = \textbf{Weight}_{\textbf{initial RR salt}} - \textbf{Weight}_{\textbf{RR salt (crystal)}} \quad \textbf{(58)}$$

The theoretical weight of RS salt dissolved in the solution is calculated by the difference as **(59)**:

$$\textbf{Weight}_{\textbf{RS salt in solution}} = \textbf{Weight}_{\textbf{initial RS salt}} - \textbf{Weight}_{\textbf{RS salt (crystal)}} \quad \textbf{(59)}$$

The total weight of salt present dissolves in solution is calculated as **(60)**:

$$\textbf{Total Weight}_{\textbf{salt in solution}} = \textbf{Weight}_{\textbf{RR salt in solution}} + \textbf{Weight}_{\textbf{RS salt in solution}} \quad \textbf{(60)}$$

The theoretical ratio of RR salt present in the filtrate is calculated as **(61)**:

$$\textbf{RR ratio}_{\textbf{in the filtrate}} = \textbf{Weight}_{\textbf{RR salt in solution}} \times 100 / \textbf{Total Weight}_{\textbf{salt in solution}} \quad \textbf{(61)}$$

The theoretical ratio of RS salt present in the filtrate is calculated as **(62)**:

RS ratio $_{\text{in the filtrate}}$ **= Weight** $_{\text{RS salt in solution}}$ **x 100 / Total Weight** $_{\text{salt in solution}}$ **(62)**

The molecular weights of the acid, base, diastereomer salt and the solvent used are as follows:

$MW_{\text{2-phenylpropionic acid}}$ = 150.18 g/mol

$MW_{\text{(R)-1-phenylethylamine}}$ = 121.18 g/mol

$MW_{\text{(R)-1-phenylethylammonium-(R,S)-2-phenylpropanoate}}$ = 271.36 g/mol

MW_{ethanol} = 46 g/mol.

For all the three systems studied (A1, A2 and A3), the volume of the filtrate has been measured. Through out the equilibrium of the A1 system, there has been loss of solvent noticed, due the small quantity of the filtrate obtained after equilibrium, at the end. Compared to the initial RR/RS ratio of the acid, the amount of crystallised solid is very little. So there has also been loss of sample through out the equilibrium (or most probably during filtration process, on filter paper, etc).

Compared to the initial RR/RS ratio (**Table_35** and **Table_36**), in the crystallised solid, the percentage of RR-diastereomer salt has increased at high RR ratio and at low initial RR ratio, the composition of RS-diastereomer has increased. In the filtrate, the percentage of RS-diastereomer has slightly increased at high initial RR ratio and the percentage of RR-diastereomer salt has increased at low initial RR-enantiomer.

For initial starting ratio of 90/10, 50/50 and 40/60, the theoretical and measured RR/RS ratios of the filtrate are in good agreement with a difference of less than 7%. When we go higher in initial RS ratio, the theoretical and measured filtrate compositions are varying.

Table_35 Equilibrium of A1 at T=30°C

Initial					**Crystallised Solid**				**Filtrate**
Initial starting ratio measured	Total salt dissolved (g) measured	Weight of RR salt (g) calculated	Weight of RS salt (g) calculated	Weight solvent added (g) measured	Solid RR/RS ratio measured	Weight of crystals (g) measured	Weight RR salt (g) calculated	Weight RS salt (g) calculated	RR/RS ratio of dissolved salt measured
100/0	0.5666	0.5666	0.0000	4.7400	100/0	0.0835	0.0835	0.0000	100/0
90/10	0.5749	0.5175	0.0574	4.7400	97.3/2.7	0.0158	0.0154	0.0004	85.8/14.2
80/20	0.5392	0.4313	0.1079	4.7400	-	0.0065	-	-	82.5/17.5
75/25	0.5753	0.4315	0.1438	4.7400	-	-	-	-	75.7/24.3
60/40	0.5708	0.3425	0.2283	4.7400	-	-	-	-	58.3/47.6
50/50	0.5606	0.2803	0.2803	4.7400	-	-	-	-	52.4/47.6
40/60	0.5988	0.2395	0.3593	4.7400	14.8/85.2	0.0456	0.0067	0.0389	48.8/51.5
25/75	0.5748	0.1437	0.4311	4.7400	4.4/95.6	0.0937	0.0041	0.0896	36.7/63.3
20/80	0.5798	0.1159	0.4639	4.7400	4.1/95.9	0.1211	0.0050	0.1161	34.3/65.7
0/100	0.5592	0.0000	0.5592	4.7400	0/100	0.2500	0.0000	0.2500	0/100

Filtrate By Difference				**Filtrate Calculatd Recovery Assuming 100%**			
Weight of RR salt in solution by difference (g) calculated	Weight of RS salt in solution by difference (g) calculated	Total weight of salt in solution (g) calculated	Theoretical RR/RS ratio calculated	Theoretical weight of solid in filtrate (g) calculated assuming 100% recovery	Weight of filtrate assuming no solvent loss (g) calculated	Weight RR salt (g) Calculated in filtrate	Weight RS salt (g) Calculated in filtrate
0.4831	0.0000	0.4831	100/0	0.4831	5.2231	0.4831	0.0000
0.5021	0.0570	0.5591	89.8/10.2	0.5591	5.2991	0.4797	0.0794
-	-	-	-	0.5327	5.2727	0.4395	0.0932
-	-	-	-	-	-	-	-
-	-	-	-	-	-	-	-
-	-	-	-	-	-	-	-
0.2328	0.3204	0.5532	42.1/57.9	0.5532	5.2932	0.2683	0.2849
0.1396	0.3415	0.4811	29/71	0.4811	5.2211	0.1765	0.3046
0.1109	0.3478	0.4587	24.2/75.8	0.4587	5.1987	0.1573	0.3014
0.0000	0.3092	0.3092	0/100	0.3092	5.0492	0.0000	0.3092

Table_36 Equilibrium of A1 at T=50°C

Initial					Crystallised Solid				Filtrate Measured	
Initial starting ratio measured	Total salt dissolved (g) measured	Weight of RR salt (g) calculated	Weight of RS salt (g) calculated	Weight solvent added (g) measured	Solid RR/RS ratio measured	Weight of crystals (g) measured	Weight RR salt (g) calculated	Weight RS salt (g) calculated	RR/RS ratio of dissolved salt measured	Weight of filtrate (g) measured
100/0	0.5502	0.5502	0.0000	2.3700	100/0	0.1510	0.1510	0.0000	100/0	2.1957
90/10	0.5580	0.5022	0.0558	2.3700	98.5/1.5	0.0621	0.0612	0.0009	88.1/11.9	2.5328
80/20	0.5594	0.4475	0.1119	2.3700	-	-	-	-	79.3/20.7	2.4393
75/25	0.5849	0.4387	0.1462	2.3700	-	-	-	-	73.5/26.5	2.6193
60/40	0.5643	0.3386	0.2257	2.3700	-	-	-	-	60.1/39.9	2.7494
50/50	0.5621	0.2810	0.2810	2.3700	38.6/61.4	0.0356	0.0137	0.0219	53.4/46.6	2.1304
40/60	0.5872	0.2349	0.3523	2.3700	20.4/79.6	0.0554	0.0113	0.0441	44.8/55.2	2.5914
25/75	0.5616	0.1404	0.4212	2.3700	18.1/81.9	0.1855	0.0336	0.1519	43.5/56.5	1.6126
20/80	0.5992	0.1198	0.4794	2.3700	13.4/86.6	0.1062	0.0142	0.0920	28.6/71.4	1.9086
10/90	0.5688	0.0569	0.5119	2.3700	11.4/88.6	0.2796	0.0319	0.2476	27/73	1.6023
0/100	0.5491	0.0000	0.5491	2.3700	0/100	0.3145	0.0000	0.3145	0/100	1.4678

Filtrate By Difference				Filtrate Calculated Recovery Assuming 100%			
Weight of RR salt in solution by difference (g) calculated	Weight of RS salt in solution by difference (g) calculated	Total weight of salt in solution (g) calculated	Theoretical RR/RS ratio calculated	Theoretical weight of solid in filtrate (g) calculated assuming 100% recovery	Weight of filtrate assuming no solvent loss (g) calculated	Weight RR salt (g) Calculated in filtrate	Weight RS salt (g) Calculated in filtrate
0.3992	0.0000	0.3992	100/0	0.3992	2.7692	0.3992	0.0000
0.4410	0.0549	0.4959	88.9/11.1	0.4959	2.8659	0.4369	0.0590
-	-	-	-	-	-	-	-
-	-	-	-	-	-	-	-
-	-	-	-	-	-	-	-
0.2673	0.2591	0.5264	50.8/49.2	0.5265	2.8965	0.2811	0.2454
0.2236	0.3082	0.5318	42/58	0.5318	2.9018	0.2382	0.2936
0.1068	0.2693	0.3761	28.4/71.6	0.3761	2.7461	0.1636	0.2125
0.1056	0.3874	0.4930	21.4/78.6	0.4930	2.8630	0.1410	0.3520
0.0250	0.2643	0.2893	8.6/91.4	0.2892	2.6592	0.0781	0.2111
0.0000	0.2346	0.2346	0/100	0.2346	2.6046	0.0000	0.2346

APPENDIX 8: EQUILIBRIUM OF A2 AT 30 AND 50°C

All the calculations presented in **Table_37** and **Table_38** have been done using the equations, **(46)** to **(62)**, as presented in **APPENDIX 7**.

The molecular weights of the acid, base, diastereomer salt and the solvent used are as follows:

$MW_{\text{2-phenylbutyric acid}}$ = 164.20 g/mol

$MW_{\text{(R)-1-phenylethylamine}}$ = 121.18 g/mol

$MW_{\text{(R)-1-phenylethylammonium-(R,S)-2-phenylbutyrate}}$ = 285.38 g/mol

MW_{ethanol} = 46 g/mol.

In the equilibrium measurements at 30°C, presented in **Table_37**, we have observed loss of solvent, after equilibrium. After equilibrium, the percentage of RS-diastereomer has increased, in the crystallised solid, compared to the initial RR/RS ratio, except in the case of RR/RS ratio of 80/20. In the filtrate, the percentage of RS-diastereomer has increased compared to the initial RR/RS ratio. Theoretical RR/RS ratio of the filtrate is not very well matching with the measured RR/RS ratio of the filtrate.

After equilibrium at 50°C, as presented in **Table_38**, the percentage of RR-diastereomer in the crystallised solid has increased compared to the initial RR/RS ratio. In the case of the measured filtrate, the percentage of RS-diastereomer has increased compared to the initial RR/RS ratio from 100/0 to 30/70 and under these initial compositions, from 25/75 to 10/90, the composition of the filtrate has not changed very much.

Table_37 Equilibrium of A2 at T=30°C

Initial					**Crystallised Solid**				**Filtrate Measured**	
Initial starting ratio measured	Total salt dissolved (g) measured	Weight of RR salt (g) calculated	Weight of RS salt (g) calculated	Weight solvent added (g) measured	Solid RR/RS ratio measured	Weight of crystals (g) measured	Weight RR salt (g) calculated	Weight RS salt (g) calculated	RR/RS ratio of dissolved salt measured	Weight of filtrate (g) measured
100/0	1.7974	1.7974	0	4.7400	100/0	1.7469	1.7469	0.0000	100/0	0.8330
90/10	1.8251	1.6426	0.1825	4.7400	76.7/23.3	1.6005	1.2276	0.3729	74.8/25.2	2.1789
80/20	1.8011	1.4409	0.3602	4.7400	98.1/1.9	1.5977	1.5673	0.0304	56.1/43.9	0.4752
75/25	1.8053	1.3540	0.4513	4.7400	-	1.3343	-	-	50.8/49.2	0.8462
60/40	1.8254	1.0952	0.7302	4.7400	-	0.9618	-	-	36.8/63.2	1.3798
50/50	1.8103	0.9051	0.9051	4.7400	-	0.9430	-	-	32.7/67.3	2.1348
40/60	1.8277	0.7311	1.0966	4.7400	-	0.5858	-	-	26.4/73.6	2.5456
25/75	1.9238	0.4829	1.4429	4.7400	0/100	1.2405	0.0000	1.2405	21.9/78.1	2.1505
20/80	1.8419	0.3684	1.4735	4.7400	0/100	0.4080	0.0000	0.4080	19.9/80.1	2.6627
0/100	1.8113	0	1.8113	4.7400	0/100	0.5146	0.0000	0.5146	0/100	3.7172

Filtrate By Difference				**Filtrate Calculated Assuming 100% Recovery**			
Weight of RR salt in solution by difference (g) calculated	Weight of RS salt in solution by difference (g) calculated	Total weight of salt in solution (g) calculated	Theoretical RR/RS ratio calculated	Theoretical weight of solid in filtrate (g) calculated assuming 100% recovery	Weight of filtrate assuming no solvent loss (g) calculated	Weight RR salt (g) Calculated in filtrate	Weight RS salt (g) Calculated in filtrate
0.0505	0	0.0505	100/0	0.0505	4.7905	0.0504	0.0000
0.4150	-	-	-	0.2246	4.9646	0.1680	0.0566
-	0.3298	-	-	0.2034	4.9434	0.1141	0.0893
-	-	-	-	0.4710	5.2110	0.2393	0.2317
-	-	-	-	0.8636	5.6036	0.3178	0.5458
-	-	-	-	0.8673	5.6073	0.2836	0.5837
-	-	-	-	1.2419	5.9819	0.3279	0.9140
0.4829	0.2024	0.6853	70.5/29.5	0.6833	5.4233	0.1496	0.5337
0.3684	1.0655	1.4339	25.7/74.3	1.4339	6.1739	0.2853	1.1486
0	1.2967	1.2967	0/100	1.2967	6.0367	0.0000	1.2967

Table_38 Equilibrium of A2 at T=50°C

Initial					Crystallised Solid				Filtrate Measured
Initial starting ratio measured	Total salt dissolved (g) measured	Weight of RR salt (g) calculated	Weight of RS salt (g) calculated	Weight solvent added (g) measured	Solid RR/RS ratio measured	Weight of crystals (g) measured	Weight RR salt (g) calculated	Weight RS salt (g) calculated	RR/RS ratio of dissolved salt measured
100/0	2.5267	2.5267	0	4.7400	100/0	2.5020	2.5020	0.0000	100/0
90/10	2.5425	2.2882	0.2543	3.1600	96.81/3.19	1.1028	1.0676	0.0352	71.1/28.9
80/20	2.5304	2.0243	0.5061	3.9500	92.86/7.15	1.1361	1.0550	0.0811	60.4/39.6
75/25	2.5005	1.8754	0.6251	4.7400	91.4/8.6	1.8660	1.7055	0.1605	42.6/57.4
70/30	2.4955	1.7468	0.7487	3.1600	84.1/15.9	1.0364	0.8716	0.1648	52.3/47.7
60/40	2.4744	1.4846	0.9898	3.1600	81.94/18.06	0.5631	0.4589	0.1042	49.4/50.6
50/50	2.5189	1.2594	1.2594	4.7400	86.9/13.1	1.8747	1.6291	0.2456	36.1/63.9
40/60	2.4629	0.9852	1.4777	3.1600	58.4/41.6	0.7538	0.4402	0.3136	30.7/69.3
30/70	2.0981	0.6294	1.4687	3.1600	43.3/56.7	0.4421	0.1914	0.2507	26.3/73.7
25/75	2.4829	0.6207	1.8622	4.7400	32.5/67.5	0.1416	0.0460	0.0956	26.4/73.6
20/80	1.7149	0.3430	1.3719	3.1600	68.1/31.9	0.1763	0.1201	0.0562	21.9/78.1
15/85	3.5752	0.5363	3.0389	5.5300	40.3/59.7	0.2529	0.1019	0.1510	16.1/83.9
10/90	3.5127	0.3513	3.1614	5.5300	33.3/66.7	0.4748	0.1581	0.3167	12.6/87.4
0/100	2.4906	0	2.4906	4.7400	0/100	0.0867	0.0000	0.0867	0/100

Filtrate By Difference				Filtrate Calculated Assuming 100% Recovery			
Weight of RR salt in solution by difference (g) calculated	Weight of RS salt in solution by difference (g) calculated	Total weight of salt in solution (g) calculated	Theoretical RR/RS ratio calculated	Theoretical weight of solid in filtrate (g) calculated assuming 100% recovery	Weight of filtrate assuming no solvent loss (g) calculated	Weight RR salt (g) calculated in filtrate	Weight RS salt (g) calculated in filtrate
0.0247	0	0.0247	100/0	0.0247	4.7647	0.0247	0.0000
1.2206	0.2191	1.4397	84.8/15.2	1.4397	4.5997	1.0236	0.4161
0.9693	0.4250	1.3943	69.5/30.5	1.3943	5.3443	0.8421	0.5522
0.1699	0.4646	0.6345	26.8/73.2	0.6345	5.3745	0.2703	0.3642
0.8752	0.5839	1.4591	60/40	1.4591	4.6191	0.7631	0.6960
1.0257	0.8856	1.9113	53.7/46.3	1.9113	5.0713	0.9442	0.9671
-	1.0138	-	-	0.6442	5.3842	0.2325	0.4117
0.5450	1.1641	1.7091	31.9/68.1	1.7091	4.8691	0.5247	1.1844

0.4380	1.2180	1.6560	26.4/73.6	1.6560	4.8160	0.4355	1.2205
0.5747	1.7666	2.3413	24.5/75.5	2.3413	7.0813	0.6181	1.7232
0.2229	1.3157	1.5386	14.5/85.5	1.5380	4.6980	0.3368	1.2012
0.4344	2.8879	3.3223	13.1/86.9	3.3223	8.8523	0.5349	2.7874
0.1932	2.8447	3.0379	6.4/93.63	3.0379	8.5679	0.3828	2.6551
0	2.4039	2.4039	0/100	2.4039	7.1439	0.0000	2.4039

APPENDIX 9: EQUILIBRIUM OF A3 AT 30 AND 50°C

All the calculations presented in **Table_39** and **Table_40** have been done using the equations, **(46)** to **(62)**, as presented in **APPENDIX 7**.

$MW_{\text{mandelic acid}}$ = 152.15 g/mol
$MW_{\text{(R)-1-phenylethylamine}}$ = 121.18 g/mol
$MW_{\text{(R)-1-phenylethylammonium-(R,S)-mandelate}}$ = 273.33 g/mol
MW_{ethanol} = 46 g/mol.

For the results presented in **Table_39**, when we go higher in initial RS-composition, we get less crystallised solid after equilibrium and the volume of filtrate measured was quite high, explaining that there was very low loss of filtrate. The percentage of RR-diastereomer has increased through out the whole crystallised solid, compared to the initial RR/RS ration. And the percentage of RS-diastereomer has increased through out the filtrates measured, compared to the initial RS-composition.

For the results presented in **Table_40**, when we go high in initial RS-composition, we only obtained little amount of crystallised solid compared to the total salt dissolved initially. The percentage of RR-diastereomer has increased in the crystallised solid compared to the initial RR/RS ratio and the percentage of the RS-diastereomer has increased in the measured filtrate up to initial RR/RS ratio of 25/75. The theoretical and measured RR/RS ratio of the filtrate is in good agreement, except for the initial RR/RS ratio of 60/40.

Table_39 Equilibrium of A3 at T=30°C

Initial					Crystallised Solid				Filtrate Measured	
Initial starting ratio measured	Total salt dissolved (g) measured	Weight of RR salt (g) calculated	Weight of RS salt (g) calculated	Weight of solvent added (g) measured	Solid RR/RS ratio measured	Weight of crystals (g) measured	Weight RR salt (g) calculated	Weight RS salt (g) calculated	RR/RS ratio of dissolved salt measured	Weight of filtrate (g) measured
100/0	1.1061	1.1061	0	4.7400	100/0	0.9444	0.9444	0.0000	100/0	3.5718
90/10	1.1348	1.0213	0.1135	4.7400	96/04	0.5911	0.5675	0.0236	82/18	3.9046
80/20	1.1402	0.9122	0.2280	4.7400	89/11	0.8407	0.7482	0.0925	44.3/55.7	0.9912
75/25	1.1345	0.8509	0.2836	4.7400	86.6/13.4	0.7826	0.6777	0.1049	41.7/58.3	2.0523
60/40	1.1332	0.6799	0.4533	4.7400	76.4/23.6	0.6723	0.5136	0.1587	30/70	3.0774
50/50	1.1041	0.5520	0.5520	4.7400	71.4/28.6	0.5752	0.4107	0.1645	25.3/74.7	3.2130
40/60	1.1316	0.4526	0.6790	4.7400	65.7/34.3	0.4277	0.2810	0.1467	18.8/81.2	4.4831
25/75	1.1131	0.2783	0.8348	4.7400	60/40	0.2690	0.1614	0.1076	13.5/86.5	5.4036
20/80	1.1246	0.2249	0.8997	4.7400	55.8/44.2	0.1802	0.1006	0.0796	11.3/88.7	5.5047
10/90	1.1341	0.1134	1.0207	4.7400	27/73	0.0466	0.0126	0.0340	9.2/90.8	5.6102
0/100	1.1156	0	1.1156	4.7400	-	0.0092	-	-	0/100	5.7490

Filtrate By Difference				Filtrate Calculated Assuming 100% Recovery			
Weight of RR salt in solution by difference (g) calculated	Weight of RS salt in solution by difference (g) calculated	Total weight of salt in solution (g) calculated	Theoretical RR/RS ratio calculated	Theoretical weight of solid in filtrate (g) calculated assuming 100% recovery	Weight of filtrate assuming no solvent loss (g) calculated	Weight RR salt (g) Calculated in filtrate	Weight RS salt (g) Calculated in filtrate
0.1617	0	0.1617	100/0	0.1617	4.9017	0.1617	0.0000
0.4538	0.0899	0.5437	83.5/16.5	0.5437	5.2837	0.4458	0.0979
0.1640	0.1355	0.2995	54.7/45.3	0.2995	5.0395	0.1327	0.1668
0.1732	0.1787	0.3519	49.2/50.8	0.3519	5.0919	0.1467	0.2052
0.1663	0.2946	0.4609	36/64	0.4609	5.2009	0.1383	0.3226
0.1413	0.3875	0.5288	26.7/73.3	0.5289	5.2689	0.1338	0.3951
0.1716	0.5323	0.7039	24.4/75.6	0.7039	5.4439	0.1323	0.5716
0.1169	0.7272	0.8441	13.8/86.2	0.8441	5.5841	0.1139	0.7302
0.1243	0.8201	0.9444	13.2/86.8	0.9444	5.6844	0.1067	0.8377
0.1008	0.9867	1.0875	9.3/90.7	1.0875	5.8275	0.1000	0.9875
0	-	-	-	1.1064	5.8464	0.0000	1.1064

Table_40 Equilibrium of A3 at T=50°C

Initial					Crystallised Solid				Filtrate Measured	
Initial starting ratio measured	Total salt dissolved (g) measured	Weight of RR salt (g) calculated	Weight of RS salt (g) calculated	Weight solvent added (g) measured	Solid RR/RS ratio measured	Weight of crystals (g) measured	Weight RR salt (g) calculated	Weight RS salt (g) calculated	RR/RS ratio of dissolved salt measured	Weight of filtrate (g) measured
100/0	1.5173	1.5173	0	4.7400	100/0	1.2181	1.2181	0.0000	100/0	3.2926
90/10	1.5288	1.3759	0.1529	4.7400	93.3/6.7	1.2055	1.1247	0.0808	78.4/21.6	0.0420
80/20	1.5326	1.2261	0.3065	4.7400	90.2/9.8	1.1364	1.0250	0.1114	51.8/48.2	0.6145
75/25	1.5999	1.1999	0.4000	4.7400	87.9/12.1	1.0117	0.8893	0.1224	49.2/50.8	2.7029
60/40	1.5435	0.9261	0.6174	4.7400	80.5/19.5	0.8333	0.6708	0.1625	35.5/64.5	2.3016
50/50	1.5193	0.7596	0.7596	4.7400	73.6/26.4	0.6912	0.5087	0.1825	29.7/70.3	2.4801
40/60	1.5230	0.6092	0.9138	4.7400	66.1/33.9	0.5505	0.3639	0.1866	24.9/75.1	4.2293
25/75	1.5442	0.3861	1.1581	4.7400	60/40	0.1926	0.1156	0.0770	19.2/80.8	5.2231
20/80	1.5243	0.3049	1.2194	4.7400	56.6/43.4	0.1447	0.0819	0.0628	17.4/82.6	4.8711
10/90	1.5388	0.1539	1.3849	4.7400	-	0.0036	-	-	11.2/88.8	5.3800
0/100	1.5137	0	1.5137	4.7400	-	0.0078	-	-	0.1/99.9	5.9275

Filtrate By Difference				Filtrate Calculated Recovery Assuming 100%			
Weight of RR salt in solution by difference (g) calculated	Weight of RS salt in solution by difference (g) calculated	Total weight of salt in solution (g) calculated	Theoretical RR/RS ratio calculated	Theoretical weight of solid in filtrate (g) calculated assuming 100% recovery	Weight of filtrate assuming no solvent loss (g) calculated	Weight RR salt (g) Calculated in filtrate	Weight RS salt (g) Calculated in filtrate
0.2992	0	0.2992	100/0	0.2992	5.0326	0.2992	0.0000
0.2512	0.0721	0.3233	77.7/22.3	0.3233	5.0633	0.2535	0.0698
0.2011	0.1951	0.3962	50.8/49.2	0.3962	5.1362	0.2052	0.1910
0.3106	0.2776	0.5882	52.8/47.2	0.5882	5.3282	0.2894	0.2988
1.2553	0.4549	1.7102	73.4/26.6	0.7102	5.4502	0.2521	0.4581
0.2509	0.5771	0.8280	30.3/69.7	0.8281	5.5681	0.2459	0.5822
0.2453	0.7272	0.9725	25.2/74.8	0.9725	5.7125	0.2421	0.7304
0.2705	1.0811	1.3516	20/80	1.3516	6.0916	0.2595	1.0921
0.2230	1.1566	1.3796	16.2/83.8	1.3796	6.1196	0.2400	1.1396
-	-	-	-	1.5352	6.2752	0.1719	1.3633
-	-	-	0/100	1.5059	6.2459	0.0015	1.5044

APPENDIX 10: SEPARABILITY CALCULATION SHEET OF A1 AT DIFFERENT TEMPERATURES

All the calculations presented in **Table_41**, **Table_42** and **Table_43** have been done using the equations, **(46)** to **(62)**, as presented in **APPENDIX 7**.

Table_41 Separability measurements of A1 at T=30°C

Initial							**Crystallised Solid**			**Filtrate Measured**
Initial starting ratio measured	Total salt dissolved (g) measured	Weight of RR salt (g) calculated	Weight of RS salt (g) calculated	Weight solvent added (g) measured	Solid recovery conditions Temperature, Time	Solid RR/RS ratio measured	Weight of crystals (g) measured	Weight RR salt (g) calculated	Weight RS salt (g) calculated	RR/RS ratio of dissolved salt measured
100/0	0.8386	0.8386	0	6.3200	29.8°C on the day	100/0	0.1845	0.1845	0	-
90/10	0.5643	0.5079	0.0564	3.9500	6.2°C 21 days	95/05	0.3714	0.3528	0.0186	85.4/14.6
80/20	0.6201	0.4961	0.1240	3.9500	6.2°C 21 days	88.5/11.5	0.3821	0.3381	0.0440	64.6/35.4
75/25	1.0872	0.8154	0.2718	6.3200	29.8°C 7 days	72.7/27.3	0.1667	0.1212	0.0455	-
60/40	0.7495	0.4497	0.2998	3.9500	29.6°C in few hours	12.6/87.4	0.1138	0.0143	0.0995	65.7/34.3
50/50	0.8583	0.4291	0.4291	5.5300	29.8°C on the day	5.1/94.9	0.0998	0.0051	0.0947	-
40/60	0.5135	0.2054	0.3081	3.9500	29.6°C in few hours	12.7/87.3	0.0873	0.0111	0.0762	48.5/51.5
25/75	0.6317	0.1579	0.4738	6.3200	20.3°C 28 days	3.1/96.9	0.1633	0.0051	0.1582	34.4/65.6
20/80	0.3757	0.0751	0.3006	3.9500	6.2°C 21 days	9.7/90.3	0.2066	0.0200	0.1866	36.5/63.5
10/90	0.3187	0.0319	0.2868	3.9500	29.6°C in few hours	4.5/95.5	0.0591	0.0027	0.0564	14.8/85.2
0/100	0.4656	0	0.4656	6.3200	29.8°C 12 days	0/100	0.1842	0	0.1842	0.63/99.37

Filtrate Measured	**Filtrate By Difference**				**Filtrate Calculated Assuming 100% Recovery**			
Weight of filtrate (g) measured	Weight of RR salt in solution by difference (g) calculated	Weight of RS salt in solution by difference (g) calculated	Total weight of salt in solution (g) calculated	Theoretical RR/RS ratio calculated	Theoretical weight of solid in filtrate (g) calculated assuming 100% recovery	Weight of filtrate assuming no solvent loss (g) calculated	Weight RR salt (g) calculated in filtrate	Weight RS salt (g) calculated in filtrate
-	0.6541	0	0.6541	100/0	0.6541	6.9741	-	-
2.1557	0.1551	0.0378	0.1929	80.4/19.6	0.1929	4.1429	0.1647	0.0282
2.5736	0.1580	0.0800	0.2380	66.4/33.6	0.2380	4.1880	0.1537	0.0845
-	0.6942	0.2263	0.9205	75.4/24.6	0.9205	7.2405	-	-
4.2201	0.4354	0.2003	0.6357	68.5/31.5	0.6357	4.5857	0.4176	0.2181
-	0.4240	0.3344	0.7584	55.9/44.1	0.7585	6.2885	-	-
4.1138	0.1943	0.2319	0.4262	45.6/54.4	0.4262	4.3762	0.2067	0.2195
-	0.1528	0.3156	0.4684	32.6/67.4	0.4684	6.4833	0.1611	0.3073
2.8022	0.0551	0.1140	0.1691	32.6/67.4	0.1691	4.1191	0.0617	0.1074
3.9688	0.0292	0.2304	0.2596	11.2/88.8	0.2596	4.2096	0.0384	0.2217
-	0	0.2814	0.2814	0/100	0.2814	6.6014	0.0018	0.2796

In the case of separability measurements temperature and the duration of crystallisation are not the same for all the RR/RS ratios. Some of them have crystallised at 30°C (**Table_41**), but for some other compositions, crystallisation took place at lower temperatures.

For the separability measurements done at 30°C (**Table_41**), when we go down the initial RR/RS ratio, below 75/25, the percentage of RS composition increases in the crystallised solid and this is not the case for initial RR/RS ratio over 75/25. And in the filtrate, the percentage of RR diastereomer has increased for initial RR/RS ratio under 75/25. The RR/RS ratio of the measured filtrate is much closer to the theoretical RR/RS ratio calculated.

For the separability measurements done at 20°C (**Table_42**), except the starting ratio containing pure RR and / or RS enantiomer, the rest of the compositions are crystallising at 19.9°C within very few days. The pure starting acid containing samples have crystallised at low temperatures

and the crystallisation period is about a month. Above the starting RR ratio of 50%, the crystallised products have an increase in the RR composition and below 50% of starting RR ratio, the crystallised solid materials have an increase in the RS diastereomer salt. Measured RR/RS ratio in the filtrate and the theoretical RR/RS ratio calculated are in good agreement.

Table_42 Separability measurements of A1 at T=20°C

Initial						**Crystallised Solid**				**Filtrate Measured**
Initial starting ratio measured	Total salt dissolved (g) measured	Weight of RR salt (g) calculated	Weight of RS salt (g) calculated	Weight solvent added (g) measured	Solid recovery conditions Temperature, Time	Solid RR/RS ratio measured	Weight of crystals (g) measured	Weight RR salt (g) calculated	Weight RS salt (g) calculated	RR/RS ratio of dissolved salt measured
100/0	0.8304	0.8304	0	6.3200	5.8°C 30 days	100/0	0.2635	0.2635	0	100/0
75/25	1.0227	0.7670	0.2557	6.3200	19.9°C 5 days	89.9/10.1	0.3611	0.3246	0.0365	65.7/34.3
50/50	0.8463	0.4231	0.4231	5.5300	19.9°C 5 days	8.0/92.0	0.1511	0.0121	0.1390	61.2/38.8
25/75	0.6620	0.1655	0.4965	6.3200	19.9°C 5 days	4.5/95.5	0.1638	0.0074	0.1638	35.2/64.8
0/100	0.4685	0	0.4685	6.3200	3.8°C 33 days	0/100	0.0636	0	0.0636	99.6/0.4

Filtrate By Difference				**Filtrate Calculated Recovery Assuming 100%**			
Weight of RR salt in solution by difference (g) calculated	Weight of RS salt in solution by difference (g) calculated	Total weight of salt in solution (g) calculated	Theoretical RR/RS ratio calculated	Theoretical weight of solid in filtrate (g) calculated assuming 100% recovery	Weight of filtrate assuming no solvent loss (g) calculated	Weight RR salt (g) calculated in filtrate	Weight RS salt (g) calculated in filtrate
0.5669	0	0.5669	100/0	0.5669	6.8869	0.5669	0
0.4424	0.2192	0.6616	66.9/33.1	0.6616	6.9816	0.4347	0.2269
0.4110	0.2841	0.6951	59.1/40.9	0.6952	6.2252	0.4255	0.2697
0.1581	0.3327	0.4908	32.2/67.8	0.4982	6.8182	0.1754	0.3228
0	0.4049	0.4049	0/100	0.4049	6.7249	0.4033	0.0016

Table_43 Separability measurements of A1 at T=2°C

Initial						**Crystallised Solid**				**Filtrate Measured**
Initial starting ratio measured	Total salt dissolved (g) measured	Weight of RR salt (g) calculated	Weight of RS salt (g) calculated	Weight solvent added (g) measured	Solid recovery conditions Temperature, Time	Solid RR/RS ratio measured	Weight of crystals (g) measured	Weight RR salt (g) calculated	Weight RS salt (g) calculated	RR/RS ratio of dissolved salt measured
75/25	1.0236	0.7677	0.2559	6.3200	3.9°C 2 days	86.5/13.5	0.5539	0.4791	0.0748	59.8/40.2
50/50	0.8612	0.4306	0.4306	5.5300	3.9°C 4 days	32.1/67.9	0.3828	0.1229	0.2599	58.7/41.3
25/75	0.6311	0.1578	0.4733	6.3200	3.9°C 2 days	3.5/96.5	0.2656	0.0093	0.2563	42.9/57.1
0/100	0.4951	0	0.4951	6.3200	4.7°C on the day	0/100	0.2765	0	0.2765	0/100

Filtrate By Difference				**Filtrate Calculated Recovery Assuming 100%**			
Weight of RR salt in solution by difference (g) calculated	Weight of RS salt in solution by difference (g) calculated	Total weight of salt in solution (g) calculated	Theoretical RR/RS ratio calculated	Theoretical weight of solid in filtrate (g) calculated assuming 100% recovery	Weight of filtrate assuming no solvent loss (g) calculated	Weight RR salt (g) calculated in filtrate	Weight RS salt (g) calculated in filtrate
0.2886	0.1811	0.4697	61.4/38.6	0.4697	6.7897	0.2809	0.1888
0.3077	0.1707	0.4784	64.3/35.7	0.4784	6.0084	0.2808	0.1976
0.1485	0.2170	0.3655	40.6/59.4	0.3655	6.6855	0.1568	0.2087
0	0.2186	0.2186	0/100	0.2186	6.5386	0	0.2186

When the temperature has been set at 2°C (**Table_43**) and when we go down the temperature starting from 30°C towards 2°C, with a rate of 0.5°C/min, all the different initial compositions have crystallised within few days at lower temperature. For the initial staring ratio of 75/25, there is an increase in RR-diastereomer in the crystallised solid and an increase in the RS-diastereomer in the measured filtrate. For all other samples, there is an increase in RS-diastereomer in the crystallised solid and an increase in the RR-diastereomer in the measured filtrate. The compositions of measured filtrates and the calculated filtrates (by differences) are in good agreement.

APPENDIX 11: SEPARABILITY CALCULATION SHEET OF A2 AT DIFFERENT TEMPERATURES

All the calculations presented in **Table_44**, and **Table_45** have been done using the equations, **(46)** to **(62)**, as presented in **APPENDIX 7**.

Table_44 Separability measurements of A2 at T=30°C

Initial							**Crystallised** **Solid**			**Filtrate**	**Measured**
Initial starting ratio measured	Total salt dissolved (g) measured	Weight of RR salt (g) calculated	Weight of RS salt (g) calculated	Weight solvent added (g) measured	Solid recovery conditions Temperature, Time	Solid RR/RS ratio measured	Weight of crystals (g) measured	Weight RR salt (g) calculated	Weight RS salt (g) calculated	RR/RS ratio of dissolved salt measured	Weight of filtrate (g) measured
100/0	0.2555	0.2555	0	5.5300	15.7°C 10 days	100/0	0.0459	0.0459	0	94.4/5.6	0.8003
90/10	0.2157	0.1941	0.0216	3.9500	19.8°C 6 days	85.2/14.8	0.0342	0.0291	0.0051	77.3/22.7	3.8564
80/20	0.2548	0.2038	0.0510	3.9500	6.2°C 19 days	85.2/14.8	0.0550	0.0469	0.0081	54.1/45.9	0.5403
75/25	0.3697	0.2773	0.0924	5.5300	19.8°C 8 days	100/0	0.0150	0.0150	0	71.3/28.7	0.7947
60/40	0.3325	0.1995	0.1330	3.9500	19.8°C 6 days	74.2/14.8	0.0327	0.0243	0.0084	50.8/49.2	3.6142
50/50	0.5687	0.7843	0.7843	5.5300	6.0°C 15 days	80.1/19.9	0.1353	0.1084	0.0269	-	-
40/60	0.5801	0.2321	0.3480	3.9500	24.7°C 4 days	41.2/58.8	0.0738	0.0304	0.0434	33.9/66.1	2.8886
25/75	1.5609	0.3902	1.1707	4.7400	15.7°C 10 days	35.1/64.9	1.4605	0.5126	0.9479	-	-
20/80	2.1582	0.4317	1.7265	3.9500	24.7°C 4 days	26/74	1.9090	0.4963	1.4127	None	None
10/90	2.1633	0.2163	1.9470	3.9500	24.7°C 4 days	13.3/86.7	1.0879	0.1447	0.9432	15.2/84.8	0.3907
0/100	2.3527	0	2.3527	4.7400	30.1°C 3 days	0/100	1.5223	0	1.5223	-	-

Filtrate Measured	**Filtrate By Difference**				**Filtrate Calculated Assuming 100% Recovery**			
Weight of filtrate (g) measured	Weight of RR salt in solution by difference (g) calculated	Weight of RS salt in solution by difference (g) calculated	Total weight of salt in solution (g) calculated	Theoretical RR/RS ratio calculated	Theoretical weight of solid in filtrate (g) calculated assuming 100% recovery	Weight of filtrate assuming no solvent loss (g) calculated	Weight RR salt (g) calculated in filtrate	Weight RS salt (g) calculated in filtrate
-	0.2096	0	0.2096	100/0	0.2096	5.7396	0.1979	0.0117
3.8564	0.1650	0.0165	0.1815	90.9/9.1	0.1815	4.1315	0.1403	0.0412
0.5403	0.1569	0.0429	0.1998	78.5/21.5	0.1998	4.1498	0.1081	0.0917
-	0.2923	0.0924	0.3847	76/24	0.3547	5.8847	0.2529	0.1018
3.6142	0.1752	0.1246	0.2998	58.4/41.6	0.2998	4.2498	0.1523	0.1475
-	0.6759	0.7574	1.4333	47.2/52.8	0.4334	5.9634	-	-
2.8886	0.2017	0.3046	0.5063	39.8/60.2	0.5063	4.4563	0.1716	0.3347
-	-	0.2228	-	-	0.1004	4.8404	-	-
None	-0.0646	0.3138	-	-	0.2492	4.1992	-	-
0.3907	0.0716	1.0038	1.0754	6.6/93.4	1.0754	5.0254	0.1635	0.9119
-	0	0.8304	0.8304	0/100	0.8304	5.5704	0	0.8304

For the separability measurements done at 30°C (**Table_44**), different starting RR/RS compositions have different solid recovery temperatures and times. In all the cases, except for the initial RR/RS ratio of 90/10, the crystallised solids have an increase in RS-diastereomer. The RR/RS ratios of the measured filtrates do not match matching with the theoretical RR/RS ratio of the filtrate calculated (by difference).

Table_45 Separability measurements of A2 at T=3°C

Initial						**Crystallised Solid**				**Filtrate Measured**	
Initial starting ratio measured	Total salt dissolved (g) measured	Weight of RR salt (g) calculated	Weight of RS salt (g) calculated	Weight solvent added (g) measured	Solid recovery conditions Temperature, Time	Solid RR/RS ratio measured	Weight of crystals (g) measured	Weight RR salt (g) calculated	Weight RS salt (g) calculated	RR/RS ratio of dissolved salt measured	Weight of filtrate (g) measured
75/25	0.3377	0.2533	0.0844	5.53	3.8°C 1 day	97.1/2.9	0.0919	0.0892	0.0027	66.3/33.7	1.9847
50/50	0.5970	0.2985	0.2985	5.53	3.9°C 2 days	66.4/33.6	0.1328	0.0882	0.0446	42.8/57.2	1.8128
25/75	1.5614	0.3903	1.1711	4.74	36.8°C on the day during T decrease	52.7/47.3	0.6451	0.3400	0.3051	23.4/76.6	1.2829

Filtrate By Difference				**Filtrate Calculated Assuming 100% Recovery**			
Weight of RR salt in solution by difference (g) calculated	Weight of RS salt in solution by difference (g) calculated	Total weight of salt in solution (g) calculated	Theoretical RR/RS ratio calculated	Theoretical weight of solid in filtrate (g) calculated assuming 100% recovery	Weight of filtrate assuming no solvent loss (g) calculated	Weight RR salt (g) calculated in filtrate	Weight RS salt (g) calculated in filtrate
0.0892	0.0817	0.1709	52.2/47.8	0.2458	5.7758	0.1630	0.0828
0.0882	0.2539	0.3421	25.8/74.2	0.5524	6.0824	0.2364	0.3160
0.3400	0.8660	1.2060	28.2/71.8	0.9163	5.6563	0.2144	0.7019

For the separability measurements done at 3°C (**Table_45**), compounds of initial composition of 75/25 and 50/50 have crystallised at very low temperatures within two days, but the compound of initial composition 25/75 has crystallised during the temperature decrease. In all three compositions studied here, the percentage of RR-diastereomer has increased in the crystallised solid and the percentage of RS-enantiomer has increased in the filtrate.

APPENDIX 12: SEPARABILITY CALCULATION SHEET OF A3 AT 30°C

All the calculations presented in **Table_46**, have been done using the equations, **(46)** to **(62)**, as presented in **APPENDIX 7**.

Table_46 Separability measurements of A3 at T=30°C

Initial						**Crystallised Solid**				**Filtrate**	**Measured**
Initial starting ratio measured	Total salt dissolved (g) measured	Weight of RR salt (g) calculated	Weight of RS salt (g) calculated	Weight solvent added (g) measured	Solid recovery conditions Temperature, Time	Solid R/S ratio measured	Weight of crystals (g) measured	Weight RR salt (g) calculated	Weight RS salt (g) calculated	R/S ratio of dissolved salt measured	Weight of filtrate (g) measured
100/0	0.3113	0.3113	0	4.74	29.7°C 1 day	100/0	0.1553	0.1553	0	100/0	3.7653
90/10	0.3115	0.2803	0.0312	4.74	29.7°C 1 day	97.9/2.1	0.1299	0.1272	0.0027	81.3/18.7	4.4998
80/20	0.3137	0.2510	0.0627	4.74	24.7°C 5 days	95.5/5.0	0.1041	0.0994	0.0047	69.4/30.6	4.3300
75/25	0.3458	0.2594	0.0864	4.74	20.2°C 8 days	91.6/8.4	0.1560	0.1429	0.0131	57.6/42.4	3.9174
60/40	0.3880	0.2328	0.1552	4.74	15.3°C 12 days	82.9/17.7	0.1574	0.1305	0.0269	38.1/16.9	3.9384
50/50	0.4940	0.2470	0.2470	4.74	20.2°C 9 days	79.7/20.3	0.1797	0.1432	0.0365	29.3/70.7	4.3933
40/60	0.6058	0.2423	0.3635	4.74	15.3°C 12 days	71.7/28.3	0.2052	0.1471	0.0581	20.0/80.0	4.0160
25/75	1.0098	0.2524	0.7574	4.74	20.2°C 9 days	54.6/45.4	0.3289	0.1796	0.1493	9.9/90.1	4.5127
20/80	1.2780	0.2556	1.0224	4.74	15.3°C 15 days	45.2/54.8	0.4534	0.2049	0.2485	5.6/94.4	4.0566

Filtrate By Difference				Filtrate Calculated Recovery Assuming 100%			
Weight of RR salt in solution by difference (g) calculated	Weight of RS salt in solution by difference (g) calculated	Total weight of salt in solution (g) calculated	Theoretical R/S ratio calculated	Theoretical weight of solid in filtrate (g) calculated assuming 100% recovery	Weight of filtrate assuming no solvent loss (g) calculated	Weight RR salt (g) calculated in filtrate	Weight RS salt (g) calculated in filtrate
0.1560	0	0.1560	100/0	0.1560	4.8960	0.1560	0
0.1531	0.0285	0.1816	84.3/15.7	0.1816	4.9216	0.1513	0.0303
0.1516	0.0580	0.2096	72.3/27.7	0.2096	4.9496	0.1455	0.0641
0.1165	0.0733	0.1898	61.4/38.6	0.1898	4.9298	0.1093	0.0805
0.1023	0.1283	0.2306	44.4/55.6	0.2306	4.9706	0.0878	0.1428
0.1038	0.2105	0.3143	33/67	0.3143	5.0543	0.0921	0.2222
0.0952	0.3054	0.4006	23.7/76.3	0.4006	5.1406	0.0801	0.3205
0.0728	0.6081	0.6809	10.7/89.3	0.6809	5.4209	0.0674	0.6135
0.0507	0.7739	0.8246	6.1/93.9	0.8246	5.5646	0.0462	0.7784

For the separability measurements done at 30°C, all the RR/RS compositions have different crystallisation temperatures and times. In all cases, the crystallised solid has an increase in the percentage of RR-diastereomer and the filtrate has an increase in the percentage of RS-diastereomer. The RR/RS ratio of the measured filtrate and the theoretical RR/RS ratio calculated are in good agreement.